

VOLUME 17

NUMBER 1

2024

ISSN 2218-7979  
eISSN 2409-370X

International Journal of  
**Biology**  
and **Chemistry**



Al-Farabi Kazakh National University

International Journal of Biology and Chemistry is published twice a year by  
al-Farabi Kazakh National University, al-Farabi ave., 71, 050040, Almaty, Kazakhstan  
website: <http://ijbch.kaznu.kz/>

Any inquiry for subscriptions should be sent to:  
Prof. Mukhambetkali Burkitbayev, al-Farabi Kazakh National University  
al-Farabi ave., 71, 050040, Almaty, Kazakhstan  
e-mail: [Mukhambetkali.Burkitbayev@kaznu.edu.kz](mailto:Mukhambetkali.Burkitbayev@kaznu.edu.kz)

## **EDITORIAL**










The most significant achievements in the field of natural sciences are reached in joint collaboration, where important roles are taken by biology and chemistry. Therefore publication of a Journal, displaying results of current studies in the field of biology and chemistry, facilitates highlighting theoretical and practical issues and distribution of scientific discoveries.

One of the basic goals of the Journal is to promote the extensive exchange of information between the scientists from all over the world. We welcome publishing original papers and materials of biological and chemical conferences, held in different countries (by prior agreement, after the process of their subsequent selection).

Creation of International Journal of Biology and Chemistry is of great importance, since scientists worldwide, including other continents, might publish their articles, which will help to widen the geography of future collaboration.

The Journal aims to publish the results of the experimental and theoretical studies in the field of biology, biotechnology, chemistry and chemical technology. Among the emphasized subjects are: modern issues of technologies for organic synthesis; scientific basis of the production of biologically active preparations; modern issues of technologies for processing of raw materials; production of new materials and technologies; study on chemical and physical properties and structure of oil and coal; theoretical and practical issues in processing of hydrocarbons; modern achievements in the field of nanotechnology; results of studies in various branches of biology, chemistry and related technologies.

We hope to receive papers from the leading scientific centers, which are involved in the application of the scientific principles of biological and chemical sciences on practice and fundamental research, related to production of new materials, technologies well ecological issues.

E.S. Seitkozhanova<sup>1</sup> , S.M. Shalgimbayeva<sup>1</sup> , S.S. Barinova<sup>2</sup> ,  
 Dh. Makhmetova<sup>1</sup> , G.B. Jumakhanova<sup>1\*</sup> , A.E. Nurgaliev<sup>3</sup> ,  
 Z.S. Omarova<sup>1</sup> , D.A. Yussayeva<sup>1</sup> , G.T. Zhanysbay<sup>1</sup> 

<sup>1</sup>Al-Farabi Kazakh National University, Almaty, Kazakhstan

<sup>2</sup>Institute of Evolution, University of Haifa, Haifa, Israel

<sup>3</sup>Charyn State National Natural Park, Alma-Ata's region, Kazakhstan

e-mail: gkaznu@gmail.com

(Received 3 October 2023; received in revised form 12 December 2023; accepted 28 December 2023)

## Study of Charyn river naked osman (*Diptychus dybowskii*) nutrition and ichthyopathological analysis

**Abstract.** The paper discusses the study of nutrition and ichthyopathological analysis of naked osman from the Charyn River, which is located on the territory of the Charyn State National Natural Park in the Almaty region. The naked osman belongs to the carp family. The fish does not have any scales on other part of the body except the lateral line. The naked osman currently dwells in Kazakhstan, China, Kyrgyzstan, Uzbekistan, India, Nepal and other Asian countries. The purpose of the work is to determine the Charyn River's food base and water condition by studying the food spectrum, fish pathology. To carry out the given study the fish were caught in the autumn in 2021. Only 15 samples of the caught fish were taken for the analysis. According to the ichthyological analysis results, the absolute length of 15 samples of the fish ranged from 8.3 cm to 12.7 cm, and their mass was from 4.81 g to 17.60 g. The standard quantitative – weight method was used for ichthyotrophological research. The special histological method was employed for ichthyopathological study. According to the ichthyotrophological study, the fullness index was about 10.75%00, and insect larvae were an essential food. Histological studies did not reveal an obvious pathology. As a result, the nutrient reserves in the reservoir were found to be at a good level and the external environment was found not to produce a negative effect on the fish.

**Key words:** Charyn River, naked osman, *Diptychus dybowskii*, ichthyotrophology, ichthyopathology, nutrition study.

### Introduction

The territory of the Republic of Kazakhstan has 85,000 rivers and temporary water bodies. The distribution of water resources in Kazakhstan is uneven. One-third of water resources is for the eastern regions, and 1/4 is for the southeastern and southern regions [1]. One of the largest rivers, the Ili, provides Lake Balkhash with water. 30% of the Ili River water resources is on Kazakhstan territory. Besides Sharyn and Shelek, there are several mountain rivers such as Turgen, Esik, Talgar, Kaskelen which flow into the Ili River on the left [2].

The source of the Sharyn River originates from the southern ranges of the Ketmen Mountains. Kegen, the middle part of the river, that is also called Sharyn flows from the exit to Zhalanash hill [3,4]. The acclimatization works of the last century led to

the migration of such fish as carp, pikeperch, bream, asp, catfish, roach, grass carp, white and spotted silver carp to the Balkhash-Ili basin. Over the past 14 years, alien species from China have appeared, but they were included in the Red Book as native species (rudd fish, Balkhash perch). Other aborigines (catfish, naked osman) migrated to mountain rivers. In addition, the habitat of rudd fish is the Sharyn River and Kaskelen Bay [5,6].

The naked osman is one of the main species inhabiting in the Sharyn River. Naked osman is found in mountainous regions of Central Asia. The short length of the head, a small indicator of the maximum height of the body, a high caudal stem and shortened pectoral fins are the characteristics of the Sharyn Osman. These morphological features determine the “long and slender” body shape of the naked osman compared to the body

shape of the remaining geographical races of this species [7-9].

Naked osman belongs to bentophages by the nutrition type. Ichthyotrophological studies were carried out by the method of benthos fish nutrition study. The studies of the nutrition of bentophages differ in the stomach presence or absence as well as in the sections of the digestive fish canal. In fish with a stomach, food is better preserved and more easily digested. When investigating fish with no stomach, food is digested throughout the digestive tract. The nutrition of benthos fish with no stomach was carried out by combined method, which includes methods for benthos, planktonophage and predatory fish [10]. Ichthyopathological studies of the fish were made by the special histological methods. As numerous studies show histopathological changes can be an excellent bioindicator of the biological effects of environmental influences on the organism. They can range from the presence of minor parasitic infestation to severe necrotic processes and indicate tumor formations. Histological changes can rarely be caused by the effects of a particular substance. These changes are a general response to the impact of the entire complex of environmental toxicants. Histological processing of the materials obtained in the the study included the following operations: dehydration, paraffin freezing, cutting with microtome and studying under the microscope [11-13].

The given research is considered to be relevant due to the fact that the study of the Charyn River ichthyopathological and ichthyotrophological characteristics has conducted for the first time. So, the investigation of its ichthyofauna, nutritious resources and water conditions through fish and their pathology is an important part of the given research. The ichthyotrophological and ichthyopathological studies of Charyn River naked osman have been made for the first time which makes the given study more valuable and novel in the field of ichthyology.

The aim of the study is to determine the nutritional base of the Sharyn River and the state of the fish by conducting the naked osman ichthyotrophological and ichthyopathological studies.

### Materials and methods

To determine the food spectrum and conduct histological studies the species of naked osman (*Diptychus dybowski*) were caught in the autumn of 2021 in the Charyn River using the following coordinates: inspection 1, part 5, allotment 8 ( $43^{\circ}40'14.84''\text{N}$ ,  $79^{\circ}23'24.17''\text{E}$ ; Figure 1, A), inspection 5, part 49, allotment 7 ( $43^{\circ}30'31.87''\text{N}$ ,  $79^{\circ}13'20.20''\text{E}$ ; Figure 1, B), inspection 19, part 120, allotment 7 ( $43^{\circ}21'40.81''\text{N}$ ,  $79^{\circ}9'52.81''\text{E}$ ; Figure 1, C).



**Figure 1** – The coordinates used for fish catch in the Charyn River.

Note: A –  $43^{\circ}40'14.84''\text{N}$ ,  $79^{\circ}23'24.17''\text{E}$ ; B –  $43^{\circ}30'31.87''\text{N}$ ,  $79^{\circ}13'20.20''\text{E}$ ; C –  $43^{\circ}21'40.81''\text{N}$ ,  $79^{\circ}9'52.81''\text{E}$

The caught fish were preliminary placed in 10% formalin, then they were delivered to the laboratory where 15 samples of the fish were selected for analysis (Figure 2).



**Figure 2** – Naked osman used for study

In the laboratory of the Department of Biodiversity and Bioresources, Al-Farabi Kazakh National University, ichthyological, ichthyotrophological and ichthyopathological studies of 15 samples of the fish were made. Ichthyological studies and measurements were made using Pravdin method. During the ichthyological studies, absolute and short length of the samples were measured using a caliper, large and small weights were determined using the MW-Micro Digital Computing Scale (Korea). The indicator of fish fatness was calculated according to Fulton and Clark formula [14,15].

The components of food in the digestive tract of naked osman were investigated by a standard weight-quantity method. Processing was performed quantitatively, i.e., by counting and measuring the gastrointestinal tract. During the ichthyotrophological analysis, the gastrointestinal tract of fish was taken, the intestine was divided into 3 parts, and the nutrient node of each section was placed onto filter paper and dried. The dried nutrient node was weighed on an EP613C torzion scale (Switzerland). The nutrient node composition of food supply was determined by a binocular magnifying glass (MBS-9 stereomicroscope (SCOPICA, Russian)) and a microscope (MicroOptix light microscope (MicroOptx, Inc., Austria)) [10,16-18].

To identify the physiological state of the fish organs, a histological study was conducted using special histological methods. The fragments of different organs were placed in cassettes and prepared for dehydration using the research method. Dehydration process is carried out in a battery of

butyl and ethyl alcohol starting with 70° alcohol and then increasing its concentration by 10°. The materials were transferred from one solution to another. They were dried on the filter paper. The time of each alcohol exposure was 35 minutes. After the material was immersed in alcohol, it was dipped in alcohol – butanol mixture, and then it was placed in pure butanol. After the immersion in butanol-II, the material was put in molten paraffin. Then it was placed in a thermostat overnight at 56° C to impregnate the sample with paraffin. When the material solidified in paraffin, a microtome was used to obtain 5-micron histological sections. To remove paraffin from the surface of the sections before their coloring, they were passed through the solutions of xylene-I, xylene-II, then 96 percent ethanol-I, 96 percent ethanol-II, 70 percent ethanol. The colored sections were investigated using optical microscope (Motic BA-400 microscope (Motic Asia, Hong Kong, China)) [11,12,19]. Statistical data processing was done by standard methods and statistical programs in Microsoft Excel.

## Results and discussion

Ichthyological analysis allowed determining the value of the fish length, large and small weight. The absolute length of the studied fish ranged from 8.3 cm to 12.7 cm, the average length was 10.7 cm, the large weight was from 4.81 to 17.60 g, the average weight was 10.3 g (Table 1).

**Table 1** – Length and weight of the studied naked osman

No.	L, cm	l, cm	Q, g	q, g
1	12.7	10.5	17.60	14.06
2	11.2	9.1	13.81	10.35
3	11.8	9.6	13.62	10.81
4	11.1	8.9	10.63	8.81
5	11	9	10.70	9.23
6	11.5	9.4	12.01	10.06
7	10.7	8.9	9.74	8.42
8	11.1	9	10.95	9.22
9	10.7	8.6	10.23	8.39
10	10.7	8.6	10.91	8.74
11	10.8	8.5	9.82	7.69
12	10.1	8.4	8.34	7.21
13	9.6	7.8	6.21	5.40
14	8.8	7.1	5.23	4.43
15	8.3	6.7	4.81	3.91

Table 1 shows the data measured in the ichthyological study. The table gives the values of the absolute length (L), short length (l), large (Q) and small (q) weight, which show notable changes in the parameters.

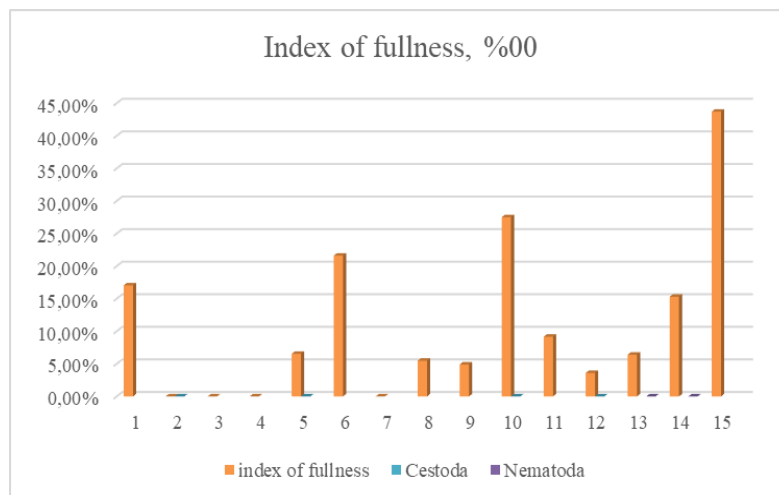
The fish fatness was calculated using the Fulton and Clark formula, Fulton results were from 1.31 to 1.83, Clark results were from 1.19 to 1.37 (Table 2).

Table 2 shows the results of fatness calculated by Fulton and Clark formula. According to Fulton formula, the maximum value was 1.27, and the minimum was 0.7. According to Clark formula the maximum value was 0.74, and the minimum was 0.61. These indicators demonstrate a good level of fish fatness.

During ichthyotrophic studies, fullness index of 15 samples of naked osman was calculated. The overall value of the fullness index was 161.22%00 and the average value was 10.75% (Figure 3).

**Table 2** – Fatness results of the studied fish by Fulton and Clark

No.	Fulton	Clark
1	0.86	0.67
2	1.27	0.74
3	0.83	0.66
4	0.78	0.64
5	0.80	0.69
6	0.79	0.66
7	0.80	0.69
8	0.80	0.67
9	0.84	0.68
10	0.89	0.71
11	0.79	0.61
12	0.81	0.7
13	0.70	0.61
14	0.82	0.69
15	0.84	0.68
medium	0.84	0.68



**Figure 3** – Fullness index of the studied naked osman

Figure 3 shows the fullness index variability. Of the 15 fish species studied, 4 were completely free and cestodes were shown to be found in 4 samples and nematodes were present in 2 samples.

The results of ichthyotrophic studies mainly indicates the presence of insect fragments and unidentified pieces of digested food in the digestive tract of the naked osman (Figure 4).

Figure 4 illustrates the chitinous legs and claws of the insect found in the nutrient node, where completely digested food was also discovered but it could not be identified.

Fragments and nests of caddisfly larvae were discovered in the intestine (Figure 5).

The images given above show the parts of the caddisfly larvae which consist of a nest and fragments of a wing mixed with digested food. Nests are usually made of stones and plants, wings have a chitinous structure, so they cannot be digested.

In addition, the fragments of water beetle larvae were present in the intestine part (Figure 6).

The image above illustrates the part of the water beetle chitinous head and the digested food elements. Since the parts of the insects are chitinous, they cannot be completely digested.

Nematodes were in 4 species of the studied fish, and cestodes were in 2 species (Figure 7).



**Figure 4** – A, B – Images of insect fragments and pieces of naked osman digested food

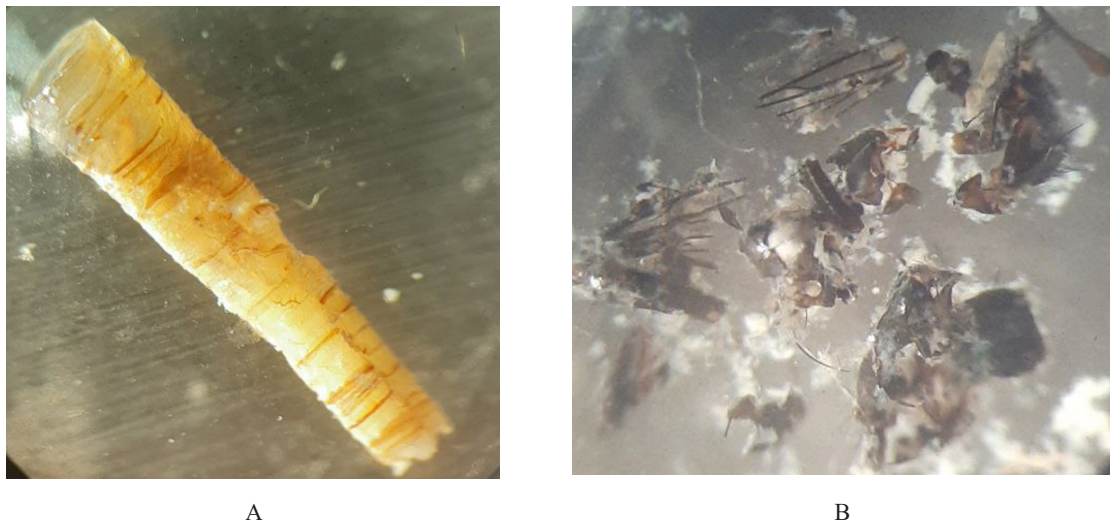


**Figure 5** – A – Image of caddisfly larvae nest. B – Image of caddisfly larvae fragments



**Figure 6** – Images of water beetle larvae fragment



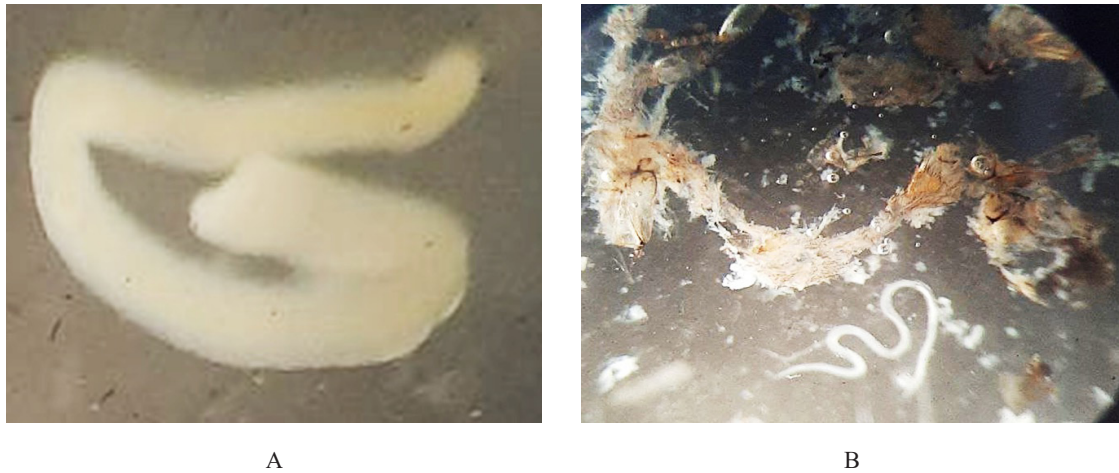


**Figure 7** – A- Image of cestoda found in intestine part.  
B – Image of nematoda found in intestine part

Figure 7 shows the cestodas and nematodas found inside the intestinal tract of the samples. In total, 4 nematodes and about 17 cestosdes were found in 15 fish.

The repetition frequency of the identified fragments and the number of fragments were determined using Microsoft Excel (Table 3).

**Table 3** – The repetition frequency and the number of components in the digestive tract of the naked osman

Components	The repetition frequency	The number of components
Insect	90%	83.30%
Larvae of water beetle	20%	4.50%
Caddisfly larvae	30%	6.10%
Plant	20%	6.10%

From the results we can see that the food spectrum of the studied fish consists mainly of insects and their larvae. The naked osman eats plants very rarely, however the intestinal sections contain plants because the caddisfly larvae can build their nests near plants.

The results of histological studies demonstrate that the condition of the gills of 15 samples of naked osman was normal. Hyperplasia was one of the most frequent changes in histological preparation analysis (Figure 8).

The study of histological samples of fish muscles showed no pathological changes. The largest and

smallest cross-sectional sizes of the muscles were taken for study and compared. The smallest muscles were 35.03 nm, 33.83 nm, 42.51 nm, and the largest muscles were 82.71 nm, 86.22 nm, 93.35 nm (Figure 9).

There is no pathology in the histological samples of the naked osman stomach parts taken for the study. The walls are not damaged and straight (Figure 10).

Histological tests of the studied fish the liver showed no pathology. Stem cells lined with blood capillaries are clearly visible. Hepatocyte cells were basophilic. No fat content was observed in these fish species (Figure 11).

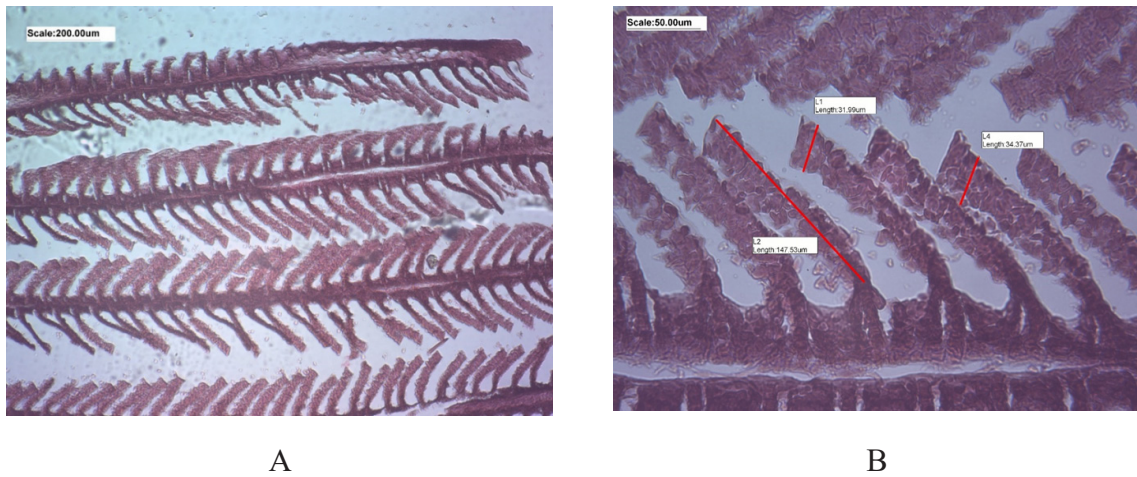


**Figure 8** – Images of histological section of naked osman gills coloured by haematoxylin-eosin A-10x magnifying, B-40x magnifying

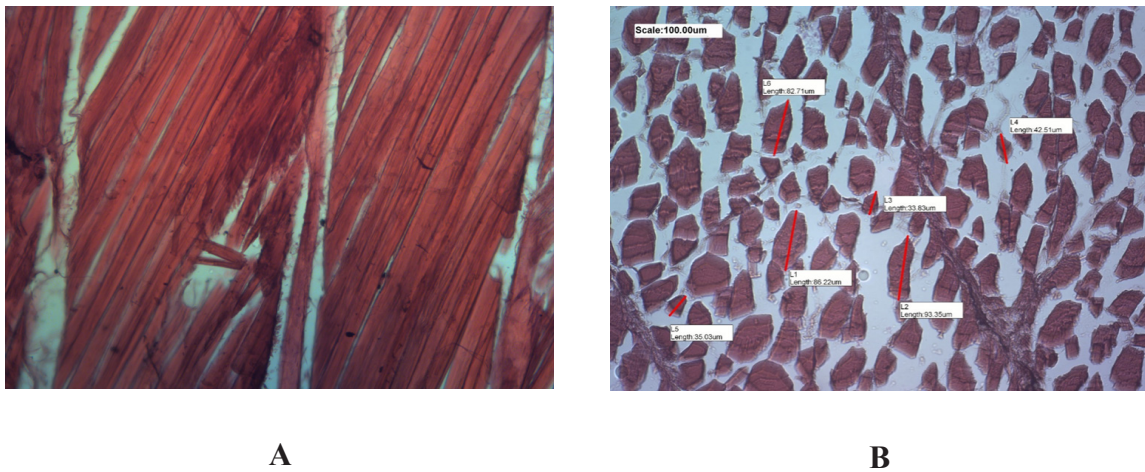


**Figure 9** – A, B- 20 x image of histological section of the naked osman muscles colored by haematoxylin-eosin

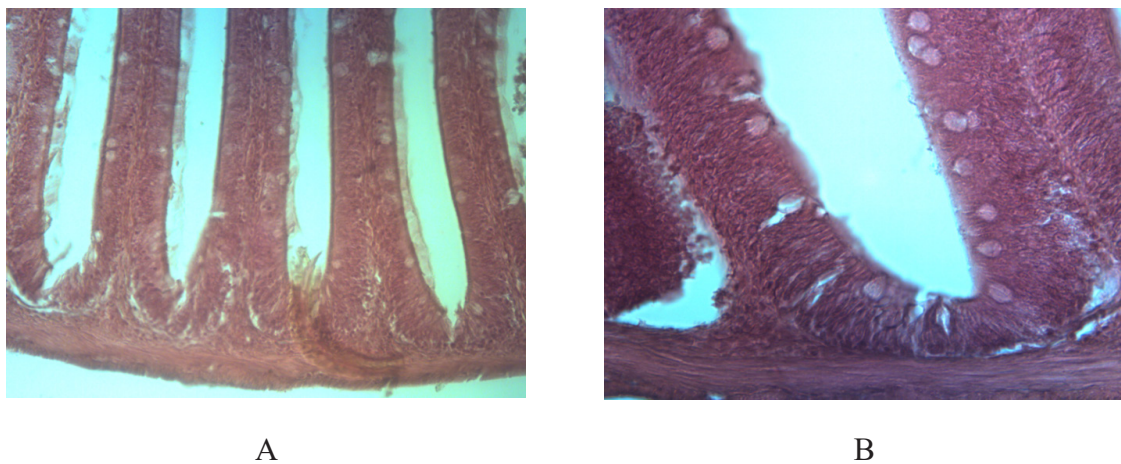


**Figure 10** – Image of histological section of the naked osman stomach parts colored by haematoxylin- eosin 20x magnifying, B- 40x magnifying

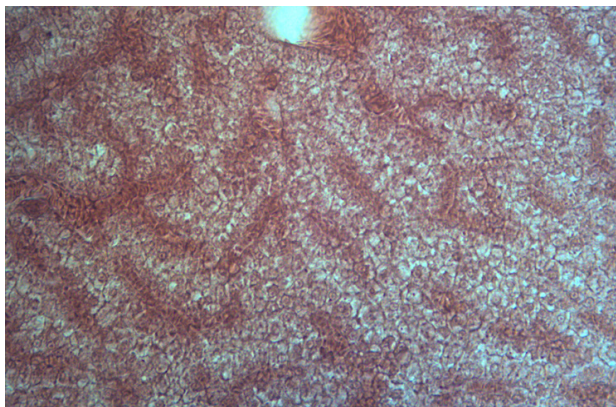


**Figure 12** – 20x image of histological section of the naked osman liver colored by haematoxylin-eosin

The research gives a detailed analysis of the naked osman food spectrum and its ichthyopathological state. It reveals the Charyn River nutritious resources and water conditions. The given study is considered to be a pioneering one since such investigations have never been conducted before and the objects used for the study have also been never researched.

### Conclusion

The results of ichthyotrophological studies indicate 90% of insect fragments, 30% of caddisfly larvae, 20% of water beetle larvae and plants. The composition of these samples included 83.30% of the fragments of insects, 4.5% of the larvae of water

beetles, 6.10% of the larvae of caddisflies and plants. The studied fish are benthophagous, according to the frequency of food fragments and their number of components, insect larvae fragments was their main food. Out of 15 fish, 4 had completely empty digestive tract. 11 fish samples had digested food in their tract, the total fullness index equaled 161.22%00. The studies also showed the sufficient supply of nutrients to the reservoir.

Histological analysis revealed that protozoal infestation caused such changes as hyperplasia and lamella shortening in gills in addition to the normal state of the structure of the gill lamella of the fish. There are no pathologies very dangerous for the fish in the digestive system of the fish. Epithelium desquamation was observed on some villi of the fish intestine. The liver was in a normal state. Hepatocyte cells were arranged in a right order and were clearly visible. In most cases, the fibers of the fish skeleton muscles were normal, the sarcolemma was not damaged, the horizontal lines were also clearly visible, and the nuclei were located on the periphery. According to the study results the external environment produced no negative effect on the body of the naked osman. As the nutrition results of the Sharyn River fish show, nutrition base is good which prevents pathologies in organisms. Results can be useful for further studies on naked osman and on the Charyn River. In addition, ichthyotrophological and histological methods were improved which allows using them in trophology and histology.

### References

1. Berdygulova G.E. (2014) The current state of Kazakhstan's transboundary rivers and the problems of their joint use [Sovremennoe sostojanie transgranichnyh rek kazahstana i problemy ih sovmestnogo ispol'zovanija]. Almaty: KazNPU, 4 p., ISSN 1728-8975
2. Amirgalieva A.S. (2021) Assessment of changes in water resources and prospects for forecasting the water content of the main rivers of the Ile-Balkhash basin in the conditions of modern climate warming [Ocenka izmenenija vodnyh resursov i perspektivy prognoza vodnosti osnovnyh rek Ile- Balhashskogo bassejna v uslovijah sovremennogo potepnenija klimata]. Dis. cand. biol. sciences., Almaty, 127 p.
3. Kerimbay B.S., Musabayeva M.N., Kerimbay N.N. (2021) Determination of biomass productivity of vegetation of the Sharyn River basin [Opredelenie produktivnosti biomassy rastitel'nosti bassejna reki Sharyn]. *Hydrometeorology and ecology*, no. 1, pp. 72-79.
4. Kazangapova N.B. (2019) The current state of the recreational potential of the natural environment of the Sharyn SNNP (State National Natural Park) Collective monograph. Almaty, Publishing house of Tau Kainar LLP, 204 p., ISBN 978-601-7059-63-7
5. Ablaisanova G.M., Barakbayev T.T., Pazylbekov M.Zh. (2016) The modern composition of the ichthyofauna of the Kapshagai reservoir and the Ili River [Sovremennij sostav ihtiofauny Kapshagajskogo vodohranilishha i reki Ili]. Almaty: Kazakh Research Institute of Fisheries LLP
6. Ismukhanov Kh.K., Skakun V.A. (2008) The current state of biodiversity of the transboundary Ili River and Kapchagai reservoir, the impact of migrating alien species on their ecosystem [Sovremennoe sostojanie bioraznoolbracija transgranichnoj reki Ili i Kapchagajskogo vodohranilishha, vlijanie migrirujushhih chuzherodnyh vidov na ih jekosistemu]. Almaty, 273 p.
7. Timirkhanov S.R., Karabekova D.U. (2015) Naked Osman (*Gymnodiptychus Dybowskii* (Kessler, 1874)) Of Central Asia: Review And Systematic Structure [Golyj Osman (*Gymnodiptychus Dybowskii* (Kessler, 1874)) Central'noj Azii: Obzor I Sistematičeskaja Struktura]. *Science, New Technologies and Innovations of Kyrgyzstan*, no. 4, pp. 119-122.

8. Khusainova N.Z. (1966) Biological foundations of fisheries in the reservoirs of Central Asia and Kazakhstan [Biologicheskie osnovy rybnogo hozjajstva na vodoemah Srednej Azii i Kazahstana]. Alma-Ata: Nauka, pp. 219-222.
9. Timirkhanov S.R. (2010) Ecological variability of the naked osman (*Gymnodiptychus Dybowskii* (Kessler, 1874)) in the reservoirs of Central Asia and Kazakhstan. *Bulletin of KazNU. Ecological series*, vol. 28, no. 2, pp. 82-86.
10. Pavlovsky E.N. (1961) Guide to the study of fish nutrition in natural conditions [Rukovodstvo po izucheniju pitaniya ryb v estestvennyh usloviyah]. Moscow: Publishing House of the USSR Academy of Sciences, 244 p.
11. Mikodina E.V. et al. (2009) Histology for ichthyologists: Experience and advice [Gistologiya dlja ihtiologov: Opyt i sovery]. Moscow: Publishing House VNIRO, 112 p. ISBN 978-5-85382-365-5.
12. Shalgimbayeva S.M., Omarova Zh.S., Dzhumakhanova G.B. (2021) The Basics of Microtechnics methodological manual [Mikrotehnika negizderi Adistemelik nusqaýlyq]. Almaty: Qazaq University, 85 p. ISBN 978-601-04-5012-7
13. Mohamed F.A.S. (2009) Histopathological Studies on *Tilapia zillii* and *Solea vulgaris* from Lake Qarum, Egypt. *World journal of Fish and Marine Sciences*, vol. 1, no. 1, pp. 29-39. ISSN 1992-0083
14. Mitrofanov V.P., Dukravets G.M., Melnikov V.A., Baimbetov A.A. (1988) Fish of Kazakhstan 3-vol. Almaty: "Nauka", pp. 93-105. ISBN: 978-5-458-47520-4
15. Pravdin I.F. (1966) Guide to the study of fish [Rukovodstvo po izucheniju ryb]. – Moscow: Pischevaja promyshlennost, 376 p.
16. Borutsky E.V., Zheltenkova M.V., Verigina I.A et al. (1974) Methodical manual for the study of nutrition and food relations of fish in natural conditions [Metodicheskoe posobie po izucheniju pitaniya i pishhevyyh otnosheniy ryb v estestvennyh usloviyah]. Moscow, Nauka, 254 p.
17. Desai V.R. (1970) Studies on the fishery and biology of *Tor tor* (Hamil-ton) from river Narmada. *J. Inland Fish. Soc. India*. vol. 2, no. 5, pp. 101-112.
18. Biswas S.P. (1993) Manual of methods in fish biology. New Delhi: South Asian Publishers, 157 p.
19. Shalgimbaeva S.M., Ibragimova N.A., Jumakhanova G.B., Popov N., Omarova Zh.S., Kairat B.K., Rakybayeva A.A. (2019) Biomarkers of effect: gross and histopathological indicators atherina boyeri of the caspian sea, kazakhstan sector. *Experimental Biology*, vol. 78, no. 1, pp. 130-137. ISSN 1563-0218

#### **Information about authors**

Seitkozhanova Elnaz – master's student, Department of Biodiversity and Bioresources, Al-Farabi Kazakh National University (Almaty, Kazakhstan, email: seitkozhanova0703@mail.ru)

Shalgimbayeva Saule – associate professor, Department of Biodiversity and Bioresources, Al-Farabi Kazakh National University (Almaty, Kazakhstan, email: S.Saule777@gmail.com)

Barinova Sophia – PhD, Associate Professor, Institute of Evolution, Laboratory of Biodiversity and Ecology of Algae, University of Haifa (Haifa, Israel, email: sophia@evo.haifa.ac.il)

Makhmetova Dzhamilya – Senior lecturer, Faculty of foreign languages, Al-Farabi Kazakh National University (Almaty, Kazakhstan, email: djamilamakhmetova@gmail.com)

Jumakhanova Gaukhar – (corresponding author) – PhD, Senior lecturer at the Department of Biodiversity and Bioresources, al-Farabi National University (Almaty, Kazakhstan, email: gkaznu@gmail.com)

Nurgaliev Arsen – Senior Researcher, Department of Protection and Reproduction of Wildlife, Charyn State National Natural Park (Kazakhstan, email: arsen\_nurgaliev@mail.ru)

Omarova Zhanar – PhD, Associate Professor, Department of Biodiversity and Bioresources, al-Farabi National University (Almaty, Kazakhstan, email: omarova.zh19@gmail.com)

Yussayeva Damira – Senior Lecturer, Department of Biodiversity and Bioresources, al-Farabi National University (Almaty, Kazakhstan, email: damira.yusaeva.74@mail.ru)

Zhanyrbay Gulmaral – master's student, Department of Biodiversity and Bioresources, al-Farabi National University (Almaty, Kazakhstan, email: gulmaral.zhanyrbay@mail.ru)

M. Ozdal\* , O. Gulmez , E. Gökçe , O.F. Algur 

Ataturk University, Faculty of Science, Department of Biology, Erzurum, Turkey

\*e-mail: murat.ozdal@yahoo.com

(Received 2 April 2024; received in revised form 10 May 2024; accepted 23 May 2024)

## Purification and characterization of glutaminase and urease-free L-asparaginase from *Bacillus atrophaeus* with acrylamide reduction potential

**Abstract.** L-asparaginase (L-asnase) is a versatile enzyme with uses in food industry and medicine. Current study aimed to isolate L-asnase producing microorganism/s without urease and glutaminase and optimize L-asnase production. First, screening and isolation of L-asnase-producing bacterial strains that did not produce glutaminase and urease from chicken gizzards were performed. For this purpose, the enzyme producing bacteria were screened on the agar medium supplied with substrate and phenol red indicator dye. Among the isolated bacteria, 1 isolate showed L-asnase free of glutaminase and urease. The selected strain was identified by biochemical, morphological and 16s rRNA sequencing. The selected strain was identified as *Bacillus atrophaeus* by 16S rRNA sequencing. The effects of incubation temperature (30°C) and time (72 hours), medium pH (8.0) and nutritional sources (glucose and NaNO<sub>3</sub>) on L-asnase production were determined. L-asnase was purified with acetone, and its molecular weight was determined to be 42 kDa by SDS-Page. Enzyme kinetics were also calculated, and it was determined that  $V_{max}$  was 43  $\mu\text{mol/mL/min}$  and  $K_m$  was 2.7 mM. L-asnase activity was highest at 40 °C and the optimal pH was 8.0. L-asnase activity was stimulated by Mn<sup>2+</sup>, Mg<sup>2+</sup>, and Ca<sup>2+</sup> but inhibited by Co<sup>2+</sup>, Na<sup>+</sup>, Zn<sup>2+</sup>, and Hg<sup>2+</sup>. L-asnase was utilized to treat potato chips before they were fried in order to assess its capacity to mitigate acrylamide. The result was an 80% reduction in acrylamide concentration when compared to the untreated control. Based on these findings, it appears that L-asnase could have potential use in the food industry.

**Key words:** L-asparaginase, *Bacillus atrophaeus*, production, purification, acrylamide.

### Introduction

L-asparaginase (E.C.3.5.1.1, L-asnase) is an enzyme of the hydrolase group. This enzyme hydrolyzes L-asparagine to ammonia and L-aspartate [1]. L-asnase has many applications in the health and food fields. L-asnase is a chemotherapeutic agent in the treatment of leukemia, Hodgkin's disease, melanosarcoma, lymphosarcoma, and reticulosarcoma [1–3]. L-asnase is eco-friendly, biodegradable, safe, and can reach the desired area directly. L-asnase is important in reducing potential carcinogenic and neurotoxic acrylamide in food technology [4]. Apart from chemical and physical methods, enzymatic methods are also used to prevent acrylamide formation, which occurs when starchy foods are heated to high temperatures by frying or baking [5,6]. Acrylamide is formed by the Maillard reaction of L-asparagine and reducing sugars, which are naturally found in foods (coffee, crackers, and chips). The World Health Organization has declared acrylamide as a carcinogen due to its potential for mutagenicity and toxicity [7]. It is crucial to maintain

desirable textural, nutritional and sensory qualities while reducing acrylamide formation. The easiest and most efficient method for preventing or reducing the formation of acrylamide is to utilize L-asnase [3]. Acrylamide formation can be reduced by using L-asnase before heat treatment of foods [8]. It is also known that L-asnase has antioxidant characteristics [9].

Due to its increasing use in the food and health fields, the market for L-asnase is constantly increasing. The market for L-asnase is estimated to be US\$413.2 million in 2019 and will increase to US\$435.8 million by 2025. Currently, L-asnase, which is used in clinical applications, is produced by *Escherichia coli* and *Erwinia chrysanthemi*. As cancer cases are expected to increase in the coming years, there will be an increase in demand for and use of L-asnase [10].

L-asnase is produced by a wide range of bacteria, fungi, actinomycetes, algae, and plants. Microorganisms are the most suitable sources for the production of L-asnase. However, this enzyme causes undesired side effects (liver, kidney, and

pancreas problems, hepatotoxicity, neurotoxicity, allergic reactions, coagulation anomalies) due to its impurities (glutaminase, urease). Therefore, extra purification steps are required to remove glutaminase and urease [11]. Isolation of glutaminase and urease-free L-asnase producing isolates is unquestionably advantageous in order to reduce purification steps. The aim of this study is to optimize and characterize the glutaminase- and urease-free L-asnase production of newly isolated *B. atrophaeus*. The application potential of the L-asnase in acrylamide reduction in potato chips was also evaluated.

## Materials and methods

### *Collecting samples and isolating bacterial strains.*

The gizzard samples from the local slaughterhouse were transported directly to the laboratory, after which samples were taken aseptically from the gizzard. Phosphate-buffered saline was added at 5 mL for each gram of sample, and the falcon tube was shaken for 60 s. Serial dilutions were prepared from the resulting homogenate, spread on Nutrient Agar (NA, Merck, Germany) plates, and incubated at 37 °C for 2 days. Individual representative colonies were selected for purification and plated on fresh NA plates. At -86 °C, pure cultures were cryopreserved in Nutrient Broth with 20% glycerol for later use.

*Selection of bacterial isolates for L-asnase production.* Isolated bacteria were screened using M9 agar plates (% 1.5 agar) containing phenol red and L-asparagine (10 g/L). M9 consisted of (g/L): 2 glucose, 3 KH<sub>2</sub>PO<sub>4</sub>, 0.5 MgSO<sub>4</sub>·7H<sub>2</sub>O, 0.1 CaCl<sub>2</sub>·2H<sub>2</sub>O, 10 L-asparagine, 0.5 NaCl and 6 Na<sub>2</sub>HPO<sub>4</sub>. Phenol red 0.009% (w/v) was added as an indicator dye. On M9 agar plates, separated pure cultures were streaked, and the color change formation was observed for two days at 30 °C. Isolates with pink colored regions around bacterial colonies were evaluated as L-asnase producing strains.

*Screening of bacterial isolates for glutaminase and urease production.* Both quantitative and qualitative techniques were applied to evaluate whether the isolated bacteria produced urease and glutaminase. Glutaminase or urease producing isolates were determined on phenol red indicator plates [12]. Pre-culture of the isolates was grown overnight at 30 °C and 150 rpm in Nutrient Broth. The following day, 1 mL of pre-culture (OD<sub>600</sub> 1) was added to 50 mL of M9 broth media in 250 mL flasks, and the mixture was incubated for 4 days at 30 °C at 140 rpm. It was determined using M9 media containing L-glutamic acid or urea as the sole nitrogen source, respectively. NaNO<sub>3</sub> was used as the only source of nitrogen while

preparing control plates. Glutaminase and urease activities were evaluated using the Nesslerization procedure outlined below to assess L-asnase activity. The buffer combination containing L-asparagine-Tris-HCl was substituted with L-glutamine-Tris-HCl and urea-Tris-HCl, respectively, and the enzyme activity was determined using the same approach as stated below.

### *Identification of L-asnase producer bacterium.*

Abis Online Software was used for both morphological and biochemical tests to identify the bacterium [13]. The bacterium producing L-asnase was then identified based on 16S rDNA sequencing using universal primer sets 27F and 1102R. The obtained sequence was aligned and compared with the sequences deposited in GenBank (<http://www.ncbi.nlm.nih.gov/BLAST>) and submitted to GenBank.

*Analytical methods.* The L-Asnase activity was determined by quantifying ammonia formation in the culture supernatant using Nessler's reagent. The enzymatic reaction mixture contains 900 µl of 0.04 M L-asparagine in 50 mM M Tris-HCl buffer (pH 8.6) and 100 µL of crude enzyme. For 30 min, enzyme substrate mixtures were incubated at 37 °C. At the end of the incubation, 100 µL of 1.5 M trichloroacetic acid (TCA) was added to stop the activity, and the mixture was incubated for 15 min. at 20 °C for color development. To separate precipitates from the reaction mixture, it was centrifuged at 8,000 rpm for 6 min. Then, 200 µL of Nessler reagent was added to the sample containing 200 µL of supernatant and 1.6 mL of distilled water, and the amount of ammonia released was determined using the UV visible spectrophotometer at 425 nm. At 37 °C, one unit of L-Asnase activity was stated the quantity of enzyme that produced 1 µmole ammonia per minute [11,12].

*Enhancement of L-Asnase production using one factor at a time approach.* The influence of carbon and nitrogen sources on L-Asnase production was investigated. For this purpose, six different carbon sources (2 g/L) such as glucose, fructose, mannitol, lactose, glycerol and sucrose and six different nitrogen sources (1 g/L) such as ammonium nitrate, ammonium sulfate, ammonium chloride, bacto peptone, tyrtone, and yeast extract were added to M9 broth. The effects of different temperatures (25-40 °C), pH (5-10), and incubation times (24-96 hours) on L-asnase production were tested.

*Purification of L-asnase.* *B. atrophaeus* AspK1 was grown for 48 h at 180 rpm and 30 °C in optimized M9 medium containing L-asparagine. At the end of the period, the culture medium was centrifuged at 10,000 rpm for 15 min., the supernatant was taken, and the bacterial cells were discarded. Chilled

acetone (-18 °C) was added to the supernatant (crude enzyme) at a rate of 60% to precipitate the proteins and mixed with a constant stirrer at 4 °C for 5 h. Then, centrifugation was done at 15,000 rpm and 4 °C for 20 min. Precipitated proteins were dissolved in 50 mM Tris-HCl buffer (pH 8.0) and washed by ultrafiltration (Amicon® Ultra-15 centrifugal filter units, 10 kDa cutoff) at 5000 rpm at 4 °C [14]. Utilizing Biological LP Chromatography Systems (Biorad, USA), anion exchange chromatography was employed to carry out the remaining purification process. After washing out, concentrated enzyme solution was filtered through a 0.45 µm syringe filters and loaded onto HiTrap Q HP column (GE Healthcare) pre-equilibrated with 20 mM Tris-HCl, pH 8.0. During elution, 2 mL fractions were collected at a flow rate of 0.5 mL/min with a rising linear gradient of NaCl (50-500 mM) in a buffer of 20 mM Tris-HCl pH 8.0. Elution fractions were collected, and protein concentration was measured according to the Lowry Method [15].

*Determination of molecular weight and kinetic constants ( $K_m$  and  $V_{max}$ ).* Using 12% (v/v) polyacrylamide gel stained with Coomassie Brilliant Blue R-250 following electrophoresis, crude and purified L-asnase fractions were subjected to SDS-PAGE analysis. By comparing the relative mobilities with the Precision Plus Protein Unstained Standard (250-10 kDa), the molecular weights of the samples were determined.

Using L-asparagine as the substrate at dosages ranging from 0.2-4 mM, the Michaelis-Menten constant ( $K_m$ ) and maximum velocity ( $V_{max}$ ) of pure L-asnase from *B. atrophaeus* AspK1 were assessed.

*Enzyme characterization.* The activity of purified L-asnase was measured at various pH, temperatures, incubation times, and metal ion concentrations. The purified enzyme was studied in buffers of 50 mM pH between 3-10. Potassium phosphate (pH 3-7), Tris-HCl (pH 8-9), and glycine-NaOH (pH 10) were selected as buffers and used for residual activity determination. The L-asnase activity was determined at a temperature ranging from 20 to 80 °C. The thermal stability of L-asnase was tested by pre-incubating at different temperatures for 1-5 hours. Metal ions of salt solutions at 1 mM and 10 mM concentrations, such as  $MgSO_4$ ,  $CoCl_2$ ,  $FeCl_2$ ,  $CuCl_2$ ,  $ZnCl_2$ , and  $CaCl_2$  were used for the determination of enzyme activity.

*Application of L-asnase in potato chips.* After being cleaned, the potatoes were peeled and chopped into 2 mm slices. In addition, distilled water was used to rinse the starch particles that had adhered to the potato's surface. For forty minutes, the

potato chips were submerged in a crude enzyme solution containing 40 U/mL at 40 °C, and dried on blotting paper. The potato chips were cooked for 5 min at 180 °C, dried for 20 min. at 60 °C, and then chilled to room temperature. n-hexane was used three times to de-oil potato chips that were pureed and homogenized in a centrifuge tube. Acetonitrile was used to extract acrylamide. Finally, a 0.22 mm microporous membrane filter was used to remove resuspended liquids for additional examination [16]. Acrylamide analysis was performed using an LC-MS/MS (Agilent 6460 Triple Quadrupole) with a mass-selective detector (MSD, Agilent 7000). The injection volume was 10 µL, and the solvent system consisted of 0.1% formic acid in water and 0.1% formic acid in methanol at a flow rate of 0.3 mL/min at 30 °C.

## Results and discussion

*Isolation of bacterial species.* Nine bacteria isolated from chicken gizzards. The digestive systems of animals provide very favorable environments for the life of microorganisms [17]. Bacteria in the digestive system can produce many enzymes that aid digestion. The chicken gizzard, which is one of these environments, constitutes a very complex environment. In the proximal intestine, such as the gizzard and small intestine, microorganisms compete with the host for energy. *Lactobacillus* and *Clostridium* species are dominant in the gizzard [18,19]. It was also identified in genera such as *Bacillus*, *Enterococcus*, *Corynebacterium*, *Weissella*, *Geobacillus* and *Planococcus* [20]. Spore-forming *Bacillus* species are widely found in ecosystems due to their high resistance to environmental stresses.

Isolated bacteria were screened for L-asnase, L-glutaminase and urease activity on L-asparagine-, L-glutamine- and urea-agar plates containing phenol red as an indicator. When these substrates break down, the released ammonia reacts with water to form  $NH_4OH$ , which increases the pH of the medium. In these environments containing phenol red as a pH indicator, the pink color formation with an increase in pH is an indication of the production of the relevant enzyme [12]. L-asnase, used in chemotherapy, has possible side effects due to its impurities. Therefore, there is a need to discover new high-purity enzyme production sources for therapeutic uses [21]. Since the AspK1 isolate did not produce L-glutaminase or urease, there was no color change in the solid medium containing L-glutamine and urea, and it was determined that it showed a pink-colored region on the L-asparagine plate. This showed that

it produced L-asnase without producing glutaminase or urease. In addition, isolates were screened by spectrophotometry using the Nesslerization method and the AspK1 isolate was identified as the L-asnase producer without glutaminase and urease activity.

*Identification of the glutaminase and urease-free L-asnase producing bacterium.* Biochemical tests and physical properties showed that the AspK1 strain is a Gram positive, catalase positive, oxidase negative, aerobic, rod, pale brown pigmented, motile, and endospore forming organism (Table 1).

A 1463 bp 16S rRNA sequence was screened by BLAST (GenBank, NCBI) based on the result of the genetic analysis of the AspK1 strain. The nucleotide sequence is recorded in GenBank with the accession number MW866485.1, and Figure 1 shows species closely related to *B. atrophaeus* in the phylogenetic tree.

**Table 1** – Morphological and biochemical characteristics of strain AspK1

Characteristic	Result
Gram	+
Shape	Rods
Motility	+
Endospore	Ellipsoidal
Pigment	Brown
Oxidase	-
Catalase	+
Urease	-
Starch hydrolysis	+
Nitrate reduction	+
Anaerobic growth	-

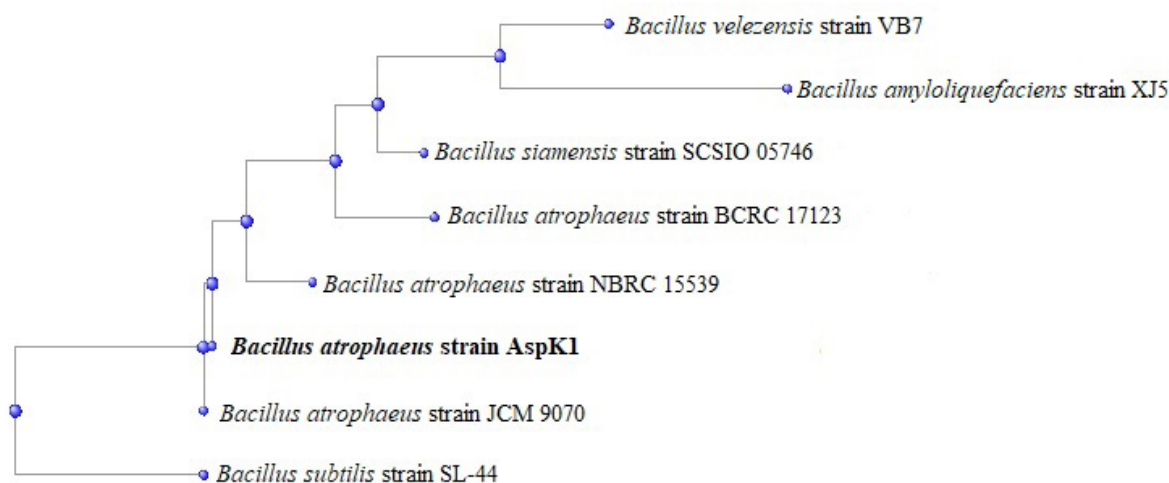


**Figure 1** – Phylogenetic tree based on the 16s rDNA sequences of strain AspK1

*Optimization of culture conditions for the production of L-asnase.* Nutritional and environmental conditions highly affect enzyme production by microorganisms. These properties differ from one organism to another. The optimum temperature for L-asnase production by *B. atrophaeus* AspK1 was determined to be 30°C (Figure 2a). *Bacillus* species have been reported to produce L-asnase within the temperature range of 25–40 [22].

In addition to temperature, the pH of the culture medium is important in enzyme production as it affects metabolism. Maximum L-asnase production was noted at pH 8.0, followed by a gradual decrease (Figure 2b). Similar to this study, El-Fakharany

et al. [23] reported an optimum pH of 8.2 for *B. halotolerans*.

The effect of incubation time on the production of L-asnase is presented on Figure 2c. Maximum L-asnase was achieved in M9 at 48 hours and then gradually decreased. This result is consistent with the result of L-asnase production by *B. velezensis* [21].

The effect of various carbon sources on L-asnase production by *B. atrophaeus* AspK1 was evaluated. It was determined that the synthesis of L-asnase was highest when glucose was used and lowest when sucrose was present (Figure 2d). Similar results have been reported for *B. subtilis* [24], *B. velezensis* [21], *B.*



*altitudinis* [25], *B. licheniformis* [26], *B. halotolerans* [23] and *Brevibacillus borstelensis* [27].

For L-asnase production from *B. atrophaeus* AspK1, both organic and inorganic nitrogen sources were investigated. Inorganic nitrogen sources have generally resulted in high enzyme production. In this study, the highest L-asnase production with *B. atrophaeus* AspK1 was obtained when  $\text{NH}_4\text{NO}_3$  was

used among the nitrogen sources. In the presence of yeast extract, the least amount of L-asnase was produced (Figure 2e). In L-asnase production,  $\text{NH}_4\text{Cl}$  for *B. velezensis* [26] and  $(\text{NH}_4)_2\text{SO}_4$  for *B. licheniformis* [26] were determined as suitable nitrogen sources. As a nitrogen source,  $\text{NaNO}_3$  was found suitable for *Paenibacillus validus* and *Streptococcus* sp. [28].

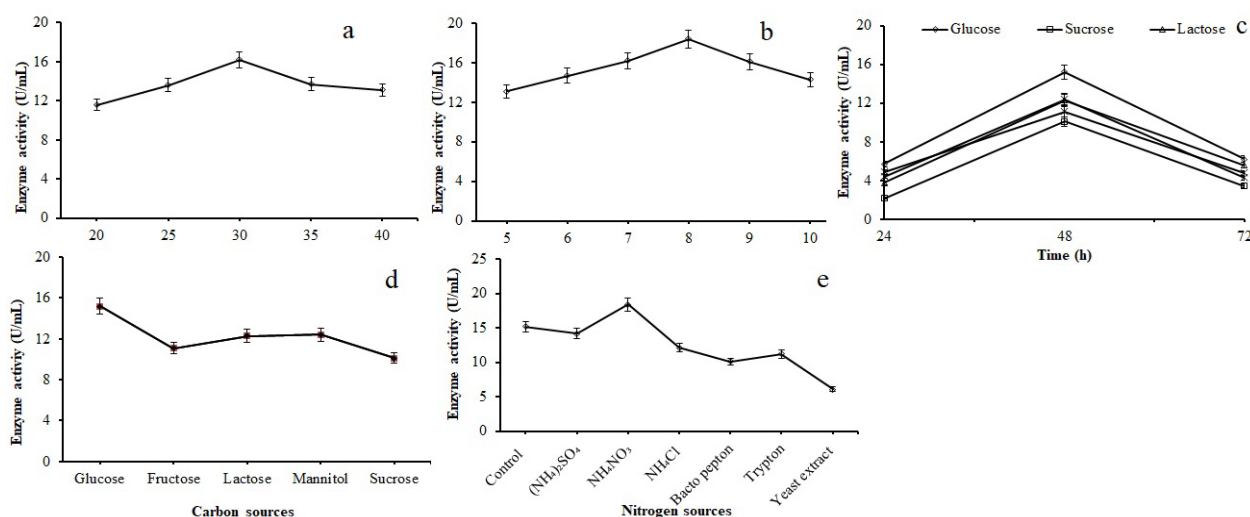


**Figure 2** – The impact of a) temperature, b) pH, c) time, d) carbon sources, e) nitrogen sources on L-Asp production by *B. atrophaeus* strain AspK1

*Purification and characterization of L-asnase.* Extracellular L-asnase found in the cell-free supernatant was used as the source of the crude enzyme. Cells in the broth culture medium were removed by centrifugation at 10,000 rpm for 15 min after 48 h of incubation. The L-asnase was purified

using 60% (v/v) chilled cold acetone precipitation followed by Amicon® Ultra-15 centrifugal filter and anion exchange chromatography with the HiTrap Q HP column. The purification steps, protein concentration, specific activity and yield of L-asnase are shown in Table 2.

**Table 2** – Purification steps of the L-Asp from *B. atrophaeus* AspK1

Steps	Total activity (U)	Total protein (mg)	Specific activity (U/mg)	Fold purification	Yield (%)
Crude extract	810	105	7.71	1.0	100
Acetone precipitation	578	31.5	18.34	1.5	67
Ion Exchange	288	11	26.18	4.8	34

The amount of protein in the L-asnase production medium was determined to be 105 mg. In acetone precipitation, the enzyme yield of L-asnase was measured at 67%, and its protein content was measured at 31.5 mg. It was observed that the specific activity increased in the purification of L-asnase with

acetone. A specific activity of 26.18 U/mg protein with a 34% yield and 4.8-fold purification was obtained from the final purified enzyme. In many studies, as the purification coefficient increased, the yield decreased, however, the specific enzyme activity increased [29,30].

After L-asnase was purified, its molecular mass was determined by SDS-PAGE analysis. Molecular mass in the range of 25-47 kDa is common in *Bacillus* L-asnase such as 37 kDa for *B. licheniformis* [26], 39.7 kDa for *B. velezensis* [26], 38.2 kDa for *B. amyloliquefaciens* [31], 41.5 kDa for *B. halotolerans* [23], 42 kDa for *B. australimaris* [32] and 47 kDa for *B. megaterium* [33]. The molecular weight of *B. atrophaeus* L-Asnase was determined to be (42 kDa) (Figure 3) and varied from other *Bacillus* species.

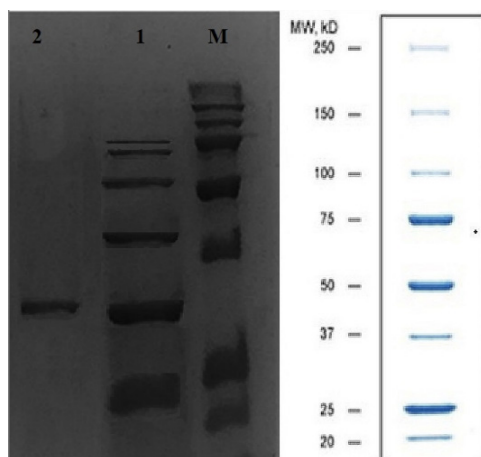


**Figure 3** – SDS-PAGE of the purified L-Asp. Note: M – standard protein markers; Lane 1 – crude enzyme; Lane 2 – purified enzyme

*Determination of kinetic constants ( $K_m$  and  $V_{max}$ ).* The  $K_m$  indicates the enzyme's affinity for its substrate, whereas the  $V_{max}$ , which is measured in

units of product generated per unit of time, indicates substrate turnover [26]. Enzyme kinetic parameters showed  $V_{max}$  at 43  $\mu\text{mol/ml/min}$  and  $K_m$  at 2.7 mM, which indicates the high affinity of this enzyme to its substrate. Many factors (origin, structure, and form of an enzyme, enzyme conditions and assay procedures) influence the kinetic features of enzymes.  $K_m$  and  $V_{max}$  values for an L-asnase from *B. velezensis* were 3.6 mM and 41.49  $\mu\text{mol/ml/min}$ , respectively [26]. The  $K_m$  was found to be 4.56 mM for the *B. australimaris* NJB19 [32]. The  $K_m$  of purified L-asnase from *B. licheniformis* was 1.4 mM [29].

*Effect of temperature and pH on L-asnase activity.* Temperature effects on L-Asnase stability were investigated at temperatures ranging from 20 to 90°C (Figure 4).

Results in Figure 4 determined that it showed maximum activity at 40°C. L-asnase activity lost approximately 60% of the total activity at 90°C. Purified L-asnase showed maximum stability after 1h incubation at 40°C, retaining more than 96% of its total activity. In addition, L-asnase lost about 40% of its activity after 5h of incubation at 80°C. L-asnase was found to be quite stable at 30-50°C and retained more than 85-70% of its activity after 5h of incubation. This reasonable thermostability of L-asnase is important for its use in biotechnological fields [31].

L-asnase purified from *B. atrophaeus* AspK1 was studied at pH 3.0-10.0 and was determined to be most active at pH 7.0. Enzyme activity decreased at lower pH values (Figure 5).

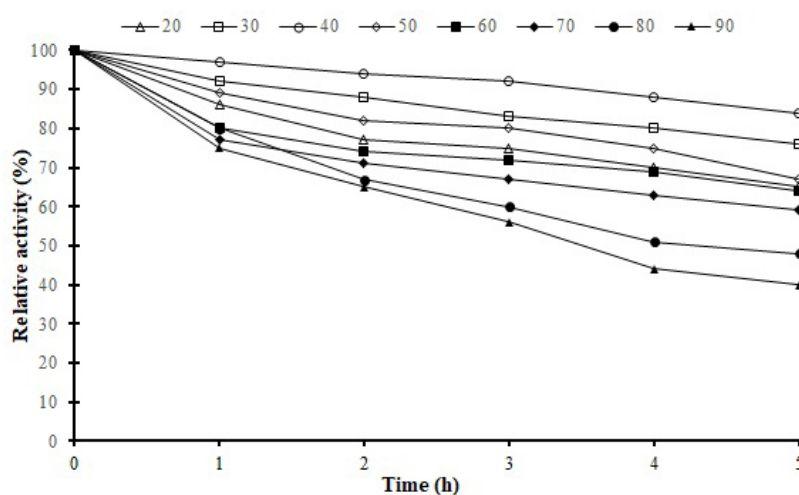


**Figure 4** – Thermostability of *B. atrophaeus* AspK1 L-Asp at different temperatures for 5 h

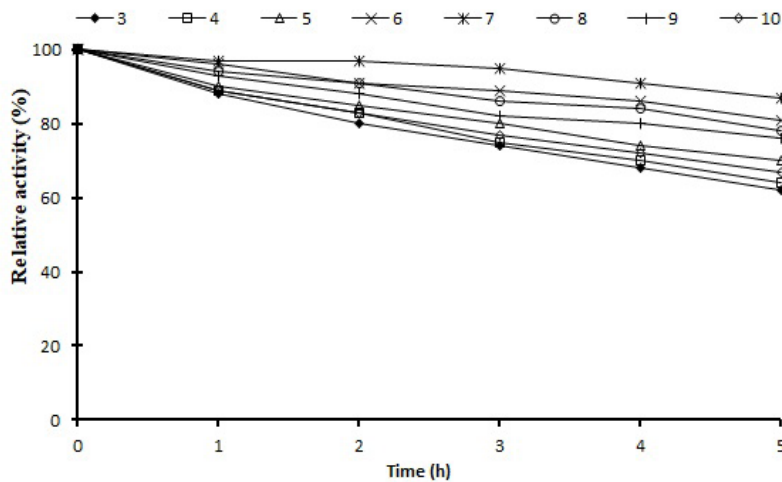


Figure 5 – pH stability of *B. atrophaeus* AspK1 L-asnase incubated in various pH for 5 h

AspK1 L-asnase retained 85% of its activity when incubated for 5h at pH 7. In a study with L-asnase obtained from *B. megaterium*, more than 80% residual activity was determined after 2h of incubation at pH 5.0-8.0 [34].

In addition, it was determined that L-asnase obtained from *B. amyloliquefaciens* showed more than 80% residual activity after 4h of incubation at pH 3.0-11.0 [31]. This is because L-asparagine, when

broken down into L-aspartic acid, causes the pH to decrease [31, 34].

*Effects of metal ions on the activity of L-asnase.* Due to their ability to attach to specific areas of the enzyme, metal ions are important for preserving both its structure and activity [14]. It was determined that the purified enzyme was sensitive to different metal ions. In this study,  $Mn^{2+}$  ions (1 mM and 10 mM) increased AspK1 L-Asnase activity by approximately 44-33% (Figure 6).

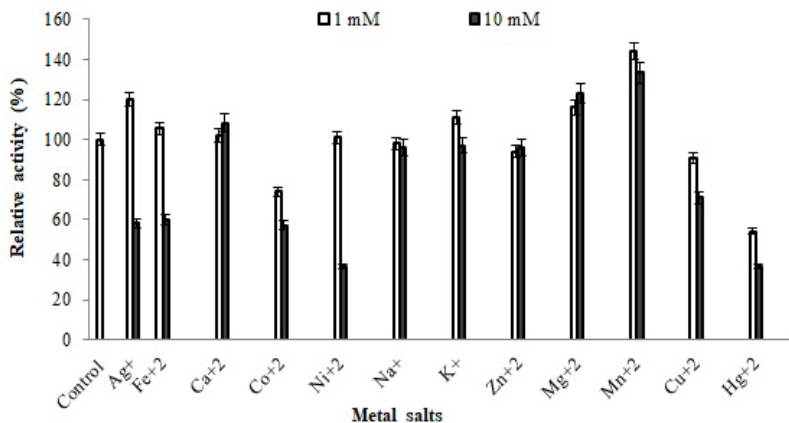


Figure 6 – Effects of different metal ions on L-Asnase from *B. atrophaeus* AspK1

L-asnase activity increased by 105-120% in the presence of 1mM  $Ag^{2+}$ ,  $K^+$  and  $Fe^{+2}$ . In addition of 10mM of  $Fe^{2+}$ ,  $Ni^{2+}$ ,  $Ag^+$ ,  $Fe^{2+}$  and  $Cu^{2+}$  decreased the activity by more than 40%. The present study determined that some metal ions ( $Ca^{2+}$ ,  $Mn^{2+}$ ,  $K^+$  and  $Mg^{2+}$ ) can be evaluated as activator for the L-asnase

produced by *B. atrophaeus*. Stimulation of L-asnase with  $Mn^{2+}$  and  $Mg^{2+}$  ions is common [31,35,36]. Also, similar to other studies, the enzyme activity was inhibited by  $Hg^{2+}$ ,  $Cu^{2+}$  and  $Co^{2+}$  [37].

*Acrylamide mitigation potential of B. atrophaeus L-asnase.* The effect of L-asnase on

the reduction of acrylamide in potato chips was examined by treating the potato slices with 40 U/mL of L-asnase. Approximately 80% less acrylamide was formed during the frying process of potato strips treated with L-asnase than when potato strips were left untreated (Figure 7).

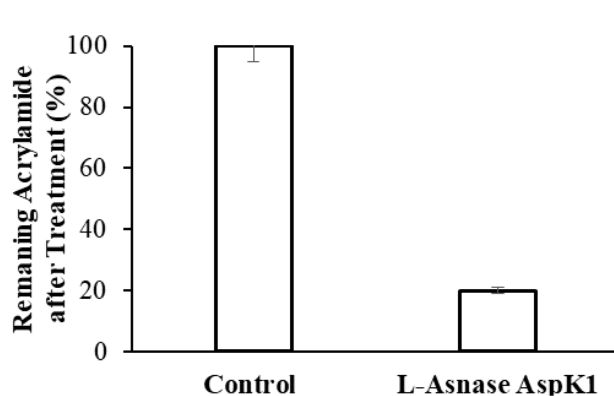


**Figure 7** – Content of acrylamide in potato chips after L-asnase treatment

Significantly, *B. atrophaeus* L-asnase's capacity to reduce acrylamide is similar to that of other microbial L-asnase that have been previously documented. In fried potatoes and baked mooncakes, for example, *Paenibacillus barengoltzii*'s L-asnase lowered acrylamide by up to 86% and 52%, respectively [37]. In parallel research, two distinct strains of *B. subtilis* were shown to have L-asnase that could reduce acrylamide by up to 80% [38] and 82% [39].

Similarly, L-asnases from *Acinetobacter soli* [8], *Cobetia amphilecti* AMI6 [40], *Aquabacterium* sp. A7-Y [41], and recombinant *Palaeococcus ferrophilus* [42] have also been shown to reduce acrylamide concentrations by up to 80%, 88.2%, 55.9%, and 79%. However, *Streptomyces koyangensis* SK4 reduced acrylamide levels in potato chips by

up to 50% [43], and L-ASNase from *Aspergillus terreus* BV-C observed 93% acrylamide reduction [44]. Recently, the amount of acrylamide in bread and potato chips was decreased by 51.7% and 66.9%, respectively, thanks to an engineered *E. coli* L-asnase [45].

Furthermore, using L-asnase produced by *Fusarium culmorum* reduced the amount of acrylamide in bread and potato chips to 86% and 94%, respectively [46]. Bhagat et al. (2016) [47] reported that the acrylamide concentration in fried potatoes treated with L-asnase from *Pseudomonas oryzae* reduced to 90%.

## Conclusion

A newly-isolated *B. atrophaeus* AspK1 was isolated for L-asnase production. The production of L-asnase has been determined to be influenced by pH, temperature, incubation period, and carbon and nitrogen sources. Glutaminase and urease-free L-asnase from *B. atrophaeus* AspK1 was found to have a molecular size of 42 kDa. The high pH and thermostability of L-asnase obtained from *B. atrophaeus* is important for its use in biotechnological fields. Glutaminase and urease-free AspK1 L-asnase could possibly be used in the pharmaceutical or food industries. Our isolated *B. atrophaeus* AspK1 enzyme significantly reduced the creation of acrylamide in potato chips. Therefore, the study is very valuable considering the commercial and vital importance of L-asnase.

## Acknowledgments

The authors would like to thank Ataturk University for the facilities and resources to complete the study. This research was supported by a grant from the research funds appropriated to Ataturk University (FBA-2019-6870), Erzurum, Turkey.

## References

1. Muneer, F., Siddique, M. H., Azeem, F., Rasul, I., Muzammil, S., Zubair, M., Nadeem, H. (2020). Microbial l-asparaginase: purification, characterization and applications. *Archives of Microbiology*, 202(5), 967–981. <https://doi.org/10.1007/s00203-020-01814-1>
2. Krishnapura, P. R., Belur, P. D., Subramanya, S. (2015). A critical review on properties and applications of microbial L-asparaginases. *Critical Reviews in Microbiology*, 1–18. <https://doi.org/10.3109/1040841X.2015.1022505>
3. Chand, S., Mahajan, R. V., Prasad, J. P., Sahoo, D. K., Mihooliya, K. N., Dhar, M. S., Sharma, G. (2020). A comprehensive review on microbial L-asparaginase: Bioprocessing, characterization, and industrial applications. *Biotechnology and Applied Biochemistry*, 67(4), 619–647. <https://doi.org/10.1002/bab.1888>
4. Akgün, B., Arıcı, M., Çavuş, F., Karataş, A. B., Ekşi Karaağaç, H., Uçurum, H. Ö. (2021). Application of L-asparaginase to produce high-quality Turkish coffee and the role of precursors in acrylamide formation. *Journal of Food Processing and Preservation*, 45(6). <https://doi.org/10.1111/jfpp.15486>

5. Abedi, E., Mohammad Bagher Hashemi, S., Ghiassi, F. (2023). Effective mitigation in the amount of acrylamide through enzymatic approaches. *Food Research International*, 172, 113177. <https://doi.org/10.1016/j.foodres.2023.113177>
6. Joshi, D., Patel, H., Suthar, S., Patel, D. H., Kikani, B. A. (2024). Evaluation of the efficiency of thermostable L-asparaginase from *B. licheniformis* UDS-5 for acrylamide mitigation during preparation of French fries. *World Journal of Microbiology and Biotechnology*, 40(3), 92. <https://doi.org/10.1007/s11274-024-03907-1>
7. Castro, D., Marques, A. S. C., Almeida, M. R., de Paiva, G. B., Bento, H. B. S., Pedrolli, D. B., Santos-Ebinuma, V. C. (2021). L-asparaginase production review: bioprocess design and biochemical characteristics. *Applied Microbiology and Biotechnology*, 105(11), 4515–4534. <https://doi.org/10.1007/s00253-021-11359-y>
8. Jiao, L., Chi, H., Lu, Z., Zhang, C., Chia, S. R., Show, P. L., Lu, F. (2020). Characterization of a novel type I L-asparaginase from *Acinetobacter soli* and its ability to inhibit acrylamide formation in potato chips. *Journal of Bioscience and Bioengineering*, 129(6), 672–678. <https://doi.org/10.1016/j.jbiosc.2020.01.007>
9. El-Gendy, M. M. A. A., Awad, M. F., El-Shenawy, F. S., El-Bondkly, A. M. A. (2021). Production, purification, characterization, antioxidant and antiproliferative activities of extracellular L-asparaginase produced by *Fusarium equiseti* AHMF4. *Saudi Journal of Biological Sciences*, 28(4), 2540–2548. <https://doi.org/10.1016/j.sjbs.2021.01.058>
10. Patel, P. G., Panseriya, H. Z., Vala, A. K., Dave, B. P., Gosai, H. B. (2022). Exploring current scenario and developments in the field of microbial L-asparaginase production and applications: A review. *Process Biochemistry*, 121, 529–541. <https://doi.org/10.1016/j.procbio.2022.07.029>
11. Ashok, A., Doriya, K., Rao, J. V., Qureshi, A., Tiwari, A. K., Kumar, D. S. (2019). Microbes Producing L-Asparaginase free of Glutaminase and Urease isolated from Extreme Locations of Antarctic Soil and Moss. *Scientific Reports*, 9(1), 1423. <https://doi.org/10.1038/s41598-018-38094-1>
12. Doriya, K., Kumar, D. S. (2016). Isolation and screening of L-asparaginase free of glutaminase and urease from fungal sp. 3 *Biotech*, 6(2), 239. <https://doi.org/10.1007/s13205-016-0544-1>
13. Sorescu, I., Stoica, C. (2021). Online Advanced Bacterial Identification Software, an Original Tool for Phenotypic Bacterial Identification. *Romanian Biotechnological Letters*, 26(6), 3047–3053. <https://doi.org/10.25083/rbl/26.6/3047-3053>
14. Gurkok, S., Ozdal, M. (2021). Purification and characterization of a novel extracellular, alkaline, thermoactive, and detergent-compatible lipase from *Aeromonas caviae* LipT51 for application in detergent industry. *Protein Expression and Purification*, 180, 105819. <https://doi.org/10.1016/j.pep.2021.105819>
15. Naganthran, A., Masomian, M., Rahman, R. N., Ali, M., Nooh, H. (2017). Improving the Efficiency of New Automatic Dishwashing Detergent Formulation by Addition of Thermostable Lipase, Protease and Amylase. *Molecules*, 22(9), 1577. <https://doi.org/10.3390/molecules22091577>
16. Chi, H., Chen, M., Jiao, L., Lu, Z., Bie, X., Zhao, H., Lu, F. (2021). Characterization of a Novel L-Asparaginase from *Mycobacterium gordonae* with Acrylamide Mitigation Potential. *Foods*, 10(11), 2819. <https://doi.org/10.3390/foods10112819>
17. Ozdal, M., Ozdal, O. G., Algur, O. F. (2016). Isolation and characterization of  $\alpha$ -endosulfan degrading bacteria from the microflora of cockroaches. *Polish Journal of Microbiology*, 65(1).
18. Sekelja, M., Rud, I., Knutsen, S. H., Denstadli, V., Westereng, B., Næs, T., Rudi, K. (2012). Abrupt Temporal Fluctuations in the Chicken Fecal Microbiota Are Explained by Its Gastrointestinal Origin. *Applied and Environmental Microbiology*, 78(8), 2941–2948. <https://doi.org/10.1128/AEM.05391-11>
19. Mosa, M., Salem, H., Bastamy, M., Amer, M. (2023). Pathogenic and Non-pathogenic Factors; Especially Infectious Bursal Disease Viruses; Affect Chicken Digestive System Microbiota and Methods of Its Evaluation and Recovery: A review. *Egyptian Journal of Veterinary Sciences*, 54(4), 733–760. <https://doi.org/10.21608/ejvs.2023.203480.1476>
20. García-Amado, M. A., Shin, H., Sanz, V., Lentino, M., Martínez, L. M., Contreras, M., Domínguez-Bello, M. G. (2018). Comparison of gizzard and intestinal microbiota of wild neotropical birds. *PLOS ONE*, 13(3), e0194857. <https://doi.org/10.1371/journal.pone.0194857>
21. Mostafa, Y., Alrumman, S., Alamri, S., Hashem, M., Al-izran, K., Alfaifi, M., Taha, T. (2019). Enhanced production of glutaminase-free L-asparaginase by marine *Bacillus velezensis* and cytotoxic activity against breast cancer cell lines. *Electronic Journal of Biotechnology*, 42, 6–15. <https://doi.org/10.1016/j.ejbt.2019.10.001>
22. Pola, M., Durthi, C. P., Rajulapati, S. B., Erva, R. R. (2018). Modelling and optimization of L-Asparaginase production from *Bacillus stratosphericus*. *Current Trends in Biotechnology and Pharmacy*, 12(4), 390–405.
23. El-Fakharany, E., Orabi, H., Abdelkhalek, E., Sidkey, N. (2022). Purification and biotechnological applications of L-asparaginase from newly isolated *Bacillus halotolerans* OHEM18 as antitumor and antioxidant agent. *Journal of Biomolecular Structure and Dynamics*, 40(9), 3837–3849. <https://doi.org/10.1080/07391102.2020.1851300>
24. Bhosale, H J; Uzma, S Z; Kadam, T. A. (2021). Isolation of L-asparaginase from marine bacterium *Bacillus subtilis* and its characterization. *Indian Journal of Geo-Marine Sciences*, 50(02). <https://doi.org/10.56042/ijms.v50i02.66090>
25. Prakash, P., Singh, H. R., Jha, S. K. (2020). Production, purification and kinetic characterization of glutaminase free anti-leukemic L-asparaginase with low endotoxin level from novel soil isolate. *Preparative Biochemistry & Biotechnology*, 50(3), 260–271. <https://doi.org/10.1080/10826068.2019.1692221>
26. Alrumman, S. A., Mostafa, Y. S., Al-izran, K. A., Alfaifi, M. Y., Taha, T. H., Elbehairi, S. E. (2019). Production and Anticancer Activity of an L-Asparaginase from *Bacillus licheniformis* Isolated from the Red Sea, Saudi Arabia. *Scientific Reports*, 9(1), 3756. <https://doi.org/10.1038/s41598-019-40512-x>
27. Mukherjee, R., Bera, D. (2023). Effect of nutritional parameters on microbial production of L-Asparaginase by novel *Brevibacillus borstelensis* ML12. *Preparative Biochemistry & Biotechnology*, 1–9. <https://doi.org/10.1080/10826068.2022.2164592>
28. Sherif M. Wakil, Adesewa A. Adelegan. (2015). Screening, Production and Optimization of L-Asparaginase From Soil Bacteria Isolated in Ibadan, South-western Nigeria. *Journal of Basic and Applied Sciences*, 11, 39–51. <https://doi.org/10.6000/1927-5129.2015.11.06>

29. Mahajan, R. V., Kumar, V., Rajendran, V., Saran, S., Ghosh, P. C., Saxena, R. K. (2014). Purification and Characterization of a Novel and Robust L-Asparaginase Having Low-Glutaminase Activity from *Bacillus licheniformis*: In Vitro Evaluation of Anti-Cancerous Properties. *PLoS ONE*, 9(6), e99037. <https://doi.org/10.1371/journal.pone.0099037>
30. Aly, N., El-Ahwany, A., Ataya, F. S., Saeed, H. (2020). *Bacillus sonorensis* L. Asparaginase: Cloning, Expression in *E. coli* and Characterization. *The Protein Journal*, 39(6), 717–729. <https://doi.org/10.1007/s10930-020-09932-x>
31. Yim, S., Kim, M. (2019). Purification and characterization of thermostable l-asparaginase from *Bacillus amyloliquefaciens* MKSE in Korean soybean paste. *LWT*, 109, 415–421. <https://doi.org/10.1016/j.lwt.2019.04.050>
32. Chakravarty, N., Sharma, M., Kumar, P., Singh, R. P. (2022). Biochemical and molecular insights on the bioactivity and binding interactions of *Bacillus australimaris* NJB19 L-asparaginase. *International Journal of Biological Macromolecules*, 215, 1–11. <https://doi.org/10.1016/j.ijbiomac.2022.06.110>
33. Pal Roy, M., Das, V., Patra, A. (2019). Isolation, purification and characterization of an extracellular L-asparaginase produced by a newly isolated *Bacillus megaterium* strain MG1 from the water bodies of Moraghat forest, Jalpaiguri, India. *The Journal of General and Applied Microbiology*, 65(3), 137–144. <https://doi.org/10.2323/jgam.2018.07.004>
34. Zhang, S., Xie, Y., Zhang, C., Bie, X., Zhao, H., Lu, F., Lu, Z. (2015). Biochemical characterization of a novel l-asparaginase from *Bacillus megaterium* H-1 and its application in French fries. *Food Research International*, 77, 527–533. <https://doi.org/10.1016/j.foodres.2015.08.031>
35. Badoei-Dalfard, A. (2015). Purification and characterization of L-asparaginase from *Pseudomonas aeruginosa* strain SN004: Production optimization by statistical methods. *Biocatalysis and Agricultural Biotechnology*, 4(3), 388–397. <https://doi.org/10.1016/j.cbab.2015.06.007>
36. El-Naggar, N. E.-A., Deraz, S. F., El-Ewasy, S. M., Suddek, G. M. (2018). Purification, characterization and immunogenicity assessment of glutaminase free L-asparaginase from *Streptomyces brolosae* NEAE-115. *BMC Pharmacology and Toxicology*, 19(1), 51. <https://doi.org/10.1186/s40360-018-0242-1>
37. Shi, R., Liu, Y., Mu, Q., Jiang, Z., Yang, S. (2017). Biochemical characterization of a novel L-asparaginase from *Paenibacillus barengoltzii* being suitable for acrylamide reduction in potato chips and mooncakes. *International Journal of Biological Macromolecules*, 96, 93–99. <https://doi.org/10.1016/j.ijbiomac.2016.11.115>
38. Onishi, Y., Prihanto, A. A., Yano, S., Takagi, K., Umekawa, M., Wakayama, M. (2015). Effective treatment for suppression of acrylamide formation in fried potato chips using L-asparaginase from *Bacillus subtilis*. *3 Biotech*, 5(5), 783–789. <https://doi.org/10.1007/s13205-015-0278-5>
39. Jia, M., Xu, M., He, B., Rao, Z. (2013). Cloning, Expression, and Characterization of <sc>l</sc>-Asparaginase from a Newly Isolated *Bacillus subtilis* B11–06. *Journal of Agricultural and Food Chemistry*, 61(39), 9428–9434. <https://doi.org/10.1021/jf402636w>
40. Farahat, M. G., Amr, D., Galal, A. (2020). Molecular cloning, structural modeling and characterization of a novel glutaminase-free L-asparaginase from *Cobetia amphilecti* AM16. *International Journal of Biological Macromolecules*, 143, 685–695. <https://doi.org/10.1016/j.ijbiomac.2019.10.258>
41. Sun, Z., Qin, R., Li, D., Ji, K., Wang, T., Cui, Z., Huang, Y. (2016). A novel bacterial type II L -asparaginase and evaluation of its enzymatic acrylamide reduction in French fries. *International Journal of Biological Macromolecules*, 92, 232–239. <https://doi.org/10.1016/j.ijbiomac.2016.07.031>
42. Wang, Y., Wu, H., Zhang, W., Xu, W., Mu, W. (2021). Efficient control of acrylamide in French fries by an extraordinarily active and thermo-stable L-asparaginase: A lab-scale study. *Food Chemistry*, 360, 130046. <https://doi.org/10.1016/j.foodchem.2021.130046>
43. Shahana Kabeer, S., Francis, B., Vishnupriya, S., Kattatheyl, H., Joseph, K. ., Krishnan, K. ., Mohamed Hatha, A. A. (2023). Characterization of L-asparaginase from *Streptomyces koyangensis* SK4 with acrylamide-minimizing potential in potato chips. *Brazilian Journal of Microbiology*, 54(3), 1645–1654. <https://doi.org/10.1007/s42770-023-00967-7>
44. Paul, V., Tiwary, B.N. (2020). An investigation on the acrylamide mitigation potential of L-asparaginase from BV-C strain. *Biocatalysis and Agricultural Biotechnology*, 27, 101677. <https://doi.org/10.1016/j.cbab.2020.101677>
45. Yuan, B., Ma, P., Fan, Y., Guan, B., Hu, Y., Zhang, Y., Ni, Y. (2022). Construction of L-Asparaginase Stable Mutation for the Application in Food Acrylamide Mitigation. *Fermentation*, 8(5), 218. <https://doi.org/10.3390/fermentation8050218>
46. Meghavarnam, A. K., Janakiraman, S. (2018). Evaluation of acrylamide reduction potential of l-asparaginase from *Fusarium culmorum* (ASP-87) in starchy products. *LWT*, 89, 32–37. <https://doi.org/10.1016/j.lwt.2017.09.048>
47. Bhagat, J., Kaur, A., Chadha, B. S. (2016). Single step purification of asparaginase from endophytic bacteria *Pseudomonas oryzae* exhibiting high potential to reduce acrylamide in processed potato chips. *Food and Bioproducts Processing*, 99, 222–230. <https://doi.org/10.1016/j.fbp.2016.05.010>







#### Information about authors

Murat Ozdal – (corresponding author) – PhD, Associate professor, Department of Biology, Faculty of Science, Ataturk University (Erzurum, Turkey, e-mail: [murat.ozdal@yahoo.com](mailto:murat.ozdal@yahoo.com))

Ozlem Gulmez – PhD, academic researcher, Department of Biology, Faculty of Science, Ataturk University (Erzurum, Turkey, e-mail: [ozlmg90@gmail.com](mailto:ozlmg90@gmail.com))

Emine Gökçe – PhD, postgraduate, Department of Biology, Faculty of Science, Ataturk University (Erzurum, Turkey, e-mail: [bylg\\_emine@hotmail.com](mailto:bylg_emine@hotmail.com))

Omer Faruk Algur – Professor, Department of Biology, Faculty of Science, Ataturk University (Erzurum, Turkey, e-mail: [offalgur@yahoo.com](mailto:offalgur@yahoo.com))

Y.M. Toishibekov<sup>1</sup> , D.Y. Toishybek<sup>1</sup> , T.T. Nurkenov<sup>1</sup> ,  
B.S. Katubayeva<sup>1</sup> , M.Y. Salmenova<sup>1</sup> , A.V. Perfilyeva<sup>2\*</sup> 

<sup>1</sup>Embryo Technology Labs, Almaty, Kazakhstan

<sup>2</sup>Institute of Genetics and Physiology, Almaty, Kazakhstan

\*e-mail: nastyaper2009@mail.ru

(Received: 15 February 2024; received in revised form: 6 March 2024; accepted: 19 March 2024)

## Optimization of cryopreservation methods for somatic cells of the Tobet dog breed

**Abstract.** The Tobet dog breed, a national heritage of Kazakhstan, is threatened with extinction and conservation measures are urgently needed. This study presents a pioneering approach to preserve the genetic diversity and survival of this endangered breed through cryopreservation and cryobanking. We have optimised methods for cryopreservation of somatic cells (fibroblasts) isolated from skin explants of Tobet dogs and investigated the effects of in vitro cultivation on cell viability. Our results emphasise the importance of selecting appropriate culture media and cryoprotectants. Dulbecco's Modified Eagle Medium (DMEM) and ethylene glycol (EG) were found to be the most effective agents for increasing the growth rate and viability of fibroblasts after thawing. Through careful experimentation, including the evaluation of equilibrium and non-equilibrium cryopreservation techniques and the application of various cryoprotectants, we have established the first Tobet cryobank for somatic cells. The establishment of a cryobank represents a significant step towards the conservation of the Tobet dog breed and provides a model for the conservation of other endangered species. This study not only contributes to the preservation of Kazakhstan's cultural and biological heritage, but also opens up new avenues for the application of biotechnological approaches to wildlife conservation.

**Key words:** Tobet, cryopreservation, fibroblast, equilibrium programmable cryoconservation, non-equilibrium cryoconservation.

### Introduction

Dogs of the national breed Tobet have been true friends and protectors of the Kazakh people for many centuries. But today they themselves need to be saved. Unfortunately, this unique breed is almost lost. Hundreds of years of work of our ancestors in breeding an ideal dog, a reliable guardian, a surprisingly strong and resistant dog can be in vain.

Currently, work to preserve, develop and restore the national Kazakh dog breeds, including the Tobet, is supported by the state. The success of this work will depend on civilized breeding work with them, which must be based on a scientific foundation. The modern arsenal of breeding methods has been significantly expanded by breakthrough achievements and new approaches in genetics, genomics, cytogenetics, and biotechnology.

Cryopreservation (i.e., freezing cells and tissues with cryoprotectants that ensure their long-term viable storage) followed by cryobanking (i.e.,

storing viable cells) may be a promising strategy to save an endangered breed. The effectiveness of cryobiological methods in conserving valuable livestock breeds and rare wildlife species has been demonstrated in some studies [1,2]. It has been shown that even a limited number of samples collected for long-term cryobanking can preserve genetic variation within a population. Today, cryobanks are used for the conservation and reproduction of such unique species as the giant panda (*Ailuropoda melanoleuca*), cheetah (*Acinonyx jubatus*), black-footed ferret (*Mustela nigripe*), Siberian crane (*Leucogeranus leucogeranus*), great bustard (*Chlamydotis undulata*), etc. [3-6] for supraregional IVF procedures of coral reefs [7]. However, little research has been conducted to develop procedures for cryopreservation of canine germplasm. Studies on sperm cryopreservation are more numerous [8-15]. In Kazakhstan, the successful cryopreservation of the sperm of a valuable producer of the Kazakh national breed Tazy is described [16]. Such artificial insemination with cryopreserved

sperm offers several advantages, including avoiding the stress associated with transporting the animal, solving the problem of reproduction associated with the behavior (aggressiveness or indifference) of the partner, and the quarantine imposed on the animal [11]. However, research on cryopreservation of canine somatic tissue, oocytes, and gonadal tissue is still insufficient [17-19], and is a priority in the field of canine germplasm cryobanking. It should be kept in mind that such cryobanking can only be successful if the protocol is optimized for specific species and possibly even breeds.

In this context, the aim of this study was to investigate the scientific basis for the long-term conservation of the somatic cells of the Kazakh national breed Tobet using various cryopreservation methods.

### Materials and methods

The main object of the study were dogs of Tobet breed. The collection of biomaterials from Tobet dogs was carried out during expeditions, exhibitions, and special events. Testing for compliance with the breed characteristics of the Kazakh Tobet breed was carried out by cynologists from “KANSONAR”, who met the qualification requirements and were experts in Kazakh national breeds and in the group such as the Central Asian Shepherd Dog (CAS), to which the Tobet belongs. The main document for conducting the test and establishing the breed standard that guided the experts was the breed standard for the Kazakh Tobet, which was approved by the Order of the Ministry of ecology and natural resources of the Republic of Kazakhstan dated 30 March 2023 No.101 “On the Approval of Standards for Kazakh Dog Breeds.”

We used samples of skin explants from Tobet dogs. This type of biomaterial, obtained after ear cropping, was only collected from puppies of Tobet dogs. Ear cropping was performed by a professional veterinarian, was planned, and was only performed after the dog owner had signed a consent form for this procedure. The biomaterial was used for isolation and *in vitro* culture of somatic cells (fibroblasts) and is necessary for the subsequent establishment of a Tobet somatic cell cryobank.

The study was approved by the bioethics committee of the RSE at REM Institute of Molecular Biology and Biochemistry named after M.A.Aitkhozhin CS MSHE RK (Protocol No. 1, August 18, 2023). The study is based on the “Bioethical rules for conducting research on

humans and animals” and is in accordance with the legislation of the Republic of Kazakhstan and the The European Convention on Bioethics. In the study, no experiments are conducted on the animals themselves, i.e., dogs; only biomaterials collected from dogs are used. The collection of all types of biomaterials mentioned in the study is a minimally invasive procedure that causes no harm to the dog.

*In vitro culture of somatic cells (fibroblasts) isolated from skin explants.* For the isolation and *in vitro* culture of somatic cells, fibroblasts, skin samples from the auricle of Tobet puppies were used during their docking (partial or complete removal of the external visible flap of the ear and/or ear cartilage of the animal), according to the external description of the breed, in a veterinary clinic by qualified specialists – veterinarians. Next, skin samples were treated with ethyl alcohol, placed in 15 ml plastic tubes with 10 ml of DMEM transport medium (Sigma, USA) containing 10% FBS and antibiotics at standard concentrations and transported to the laboratory.

In the laboratory, under the conditions of a sterile laminar flow hood (Esco, Singapore), skin samples were pre-rinsed twice in a DPBS solution (Sigma) for several minutes, the remaining hair was removed from their surface, then cut with a scalpel into pieces measuring approximately 1-2 mm<sup>2</sup> in a small volume of complete medium. After grinding, the tissue pieces were placed on the bottom of plastic culture mats with a surface area of 25 cm<sup>2</sup> and covered with complete culture medium in a volume of 3 ml, followed by observation of the release of fibroblasts from the explants and cell proliferation. For further *in vitro* culture of fibroblasts, DMEM nutrient medium (Sigma, USA) containing fetal bovine serum (Sigma, USA), L-glutamine (Sigma, USA) was used, and to suppress microflora, an antibiotic solution was added to the nutrient medium (Sigma, USA).

Further culturing of the explants was carried out in a CO<sub>2</sub> incubator (Binder, Germany), under conditions: 37°C, 5% CO<sub>2</sub> and 85% humidity for 4-5 days, without touching or moving the culture dishes. Using an inverted microscope Axiovert 40 CFL (Zeiss, Germany), the initial release and migration of single fibroblasts from the explant and the subsequent appearance of the growth zone were recorded. Cells were cultured in complete culture medium until they reached a monolayer in culture mats. To maintain the normal functioning of the cell culture, as well as to prevent negative phenomena, periodically, every 5 days, the culture medium was replaced with fresh one. To avoid contamination of cultures with bacteria



or other cell lines, all manipulations were carried out in compliance with aseptic rules in a sterile box Esco (Esco, Singapore).

Since fibroblasts are adhesive cells and form a monolayer in culture, for further passaging they must be separated from the substrate and their clusters separated. Cell dissociation and separation of the monolayer from the surface of the culture plastic was carried out using a warm 0.25% trypsin solution. The cells separated from the surface were collected into a 15-ml tube and washed by centrifugation. The resulting fibroblast pellet was resuspended in fresh culture medium, transferred to 2 new culture mats, and subsequent culturing was continued to increase the cell population, or the cells were frozen.

*Study of the viability of somatic cells (fibroblasts) of the Tobet breed.* Cell viability was assessed using the trypan blue dye exclusion method. The cell suspension was mixed with a 0.4% trypan blue solution and introduced into Goryaev's chamber. Separately stained (dead) and unstained (live) cells were counted under microscopy, thereby calculating the relative number (percentage) of living cells.

*Slow freezing (Non-Equilibrium Cryopreservation, NEC) using various cryoprotectants (dimethyl sulfoxide and ethylene glycol).* Fibroblasts were frozen using 0.5 ml straws (CryoBioSystem, France). For this purpose, the cell suspension was centrifuged for 10 min at 300 g. The cell sediment was resuspended in various cryoprotectants at the rate of 1-10 million cells per 1 ml of FTS, filled into 0.5 ml straws, which were placed for equilibration in a freezer chamber at  $-70^{\circ}\text{C}$ . Then, after 24 hours, the straws with cells were transferred to a Dewar flask with liquid nitrogen. Various cryoprotectants were used for freezing: 10% dimethyl sulfoxide (DMSO) and 10% ethylene glycol (EG).

*Slow program freezing (Equilibrium Programmable Cryoconservation, EPC) using a program freezer and various cryoprotectants (dimethyl sulfoxide and ethylene glycol).* For equilibrium cryopreservation of cells, the slow freezing method was used using a Planer Kryo 330 – 3.3 software freezer (Planer, UK) (Figure 1). Fibroblasts were frozen in 2 different cryoprotectants: 1.5 M DMSO (Sigma, USA) and 1.5 M ethylene glycol (Sigma, USA), prepared in DMEM and 10% BSA. When diluting with a cryoprotector, a cell concentration of  $2 \times 10^6$  cells/ml was maintained. For cryopreservation and further storage, 0.5 ml straws (CryoBioSystem, France) were filled with samples with a cryoprotector; the end of the straw was sealed.

The samples were then placed in a refrigerator and kept for 2 hours at  $5^{\circ}\text{C}$ . This procedure is necessary for equilibration and stabilization of cells in the cryoprotectant solution. Then they were frozen in a program freezer. For freezing, the following regime was used: from  $5^{\circ}\text{C}$  to  $-40^{\circ}\text{C}$  at a rate of  $-1^{\circ}\text{C}/\text{min}$ , from  $-40^{\circ}\text{C}$  to  $-85^{\circ}\text{C}$  at a rate of  $-4^{\circ}\text{C}/\text{min}$  (Figure 1), and then the straws were transferred to liquid nitrogen for storage.

*Thawing cells after freezing.* Thawing of cells was carried out using a standard method (Freshney). The cryovial with cells was transferred from the Dewar flask to a water bath with a temperature of  $37^{\circ}\text{C}$ , having previously been kept at room temperature to evaporate the remaining liquid nitrogen from the test tube. After complete thawing, the cell suspension was washed from DMSO and fetal serum in a 20-fold excess of RPMI-1640 medium by centrifugation at 160 g for 10 min. Cells were then resuspended in complete RPMI-1640 culture medium containing 10% FCS, 2 mM L-glutamine, and antibiotics. After this, cell viability was determined by trypan blue exclusion and subjected to further cultivation.

*Statistical data processing.* For statistical processing, the ANOVA application program was used. We calculated the arithmetic mean, the mean square error of the arithmetic mean, and the reliability of the difference in means P using the Student's test.

## Results and discussion

The study of the effects of *in vitro* cultivation of somatic cells on their viability is of strategic importance in the context of the conservation of valuable animal breeds, as it allows to develop optimal conditions for maintaining and ensuring high viability of their cells.

In this study, to isolate somatic cells, in particular fibroblasts, skin samples obtained from the auricle of a Tobet dog were used. The release of fibroblasts from explants and cell proliferation were monitored by microscopy. The rate of spreading and growth in culture dishes made of various materials (plastic and glass Petri dishes, plastic culture flasks) was assessed.

Observation of the release of cells from the explant tissue showed that, regardless of the method of explantation (in culture mats or in Petri dishes under a cover glass), the release of single cells from the explant tissue (Figure 1a) began no earlier than the 6th day of cultivation (on average 8-10th day after sowing) and was accompanied by cell division until a monolayer was reached (Figures 1b-d).

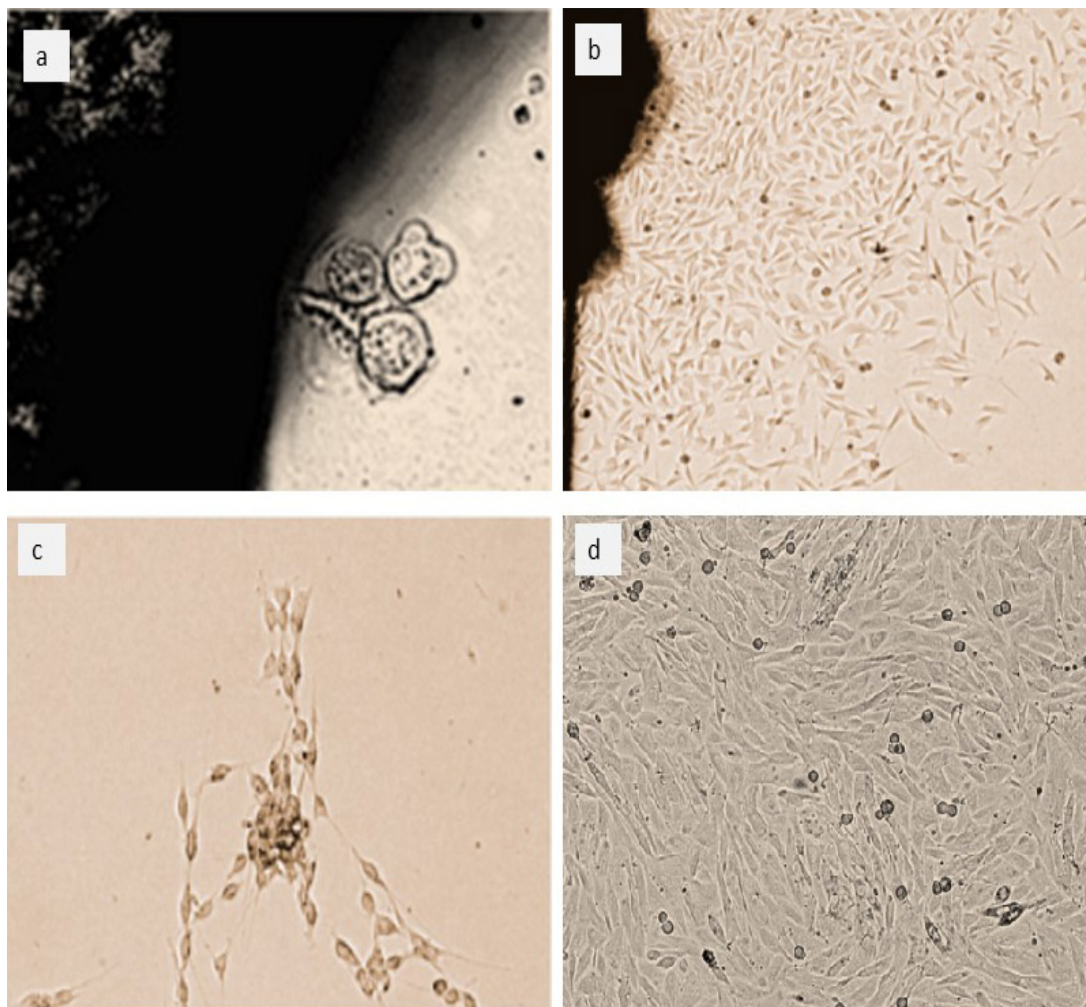


**Figure 1** – Output of fibroblasts from explant tissue obtained from the skin of a Tobet dog.

Note: a – output of single fibroblasts from explant tissue obtained from the skin of a Tobet dog;

b – release and proliferation of fibroblasts from explant tissue obtained from skin on the 14th day of culturing (Tobet dog);

c – an island of dividing fibroblasts from the stroma of an explant obtained from the skin on the 14th day of culture (Tobet dog);

d – monolayer of fibroblasts from the stroma of the explant obtained from the skin on the 28th day of culture (Tobet dog)

Already 10-12 days after the fibroblasts emerged from the explant, the monolayer occupied approximately 1/3 of the surface of a culture mattress with an area of 25 cm<sup>2</sup> or a Petri dish with a diameter of 60 mm.

When comparing the effectiveness of the two culture media used (RPMI-1640 and DMEM), preference was given to DMEM. When cultured in this medium, fibroblasts emerged from the explant several days earlier, and their growth rate was also noticeably higher.

Passaging of fibroblasts was carried out to increase cell mass, as well as to obtain a monoculture. Since fibroblasts are adherent cells, proteolytic enzymes, the main of which is trypsin, are most often used to

separate them from the surface of the culture dish. In our studies, the use of this enzyme alone turned out to be effective and sufficient for almost complete removal of the fibroblast monolayer from the surface of the culture dish. The optimal incubation time with trypsin was 7-10 minutes at 37°C. To prevent further action of the enzyme, 5-20 ml of 10% full complete media was added. The disaggregated cell suspension was transferred into new culture vessels, diluted 2-fold with fresh culture medium. Cell counting after trypsin dissociation showed that the percentage of living cells was  $91.7 \pm 0.6$ .

The dynamics of the process of desorption of fibroblasts from the surface of plastic Petri dishes is presented on Figure 2.

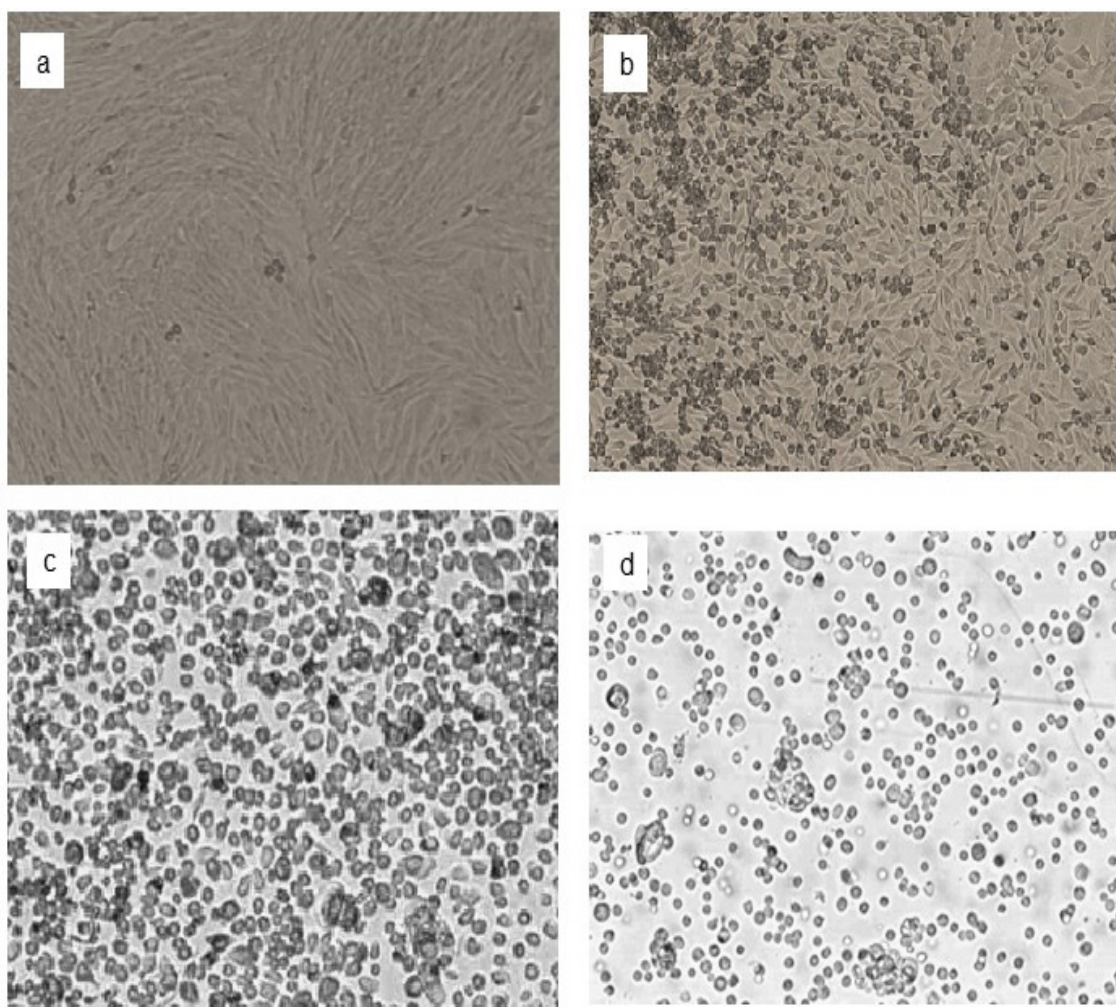


**Figure 2** – The dynamics of the process of desorption of fibroblasts from the surface of plastic Petri dishes.

Note: a – monolayer of fibroblasts obtained from a skin explant after washing with a buffer solution;  
 b – culture of fibroblasts obtained from a skin explant 40 seconds after the addition of trypsin;  
 c – culture of fibroblasts obtained from a skin explant 5 minutes after the addition of trypsin;  
 d – culture of fibroblasts obtained from a skin explant 10 minutes after the addition of trypsin and after resuspension

After the next passage, carried out after the cell culture reached the confluency state, the cell growth rate increased significantly. Moreover, the cell culture became more homogeneous. So, after the 5th passage we received an almost pure monoculture.

*Study the effect of slow freezing NEC using various cryoprotectants (dimethyl sulfoxide and ethylene glycol) on the viability of frozen-thawed fibroblasts of Tobet dogs.* Slow freezing using cryoprotectants has been shown to be an effective method of preserving animal genetic material [2,20]. Despite the extensive studies on this method and the effective protocols available, the individual characteristics and response to cryopreservation procedures can vary considerably depending on the cell type and animal species or

breed [21-27], making it necessary to individualise the approaches and optimise the protocols to produce viable cell lines.

As is known, the viability of cells during freezing is influenced by several factors, the main of which is the composition of the cryoprotectant and the freezing regime. The action of this factor is aimed at the formation of hexagonal ice crystals to preserve the integrity of the cytoplasmic membranes of cells. At the same time, it was revealed that there are species differences between cells in biophysical parameters: surface area, cell volume and membrane permeability of water. However, theoretical models have now been defined for different cell types, but these models do not correspond to fibroblasts (cell

size). Despite these differences, it is quite possible to use them to optimize the conditions for increasing the cryoviability of fibroblasts of various animal species and breeds.

The experiment used the simplest and most common method of cryopreservation. The results of assessing the viability rate of cells (fibroblasts) of Tobet dogs subjected to cryopreservation are presented in Table 1.

The viability rate of Tobet dog fibroblasts using various cryoprotectors: 10% DMSO and 10% EG, as well as the use of slow freezing NEC was  $54.3 \pm 1.1\%$  and  $65.7 \pm 1.1\%$  respectively. Static analysis by Student did not reveal significant differences ( $P > 0.05$ ). However, it should be noted that when using the 10% EG, the viability rate of frozen-thawed fibroblasts of Tobet dogs is higher than when using the 10% DMSO.

**Table 1** – Effect of various cryoprotectants and slow freezing NEC on the viability of Tobet fibroblasts

Cryoprotector/freezing mode	Relative number of living cells before freezing, %	Relative number of living cells after thawing, %
DMSO/ NEC	$91.7 \pm 0.6a$	$54.3 \pm 1.1b$
EG/ NEC	$91.7 \pm 0.6a$	$65.7 \pm 1.1c$

Note, ab, bc  $P > 0.05$

Study the effect of slow program freezing EPC using a program freezer and various cryoprotectants (dimethyl sulfoxide and ethylene glycol) on the viability of frozen-thawed fibroblasts of Tobet dogs.

In contrast to the previous method, EPC requires high-tech equipment. However, it offers a more precise and controlled freezing process with the possibility to programme temperature changes and thus avoid the formation of intracellular ice crystals.

In this study, the viability rates of frozen fibroblasts from Tobet dogs with EPC were analysed and compared with those of NEC. The cryoprotectants DMSO and EG were also used in the experiment and the Planer Kryo-330 software freezer was utilised.

The possibilities of using this equipment allow you to program the freezing mode and maintain the freezing temperature with an error of 0.01 degrees Celsius.

During the experiment, it was revealed that the viability rate of fibroblasts from Tobet dogs using various cryoprotectors: 10% DMSO and 10% EG using slow program freezing EPC was  $60.7 \pm 1.1\%$  and  $75.7 \pm 0.9\%$ , respectively (Table 2), which was higher than when using NEC (Figure 3). Statistical analysis by Student did not reveal significant differences ( $P > 0.05$ ). As in the previous case, the viability of thawed fibroblasts from Tobet dogs was higher when 10% EG was used than when 10% DMSO was used.

**Table 2** – Effect of various cryoprotectants and the use of slow program freezing EPC on the viability of fibroblasts of the Tobet breed

Cryoprotector/freezing mode	Relative number of living cells before freezing, %	Relative number of living cells after thawing, %
DMSO/EPC	$91.7 \pm 0.6a$	$60.7 \pm 1.1b$
EG/ EPC	$91.7 \pm 0.6a$	$75.7 \pm 0.9c$

Note, ab, bc  $P > 0.05$

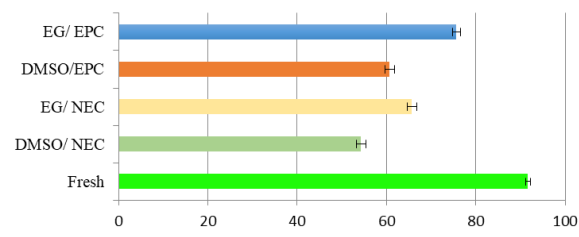


**Figure 3** – Viability of fibroblasts from dogs of the Tobet breed when using various cryoprotectants and different freezing methods

The development of methods and the study of the characteristics of the cryopreservation of somatic cells of Tobet breed dogs have allowed us to reach the following conclusions and methodological recommendations that can be used for a more effective conservation of the genetic resources of the Tobet breed:

- when comparing the effectiveness of the two culture media used (RPMI-1640 and DMEM), preference was given to DMEM. When cultured in this medium, the release of fibroblasts from the explant was observed several days earlier, and their growth rate was also noticeably higher;

- in our studies, the use of only one enzyme, a warm 0.25% trypsin solution, turned out to be effective and sufficient for almost complete removal of the fibroblast monolayer from the surface of the culture dish. The optimal incubation time with trypsin was 7-10 minutes at 37 °C;

- during the studies, it was revealed that the most optimal cryoprotector when using slow freezing methods is EG;

- it was found that the use of a software freezer for slow freezing of fibroblasts from Tobet dogs is the most effective.

## Conclusion

In this study, the methods were optimised and the properties of cryopreservation of somatic cells

(fibroblasts) from Tobet's dogs isolated from skin explants were investigated. The influence of *in vitro* cultivation on their viability was investigated. Their viability was determined during equilibrium and non-equilibrium cryopreservation using different cryoprotectants. Based on the investigations, the most effective approaches were proposed and the first cryobank with somatic cells (fibroblasts) from Tobet's dogs was established. The establishment of the first Tobet dog somatic cell cryobank is a huge step towards the preservation of this unique breed. The results of this study are groundbreaking for similar endeavours as they demonstrate the integration of traditional breeding values with cutting-edge biotechnological approaches.

## Acknowledgments

We would like to thank the dog breeders and owners who provided us with samples and information about this unique breed. Our special thanks to the veterinarians and members of "Kansonar" who helped with sampling and provided expert guidance.

This work was supported by the Committee of Science, Ministry of Science and Higher Education of Republic of Kazakhstan (Targeted funding programme #BR21881977, Agreement No.417-TPF-23-25 from November 15, 2023).

## References

- Woelders H, Windig J, Hiemstra SJ. How Developments in Cryobiology, Reproductive Technologies and Conservation Genomics Could Shape Gene Banking Strategies for (Farm) Animals. *Reproduction in Domestic Animals*. 2012; 47(SUPPL.4):264–273.
- Silva AR, Lima GL, Peixoto GCX, Souza ALP. Cryopreservation in mammalian conservation biology: current applications and potential utility. *Research and Reports in Biodiversity Studies*. 2015; 4:1–8.
- Herrick JR. Assisted reproductive technologies for endangered species conservation: Developing sophisticated protocols with limited access to animals with unique reproductive mechanisms. Vol. 100, *Biology of Reproduction*. 2019.
- Morrow CJ, Penfold LM, Wolfe BA. Artificial insemination in deer and non-domestic bovids. *Theriogenology*. 2009; 71(1).
- Andrabi SMH, Maxwell WMC. A review on reproductive biotechnologies for conservation of endangered mammalian species. Vol. 99, *Animal Reproduction Science*. 2007.
- Ballou JD. Strategies for maintaining genetic diversity in captive populations through reproductive technology. *Zoo Biol*. 1984;3(4).
- Hagedorn M, Spindler R, Daly J. Cryopreservation as a tool for reef restoration. In: *Advances in Experimental Medicine and Biology*. 2019.
- Hollinshead FK, Hanlon DW. Factors affecting the reproductive performance of bitches: A prospective cohort study involving 1203 inseminations with fresh and frozen semen. *Theriogenology*. 2017; 101.
- Mason SJ, Rous NR. Comparison of endoscopic-assisted transcervical and laparotomy insemination with frozen-thawed dog semen: A retrospective clinical study. *Theriogenology*. 2014; 82(6).
- Mason SJ. A retrospective clinical study of endoscopic-assisted transcervical insemination in the bitch with frozen-thawed dog semen. *Reproduction in Domestic Animals*. 2017; 52.
- Suzuki H, Watanabe H, Abe Y. Assisted reproductive techniques for canines: preservation of genetic material in domestic dogs. *Journal of Reproduction and Development*. 2022; 68(1).
- Cheema RS, Kaur S, Mavi GK, Singh AK, Honparkhe M, Gandotra VK. *In vitro* evaluation of Labrador dog spermatozoa cryopreserved in Tris-citric acid-fructose buffer supplemented with different combinations of extracellular and intracellular cryoprotectants. *Anim Biotechnol*. 2021;32(3).

Rota A, Milani C, Romagnoli S, Zucchini P, Mollo A. Pregnancy and conception rate after two intravaginal inseminations with dog semen frozen either with 5% glycerol or 5% ethylene glycol. *Anim Reprod Sci.* 2010; 118(1).

Rota A, Milani C, Cabianca G, Martini M. Comparison between glycerol and ethylene glycol for dog semen cryopreservation. *Theriogenology.* 2006; 65(9).

Martins-Bessa A, Rocha A, Mayenco-Aguirre A. Comparing ethylene glycol with glycerol for cryopreservation of canine semen in egg-yolk TRIS extenders. *Theriogenology.* 2006; 66(9).

Akulova Oksana. Najti i zamorozit' [Find and freeze]. *Vremja*, 2023, May 3 [cited 2023 Jul 1]; Available from: <https://time.kz/articles/reporter/2023/05/03/najti-i-zamorozit>

Suzuki H, Ishijima T, Maruyama S, Yanagimoto Ueta Y, Abe Y, Saitoh H. Beneficial effect of desialylated erythropoietin administration on the frozen-thawed canine ovarian xenotransplantation. *J Assist Reprod Genet.* 2008; 25(11-12).

Hariya M, Suzuki H. Incidence of Apoptotic Cells after Vitrification in Canine Ovarian Tissues. *J Mamm Ova Res.*, 2016; 33(1).

Ishijima T, Kobayashi Y, Lee DS, Ueta YY, Matsui M, Lee JY, et al. Cryopreservation of canine ovaries by vitrification. *J Reprod Dev.* 2006; 52(2).

Whaley D, Damyar K, Witek RP, Mendoza A, Alexander M, Lakey JRT. Cryopreservation: An Overview of Principles and Cell-Specific Considerations. Vol. 30, *Cell Transplantation.* 2021.

Wang S, Yuan X, Zhou J, Jin J, Zuo Q, Li B. Comparison of the effects of three cryoprotectants on the cryopreservation of mouse subcutaneous tissue under different conditions. *Exp Ther Med.* 2020

Cao J, Xie Y, Wang J, Huang Y, Zhang X, Xiao T, et al. Evaluating the Effects of Cryopreservation on the Viability and Gene Expression of Porcine-Ear-Skin Fibroblasts. *Genes.* 2023; 14(3).

Santiago-Moreno J, Castaño C, Toledano-Díaz A, Coloma MA, López-Sebastián A, Prieto MT, et al. Semen cryopreservation for the creation of a Spanish poultry breeds cryobank: Optimization of freezing rate and equilibration time. *Poult Sci.* 2011; 90(9).

Tan J, Guo YY, Zhou XL. Study on Optimization of Slow Freezing Protocol of Mouse Testis. *Progress in Biochemistry and Biophysics.* 2022; 49(10).

Cardoso B, Sánchez-Ajofrín I, Castaño C, García-álvarez O, Estes MC, Maroto-Morales A, et al. Optimization of sperm cryopreservation protocol for peregrine falcon (*Falco peregrinus*). *Animals.* 2020; 10(4).

Rodenas C, Parrilla I, Roca J, Martínez EA, Lucas X. Effects of Rapid Cooling Prior to Freezing on the Quality of Canine Cryopreserved Spermatozoa. *J Reprod Dev* [Internet]. 2014 [cited 2023 Nov 30];60(5):355. Available from: [/pmc/articles/PMC4219992/](https://pubmed.ncbi.nlm.nih.gov/24219992/)

Hussain M, Kumar M, Uddin K, Nath R, Sultana S. Additives used in semen preservation in animals: A short review. *Int J Chem Stud.* 2018;6(5).

#### **Information about authors**

Toishibekov Yerzhan Makenovich – Doctor of Biology Sciences, Associate Professor, LLP “Embryo Technology Labs” (Almaty, Kazakhstan, e-mail: [toishibekov@yandex.ru](mailto:toishibekov@yandex.ru))

Toishybek Dinmukhamed Yerzhanuly – Junior researcher, LLP “Embryo Technology Labs” (Almaty, Kazakhstan, e-mail: [dimash1212@gmail.com](mailto:dimash1212@gmail.com))

Nurkenov Tulendy Tuleshevich – PhD, LLP “Embryo Technology Labs” (Almaty, Kazakhstan, e-mail: [nurkenovtulendy@gmail.com](mailto:nurkenovtulendy@gmail.com))

Katubayeva Bibigul Serikovna – MS, LLP “Embryo Technology Labs” (Almaty, Kazakhstan, e-mail: [bibigul-82@mail.ru](mailto:bibigul-82@mail.ru))

Salmenova Madina Yerkenovna – MS, LLP “Embryo Technology Labs” (Almaty, Kazakhstan, e-mail: [leleo@bk.ru](mailto:leleo@bk.ru))

Perfilyeva Anastassiya – Candidate of biological sciences, leading researcher, Institute of Genetics and Physiology (Almaty, Kazakhstan, e-mail: [nastyaper2009@mail.ru](mailto:nastyaper2009@mail.ru))

A.K. Shokan<sup>1,2\*</sup>, D.M. Yergozova<sup>1,2</sup>, T.N. Kobylina<sup>1,2</sup>,  
 N.O. Kudrina<sup>1,2</sup>, Yu.A. Litvinenko<sup>1,2</sup>, G.A. Seitimova<sup>1,2</sup>,  
 T.E. Kulmanov<sup>1</sup>, N.V. Terletsкая<sup>1,2</sup>, I.M. Zharkova<sup>1</sup>

<sup>1</sup>Al-Farabi Kazakh National University, Almaty, Kazakhstan

<sup>2</sup>Institute of Genetic and Physiology, Almaty, Kazakhstan

\*e-mail: aksholpan.shokan@gmail.com

(Received 21 November 2023; received in revised form 20 February 2024; accepted 25 March 2024)

## Effect of the complex extract from *Rumex* plants on quantitative parameters of blood cells and bone marrow *in vivo*

**Abstract.** Assessment of the composition of peripheral blood cells and red bone marrow in preclinical studies is a key component of program for analysis of biologically active compounds obtained from the plant materials. Current study concerns effect of the complex extract from *Rumex* plants (*R. confertus*, *R. tianschanicus*, *R. thyrsiflorus*) on parameters of blood cells and bone marrow of laboratory animals. During the study, data were obtained on the effect of the extract on hematopoiesis when administered at 100 mg/kg of animal weight. The results obtained show that application of the extract is accompanied by a statistically significant increase in the number of neutrophil precursors, such as myeloblasts and band neutrophils ( $p \leq 0.05$ ). According to our results the extract we obtained from *Rumex* plants does not cause inhibition of early bone marrow precursors and is safe and non-toxic.

**Key words:** *Rumex*, extract, peripheral blood cells, red bone marrow, hematopoiesis.

### Introduction

One of the crucial elements during the of assessment anticancer, anticonvulsant, antimicrobial, and anti-inflammatory medications is examination of the red bone marrow (RBM), which stands as a crucial element in evaluating a potential drug in preclinical studies. This becomes particularly pertinent when [1]. Should a drug under scrutiny possess a high likelihood of impacting RBM, it becomes imperative to establish a procedure for bone marrow extraction to compute the myelogram, alongside ensuring the availability of a specialist capable of conducting such analysis. In cases where the investigated drug is entirely novel or its effects on RBM remain untested, and significant alterations in peripheral blood counts are detected, the decision to delve into RBM studies should precede the final phase of the investigation [2].

Use of medicinal plants and their substances is not only a growing global trend [3-11]. Our studies show that biologically active compounds (BAC) of the *Rumex* genus have wound-healing properties and a chemical structure comparable to drugs for the treatment of gastric reflux [12]. In Kazakhstani Tien

Shan, a wild variety of *Rumex* (*R.*) *tianschanicus* grows – one of the industrial crops offered for harvesting [10]. A study of the composition of *R. tianschanicus* showed the presence of flavonoids, which are renowned for their anti-inflammatory effect, in the leaves, roots and stems of the aforementioned plants [14]. In addition, the plant contains anthracene derivatives, which are reported to have a protective effect on the stomach. Furthermore, components like tannins, naphthols, coumarin and polysaccharides were also found in the plants [15].

To evaluate diseases, blood and bone marrow characteristics are often examined. The research [16] advises the use of the bone marrow cytology and preclinical toxicity studies as the basis for determining the effects of test materials on the hematological system. In some studies, the etiology of hematological changes is determined by analyzing indicators of total lymphocytes, granulocytes and hemoglobin. Mohamed et al. [17] illustrated the changes that occur with acetylsalicylic acid treatment, including noteworthy neutropenia, lymphocytopenia and eosinophilia, while basophils and monocytes are intermediate. Rats with inflammation tend to have more white blood cells overall [18]. According to

the studies [19], some animals may have delayed erythropoiesis and suppressed myelopoiesis, which may lead to a decrease in peripheral red blood cells and granulocytes.

### Materials and methods

*Experimental animals.* Animals used in this experiment were thirty white mongrel laboratory rats of both sex of three months' age, weight 180-220 g. Rats were acquired from the biological clinic of Al-Farabi Kazakh National University. The lab rats were kept in cages made of wire mesh, given a vitamin-enriched and well-balanced meal diet and unlimited access to water. Lab rats were divided into three groups, each consisting of 10 rats. Order No. RK DSM-255/2020 by the Minister of Health Care, Republic of Kazakhstan from December 11, 2020 established the guiding principles for animal research. All preclinical animal experiments were conducted with the approval of the ethical commission of the

Institute of Genetics and Physiology (protocol No. 07-05/68 from June 17, 2020). In addition, throughout the course of the study, the behavior and health of the experimental animals were observed and evaluated to those of the control animals. The regional ethical commission gave its approval for application of animals in this experiment as part of a Program-Target Financing "Adoption of innovative genomic technologies for defending organisms from mutagenic effects, increasing the productivity of natural resources, and improving the quality of life of the population."

*Collection of raw materials.* Taking into account the data obtained on the area of germination in the territories of our mountains, it can be assumed that the species under study feels good in such conditions. This is an indicator that it is not for nothing that this species is medicinal and grows in mountainous areas and we collected it. The place of growth of this species where we collected it (Figure 1).



Figure 1 – Scheme map with marks of plants collection

Plant materials were collected in the large Almaty gorge (Almaty region, Kazakhstan) at coordinates N 43° 03' 27, E 76° 58' 17, an altitude of 2511 m above the sea level.

*Phytochemical analysis.* Qualitative reactions with minor modifications were carried out for the presence of the main groups of biologically active compounds in the extract from *Rumex* plants, using standard methods. Phytochemical analysis of the

underground part of sorrel for various classes of compounds was carried out using two-dimensional and one-dimensional paper chromatography methods by comparison with taps in various solvent systems: butyl alcohol-acetic acid-water (40:12.5:29); butyl alcohol-acetic acid-water (4:1:5); 2% acetic acid and 15% acetic acid using specific developers; the following were found: carbohydrates (reactions with o-toluidine and urea), anthraquinones (by reaction



with alkali), flavonoids (Gage's reaction), phenols (reaction with iron-ammonium alum).

*Determination of the quantitative content of the main groups of biologically active substances.* According to generally accepted methods of the State Pharmacopoeia of the Republic of Kazakhstan, 1st edition and the State Pharmacopoeia of the USSR, the quantitative contents of the main groups of biologically active substances were determined [28].

*Design of studies.* Two groups of the animals (each with ten rats) were formed randomly. The first group was a control group, the second group obtained 100 milligrams of extract per kilogram. The water and extracts were administered perioral for 10 days using a pipette. The lab rats were subsequently sacrificed through the cardiac fence while sedated. Saline solution was used to obtain a sample of bone marrow, which was then sent for cytological staining. Also to ensure the reliability of the results, the experiment was repeated 3 times.

*Carrying out hematological analysis.* The results of a general blood test were obtained on a hematological analyzer Sysmex KX-21 (Japan), which includes 18 counting parameters: red blood cells ( $10^{12}/L$ ), leukocytes ( $10^9/L$ ), platelets ( $10^9/L$ ), hemoglobin (g/L), hematocrit (L/L), erythrocyte indices (fL), platelet indices (fL), lymphocytes, neutrophils, mixed cells (% and  $10^9/L$ ).

*Evaluation of bone marrow cytology.* Twenty treated rats and ten control rats were studied. Bone marrow was extracted using the left and right tibias. After the bone was dissected neatly, the bottom section of the tibia was compressed using fine forceps. The fractured top end's thick pink marrow was taken and put on a glass slide. A droplet of saline was added

as a diluent and delicately mixed with the marrow. Giemsa's guidelines were followed while staining thin smears with Azur-eosin and May-Grunwald (Pappenheim modification). First, a suitable amount of undiluted May-Grunwald stain is applied to the smear. Then, the stain is drained off the glass after 3 minutes, and the smear is stained for 10-12 minutes with a Giemsa stain solution before being rinsed with clean tap water. This staining approach combines the May-Grunwald stain's ability to detect cell granularity with the evident staining of the nucleus structure with Giemsa solution. Several hundred cells were discovered and counted. I.A. Kassirsky and G.A. Alekseev's classifications assisted in cell identification. Each sample was analyzed and cell counted using microscope Micro Opix MX 700 (T) (West Medica, Brown Boveri-StaBe 6, B17-1 2351 Wiener Neudorf, Austria), with HD camera CAM V1200C (West Medica, Brown Boveri-StaBe 6, B17-1 2351 Wiener Neudorf, Austria).

*Statistical analysis.* To show all data, the mean and standard error of the mean are employed. The Student t-test was used to examine the statistical significance of group differences; the significant result was  $p \leq 0.05$ .

## Results and discussion

The impact of *R. tianschanicus* extract on red bone marrow cytology. Figure 2 illustrates a wide range of blood cells, primarily progenitors and a few mature cells. According to Figure 3, the inflammatory process begins when the number of neutrophil progenitors grows. Finally, Figure 4 illustrates the blood count slowly improving, demonstrating the calming impact of extract therapy.

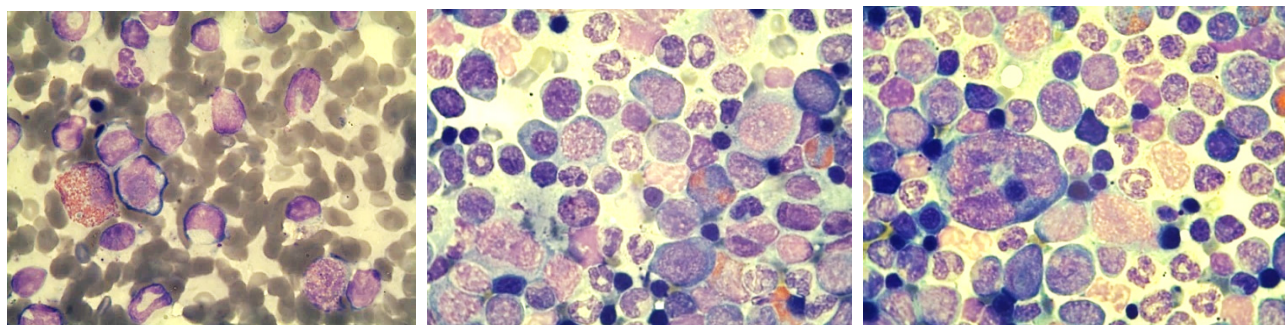


**Figure 2** – Photomicrograph of control group's cytology of red bone marrow (May Grunwald-Giemsa (MGG) staining, magnification  $\times 100$ , immersion oil)

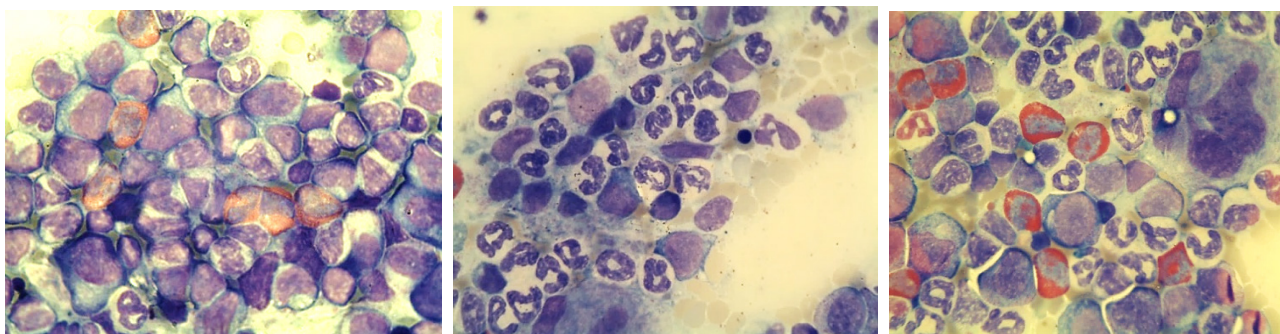


**Figure 3** – Photomicrograph of acute gastritis group' cytotology of red bone marrow (May Grunwald-Giemsa (MGG) staining, magnification  $\times 100$ , immersion oil)

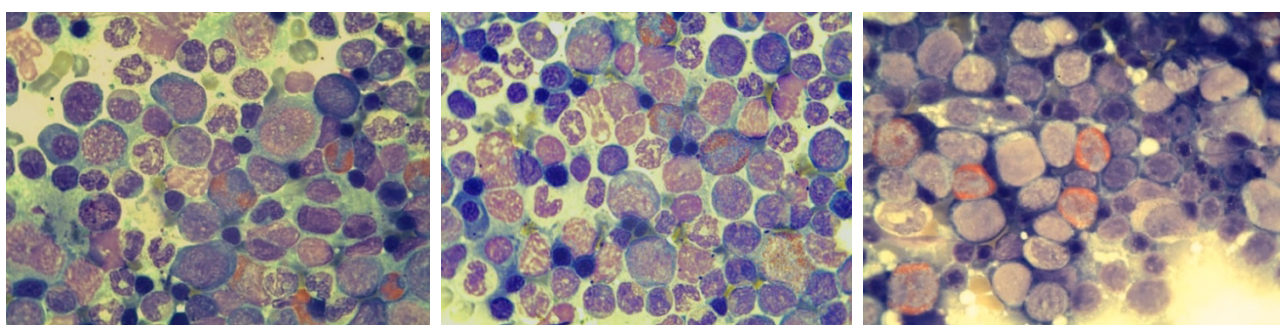


**Figure 4** – Photomicrograph of extract treatment group' cytotology of red bone marrow (May Grunwald-Giemsa (MGG) staining, magnification  $\times 100$ , immersion oil)

According to a morphological study of the structure, there were no unusual forms or qualitative abnormalities in gastritis and treatment.

The obtained data for determining the quantitative content of biologically active compounds in the underground part of sorrel extract show that this plant material is rich in flavonoids and polyphenols. The results of the analysis are presented in Table 1.

From the Table 1 we can conclude that, in terms of the quantitative content of biologically active compounds, the content of flavonoids and polyphenols dominates in the lower layers of

*R. tianschanicus* and the herbal medicine obtained on its basis.

As a result of the research, two known compounds, flavonoids and anthraquinones, were isolated from the complex extract *Rumex*. As shown in other studies, these compounds have anti-inflammatory and cell proliferation-stimulating activity and can be used in the treatment of gastrointestinal diseases [11-13].

Figure 5 shows the structure of isolated compounds from an extract obtained from the roots of *R. tianschanicus*

**Table 1** – Quantitative content of the main groups of biologically active compounds (BAC)

BAC	Raw material %	Phytoextract, %
Flavonoids	5.92	14.6
Carbohydrates	2.4	1.2
Polyphenols	3.54	10.1
Phenol- and -hydroxycinnamic acids	1.36	4.8
Polysaccharides	3.52	1.4
Anthraquinones	2.2	1.78

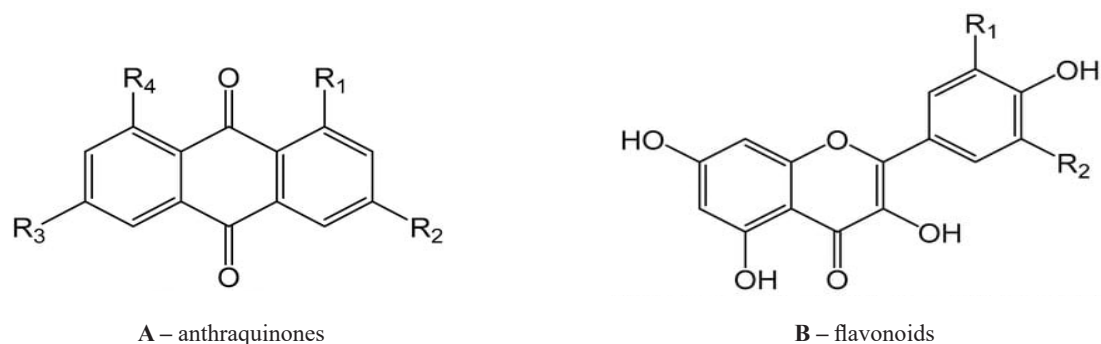


**Figure 5** – R<sub>1</sub>=OCH<sub>3</sub>, R<sub>2</sub>=H (Isoramnetin), R<sub>1</sub>=OH, R<sub>2</sub>=H (Quercetin), R<sub>1</sub>=OH, R<sub>2</sub>=OH (Myricetin) [12].

The experiment to study chronic toxicity was completed by killing the animals to obtain peripheral blood samples, which later served as material for hematological analysis. The study of the complex extract *Rumex* is confirmed by

comparative hematological parameters of the blood of experimental animals of the control group, acute and chronic toxicity of the complex extract *Rumex*, the data of which are given in the table below.

**Table 2** – Comparative hematological parameters of the blood of experimental animals of the control group, acute and chronic toxicity of the complex extract *Rumex*

Hematological indicator	International abbreviation	Control	Chronic toxicity
Total number of leukocytes, 10 <sup>9</sup> /L	WBC	6.13±1.03	7.70±1.05
Total number of red blood cells, 10 <sup>12</sup> /L	RBC	5.97±1.21	7.39±1.26
Hemoglobin level, g/L	HGB	164.20±16.32	172.80±13.85
Total platelet count, 10 <sup>9</sup> /L	PLT	919.20±154.32	719.00±152.62
Absolute neutrophil content, 10 <sup>9</sup> /L	Neut	2.76±0.54	3.14±0.51
Relative content of neutrophils, %	Neut	48.16±2.57	43.26±12.72
Absolute lymphocyte count, 10 <sup>9</sup> /L	Lymph	2.69±0.71	3.30±0.56
Relative content of lymphocytes, %	Lymph	39.40±3.65	50.96±6.57
Absolute monocyte count, 10 <sup>9</sup> /L	Mono	0.45±0.11	0.56±0.11
Relative content of monocytes, %	Mono	7.34±1.68	7.48±1.64
Absolute eosinophil count, 10 <sup>9</sup> /L	Eos	0.16±0.09	0.29±0.13
Relative content of eosinophils, %	Eos	2.62±0.98	3.22±0.69
Absolute basophil content, 10 <sup>9</sup> /L	Baso	0.04±0.06	0.24±0.43
Relative content of basophils, %	Baso	0.27±0.30	0.43±0.46

According to the results from the Table 2, when studying the chronic toxicity of a complex extract of plants of the genus *Rumex*, there were no statistically significant differences ( $p < 0.05$ ) between hematology parameters. A comparative analysis of the hematological parameters of animals in the control and experimental groups after oral administration of the extract revealed that the total number of leukocytes in the control group was  $6.13 \pm 1.03 \times 10^9/l$ ,

in the group with acute toxicity  $6.48 \pm 1.62 \times 10^9/l$ , and in the group with chronic toxicity toxicity was  $7.70 \pm 1.05 \times 10^9/l$  and did not reveal a statistically significant difference ( $p < 0.05$ ).

The total number of red blood cells in the control group was  $5.97 \pm 1.21 \times 10^{12}/l$ , in the experimental group with acute toxicity  $6.38 \pm 0.85 \times 10^{12}/l$ , in the third group after experimental treatment –  $7.39 \pm 1.26 \times 10^{12}/l$ .

The hemoglobin level in the control was  $164.20 \pm 16.32$  g/l, in the experiment with acute toxicity it was within  $170.00 \pm 19.04$  g/L, and in animals in the chronic toxicity group it was  $172.80 \pm 13.85$  g/L.

However, it was found that the concentration of the extract has a beneficial effect on the total number of platelets, from  $919.20 \pm 154.32 \times 10^9/l$  in the control group to  $825.80 \pm 175.41 \times 10^9/l$  in the group with acute toxicity and, accordingly, in the group with chronic toxicity, and amounted to  $719.00 \pm 152.62 \times 10^9/l$ . The absolute and relative content of neutrophils is  $2.76 \pm 0.54 \times 10^9/l$  and  $48.16 \pm 2.57\%$  in the control group, in the group with acute toxicity  $2.95 \pm 1.04 \times 10^9/l$  and  $45.60 \pm 9.45\%$  and in the group with chronic toxicity  $3.14 \pm 0.51 \times 10^9/l$  and  $43.26 \pm 12.72\%$ . The absolute and relative content of lymphocytes  $2.69 \pm 0.71 \times 10^9/l$  and  $39.40 \pm 3.65\%$  in the control group is higher than in the group with acute toxicity, which is  $3.27 \pm 1.15 \times 10^9/l$  and  $49.80 \pm 7.16\%$ , and the group with chronic toxicity is correspondingly higher –  $3.30 \pm 0.56 \times 10^9/l$  and  $50.96 \pm 6.57\%$ . The absolute and relative content of monocytes was  $0.45 \pm 0.11 \times 10^9/l$  and  $7.34 \pm 1.68\%$  in the control group, in the group with acute toxicity of  $0.49 \pm 0.09 \times 10^9/l$  and  $7.70 \pm 0.84\%$  and groups with chronic toxicity –  $0.56 \pm 0.11 \times 10^9/l$  and  $7.48 \pm 1.64\%$ . The absolute content of eosinophils was  $0.16 \pm 0.09 \times 10^9/l$  and the relative content was  $2.62 \pm 0.98\%$  in the control group and in the group with acute toxicity, the indicators of which were  $0.20 \pm 0.10 \times 10^9/l$  and  $3.04 \pm 0.95\%$ , and in the group with chronic toxicity  $0.29 \pm 0.13 \times 10^9/l$  and  $3.22 \pm 0.69\%$  no statistically significant changes were revealed ( $p \leq 0.05$ ). Also, considering the absolute and relative content of basophils in all three groups, no statistically significant changes were revealed ( $p \leq 0.05$ ), which is  $0.04 \pm 0.06$ ;  $0.04 \pm 0.04$ ;  $0.24 \pm 0.43 \times 10^9/l$  and  $0.27 \pm 0.30$ ;  $0.49 \pm 0.47$ ;  $0.43 \pm 0.46\%$ . Thus, all hematological blood parameters in experimental animals were within the physiological norm, which indicates the absence of toxic effects of the *Rumex* complex extract and its negative impact on hematopoiesis.

It has been established that with long-term use under the experimental conditions no hematotoxic effect was noted. With the chronic use of the complex extract *Rumex*, there are no changes in hematopoiesis indicators and no inhibition of hematopoiesis has been detected, there are no pronounced changes in the leukocyte formula, and according to the level of eosinophils and basophils, there are no allergic reactions. Thus, it can be noted that the *Rumex* complex extract is non-toxic. Consequently, no statistically significant changes  $p \leq 0.05$  in many

quantitative indicators of myelogram cell types except for the number of mature neutrophils, eosophilic metamyelocytes, monocytes and mast cells were noted. The detected statistically significant changes  $p \leq 0.05$  in the number of mature neutrophils were  $4.60 \pm 0.30$  in the control group and decreased in the group with the introduction of the extract of eosophilic metamyelocytes *Rumex* to  $1.11 \pm 0.12$ . The amount was calculated in the control –  $1.80 \pm 0.07$  and statistically significant changes  $p \leq 0.05$  were recorded in relation to the group with the introduction of the complex extract *Rumex* –  $1.12 \pm 0.21$ . In the control group, the number of monocytes was  $0.17 \pm 0.07$  and increased 2-fold in the group with the introduction of the complex extract *Rumex* –  $0.37 \pm 0.03$  relative to the control, which was also statistically detected at  $p \leq 0.05$ . And the most statistically significant change ( $p \leq 0.05$ ) of more than 30 times was observed in the number of mast cells in the control group –  $0.67 \pm 0.02$  and a decrease to –  $0.01 \pm 0.001$  in the group with the introduction of the complex extract *Rumex*.

The findings demonstrate inflammation of the stomach lining mucous membrane by an increased number of neutrophil progenitors, including myeloblasts and band neutrophils. Along with the fact that extract therapy decreased the number of neutrophil progenitors, it is assumed that the inflammation of the stomach mucosa decreased. With therapy, the initial inflammatory reaction subsided. Despite a rise in eosinophil and basophilic myelocyte production, the morphology remained unchanged. More study of this phenomenon is necessary. We may infer that the extract has a beneficial impact on the activation of erythropoiesis from the alterations in red blood cell progenitors, particularly polychromatic and orthochromatic normoblasts, as demonstrated by a sharp decline in acute gastritis with a return to the original levels in a stable condition. In addition, the number of lymphocytes dramatically increased during extract treatment, which may indicate that lymphopoiesis was activated. An increase might be attributed to the extract's unresearched immunostimulating abilities. Overall, extract has no adverse effects on the bone marrow's ability to produce blood cells.

Our data indicate a decrease in the total number of platelets associated with the use of this phytoextract, as a previously studied manifestation of *R. acetosa* antiplatelet activity by Jeong D. et al. [20]. In other hematological parameters of the control groups and with the introduction of the extract, slight increases were observed and no statistically significant

changes were detected ( $P < 0.05$ ), however, the level of hemoglobin increased in the group with the introduction of the complex herbal medicine *Rumex* in relation to the control group, although in another study, Islam R. et al. observed lower hemoglobin (HGB) in those receiving ethanol extract than in the control group [21]. In a recent investigation on the protection of hematopoiesis of the proposed extract following breast cancer [22]. The ratio of myeloid cells was reduced following the administration of the recommended extract. Similar to our findings, after extract therapy, the number of common lymphoid progenitors rises. The number of monocytes, lymphocytes, and eosinophils is decreasing while the number of neutrophils, erythrocytes, and platelets is increasing [23].

Applying a massive dosage of cortisone was found to significantly raise the ratio of myeloid to erythroid cells, taking into account earlier studies [24] concerning bone marrow. The experiment excluded the idea of decreasing RBC progenitors and growing myeloid progenitor cells, revealing information about the overall bone marrow cellularity. Myeloid proliferation or/and prevention of discharge from the bone marrow into the circulation are hypothesized to cause an increase in myeloid line cells. Data on the impact of hormone administration on the bone marrow is supported by several investigations [25]. Our conclusions were reinforced by 2015 research by Ayodeji on the age-dependency of blood parameters and biochemical markers during healing chronic toxicity. They showed that in younger rats, the lymphocyte count rose and the neutrophil count fell (3 and 6 month). The rats we utilized for the experiment and the young rats from their study are of similar age [26]. And against the

background of experimental therapy with a complex phytopreparation based on *Rumex*, were not detected any functional changes in the organs of the digestive system. During experimental administration of the extract, no deterioration or side effects were observed in rats [27]. Overall, the results confirm the beneficial and non-toxic effects of complex extract of *Rumex* plants.

## Conclusion

This investigation aimed to determine how *Rumex* extract affected myelograms and whether it would be useful in treating chaotic toxicity. The rat myelogram study's findings confirmed the predictable hypothesis. This study offers new understandings of the quantitative features of the rat myelogram during chronic toxicity and the potential therapeutic value of complex phytopreparation based on *Rumex*. The work proves that extract is not cytostatic and has erythropoiesis activation properties. Due to its therapeutic benefits against chronic toxicity, we believe the phytoextract examined in this work merits greater attention and encourage additional research into it.

## Acknowledgments

The work was supported by the program BR 21882180 "Development of a program for the conservation and development of the resource base of plants of Kazakhstan that are promising for medicine and veterinary medicine in a changing climate" (2023-2025) funded by the Committee of Science, Ministry of Science and Higher Education, Republic of Kazakhstan.

## References

1. Kang M., Park S., Chung Y., Lim J.-O., Kang J.S., Park J.H. (2022) Hematopoietic effects of *Angelica gigas* Nakai extract on cyclophosphamide-induced myelosuppression. *Plants*, 11, 3476. <https://doi.org/10.3390/plants11243476>.
2. Liu J., Wei J., Wang C., Meng X., Chen H., Deng P., Huandike M., Zhang H., Li X., Chai L. (2019) The combination of *Radix astragali* and *Radix angelicae sinensis* attenuates the IFN-gamma-induced immune destruction of hematopoiesis in bone marrow cells. *BMC Complement. Altern. Med.*, 19, 356.
3. Vasiliev A.S., Kalinkina G.I., Tikhonov V.N. Herbal medicines. – Tomsk: SSMU, 2006. – 122 p.
4. Grudzinskaya L.M., Gemedzhieva N.G., Nelina N.V., Karzhaubekova Zh.Zh. Annotated list medicinal plants of Kazakhstan. Reference publication. – Almaty: 2014. – 200 p.
5. Li J.J., Li Y.X., Li N., Zhu H.-T., Wang D., Zhang Y.-J. (2022) The genus *Rumex* (Polygonaceae): an ethnobotanical, phytochemical and pharmacological review. *Nat. Prod. Bioprospect.*, 12, 21.
6. Berillo D., Kozhahmetova M., Lebedeva L. (2022) Overview of the biological activity of anthraquinones and flavanoids of the plant *Rumex* species. *Molecules*, 27, 1204.
7. Vasas A., Orban-Gyapai O., Hohmann J. (2015) The genus *Rumex*: review of traditional uses, phytochemistry and pharmacology. *J. Ethnopharmacol.*, 175, 198-228.

8. Muzychkina R.A., Kurbatova N.V., Korulkin D.Y. (2016) Component composition and biological activity of polyphenolic metabolites of *Rumex tianschanicus* Los. KazNU Bull., 69, 22-31.
9. Muzychkina R.A. Natural anthraquinones. biological properties and physico-chemical characteristics. Phasis: M.: Russia, 1998, p. 864. ISBN 5-7036-0041-3.
10. Litvinenko Yu.A., Muzychkina R.A. (2003) Phytochemical investigation of biologically active substances in certain Kazakhstan *Rumex* species. Chem. Nat. Compd., 39: 446-449.
11. Feduraev P., Skrypnik L., Nebreeva S., Dzhobadze G., Vatagina A., Kalinina E., Pungin A., Maslennikov P., Riabova A., Krol O. et al. (2022) Variability of phenolic compound accumulation and antioxidant activity in wild plants of some *Rumex* Species (Polygonaceae). *Antioxidants*, 11, 311
12. Seitimova G.A., Shokan A.K., Tolstikova T.G., Zhukova N.A., Korulkin D.Y., Kudrina N.O., Litvinenko Y.A., Meduntseva N.D., Terletskaia N.V., Kulmanov T.E. (2023). Antiulcer activity of anthraquinone-flavonoid complex of *Rumex tianschanicus* Losinsk. *Molecules*, 28, 2347. <https://doi.org/10.3390/molecules28052347>.
13. Shokan A., Ginayatova I., Yergozova D., Kudrina N., Kurmanbaevna K. (2021) Effects of *Rumex tianschanicus* Losinsk extract on hematological indicators in experimental gastritis. *Bulletin of the Karaganda University. Biology, Medicine, Geography Series*, 103(3), 150-156. <https://doi.org/10.31489/2021bmg3/150-156>
14. Rahaman S., Mondal S. (2020) Flavonoids: A vital resource in healthcare and medicine. *PPIJ*, 8(2), 91-104. <https://doi.org/10.15406/ppij.2020.08.00285>
15. Berillo D., Kozhahmetova M., Lebedeva L. (2022) Overview of the biological activity of anthraquinones and flavanoids of the plant *Rumex* species. *Molecules*, 27(4), 1204.
16. Turinelli V., Gavazza A., Stock G., Fournel-Fleury C. (2015) Canine bone marrow cytological examination, classification and reference values: A retrospective study of 295 cases. *Res Vet Sci.*, 103, 224-230. <https://doi.org/10.1016/j.rvsc.2015.10.008>
17. Mohamed W.A., Abd-Elhakim Y.M., Ismail S.A.A. (2019) Involvement of the anti-inflammatory, anti-apoptotic, and anti-secretory activity of bee venom in its therapeutic effects on acetylsalicylic acid-induced gastric ulceration in rats. *Toxicology*, 419, 11-23. <https://doi.org/doi:10.1016/j.tox.2019.03.003>
18. Bao Y., Chen H., Hu Y., Bai Y., Zhou M., Xu A., Shao C. (2012) Combination effects of chronic cadmium exposure and gamma-irradiation on the genotoxicity and cytotoxicity of peripheral blood lymphocytes and bone marrow cells in rats. *MRGTEM*, 743(1-2), 67-74. <https://doi.org/10.1016/j.mrgentox.2011.12.025>
19. Jalgama S., Kale V., Wilbanks M., Perkins E., Meyer S. (2013) Delayed myelosuppression with acute exposure to hexahydro-1,3,5-trinitro-1,3,5-triazine (RDX) and environmental degradation product hexahydro-1-nitroso-3,5-dinitro-1,3,5-triazine (MNX) in rats. *Toxicol Appl Pharmacol*, 266(3), 443-451. <https://doi.org/10.1016/j.taap.2012.11.022>
20. Jeong D., Irfan M., Lee D.H., Hong S.B., Oh J.W., Rhee M.H. (2020) *Rumex acetosa* modulates platelet function and inhibits thrombus formation in rats. *BMC Complement Med Ther.* 23; 20(1): 98. doi: 10.1186/s12906-020-02889-5
21. Islam R., Mamat Y., Ismayil I., Yan M., Kadir M., Abdugheny A., ... Abay S. (2015) Toxicity of anthraquinones: differential effects of *Rumex* seed extracts on rat organ weights and biochemical and haematological parameters. *Phytotherapy Research*, 29(5), 777-784. doi:10.1002/ptr.5317.
22. Xie Y., Jiang Z., Yang R., Ye Y., Pei L., Xiong S. et al. (2021) Polysaccharide-rich extract from *Polygonatum sibiricum* protects hematopoiesis in bone marrow suppressed by triple negative breast cancer. *Biomed. Pharmacother.*, 137, 111338.
23. Casanova-Acebes M., Pitaval C., Weiss L., Nombela-Arrieta C., Chèvre R., A-González, N. et al. (2013) Rhythmic modulation of the hematopoietic niche through neutrophil clearance. *Cell*, 153(5), 1025-1035. <https://doi.org/10.1016/j.cell.2013.04.040>
24. Elmore S.A. (2006) Enhanced histopathology of the bone marrow. *Toxicologic pathology*, 34(5), 666-686. <https://doi.org/10.1080/01926230600939971>
25. Takeshita W.M., Gushiken V.O., Ferreira-Duarte A.P., Pinheiro-Torres A.S., Roncalho-Buck I.A., Squebola-Cola D.M., Mello G.C., Anhê G.F., Antunes E., DeSouza I.A. (2015) Staphylococcal enterotoxin A regulates bone marrow granulocyte trafficking during pulmonary inflammatory disease in mice. *Toxicol Appl Pharmacol*, 287(3), 267-275. <https://doi.org/10.1016/j.taap.2015.06.013>
26. Ajayi A.F., Olaleye B.S. (2020) Age-related changes in haematological parameters and biochemical markers of healing in the stomach of rats with acetic acid induced injury. *Toxicology Reports*, 7, 1272-1281.
27. Al-Khayri J.M., Upadhy V., Pai S.R., Naik P.M., Al-Mssallem M.Q., Alessa F.M. (2022) Comparative quantification of the phenolic compounds, piperine content, and total polyphenols along with the antioxidant activities in the *Piper trichostachyon* and *Piper nigrum*. *Molecules*, 27, 5965.
28. State Pharmacopoeia of the Republic of Kazakhstan. Vol.1.- Almaty: Zhibek zholy, 2008. – 592 p.

**Information about authors:**

*Shokan Aksholpan Kanatkyzy (corresponding author) – PhD student at the Department of Biodiversity and Bioresources, al – Farabi Kazakh National University, junior researcher at Institute of Genetic and Physiology (Almaty, Kazakhstan, email: aksholpan.shokan@gmail.com)*

*Yergozova Diana Maratkyzy (corresponding author) – PhD student at the Department Biodiversity and Bioresources, al – Farabi Kazakh National University, Senior Assistant at Institute of Genetic and Physiology (Almaty, Kazakhstan, email: diana.yergozova@gmail.com)*

*Kobylyna Tatyana Nikolaevna – PhD student at the Department of Biodiversity and Bioresources, al – Farabi Kazakh National University, researcher at Institute of Genetic and Physiology ( Almaty, Kazakhstan, email: tanya\_tanichka\_87@mail.ru)*

*Kudrina Nataliya Olegovna – Candidate of Biological Sciences, Senior Lecturer at the Department of Biodiversity and Bioresources, al-Farabi Kazakh National University, Leading researcher at Institute of Genetic and Physiology (Almaty, Kazakhstan, email: kudrina\_nat@mail.ru)*

*Litvinenko Yuliya Alekseevna – Candidate of Chemistry Sciences, Deputy head of the department for educational, method. and educational work, senior teacher at the Department of Chemistry and Technology org. substances, natural compounds and polymers, al – Farabi Kazakh National University, Leading researcher at Institute of Genetic and Physiology (Almaty, Kazakhstan, email: Yuliya\_litvinenk@mail.ru)*

*Seytimova Gulnaz Absattarovna – Associate Professor at the Department of Chemistry and Technology org. substances, natural compounds and polymers al – Farabi Kazakh National University, Leading researcher at Institute of Genetic and Physiology (Almaty, Kazakhstan, email: sitigulnaz@mail.ru)*

*Kulmanov Timur Esengalievich – candidate of Medical Sciences, Leading researcher, Head of Pharmacological research laboratory at the Institute of Genetic and Physiology (Almaty, Kazakhstan, email: kulmanovlux@mail.ru)*

*Terletskeya Nina Vladimirovna – Candidate of Biological Sciences, Associate professor at the Department of Biodiversity and Bioresources, al-Farabi Kazakh National University, Leading researcher, Head of laboratory at the Institute of Genetic and Physiology (Almaty, Kazakhstan, email: teni02@mail.ru)*

*Zharkova Irina Maratovna – Candidate of Biological Sciences, Deputy Head of Department on scientific and innovative work and international relations, Senior Lecturer at the Department of Biodiversity and Bioresources, al – Farabi Kazakh National University (Almaty, Kazakhstan, email: Irina.Zharkova@kaznu.kz)*

M. Kamalabadi , Gh. Chehardoli\* 

Hamadan University of Medical Sciences, Hamadan, Iran

\*e-mail: cheh1002@gmail.com

(Received 10 May 2024; received in revised form 25 May 2024; Accepted 5 June 2024)

## Aspects of DNA interaction with the natural heterocyclic compounds

**Abstract.** Cancer is now one of the major challenges in the medical world. An unhealthy lifestyle, and abuse or inappropriate use of drugs stimulate this disease. The drug resistance and imperfections of drugs used in cancer therapy have enforced the development of new drugs with therapeutic potential. Despite the introduction of synthetic drugs, the discovery of new drugs with natural origin has increasing attention in the treatment of diseases, recently. As natural compounds show a considerable diversity of chemical structures, they are liable for diverse mechanisms of action and interaction with target molecules. Heterocyclic natural compounds are a substantial part of natural compounds with excellent properties. These compounds possess various interaction modes with DNA. This review focus on the heterocyclic natural compounds with therapeutic potential and their binding mode with DNA.

**Key words:** Natural drugs, heterocyclic compounds, cancer, DNA binding.

### Introduction

Cancer is the third main reason of death all over the world due to poor treatments and drug resistance [1]. It is estimated that deaths caused by cancer will grow dramatically in the following decades. The DNA damage induced by chemical and physical agents plays a critical role in cancer induction. The need for the protection of DNA against damage has led to much attention on the natural compounds with antimutagenic and antioxidant properties, which have minimal or no side effects for use in cancer treatments. Natural compounds or phytochemicals are important resources of bioactive compounds for developing new potent drugs due to their anticancer activity and clinical potential [2, 3]. These promising compounds are found in plants, bacteria, mushrooms, or marine organisms [4]. From ancient civilizations until today, the use of natural compounds has been considered medicinal agents. An impressive number of FDA-approved drugs are organic compounds derived from natural sources [5-7]. Many phytochemicals have a chemopreventive effect on DNA. Most natural biologically active compounds are heterocyclic ring-containing compounds that include hetero atoms such as oxygen, sulfur, or nitrogen as a part of the carbonic ring. Heterocycles have a special place among drug molecules owing to their comprehensive properties [8, 9]. Thanks to the presence of hetero atoms in their

structure, heterocycles are able to effectively interact with receptors and enzymes through hydrogen bonding [10, 11]. These compounds can improve the pharmacokinetic and pharmaceutical properties of drug molecules through moderation of their lipophilicity [12]. It should be pointed out that the antioxidant and anti-mutagenic properties are the most important characteristics of heterocyclic natural compounds. As antioxidants can prevent DNA damage, their chronic consumption is increasing. Our survey of curcumin-derived heterocycles [13] motivated us to conduct a systematic literature review on the modes of DNA binding of natural heterocyclic compounds used as drugs.

### Major considerations

*Drug-DNA interactions.* The DNA strand is known to be the cellular target of many anti-cancer compounds. Since DNA contains genetic information, knowing the interaction mechanism of drug molecules with DNA strands is very important in biological systems. Drug interaction with the DNA strand can control cell function by regulating transcription (gene expression and protein synthesis) or by interfering with replication (the main stage in cell growth and division) [14, 15]. This aspect of DNA-interacting drugs has fascinated the field and expanded its applications. Small ligands bind



to DNA strands to mutate or inhibit their functions. Modified functions in transcription or replication can be used to treat various diseases. Anticancer drugs can interact with DNA in three ways: I) control of polymerases and transcription factors, where the drug molecules interact with proteins attached to DNA, and II) RNA-DNA binding. The structure of the triple helix or hybrid with RNA plays a critical role in the transcription of the DNA strand, and III) sticking of aromatic molecules to double-stranded DNA, which includes electrostatic interactions, intercalation between base pairs, and minor and major grooves binding [16].

*Binding modes of DNA and drug molecules.* The interaction between DNA and drug molecules can be classified into covalent and non-covalent interactions. Many drugs bind to DNA strands by forming covalent bonds within or between strands. Covalent binding of the drug to the DNA strand is irreversible, leading to complete prevention of processes related to DNA

and, finally, cell death. These covalent binders are also called alkylating agents because of adding an alkyl group to the DNA chain. The most important advantage of alkylating agents is their high binding strength to base pairs in DNA [17]. Since alkylating agents kill cancer cells by inducing significant DNA damage, they have been used as anticancer drugs [18]. Alkylating agents can bind to the N and O atoms of the DNA bases, but O6 and N7 of guanine, N1, and N3 of adenine, and N3 of cytosine are preferential sites for intercalation [19].

*Non-covalent mode of binding.* This binding mode is classified into three types, including intercalation, groove binding, and backbone binding [20]. Figure 1 displays the schematic diagram of the non-covalent mode of binding. Non-covalent interacting agents possess less cytotoxic than alkylating agents. These interactions interfere with protein-DNA interactions, and also, affect the DNA conformational, mitochondrial DNA, and its function [21].

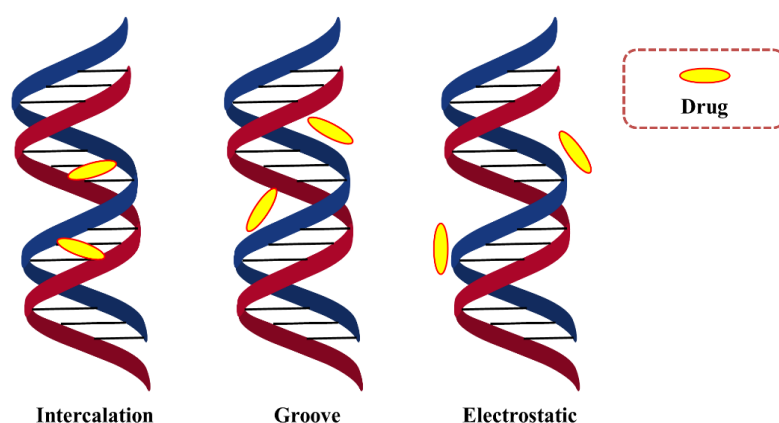


**Figure 1** – Schematic diagram of different interaction modes

DNA intercalation is defined as the insertion of planar aromatic compounds, especially planar heterocyclic compounds, between adjacent base pairs in the DNA strand through a combination of  $\pi$ - $\pi$  stacking, hydrogen bonding, and hydrophobic interactions, leading to significant changes in the DNA structure [22]. As intercalators disturb biological functions, such as DNA replication, they are used as antitumor drugs [23].

Various compounds can interact noncovalently with the minor or major groove of DNA by hydrogen bonding, and van der Waals interactions [24]. Major groove binders are often molecules with high molecular weights, such as proteins. Minor groove

binders are aromatic or hetero-aromatic compounds with concave shapes to match the groove shape [25]. These compounds often bind to adenine N3 and O2 thymidine via hydrogen bonding. Because of their ability to turn on/off gene expression, and disrupt protein-DNA interactions, minor groove binders are used in anticancer and anti-infective therapy as well as the treatment of viral, parasitic and bacterial infections [26, 27]. Backbone binding is the interaction of some molecules with phosphate groups of DNA. Metal complexes are a model of backbone binders with a positive charge and can bind with the DNA phosphate backbone with a negative charge [28].

*Methods of study of the mechanism of drug-DNA interactions.* Various analytical techniques, including UV-vis, infrared (IR), fluorescence, nuclear magnetic resonance (NMR) and circular dichroism spectroscopies, DNA melting studies, viscosity measurements, molecular docking, and electrochemical methods are employed to study the interaction nature of small molecules with DNA. This review focuses on UV-vis and fluorescence spectroscopies as the most commonly used methods.

*UV-Vis absorption spectroscopy.* UV-Vis absorption spectroscopy is one of the most commonly used techniques for studying DNA interactions with molecules because of its low cost, and simplicity. In these spectrometric studies, the changes in the absorption properties of the DNA or the molecules binding to DNA are monitored. DNA molecule shows maximum absorption at 250 nm [29]. As DNA interacts with the molecules, its structure changes, and it results in the decreasing or increasing absorption band along with the bathochromic shift or hypsochromic shift (Figure 2A).

However, DNA-binding molecules exhibit an absorption band in the visible region, which shifts to longer or shorter wavelengths. The magnitude of these shifting is considered an indicator of the interaction strength [29-32]. Intercalators usually induce hypochromism or hyperchromism effects, which mean a decrease or increase in the intensity of the absorbance band, respectively [33]. Hyperchromism arises from the damage to the double helix structure of the DNA, which leads to forming its single-stranded.[34-36] Hypochromism occurs because of the contraction of DNA in the helix axis. It also arises from the conformational changes of DNA [37, 38]. These compounds also result in bathochromic shifts of over 15 nm [39, 40]. In the case of groove binders, a decrease or increase in the absorption band occurs along with a small shifting or no shifting because the structural alteration of DNA or the binder is minimal (Figure 2B) [41]. An increase in the absorption intensity (hyperchromism) is observed in the case of the electrostatic mode of binding [16].

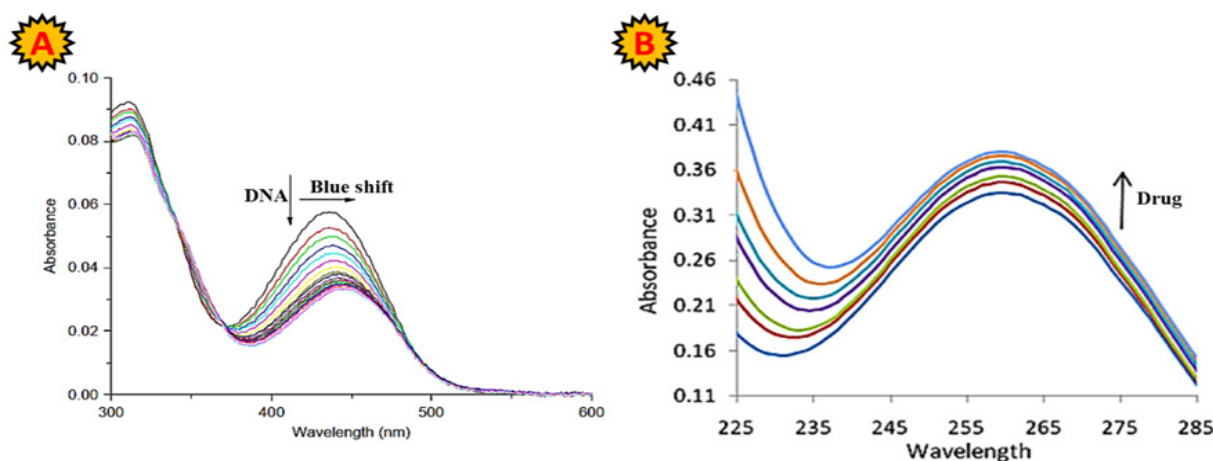


**Figure 2** – Investigating the interaction between DNA and drug using UV-vis spectroscopy related to (A) an intercalator, (B) a groove binder. It is reproduced from References [42], [43]

Concerning the absorbance changes, the binding constant ( $K$ ) of the molecule with DNA can be calculated based on the following equation, [44]:

$$\frac{A_0}{A - A_0} = \frac{\epsilon_M}{\epsilon_{Com} - \epsilon_M} + \frac{\epsilon_M}{\epsilon_{Com} - \epsilon_M} \times \frac{1}{K[DNA]}$$

Where  $K$ ,  $A_0$ , and  $A$  are the binding constant, molecule absorbance, and absorbance of molecule-DNA complex, respectively.  $\epsilon_M$  and  $\epsilon_{Com}$  represent

the absorption coefficients of the molecule and its complex with DNA.  $K$  can be obtained in two ways: i) from the intercept-to-slope ratios of  $A_0/(A - A_0)$  vs.  $1/[DNA]$  plot, ii) from the intercept-to-slope ratios of the plot of  $[DNA]$  vs.  $[DNA]/(\epsilon_M - \epsilon_{Com})$ .

*Fluorescence spectroscopy.* The other most common method to study interactions between DNA and molecules is fluorescence spectroscopy. This method has advantages over other techniques

due to its high selectivity, sensitivity, and wide linear dynamic range. Compounds containing aromatic rings possess intense fluorescence [31, 45]. The fluorescence spectroscopy and techniques based on fluorescence, such as fluorescence quenching, can be used to determine the binding mode of interaction between DNA and small molecules. Commonly, the change in the intensity of drug fluorescence in the presence of different concentrations of DNA is investigated due to the lack of fluorescence in DNA.

Fluorescence emission strongly depends on the environment, and so, the spectral shifts of about 10 to 20 nm occur in the excitation and emission spectra of binding molecules because of fluorophore transfer from high polar environments to non-polar environments [46]. Moreover, a strong interaction between DNA and binding molecules can usually lead to an increase in fluorescence intensity significantly. Thus, the fluorescence intensity enhances usually, whereas molecules bind to DNA through intercalative mode (Figure 3A) [16].

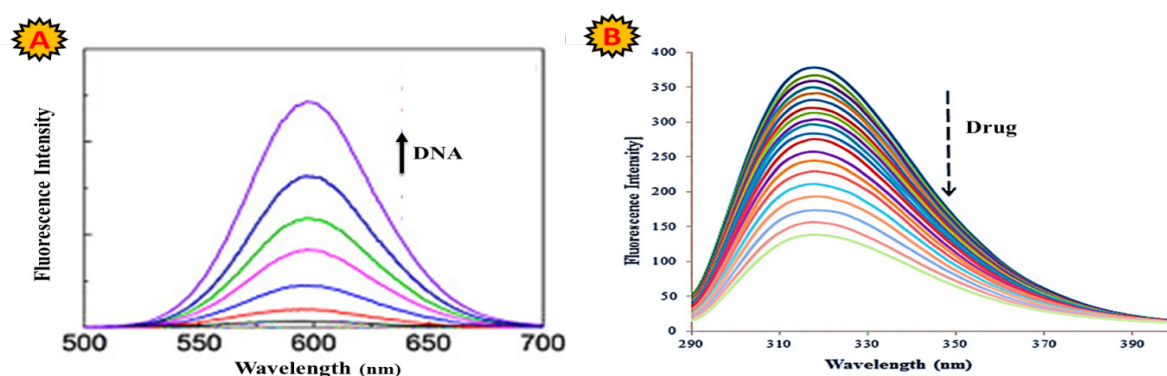


**Figure 3** – Investigating the interaction between DNA and drug using fluorescence spectroscopy related to (A) an intercalator, (B) a groove binder. It is reproduced from References [43] and [49]

It is noteworthy that when a molecule binds to the DNA groove, its fluorescence intensity decreases normally compared to before the binding to DNA (Figure 3B) [46-48].

Generally, the rotation of the molecule leads to fluorescence quenching. As intercalators incorporate into the DNA base stack, they induce a significant enhancement in the fluorescence emission.

## Results and discussion

A systematic review of articles about the interaction between natural heterocyclic compounds and DNA was conducted on the articles published from 2005 to 2022. Searches for related publications were carried out in Google scholar. This study aimed to provide practical guidance that helps researchers in the development of new drugs, especially drugs based on natural compounds. English-language original articles concerning heterocyclic compounds, natural

compounds, and the evaluation of DNA interaction were chosen. After reviewing the articles based on the title and abstract, selected full-text articles were read, and those fitted with the exclusion criteria were eliminated (Table 1).

Cancer is one of the main causes of mortality worldwide. This disease is characterized by the uncontrolled proliferation of organ cells, leading to metastasis [50]. The main aim of cancer researchers is to identify new strategies to reduce cancer treatment costs and patient suffering. Chemotherapy shows severe adverse effects such as the death of healthy cells, anemia, hair loss, etc. Also, many used medications are not effective and safe [51, 52].

Natural products and their derivatives possess a critical role in the development of chemotherapeutics due to their wide structural diversity, and pharmacological and molecular characteristics. They also reduce the side effects of chemo-radiotherapies [53, 54].

**Table 1** – Inclusion and exclusion criteria utilized in this study

Parameter	Inclusion criteria	Exclusion criteria
Language	English	Any other language
Type of publication	Original Articles	Conference articles, letters, or any other type of publication
Origin of compounds	Natural compounds	Synthetic compounds
Chemical structure	Heterocyclic compounds consisted of the single rings and fused rings.	Cyclic compounds without heteroatom

49% of all anticancer molecules approved between 1984 and 2014 were derived from natural products [55]. Note, plant-derived medicines are used in treating other degenerative diseases such as HIV/AIDS and diabetes [56].

One of the most important compounds in the innovation of new drugs is heterocyclic compounds, especially natural heterocyclic compounds. They possess unique properties, including antioxidant and anti-mutagenic properties. Also, heterocyclic compounds can effectively interact with DNA through different modes. This article has systematically

reviewed literature data on binding modes of complexes formed between the natural heterocyclic compounds and DNA. In this study, natural heterocyclic compounds were classified based on the number of their interactions with DNA as follows: single binders, dual binders, and multi binders.

*Single binders.* These compounds interact with DNA through only one binding mode. Natural compounds included in the single binders are alkaloids, flavonoids, diterpene, and carotenoids.

Figure 4 shows the structure of some of the single binders.

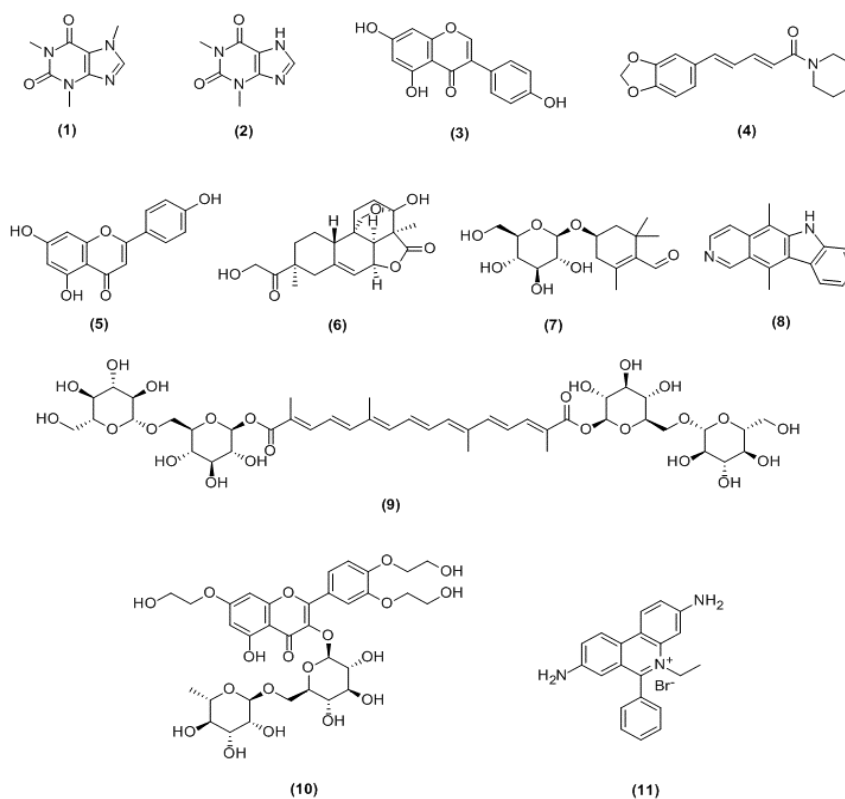


**Figure 4** – Structures of single natural binders described in the text: (1) caffeine, (2) theophylline, (3) genistein, (4) piperine, (5) apigenin, (6) annonalide, (7) picrocrocin, (8) ellipticine, (9) crocin, (10) troxertuin, (11) ethidium bromide

**Alkaloids.** These compounds are a group of nitrogen-containing compounds, naturally occurring organic compounds used as a rich source for drug discovery [57]. Most single natural binders are small alkaloids, including two to four rings, such as caffeine, theophylline, and ellipticine. Caffeine, and theophylline are alkaloids with two fused rings containing oxy and hydroxyl groups, as well as nitrogen atoms in heterocyclic rings. Nafisi et al. [58], studied the DNA interaction with theophylline and caffeine using UV-visible and FT-IR spectroscopies. The results showed that both compounds could form hydrogen binding to the A-T and G-C bases through their NH and C=O functional groups, and the groove binding mode was revealed for them. Piperine is the major alkaloid present in black pepper (Figure 4).

It possesses wide pharmacological activities, such as antimutagenic, anti-inflammatory, antioxidant, antitumor, antiapoptotic, antiarthritic antigenotoxic, antimicrobial, anti-HBV activities, etc. [59-61]. Haris et al. [62] studied the interaction mechanism between piperine and ctDNA using spectroscopy, DSC, melting, and simulation methods, for the first time. Since the UV-vis spectrum of ctDNA in the presence of piperine shows a hypochromic effect without any significant shift in the maximum wavelength (Figure 5A), it can be inferred that the DNA conformation remains unchanged. This indicates the groove binding mode between this natural alkaloid and ctDNA. Piperine exhibits a strong emission peak at 486 nm, which decayed in the presence of DNA (Figure 5B).

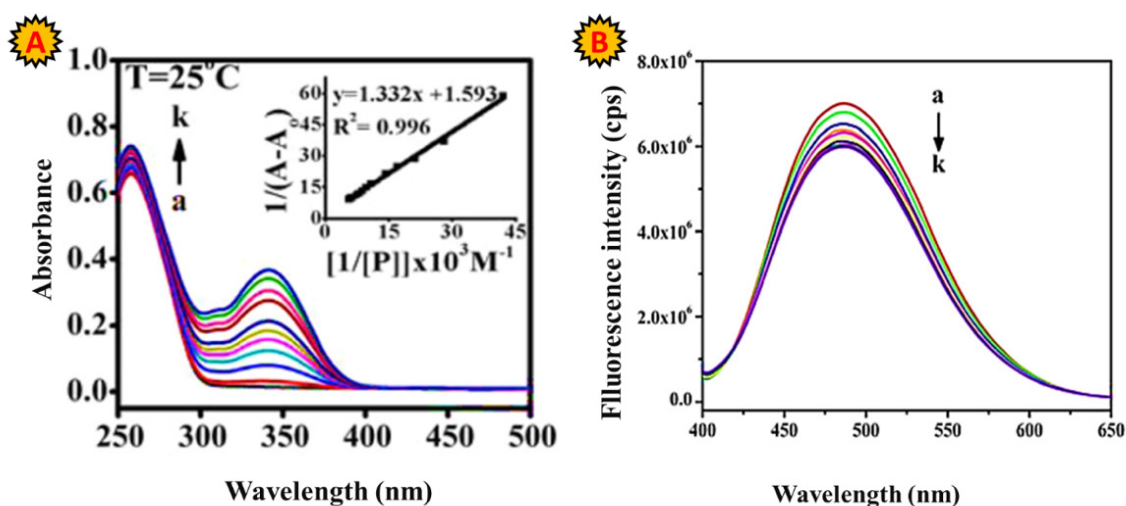


**Figure 5** – (A) UV-vis absorption spectra of ctDNA ( $100 \mu\text{mol L}^{-1}$ ) in the absence and presence of piperine ( $0\text{-}180.45 \mu\text{mol L}^{-1}$ ) in phosphate buffer solution (pH 7.0,  $100 \text{mmol L}^{-1}$  NaCl) at  $25 \text{ }^\circ\text{C}$ , (B) Fluorescence emission spectra of piperine ( $50 \times 10^{-5} \text{mol L}^{-1}$ ) in the presence of different concentrations of ctDNA ( $0\text{-}45.33 \times 10^{-6} \mu\text{mol L}^{-1}$ ) on excitation at  $342 \text{ nm}$ . Reproduced from the reference [62]

The emission quenching is an indication of the groove binding mode, and it confirms the results obtained by the UV-vis study. In this study, the results obtained from spectroscopy methods were agreement with those obtained from melting and DSC analysis. It was evident from the simulation studies that Piperine interacts with ctDNA through van der Waals and H-bonding. Ellipticine, a plant-derived alkaloid, consists of four fused rings (Figure 4). Owing to its planar structure, ellipticine acts as the intercalator and it stacks the DNA helix through interaction between its methyl groups and the thymine bases of DNA [63, 64].

**Flavonoids.** These compounds are the most abundant polyphenols found in plant-based products. Flavonoids are known to possess diverse pharmacological activities [65, 66]. They generally refer to a class of compounds formed by two phenyl rings and a heterocyclic containing oxygen atom. Most flavonoid compounds, such as genistein apigenin, and troxerutin, belong to the single binder group. Genistein is an important polyphenolic compound with anticancer property existed in our diet [67]. The interaction between genistein and DNA was investigated by Bocian et al. [68]. Their findings indicated that the phenyl ring A in the

genistein structure is not coplanar with other rings. Consequently, genistein is a DNA groove-binding molecule due to its non-planar structure. A hydrogen bond between hydroxyl groups of genistein and protons of cytidine NH is suggested (Figure 6).

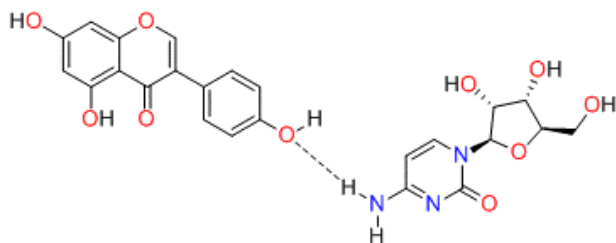


Figure 6 – The interaction between genistein and cytidine

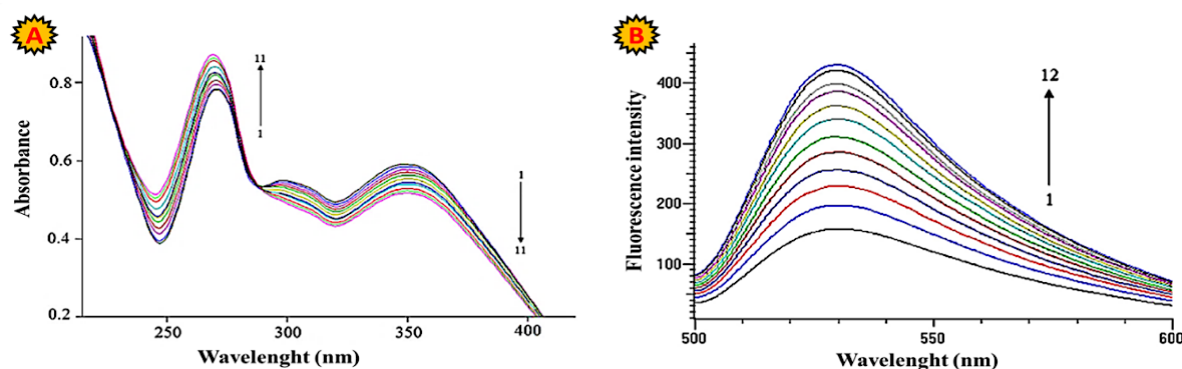


Figure 7 – (A) UV-vis absorption spectra of apigenin ( $9.10 \times 10^{-5} \text{ mol L}^{-1}$ ) in the absence and presence of DNA ( $0-8.33 \times 10^{-5} \text{ mol L}^{-1}$ ) at  $25 \text{ }^\circ\text{C}$ , (B) Fluorescence emission spectra of piperine ( $9.10 \times 10^{-5} \text{ mol L}^{-1}$ ) in the presence of different concentrations of ctDNA ( $0-4.76 \times 10^{-5} \text{ mol L}^{-1}$ ) at  $25 \text{ }^\circ\text{C}$ . It is reproduced from Ref. [70]

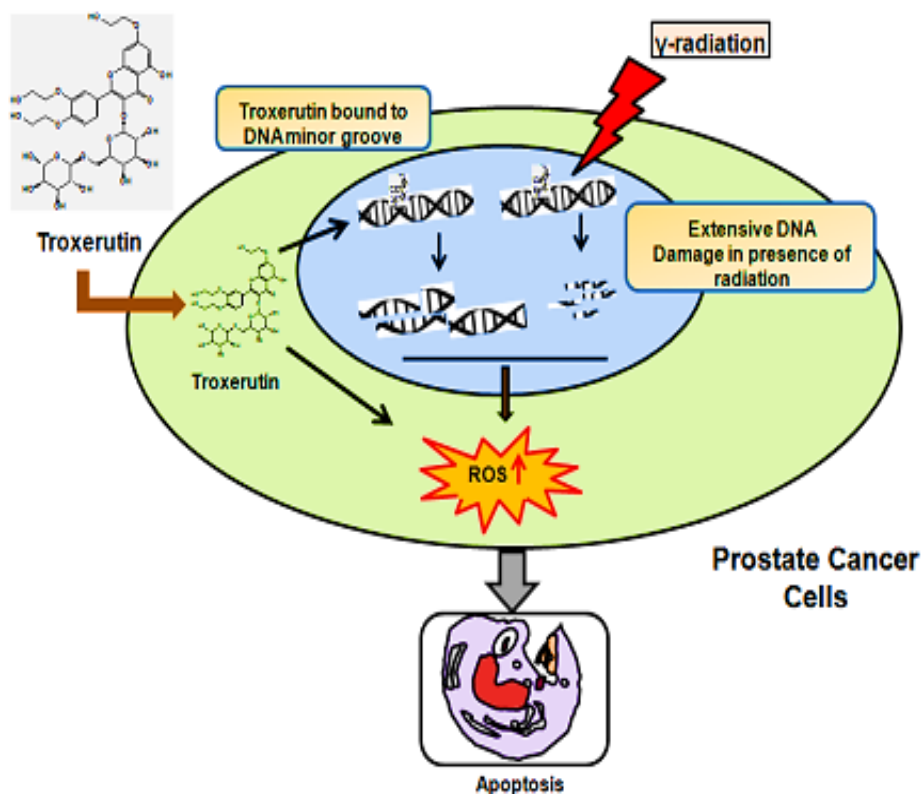
The intensity enhancement and bathochromic shift in the fluorescence emission upon molecule binding to DNA are the indicators of intercalative binding mode. The results obtained from DNA melting and viscosity measurements were consistent with the findings of fluorescence and UV-vis spectroscopies. Troxerutin is known to exhibit the radio-protective property. Panata et al. [71] reported that this flavonoid interacts with DNA through minor groove binding. They conducted competing experiments using EtBr and 4',6-diamidino-2-phenylindole (DAPI). A significant decrease in DPA fluorescence with increasing concentration of troxerutin confirmed troxerutin as a groove binder. The results of the MTT assay showed that this flavonoid could penetrate in the nucleus of cancer cells, break the DNA strand by binding to the minor grooves of DNA and induce cell death. The cytotoxicity effect of troxerutin was

enhanced in combination with gamma radiation (Scheme 1).

*Diterpene*. Annonalide (Figure 4), a pimarane-type diterpene, is also included in the class of single binders. This natural compound has attracted considerable interest because of its potential cytotoxic activity. Marques et al. [72] investigated the interaction of annonalide with DNA through fluorescence and computational studies. In this research, ethidium bromide (EB) (Figure 4) and Hoechst (HO) were used as the probes for fluorescent competition assays. EB is known as an intercalator that is widely used in competition assays. The free molecule of EB presents low emission, and when it intercalates DNA, a considerable enhancement occurs in its fluorescence emission. The presence of an intercalator in the medium can result in the displacement of EB, leading to a decrease in the

emission intensity of EB. HO is a groove binder, and the principle of its function in the competition assay is similar to EB. The spectrofluorometric titration of EB with DNA in the presence ofannonalide indicated that this natural compound binds to DNA through intercalation mode. The spectroscopic

results were confirmed by computational studies. So,annonalide is a typical DNA intercalator because it does not have the structure of general intercalators, including planarity. According to docking results, van der Walls is the main interaction between DNA andannonalide.



**Scheme 1** – The cytotoxicity effect of troxerutin in prostate cancer cells alone and in combination with  $\gamma$ -radiation. Reproduced from the reference [71]

*Carotenoids and other bioactive compounds.* Carotenoids are a large group of pigments found in animals, plants, and microorganisms [73]. They are identified with several biological functions [74]. Crocin, and picrocrocin are the studied-DNA binding molecules found in saffron (Figure 4). The studies indicated that these compounds are DNA groove binders [6, 75]. Crocin is one of the important natural carotenoids of saffron that are responsible for the anticancer property of this plant-based product [6]. Picrocrocin is a glycoside that plays a critical

role in the taste formation of saffron [76]. Bathaie et al., [6, 75] studied the interaction between important saffron carotenoids, such as crocin and picrocrocin, using spectroscopies methods. The results obtained in this study revealed that these carotenoids bind to DNA through minor groove binding due to the lack of a planar ring.

*Dual binders.* Large alkaloids, such as vincristine, are included in the category of Dual binders. The structure of dual binders studied in this review is displayed on Figure 8.

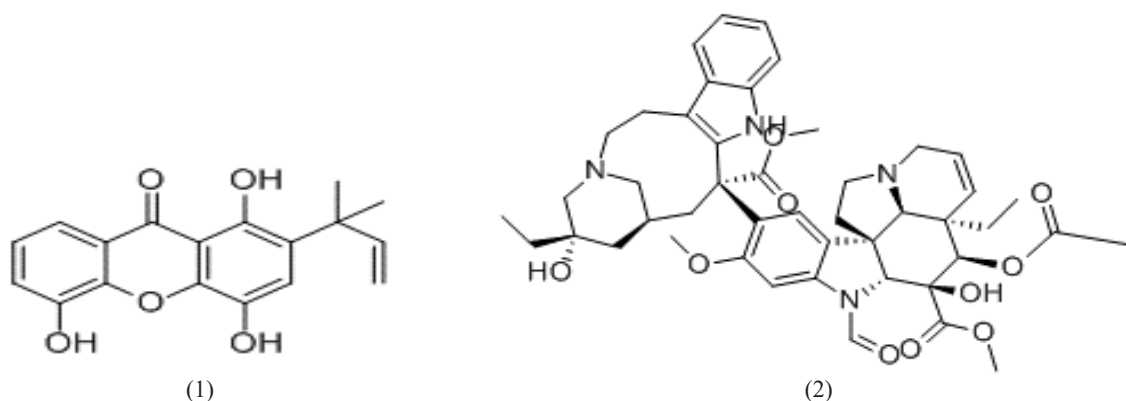


**Figure 8** – Structures of natural dual binders described in the text:  
(1) 12b-hydroxy-des-D-garcigerin, (2) vincristine

Vincristine is a natural plant alkaloid used widely for cancer therapy [77-79]. Hence, studying the mechanism of its interaction with DNA is biologically important. Tyagi et al. [80] studied the binding mode of vincristine to DNA using spectroscopic methods. The binding of vincristine to DNA caused a hypochromic effect accompanied by a bathochromic shift in the absorption of vincristine, indicating that it intercalates DNA. The results of FT-IR proposed that vincristine can also bind to DNA through guanine and cytosine, as well as phosphate backbone. Consequently, vincristine interacts with the DNA helix via external and intercalative binding modes. A few years later, Mohammadgholi et al. [81] confirmed these results.

*Xanthones* are a vast group of natural heterocyclic compounds known to have a wide range of pharmacological activities [82-84]. Wu et al., [85] investigated the interaction between 12b-hydroxy-des-D-Garcigerin (GA) and DNA using the displacement assay. In this study, acridine orange was used as the intercalator probe in the spectroscopic methods. The titration of DNA with acridine orange in the presence of GA led to changes in the absorption spectrum of GA-DNA. As these changes were similar to that of acridine orange-DNA, it could be concluded that GA acted as an intercalator. The results obtained by spectrofluorimetry confirmed the spectrophotometric result. Scatchard analysis implied the interaction of GA with DNA through electrostatic interaction (backbone binding). Consequently, GA binds to DNA through dual binding modes, including intercalation and backbone binding.

*Multiple binders.* Quercetin (Figure 9) is a natural phenolic compound with promising bioactive effects, including anticancer, antioxidant, antidiabetic,

antimicrobial, etc. [86, 87]. Study on its interaction with DNA has gained prominence in recent years. Some researchers have regarded quercetin as the intercalator [88, 89]. With regard to their results, the planar structure of quercetin plays a critical role in its binding to DNA via intercalation. Others insist on groove binders or backbone binders [90, 91]. Hence, it can be concluded that quercetin can probably bind to DNA in several ways. It is proposed that the ability of this compound as the intercalator and groove binder is concentration-dependent [88]. It is worth highlighting that this compound preferably binds to the G base [92]. It strongly interacts with the protonated form of DNA through  $\pi$ -stacking and electrostatic interactions [91].

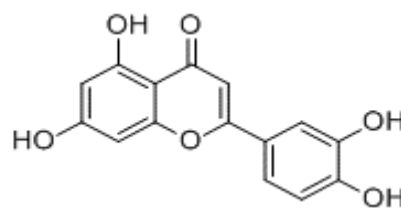


**Figure 9** – The structure of quercetin

Finally, the results of this study demonstrated that almost of natural heterocyclic compounds contain nitrogen, oxygen, or both heteroatoms. The non-planar heterocyclic compounds can form hydrogen bonding with DNA bases and act as groove binders. In the case of intercalation mode, it can be stated that this binding mode is stronger influenced by the planarity compared to the heteroatom type. It is worth noting that in all investigated studies, there was no information about the type effect of heteroatom on the interaction mode.



## Conclusion

Natural heterocyclic compounds have increasing interest in the biomedical field, especially cancer therapy, owing to their wide range of pharmaceutical properties. They exhibit different DNA binding modes. Basically, small natural heterocyclic molecules interact with DNA through two different modes: intercalation or groove binding. All studies included in this review revealed that planarity is the most important characteristic of heterocyclic compounds acting as the intercalator. The studies on large natural molecules have provided promising results about the interaction between DNA and these large molecules. Large molecules containing planar and non-planar parts in their structure can interact with DNA in more than one way. To investigate the binding modes, different techniques, including spectrometry methods, are employed. In the case of UV-vis spectroscopy, a significant increase in the absorption intensity (hyperchromism) and

redshift is typically observed for intercalation mode. In contrast, the decrease in the absorption intensity (hypochromism) is an indication of the electrostatic mode of interaction. In fluorescence spectroscopy, increasing the emission intensity is an indicator of intercalators, while decreasing the emission intensity is the indicative of groove binding and electrostatic modes. This systematic review revealed the great importance of natural heterocyclic compounds in the field of drug discovery, as well as their therapeutic potential and the mechanism of their interaction with DNA. This article and references can be helpful for researchers starting in this field.

## Acknowledgment

The authors gratefully acknowledge partial support for this work by the office of the Deputy of Research, Hamadan University of Medical Sciences (Grant number: 140008046329).

## References

1. Zaorsky, N.G., Zhang, Y., Tuanquin, L., Bluethmann, S.M., Park, H.S., and Chinchilli, V.M., (2019) Suicide among cancer patients. *Nat. Commun.* 10(1): pp. 1-7.
2. Pérez-Sánchez, A., Barrajón-Catalán, E., Ruiz-Torres, V., Agulló-Chazarra, L., Herranz-López, M., Valdés, A., Cifuentes, A., and Micol, V., (2019) Rosemary (*Rosmarinus officinalis*) extract causes ROS-induced necrotic cell death and inhibits tumor growth in vivo. *Sci. Rep.* 9(1): pp. 1-11.
3. Kaul, R., Risinger, A.L., and Mooberry, S.L., (2019) Microtubule-targeting drugs: more than antimetotics. *J. Nat. Prod.* 82(3): pp. 680-685.
4. Rejhová, A., Opatková, A., Čumová, A., Sliva, D., and Vodička, P., (2018) Natural compounds and combination therapy in colorectal cancer treatment. *Eur. J. Med. Chem.* 144: pp. 582-594.
5. Fabricant, D.S. and Farnsworth, N.R., (2001) The value of plants used in traditional medicine for drug discovery. *Environ. Health Perspect.* 109(suppl 1): pp. 69-75.
6. Bhatia, P., Sharma, A., George, A.J., Anvitha, D., Kumar, P., Dwivedi, V.P., and Chandra, N.S., (2021) Antibacterial activity of medicinal plants against ESKAPE: An update. *Heliyon.* 7(2): pp. e06310.
7. Cragg, G.M. and Newman, D.J., (2013) Natural products: a continuing source of novel drug leads. *Biochim. Biophys. Acta – Gen. Subj.* 1830(6): pp. 3670-3695.
8. Chang, C.W., Sung, H.L., Lee, C.R., and Lee, G.H., (2023) Synthesis of aryl-functionalized, 1, 5-disubstituted 1, 2, 3-triazoles and derivatives by arylation of zwitterionic ruthenium triazoloto complexes. *Journal of the Chinese Chemical Society.* 70(5): pp. 1055-1064.
9. Oudi, M., Sanchooli Tazeh, K., Hazeri, N., Fatahpour, M., and Ahmadi, R., (2019) A convenient route toward one-pot multicomponent synthesis of spirochromenes and pyranopyrazoles accelerated via quinolinic acid. *Journal of the Chinese Chemical Society.* 66(12): pp. 1721-1728.
10. Wu, Y.-J., *Heterocycles and medicine: a survey of the heterocyclic drugs approved by the US FDA from 2000 to present*, in *Progress in Heterocyclic Chemistry.* 2012, Elsevier. p. 1-53.
11. Sajjadifar, S., Zolfigol, M.A., Chehardoli, G., and Miri, S., (2013) Quinoxaline II. A practical efficient and rapid synthesis of new quinoxalines catalyzed by citric acid as a trifunctional Bronsted acid at room temperature under green condition. *Int. J. Chemtech Res.* 5(1): pp. 422-429.
12. Mallinger, A., Schiemann, K., Rink, C., Stieber, F., Calderini, M., Crumpler, S., Stubbs, M., Adeniji-Popoola, O., Poeschke, O., and Busch, M., (2016) Discovery of potent, selective, and orally bioavailable small-molecule modulators of the mediator complex-associated kinases CDK8 and CDK19. *J. Med. Chem.* 59(3): pp. 1078-1101.
13. Bahmani, A., Najafi, Z., and Chehardoli, G., (2022) Curcumin-Derived Heterocycles as Anticancer Agents. A Systematic Review. *Org Prep Proced Int* 54(6): pp. 493-510.
14. Ebadi, A., Najafi, Z., Pakdel-yeganeh, H., Dastan, D., and Chehardoli, G., (2022) Design, synthesis, molecular modeling and DNA-binding studies of new barbituric acid derivatives. *JICS:* pp. 1-12.

15. Chehardoli, G. and Bahmani, A., (2021) Synthetic strategies, SAR studies, and computer modeling of indole 2 and 3-carboxamides as the strong enzyme inhibitors: a review. *Mol. Divers.* 25(1): pp. 535-550.
16. Sirajuddin, M., Ali, S., and Badshah, A., (2013) Drug–DNA interactions and their study by UV–Visible, fluorescence spectroscopies and cyclic voltametry. *J. Photochem. Photobiol.* 124: pp. 1-19.
17. Liu, H.-K. and Sadler, P.J., (2011) Metal complexes as DNA intercalators. *Acc. Chem. Res.* 44(5): pp. 349-359.
18. Rajski, S.R. and Williams, R.M., (1998) DNA cross-linking agents as antitumor drugs. *Chem. Rev.* 98(8): pp. 2723-2796.
19. Godzieba, M. and Ciesielski, S., (2020) Natural DNA intercalators as promising therapeutics for cancer and Infectious diseases. *Curr. Cancer Drug Targets.* 20(1): pp. 19-32.
20. Ni, Y., Lin, D., and Kokot, S., (2006) Synchronous fluorescence, UV–visible spectrophotometric, and voltammetric studies of the competitive interaction of bis (1, 10-phenanthroline) copper (II) complex and neutral red with DNA. *Anal. Biochem.* 352(2): pp. 231-242.
21. Silvestri, C. and Brodbelt, J.S., (2013) Tandem mass spectrometry for characterization of covalent adducts of DNA with anticancer therapeutics. *Mass Spectrom. Rev.* 32(4): pp. 247-266.
22. Rahman, A., O’Sullivan, P., and Rozas, I., (2019) Recent developments in compounds acting in the DNA minor groove. *MedChemComm.* 10(1): pp. 26-40.
23. Li, S., Cooper, V.R., Thonhauser, T., Lundqvist, B.I., and Langreth, D.C., (2009) Stacking interactions and DNA intercalation. *J. Phys. Chem. B.* 113(32): pp. 11166-11172.
24. Alniss, H.Y., (2018) Thermodynamics of DNA minor groove binders: perspective. *J. Med. Chem.* 62(2): pp. 385-402.
25. Cai, X., Gray Jr, P.J., and Von Hoff, D.D., (2009) DNA minor groove binders: back in the groove. *Cancer Treat. Rev.* 35(5): pp. 437-450.
26. Barrett, M.P., Gemmell, C.G., and Suckling, C.J., (2013) Minor groove binders as anti-infective agents. *Pharmacol. Ther.* 139(1): pp. 12-23.
27. Neidle, S., (2001) DNA minor-groove recognition by small molecules. *Nat. Prod. Rep.* 18(3): pp. 291-309.
28. Hanczyc, P., Rajchel-Mieldzióć, P., Feng, B., and Fita, P., (2021) Identification of thioflavin T binding modes to DNA: a structure-specific molecular probe for lasing applications. *J. Phys. Chem. Lett.* 12(22): pp. 5436-5442.
29. Bhadra, K. and Kumar, G.S., (2011) Interaction of berberine, palmatine, coralyne, and sanguinarine to quadruplex DNA: a comparative spectroscopic and calorimetric study. *Biochim. Biophys. Acta – Gen. Subj.* 1810(4): pp. 485-496.
30. Sun, H., Xiang, J., Liu, Y., Li, L., Li, Q., Xu, G., and Tang, Y., (2011) A stabilizing and denaturing dual-effect for natural polyamines interacting with G-quadruplexes depending on concentration. *Biochimie.* 93(8): pp. 1351-1356.
31. Jaumot, J. and Gargallo, R., (2012) Experimental methods for studying the interactions between G-quadruplex structures and ligands. *Curr. Pharm. Des.* 18(14): pp. 1900-1916.
32. Wei, C., Wang, J., and Zhang, M., (2010) Spectroscopic study on the binding of porphyrins to (G4T4G4) 4 parallel G-quadruplex. *Biophys. Chem.* 148(1-3): pp. 51-55.
33. Kapp, L.E., Schutte-Smith, M., Twigge, L., and Visser, H.G., (2022) Synthesis, characterization and DNA binding of four imidazo [4, 5-f] 1, 10-phenanthroline derivatives. *J. Mol. Struct.* 1247: pp. 131235.
34. Rajalakshmi, S., Weyhermüller, T., Freddy, A.J., Vasanthi, H.R., and Nair, B.U., (2011) Anomalous behavior of pentacoordinate copper complexes of dimethylphenanthroline and derivatives of terpyridine ligands: Studies on DNA binding, cleavage and apoptotic activity. *Eur. J. Med. Chem.* 46(2): pp. 608-617.
35. Ariffin, E.Y., Zakariah, E.I., Ruslin, F., Kassim, M., Yamin, B.M., Heng, L.Y., and Hasbullah, S.A., (2021) Hexaferrocenium tri [hexa (isothiocyanato) iron (III)] trihydroxonium complex as a new DNA intercalator for electrochemical DNA biosensor. *Sci. Rep.* 11(1): pp. 1-14.
36. Eshkourfu, R., Čobeljić, B., Vujčić, M., Turel, I., Pevec, A., Sepčić, K., Zec, M., Radulović, S., Srdić-Radić, T., and Mitić, D., (2011) Synthesis, characterization, cytotoxic activity and DNA binding properties of the novel dinuclear cobalt (III) complex with the condensation product of 2-acetylpyridine and malonic acid dihydrazide. *J. Inorg. Biochem.* 105(9): pp. 1196-1203.
37. Dehkordi, M.F., Dehghan, G., Mahdavi, M., and Feizi, M.A.H., (2015) Multispectral studies of DNA binding, antioxidant and cytotoxic activities of a new pyranochromene derivative. *Spectrochim. Acta A Mol. Biomol. Spectrosc.* 145: pp. 353-359.
38. Lingthoingambi, N., Singh, N.R., and Damayanti, M., (2011) DNA interaction and biological activities of copper (II) complexes of alkylamidio-O-methylurea. *J. Chem. Pharm. Res.* 3(6): pp. 187-194.
39. Hasanzadeh, M. and Shadjou, N., (2016) Pharmacogenomic study using bio-and nanobioelectrochemistry: Drug–DNA interaction. *Mater. Sci. Eng. C.* 61: pp. 1002-1017.
40. Nimal, R., Unal, D.N., Erkmen, C., Bozal-Palabiyik, B., Siddiq, M., Eren, G., Shah, A., and Uslu, B., (2022) Development of the electrochemical, spectroscopic and molecular docking approaches toward the investigation of interaction between DNA and anti-leukemic drug azacytidine. *Bioelectrochemistry*: pp. 108135.
41. Moradi, S.Z., Nowroozi, A., Sadrjavadi, K., Moradi, S., Mansouri, K., Hosseinzadeh, L., and Shahlaei, M., (2018) Direct evidences for the groove binding of the Clomifene to double stranded DNA. *Int. J. Biol. Macromol.* 114: pp. 40-53.
42. Ryan, G.J., Elmes, R.B., Quinn, S.J., and Gunnlaugsson, T., (2012) Synthesis and photophysical evaluations of fluorescent quaternary bipyridyl-1, 8-naphthalimide conjugates as nucleic acid targeting agents. *Supramol. Chem.* 24(3): pp. 175-188.
43. Shahabadi, N. and Maghsudi, M., (2014) Multi-spectroscopic and molecular modeling studies on the interaction of antihypertensive drug; methyl dopa with calf thymus DNA. *Mol. Biosyst.* 10(2): pp. 338-347.
44. Benesi, H.A. and Hildebrand, J., (1949) A spectrophotometric investigation of the interaction of iodine with aromatic hydrocarbons. *J. Am. Chem. Soc.* 71(8): pp. 2703-2707.
45. Lakowicz, J.R., Principles of fluorescence spectroscopy. 2006: Springer.





46. Suh, D. and Chaires, J.B., (1995) Criteria for the mode of binding of DNA binding agents. *Bioorg. Med. Chem.* 3(6): pp. 723-728.
47. Hussain, I., Fatima, S., Siddiqui, S., Ahmed, S., and Tabish, M., (2021) Exploring the binding mechanism of  $\beta$ -resorcylic acid with calf thymus DNA: Insights from multi-spectroscopic, thermodynamic and bioinformatics approaches. *Spectrochim. Acta A Mol. Biomol. Spectrosc.* 260: pp. 119952.
48. Banerjee, A., Singh, J., and Dasgupta, D., (2013) Fluorescence spectroscopic and calorimetry based approaches to characterize the mode of interaction of small molecules with DNA. *J. Fluoresc.* 23(4): pp. 745-752.
49. Suzuki, Y. and Kawabe, Y., (2017) Fluorescence enhancement of hemicyanines bound to DNA or DNA-complex and their application to dye laser. *Opt. Mater. Express.* 7(6): pp. 2062-2068.
50. Bhatia, S., Gokhale, P., Katte, T., Acharya, S., Rasalkar, A.A., Vidapanakal, S., Manas, R., Chinnam, S., Narayanan, P., and Shettihalli, A.K., (2022) Assessing the Vulnerability of Cancer Patients for COVID-19. *ACS omega.*
51. Majolo, F., Delwing, L.K.d.O.B., Marmitt, D.J., Bustamante-Filho, I.C., and Goettert, M.I., (2019) Medicinal plants and bioactive natural compounds for cancer treatment: Important advances for drug discovery. *Phytochem. Lett.* 31: pp. 196-207.
52. Amjad, E., Sokouti, B., and Asnaashari, S., (2022) A systematic review of anti-cancer roles and mechanisms of kaempferol as a natural compound. *Cancer Cell Int.* 22(1): pp. 1-22.
53. Amjad, E., Sokouti, B., and Asnaashari, S., (2022) An investigation of 6-Shogaol effects on MCF7 cell lines through a systems biology approach. *Egypt. J. Med. Hum. Genet.* 23(1): pp. 1-19.
54. Pan, L., Chai, H.-B., and Kinghorn, A.D., (2012) Discovery of new anticancer agents from higher plants. *Front Biosci (Schol Ed)* 4: pp. 142.
55. Newman, D.J. and Cragg, G.M., (2016) Natural products as sources of new drugs from 1981 to 2014. *J. Nat. Prod.* 79(3): pp. 629-661.
56. Thomford, N.E., Senthane, D.A., Rowe, A., Munro, D., Seele, P., Maroyi, A., and Dzobo, K., (2018) Natural products for drug discovery in the 21st century: innovations for novel drug discovery. *Int. J. Mol. Sci.* 19(6): pp. 1578.
57. Debnath, B., Singh, W.S., Das, M., Goswami, S., Singh, M.K., Maiti, D., and Manna, K., (2018) Role of plant alkaloids on human health: A review of biological activities. *Mater. Today Chem.* 9: pp. 56-72.
58. Nafisi, S., Manouchehri, F., Tajmir-Riahi, H.-A., and Varavipour, M., (2008) Structural features of DNA interaction with caffeine and theophylline. *J. Mol. Struct.* 875(1-3): pp. 392-399.
59. Shrivastava, P., Vaibhav, K., Tabassum, R., Khan, A., Ishrat, T., Khan, M.M., Ahmad, A., Islam, F., Safhi, M.M., and Islam, F., (2013) Anti-apoptotic and anti-inflammatory effect of Piperine on 6-OHDA induced Parkinson's rat model. *J. Nutr. Biochem.* 24(4): pp. 680-687.
60. Murunikkara, V., Pragasam, S.J., Kodandaraman, G., Sabina, E.P., and Rasool, M., (2012) Anti-inflammatory effect of piperine in adjuvant-induced arthritic rats—a biochemical approach. *Inflamm.* 35(4): pp. 1348-1356.
61. Haq, I.U., Imran, M., Nadeem, M., Tufail, T., Gondal, T.A., and Mubarak, M.S., (2021) Piperine: A review of its biological effects. *Phytother. Res.* 35(2): pp. 680-700.
62. Haris, P., Mary, V., Haridas, M., and Sudarsanakumar, C., (2015) Energetics, thermodynamics, and molecular recognition of piperine with DNA. *J. Chem. Inf. Model.* 55(12): pp. 2644-2656.
63. Singh, M.P., Hill, G.C., Peoc'h, D., Rayner, B., Imbach, J.-L., and Lown, J.W., (1994) High-field NMR and restrained molecular modeling studies on a DNA heteroduplex containing a modified apurinic abasic site in the form of covalently linked 9-aminoellipticine. *Biochem.* 33(34): pp. 10271-10285.
64. Kizek, R., Adam, V., Hrabeta, J., Eckschlager, T., Smutny, S., Burda, J.V., Frei, E., and Stiborova, M., (2012) Anthracyclines and ellipticines as DNA-damaging anticancer drugs: recent advances. *Pharmacol. Ther.* 133(1): pp. 26-39.
65. Zhang, Z., Li, D., Luo, C., Huang, C., Qiu, R., Deng, Z., and Zhang, H., (2019) Cocrystals of natural products: Improving the dissolution performance of flavonoids using betaine. *Cryst. Growth Des.* 19(7): pp. 3851-3859.
66. Pei, R., Liu, X., and Bolling, B., (2020) Flavonoids and gut health. *Curr. Opin. Biotechnol.* 61: pp. 153-159.
67. Xie, Z., Luo, Y., Na, Z., Zhang, W., and Zong, Y., (2021) Synthesis and characterization of genistein magnetic molecularly imprinted polymers and their application in soy sauce products. *Sci. Rep.* 11(1): pp. 1-10.
68. Bocian, W., Kawęcki, R., Bednarek, E., Sitkowski, J., Ulkowska, A., and Kozerski, L., (2006) Interaction of flavonoid topoisomerase I and II inhibitors with DNA oligomers. *New J Chem.* 30(3): pp. 467-472.
69. Ono, M. and Fujimori, K., (2011) Antiadipogenic effect of dietary apigenin through activation of AMPK in 3T3-L1 cells. *J. Agric. Food Chem.* 59(24): pp. 13346-13352.
70. Zhang, S., Sun, X., Kong, R., and Xu, M., (2015) Studies on the interaction of apigenin with calf thymus DNA by spectroscopic methods. *Spectrochim. Acta A Mol. Biomol. Spectrosc.* 136: pp. 1666-1670.
71. Panat, N.A., Singh, B.G., Maurya, D.K., Sandur, S.K., and Ghaskadbi, S.S., (2016) Troxerutin, a natural flavonoid binds to DNA minor groove and enhances cancer cell killing in response to radiation. *Chem. Biol. Interact.* 251: pp. 34-44.
72. Marques, R.A., Gomes, A.O., de Brito, M.V., Dos Santos, A.L., da Silva, G.S., de Lima, L.B., Nunes, F.M., de Mattos, M.C., de Oliveira, F.C., and do Ó Pessoa, C., (2018) Annonalide and derivatives: Semisynthesis, cytotoxic activities and studies on interaction of annonalide with DNA. *J. Photochem. Photobiol. B, Biol.* 179: pp. 156-166.
73. Maoka, T., (2020) Carotenoids as natural functional pigments. *J. Nat. Med.* 74(1): pp. 1-16.
74. Seel, W., Baust, D., Sons, D., Albers, M., Eitzbach, L., Fuss, J., and Lipski, A., (2020) Carotenoids are used as regulators for membrane fluidity by *Staphylococcus xylosus*. *Sci. Rep.* 10(1): pp. 1-12.
75. Hoshyar, R., Bathaie, S.Z., and Ashrafi, M., (2008) Interaction of safranal and picrocrocin with ctDNA and their preferential mechanisms of binding to GC- and AT-rich oligonucleotides. *DNA Cell Biol.* 27(12): pp. 665-673.

76. Fernández, J.-A., (2004) Biology, biotechnology and biomedicine of saffron. *Trends Plant Sci.* : pp. 127-159.
77. Gomber, S., Dewan, P., and Chhonker, D., (2010) Vincristine induced neurotoxicity in cancer patients. *Indian J. Pediatr.* 77(1): pp. 97-100.
78. Barnett, S., Hellmann, F., Parke, E., Makin, G., Tweddle, D.A., Osborne, C., Hempel, G., and Veal, G.J., (2022) Vincristine dosing, drug exposure and therapeutic drug monitoring in neonate and infant cancer patients. *Eur. J. Cancer.* 164: pp. 127-136.
79. Mora, E., Smith, E.M.L., Donohoe, C., and Hertz, D.L., (2016) Vincristine-induced peripheral neuropathy in pediatric cancer patients. *Am. J. Cancer Res.* 6(11): pp. 2416.
80. Tyagi, G., Jangir, D.K., Singh, P., and Mehrotra, R., (2010) DNA interaction studies of an anticancer plant alkaloid, vincristine, using Fourier transform infrared spectroscopy. *DNA Cell Biol.* 29(11): pp. 693-699.
81. Mohammadgholi, A., Rabbani-Chadegani, A., and Fallah, S., (2013) Mechanism of the interaction of plant alkaloid vincristine with DNA and chromatin: spectroscopic study. *DNA Cell Biol.* 32(5): pp. 228-235.
82. Fernandes, C., Carraro, M.L., Ribeiro, J., Araújo, J., Tiritan, M.E., and Pinto, M.M., (2019) Synthetic chiral derivatives of xanthenes: Biological activities and enantioselectivity studies. *Molecules.* 24(4): pp. 791.
83. Ribeiro, J., Veloso, C., Fernandes, C., Tiritan, M.E., and Pinto, M.M., (2019) Carboxyxanthenes: Bioactive agents and molecular scaffold for synthesis of analogues and derivatives. *Molecules.* 24(1): pp. 180.
84. Klein-Júnior, L.C., Campos, A., Niero, R., Corrêa, R., Vander Heyden, Y., and Filho, V.C., (2020) Xanthenes and cancer: From natural sources to mechanisms of action. *Chem. Biodivers.* 17(2): pp. e1900499.
85. Wu, Y. and Yang, G., (2010) Interaction between Garcigenrin and DNA by spectrophotometry and fluorescence spectroscopy. *Spectrosc. Lett.* 43(1): pp. 28-35.
86. Salehi, B., Machin, L., Monzote, L., Sharifi-Rad, J., Ezzat, S.M., Salem, M.A., Merghany, R.M., El Mahdy, N.M., Kılıç, C.S., and Sytar, O., (2020) Therapeutic potential of quercetin: new insights and perspectives for human health. *ACS Omega.* 5(20): pp. 11849-11872.
87. Tang, S.-M., Deng, X.-T., Zhou, J., Li, Q.-P., Ge, X.-X., and Miao, L., (2020) Pharmacological basis and new insights of quercetin action in respect to its anti-cancer effects. *Biomed. Pharmacother.* 121: pp. 109604.
88. Das, A., Majumder, D., and Saha, C., (2017) Correlation of binding efficacies of DNA to flavonoids and their induced cellular damage. *J. Photochem. Photobiol. B, Biol.* 170: pp. 256-262.
89. Jana, B., Senapati, S., Ghosh, D., Bose, D., and Chattopadhyay, N., (2012) Spectroscopic exploration of mode of binding of ctDNA with 3-hydroxyflavone: a contrast to the mode of binding with flavonoids having additional hydroxyl groups. *J. Phys. Chem. B.* 116(1): pp. 639-645.
90. Mitrasinovic, P.M., (2015) Sequence-dependent binding of flavonoids to duplex DNA. *J. Chem. Inf. Model.* 55(2): pp. 421-433.
91. Pradhan, A.B., Haque, L., Bhuiya, S., Ganguly, A., and Das, S., (2015) Deciphering the positional influence of the hydroxyl group in the cinnamoyl part of 3-hydroxy flavonoids for structural modification and their interaction with the protonated and B form of calf thymus DNA using spectroscopic and molecular modeling studies. *J. Phys. Chem. B.* 119(23): pp. 6916-6929.
92. M Mitrasinovic, P., T Palakshan, P., Tripathi, S., and N Tripathi, A., (2013) On the affinity and specificity of quercetin for DNA. *Med. Chem.* 9(2): pp. 193-202.

#### **Information about authors**

Mahdie Kamalabadi – PhD, Researcher, Department of Medicinal Chemistry, School of Pharmacy, Medicinal Plants and Natural Products Research Center, Hamadan University of Medical Sciences, Headquarters, Shahid Fahmideh St. 6517838678, Hamadan, Iran, e-mail: mahdie.kamalabadi87@gmail.com

Gholamabbas Chehardoli – Professor, Department of Medicinal Chemistry, School of Pharmacy, Medicinal Plants and Natural Products Research Center, Hamadan University of Medical Sciences, Headquarters, Shahid Fahmideh St. 6517838678, Hamadan, Iran, e-mail: cheh1002@gmail.com

Zh.K. Batykova<sup>1\*</sup> , A.S. Kistaubayeva<sup>1</sup> ,  
I.S. Savitskaya<sup>1</sup> , V. Pidlisnyuk<sup>2</sup> 

<sup>1</sup>Al-Farabi Kazakh National University, Almaty, Kazakhstan

<sup>2</sup>Jan Evangelista Purkyně University, Ústí nad Labem, Czech Republic

\*e-mail: batyqova@gmail.com

(Received May 24, 2023; received in revised form November 28, 2023; accepted December 15, 2023)

## Isolation and study of plant growth promoting rhizobacteria from *Triticosecale Wittmack* growing in Almaty region

**Abstract.** This article presents data on isolation and characterization of native plant growth-promoting rhizobacteria (PGPR) from the rhizosphere and root-endosphere of X *Triticosecale Wittmack* growing in Almaty region. A total of 22 distinct (eighteen gram-negative and four gram-positive) bacterial isolates were identified, classified according to their spore-forming activity: eighteen non-spore-forming and four spore-forming bacteria. Bacterial isolates were screened *in vitro* for PGPR characteristics and evaluated for their beneficial effects on the early growth of triticale variety X *Triticosecale Wittmack*. The findings of our research indicated isolation of four growth-promoting bacteria (AS4, AS6, AR1, TS6), three antifungal bacteria (AR2 and AS7), and one strain of combined action, i.e. high growth-promoting and fungistatic activity (AR6). Research has demonstrated that PGPR can be utilized as biofertilizers for crop production. Study marks the beginning of a larger investigation into the bacterial diversity of the triticale variety X *Triticosecale Wittmack* in the Almaty region.

**Key words:** root-endosphere, rhizosphere, rhizobacteria, PGPR, growth stimulation.

### Introduction

Chemical fertilizers are widely used all over the world for delivery of indispensable nutrients to the soil-plant system. However, it is known that the price, availability and environmental impact of chemical fertilizing, especially nitrogen and phosphate fertilizing, especially nitrogen and phosphorus fertilizers, cause significant problems in modern agriculture [1]. Thus, there is an urgent need to identify alternative strategies that guarantee the yield of competitive crops and ensure ecological security, long-term environmental balance and sustainability within the framework of the agro-ecosystem.

Plant growth-promoting rhizobacteria (PGPR) are free-living soil microbes that aggressively colonize the rhizosphere and the roots of plants and, when applied to seeds or plants, enhance growth and yield of the plant. They have the ability to synthesize plant growth regulators. i.e., phytohormones, including indoleacetic acid (IAA), cytokinins, and gibberellins [2]; realize the possibility of strengthening the nitrogen (N<sub>2</sub>) fixation process [3]; are able to decompose inorganic phosphate and mineralize organic

phosphorus and other nutrients [4]; can synthesize siderophores necessary for plant metabolism; are able to synthesize antibiotics, enzymes and fungicidal compounds and develop antagonistic effect against phytopathogenic microorganisms due to competition with harmful microorganisms [5].

Positive effects of rhizobacteria can be observed in a multitude of ways in various crops [6-8]. For example, one of the most crucial plant growth-promoting effects of *Pseudomonas* was observed in a notable enhancement of the root biomass (20-46%) [7]. Use of *Azotobacter* as a biofertilizer has been shown to reduce the amount of chemical fertilizer required per hectare by 21-31 kg of nitrogen per hectare [8].

Understanding the indigenous bacterial population, its characteristics, ability to identify native bacteria in a given location is crucial for understanding how they are distributed and their diversity in the rhizosphere of specific crops [9, 10]. Microbial strains that are specific to a particular region can be employed as a growth-promoting inoculum in order to achieve the desired yield. Triticale is a multipurpose crop used for forage,

grain, and ethanol production. The grain can be used for human consumption or animal feed [11, 12].

### Materials and methods

In September 2022, the isolation of rhizobacteria from agricultural cereal crop rhizosphere communities was conducted. The study focused on the isolation of rhizospheric bacteria from the rhizosphere of cultivated cereal plants, specifically rye and wheat amphidiploid (*X Triticosecale* Wittmack). The triticale samples were obtained from the Kazakh Scientific Research Institute of Agriculture and Plant Production, located in the Karasay district of Almaty region. The plants were uprooted and a clod of soil was removed, after which they were placed in clean plastic bags and transported to the laboratory.

**Agrochemical soil analysis.** The preparation of the analyzed samples involves weighing them on a balance with an accuracy of  $\pm 0.0001$  g. Prepared samples are then placed in the chamber for irradiation by the X-ray fluorescence spectrometer, ensuring that they are not contaminated [13]. The instrument used in this analysis was the Focus M at the Faculty of Chemistry and Chemical Technology of al-Farabi Kazakh National University. The resulting spectrum of intensities of the characteristic fluorescence of the elements being determined is processed using software according to pre-installed calibration, content of macroelement oxides, expressed in mass percent, and the content of trace elements, expressed in mg/kg of the sample, are estimated [13]. Each sample is subjected to analysis once, with the sample placed within the X-ray fluorescence spectrometer irradiation chamber. The results are then averaged.

**Isolation of rhizosphere bacteria.** The isolation of microorganisms was conducted as follows. A soil suspension was prepared to isolate PSBs from a dilution cascade. For this purpose, 10 g of rhizosphere soil were suspended in 100 mL of sterile phosphate-buffered saline (PBS) solution (pH 7.2) and shaken at 190 rpm for 45 minutes [14]. Subsequently, serial dilutions were prepared to  $10^{-9}$ . Approximately 100  $\mu$ L of each dilution was placed on sterile Luria Bertani (LB) agar medium (Himedia, India). The medium was prepared by dissolving 10 g tryptone, 5 g yeast extract, 5 g NaCl, and 20 g agarose in 1 000 ml of distilled water. Subsequently, the pH of the medium was adjusted to 7.0. LB agar plates were incubated for 3 days at 28 °C. Single colonies were picked up and streaked on sterile LB agar plates to obtain pure cultures. Well-isolated colonies were observed for morphological characterization.

**Isolation of endophytic bacteria.** To isolate endophytic bacteria, the roots of the sample were thoroughly washed with running tap water for 10 min to remove adherent soil particles. The roots were disinfected with 70% ethanol for 1 min and then washed three times with sterile distilled water. Then the roots were surface sterilized with 3% sodium hypochlorite solution for 10 min and washed six times with sterile distilled water [16]. Then 1 g of surface sterilized root tissue was macerated with a sterilized mortar and pestle in 10 ml phosphate buffered saline (PBS), serial dilutions were prepared and 1 ml of tissue extract and diluents were applied to LB medium [17]. The plates were incubated at 28°C and monitored for the development of bacterial colonies within 2-3 days.

**Fungistatic activity of isolated bacteria.** The fungistatic activity of isolated bacteria was determined on Sabouraud's medium. The phytopathogenic fungus *Fusarium graminearum*, the causal agent of Fusarium ear blight, was selected as the test organism. The antifungal effect was quantified by measuring the width of the inhibition zones around the wells over a period of 4-5 days [18].

**Estimation of IAA phytohormone content.** The quantity of indole-3-acetic acid (IAA) produced by microorganisms was quantified using a colorimetric method with Salkowski's reagent. 1 ml of the supernatant (filtrate) was combined with 2 ml of Salkovsky reagent, which is a solution composed of 1 ml of 0.5 M  $\text{FeCl}_3$  in 50 ml of 35% HCl [19]. The color development time was approximately 30 to 40 minutes. The optical density of the colored samples was quantified on a spectrophotometer at a wavelength of 540 nm. The control was an uninoculated medium to which a reagent was added. The concentration of IAA was determined according to a calibration curve constructed in the concentration range of the substance of  $10^{-8}$  to  $10^{-2}$  g/l. IAA content was expressed in  $\mu\text{g/ml}$ .

**Determination of growth-promoting activity was developed via an inoculation of triticale seeds.** The impact of bacterial inoculation on the growth of triticale was evaluated through an experiment conducted in accordance with the conditions of the laboratory setting. The triticale seeds were subjected to surface sterilization with a 2% sodium hypochlorite solution for a period of 15 minutes, after which they were washed five times with sterile water. Subsequently, the inoculated seeds were transferred to test tubes containing the relevant strains. A series of cultures were established by inoculating 50-ml Falcon tubes with 25 ml of LB broth and maintaining

them at 200 rpm for 16 hours on a shaker. Subsequent to this period of growth, the cultures were inoculated onto water agar plates in order to permit germination of the seeds. The control consisted of seeds that had not been inoculated. After 14 days, the length of the shoots and roots was recorded [21].

## Results and their discussion

*Agrochemical soil analysis.* The results of quantitative analysis of the content of trace elements in the soil adjacent to the triticale variety X Triticosecale Wittmack are presented in Table 1.

**Table 1** – Trace elements in the soil of X Triticosecale Wittmacktriticale variety

No.	Elements	Concentration, %	Intensity, %
1	Ca	8.928	18.17
2	Ti	1.738	10.23
3	Mn	0.653	718.43
4	Fe	44.781	17.81
5	K	6.837	1.79
6	Si	26.969	0.18
7	Al	9.247	0.47
8	Cr	0.030	3.63
9	Zn	0.342	1.54
10	Sr	0.164	2.95
11	Rb	0.295	3.00
12	V	0.045	18.17

Table 1 indicates that iron (Fe), silicon (Si), aluminum (Al), potassium (K) and calcium (Ca) are prevailing in soil adjacent to X Triticosecale Wittmack.

*Isolation of rhizosphere bacteria.* Pure cultures of the bacteria were isolated from the rhizosphere of triticale. A total of 22 bacteria were isolated from rhizosphere soil of triticale. The bacteria showed colonies of various sizes and margins, ranging from white to milky white, on LB agar plates. The cells were highly motile and rod-shaped. Among the 22 bacterial isolates, 18 were identified as gram-negative, 4 as gram-positive bacteria, and 18 as non-spore-forming and 4 as spore-forming bacteria based on their spore-forming activity.

*Fungistatic activity of strains of rhizophilic bacteria.* Of the total number of 22 bacterial strains tested, only three exhibited notable antagonistic activity against the fungus *Fusarium graminearum*, with the highest inhibition of fungal growth observed at 10-12 mm in strains AS4 and AR6, indicating a high degree of antifungal activity. The AS7

strains exhibited a weak, fungistatic effect, with suppression zones found to be within 1-6 mm, while the remaining 19 strains exhibited no effect on the growth of *Fusarium graminearum*. However, they demonstrated tolerance to the fungus, with the wells remaining unovergrown with mycelium.

*Amount of phytohormone IAA determination.* The rhizobacteria under study exhibited a high level of IAA production, with a maximum observed concentration of 194.99 µg/ml (Table 2).

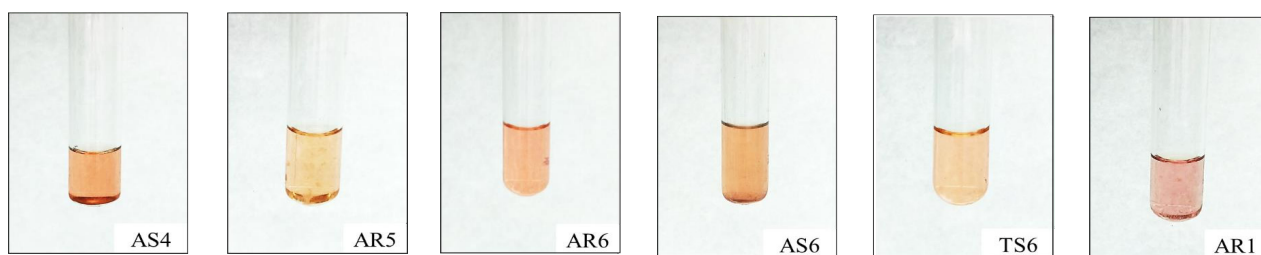
Eight of the 22 strains were found to synthesize more IAA, including those presented on Figure 1.

*Determination of growth-promoting activity.* The results of studies investigating the impact of distinct microbial isolates with varying characteristics on the growth and root development of triticale plants can be found in Table 3.

In addition, the data illustrates the disparate effects of the microbial culture fluid of various strains and its dilutions on the growth and maturation of diverse agricultural products, as depicted on Figures 2 and 3.

**Table 2** – Detection of phytohormone IAA produced by microbial strains

No.	Isolate	The amount of IAA, mcg/ml	No.	Isolate	The amount of IAA, mcg/ml
1	AS1	63.58±3.14	12	AR6	150.51±4.25
2	AS2	19.09±1.80	13	AS7	3.20±0.71
3	AS3	15.20±1.42	14	AR8	40.31±1.25
4	AS4	103.34±5.10	15	AR9	10.40±1.12
5	AS5	0	16	TS2	9.55±1.01
6	AS6	137.78±3.17	17	TS3	4.81±1.21
7	AR1	194.00±5.70	18	TS4	12.90±1.32
8	AR2	-	19	TS5	28.00±1.90
9	AR3	4.25±1.02	20	TS6	114.46±5.39
10	AR4	17.72±1.61	21	TS7	16.45±1.07
11	AR5	94.33±5.10	22	TR2	12.73±2.20

**Figure 1** – Strains with high IAA production**Table 3** – Stimulation of the growth of roots and seedlings of winter triticale by rhizobacteria, % of control

No.	Isolate	Dilution	Root length	Seedling length
1	AR1	CF	-0.9	+8.4
		1:10	+10.5	+12.2
		1:100	-13.1	-2.2
		1:1000	-	-
2	AR6	CF	-14.3	-18.2
		1:10	0	+11.6
		1:100	-15.2	+18.6
		1:1000	-	-
3	AR8	CF	+13.4	+21.4
		1:10	+6.2	+147.8
		1:100	+0.1	-9.5
		1:1000	-	-
4	TS2	CF	-8.3	-6.4
		1:10	-6.5	+3.4
		1:100	-2.0	-48.5
		1:1000	-	-
5	TS6	CF	+31.4	0
		1:10	+35.4	+21.8
		1:100	+11.8	+17.9
		1:1000	-	-
6	TS7	CF	+33.0	+7.4
		1:10	-3.4	-9.3
		1:100	+17.5	-8.3
		1:1000	-	-

\*CF – cultural fluid



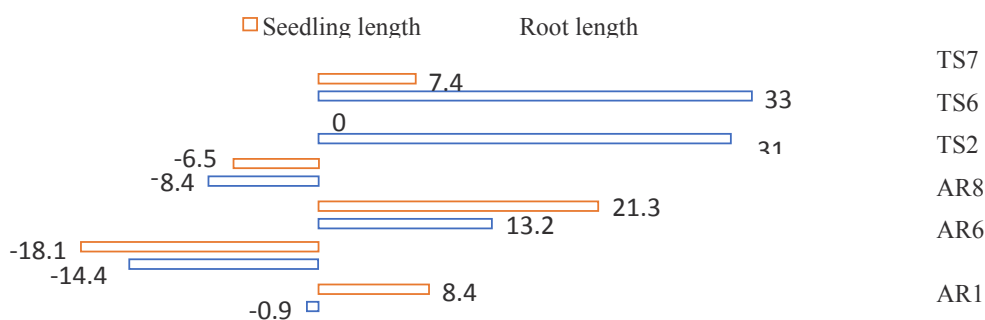


**Figure 2** – Stimulation of triticales roots and seedlings growth by rhizobacteria with dilution of cultural fluid

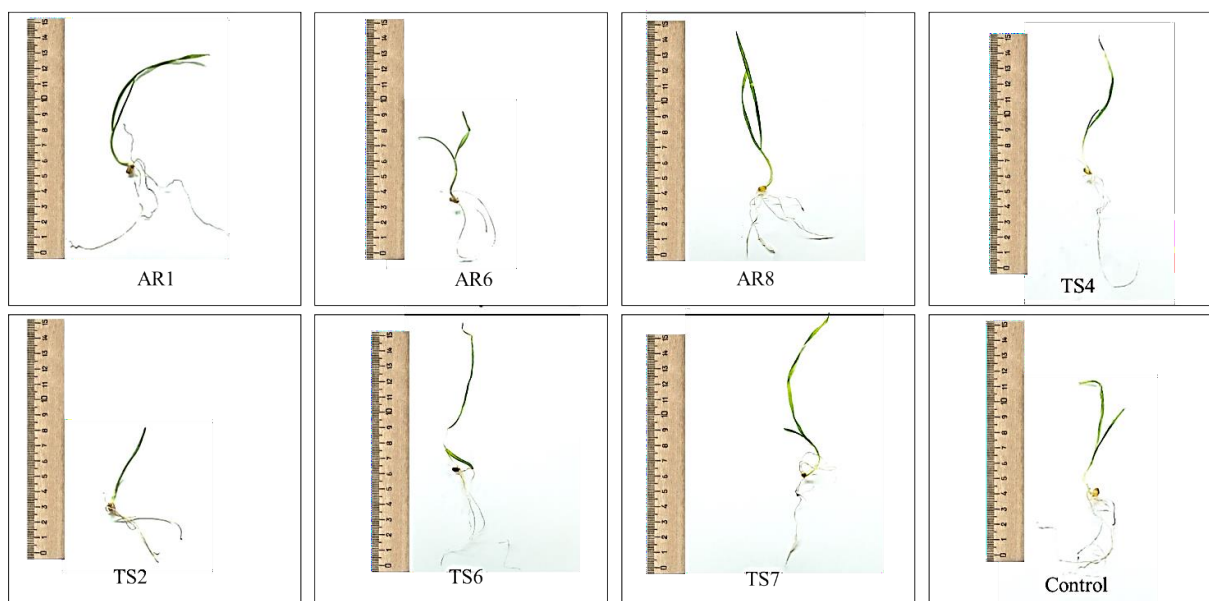


**Figure 3** – Measurement of triticales roots and seedlings growth on 14<sup>th</sup> day with dilution of cultural fluid

Development of above-the-ground and under-the-ground organs of winter triticales was most favorably affected by the cultural liquid and its 1:10 dilution of strains AR8, TS6, and AR1 and TS7. In other variants, the development of the culture was inhibited, with the exception of variant AR6.

### Conclusion

PGPR isolated from the triticales rhizosphere was reflected in their antifungal effect against *Fusarium graminearum*, which could potentially induce resistance of triticales plants. In examining the capacity of microorganisms to control the phytopathogen *Fusarium graminearum*, it was demonstrated that three strains were capable to

actively inhibit the growth of the phytopathogen, exhibiting fungistatic properties. These strains are AR6, AR2, and AS7. However, the antifungal activity of the AR2 strain was found to be particularly noteworthy, with a phytopathogen inhibition zone of  $12 \pm 0$  mm. In addition isolated rhizobacteria demonstrated the ability to synthesize the phytohormone auxin (IAA), which stimulates triticales growth, i.e. strains AS4 ( $103.33 \pm 5.10$   $\mu\text{g/ml}$ ), AS6 ( $137.77 \pm 3.16$   $\mu\text{g/ml}$ ), AR6 ( $150.49 \pm 4.23$   $\mu\text{g/ml}$ ), TS6 ( $114.45 \pm 5.37$   $\mu\text{g/ml}$ ) have the ability to synthesize phytohormones. The most prolific producer of IAA was strain AR1 ( $194.99 \pm 5.69$   $\mu\text{g/ml}$ ). An investigation into the impact of strains on the initial stages of plant growth and development revealed that the strains AR8, 38-22, TS6, AR1, and

TS7 had promoting effect on triticale growth and development. The findings of the studies indicate that five strains were identified as having growth-promoting properties (AS4, AS6, AR1, AR6, and TS6), three as having antifungal activity (AR2,

AR6, and AS7), and one as exhibiting combined effect (AR6). The outcomes of the studies serve as a foundation for the further utilisation of rhizophilic bacteria in a range of agricultural technology applications.

### References

- Olanrewaju O.S., Glick B.R., Babalola O.O. (2017) Mechanisms of action of plant growth promoting bacteria. *World J. Microbiol. Biotechnol.*, 33(11). doi: 10.1007/s11274-017-2364-9.
- Parray J.A., Jan S., Kamili A.N., Qadri R.A., Egamberdieva D., Ahmad P. (2016) Current perspectives on plant growth-promoting rhizobacteria. *J. Plant Growth Regul.*, 35; 877-902. doi: 10.1007/s00344-016-9583-4.
- Kumar A., Singh V.K., Tripathi V., Singh P.P., Singh A.K. (2018) Plant growth-promoting rhizobacteria (PGPR): Perspective in agriculture under biotic and abiotic stress. In: *New and future developments in microbial biotechnology and bioengineering, crop improvement through microbial biotechnology*, 333-342. Elsevier, ISBN 978-0-444-63987-5. <https://doi.org/10.1016/C2016-0-04330-9>
- Hakim S., Naqqash T., Nawaz M.S., Laraib I., Siddique M.J., Zia R., Mirza M.S., Imran A. (2021) Rhizosphere engineering with plant growth-promoting microorganisms for agriculture and ecological sustainability. *Front. Sustain. Food Syst.* 5:617157. doi: 10.3389/fsufs.2021.617157.
- Abbas R., Rasul S., Aslam K., Baber M., Shahid M., Mubeen F., et al. (2019) Halotolerant PGPR: a hope for cultivation of saline soils. *J. King Saud Univ.*, 31, 1195-1201. doi: 10.1016/j.jksus.2019.02.019
- Chang P., Gerhardt K.E., Huang X.-D., Yu X.-M., Glick B.R., Gerwing P.D., et al. (2014) Plant growth-promoting bacteria facilitate the growth of barley and oats in salt-impacted soil: implications for phytoremediation of saline soils. *Int. J. Phytoremediation*, 16; 1133-1147.
- Gaby J.C., Rishishwar L., Valderrama-Aguirre L.C., Green S.J., Valderrama-Aguirre A., Jordan I.K. (2018) Diazotroph community characterization via a high-throughput nifH amplicon sequencing and analysis pipeline. *Appl. Environ. Microbiol.*, 84(17). doi: 10.1128/AEM.01512-17
- Korir H., Mungai N.W., Thuita M., Hamba Y., Masso C. (2017) Co-inoculation effect of rhizobia and plant growth promoting rhizobacteria on common bean growth in a low phosphorus soil. *Front. Plant Sci.*, 8(141). doi: 10.3389/fpls.2017.00141
- Huang J., Liu Z., Li S., Xu B., Gong Y., Yang Y., Sun H. (2016) Isolation and engineering of plant growth promoting rhizobacteria *Pseudomonas aeruginosa* for enhanced cadmium bioremediation. *J Gen Appl Microbiol.*, 62(5); 258-265.
- Kuzyakov Y., Blagodatskaya E. (2015) Microbial hotspots and hot moments in soil: concept & review. *Soil Biol. Biochem.*, 83; 184-199.
- Brader G., Compant S., Vescio K., Mitter B., Trognitz F., Ma L.J. et al. (2017) Ecology and genomic insights into plant-pathogenic and plant-nonpathogenic endophytes. *Annu Rev Phytopathol.*, 55; 61-83.
- Liu Y., Chen L., Zhang N., Li Z., Zhang G., Xu Y., et al. (2016) Plant-microbe communication enhances auxin biosynthesis by a root-associated bacterium, *Bacillus amyloliquefaciens* SQR9. *Mol. Plant Microbe Interact.*, 29; 324-330. doi: 10.1094/MPMI-10-15-0239-R
- Enagbonma B.J., Fadiji A.E., Ayangbenro A.S., Babalola O.O. (2023) Communication between plants and rhizosphere microbiome: exploring the root microbiome for sustainable agriculture. *Microorganisms*, 11(8): 2003. doi: 10.3390/microorganisms11082003.
- Freitas T., Furtado N., Bastos J., Said S. (2002) Active substances against trypomastigote forms of *Trypanosoma cruzi* and microorganisms are produced in sequence by *Talaromyces flavus*. *Microbiol. Res.*, 157: 201-206.
- Chanda S., Rakholiya K., Parekh J. (2013) Indian medicinal herb: antimicrobial efficacy of *Mesua ferrea* L. seed extracted in different solvents against infection causing pathogenic strains. *J Acute Dis.*, 2: 277-281.
- Manikkam R., Venugopal G., Subramaniam B., Ramasamy B., Kumar V. (2014) Bioactive potential of actinomycetes from less explored ecosystems against *Mycobacterium tuberculosis* and other nonmycobacterial pathogens. *Int Sch Res Notices.*, 1-9.
- Tihonovich I., Provorov N. (2011) Sel'skohozyajstvennaya mikrobiologiya kak osnova ekologicheskii ustojchivogo agroproduktstva: fundamental'nye i prikladnye aspekty [Agricultural microbiology as basis of environmentally stable agroproduction: fundamental and applied aspects]. *Sel'skohozyajstvennaya biologiya*, 3; 3-9.
- Taechowisan T. (2003) Isolation of endophytic actinomycetes from selected plants and their antifungal activity. *World J Microbiol Biotechnol.*, 19; 381-385.
- Qin S., Chen H., Klenk H. (2009) *Glycomyces scopariae* sp. nov. and *Glycomyces mayteni* sp. nov., isolated from two medicinal plants in China. *Int J Syst Evol Microbiol.*, 59; 1023-1027.
- Gohain A., Gogoi A., Debnath R. (2015) Antimicrobial biosynthetic potential and genetic diversity of endophytic actinomycetes associated with medicinal plants. *FEMS Microbiology Letters* 362, no. 19: fnv158
- Weaver R.W., Frederick L.R. (1982) Rhizobium, In: *Methods of Soil Analysis, Part 2. Chemical and Microbiological Properties*, eds A.L. Page, R.H. Miller, D.R. Keeney (Madison, WI: SSSA), 1043-1067.









**Information about authors:**

*Batykova Zhuldyz Kazbekovna (corresponding author) – PhD student at the Department of Biotechnology, al-Farabi Kazakh National University (Almaty, Kazakhstan, email: batygova@gmail.com)*

*Kistaubayeva Aida Serikovna – Head of the Department of Biotechnology, Candidate of Biological Sciences, Associate Professor, Department of Biotechnology, al-Farabi Kazakh National University (Almaty, Kazakhstan, email: kistaubayeva.kaznu@gmail.com)*

*Savitskaya Irina Stanislavovna – Doctor of Biological Sciences, Professor at the Department of Biotechnology, al-Farabi Kazakh National University (Almaty, Kazakhstan, email: irasava\_2006@mail.ru)*

*Valentina Pidlisnyuk – Professor of the Department of Environmental Chemistry and Technology, Faculty of Environment, Jan Evangelista Purkyně University (Usti nad Labem, Czech Republic, email: pidlisnyuk@gmail.com)*

J. Iqra , A. Shabbir , A. Hasnain , A. Iqra ,  
S. Muqadas , A. Sajid , K. Sheraz , Sh. Khurram\* 

University of Okara, Okara, Pakistan

\*e-mail: dr.khurram@uo.edu.pk

(Received 3 May 2024; received in revised form 12 May 2024; Accepted 28 May 2024)

## The potential ameliorative effects of *Moringa oleifera* in emamectin benzoate induced toxicity in freshwater *Labeo rohita* fish

**Abstract.** Emamectin benzoate pesticide (EMB) is life-threatening chemical causing harmful effects on aquatic organisms specially fish species. Current study was aimed to understand the ameliorative role of *Moringa oleifera* against the toxic effects of emamectin benzoate on hematological, biochemical and changes in the soft tissues of *Labeo rohita*. Four groups were made. First group without chemicals is the control group, while 2<sup>nd</sup>, 3<sup>rd</sup> and 4<sup>th</sup> groups were exposed to 3.64µg/L, 7.28µg/L and 14.56µg/L EMB respectively for 30 days. Results revealed that the number of RBCs, HGB, HCT, MCV, MCH, MCHC, and WBCs were decreased while lymphocytes, monocytes, eosinophils and platelets were increased significantly. Biochemical parameters of fish including serum cholesterol, triglycerides, LDL, VLDL, albumin, globulin, blood glucose, ALT, AST, TSH, urea, creatinine, and blood urea nitrogen were significantly increased while HDL, total protein, T3 and T4 were decreased. Histological changes revealed that EMB causes degenerative effects in soft tissues of exposed fish. After using *Moringa oleifera*, all the effects were reversed and the fish was moved towards recovery. The overall results of the study showed that emamectin benzoate can alter the histological, hematological, and biochemical processes of *Labeo rohita*, thus toxic to aquatic organisms.

**Key words:** pesticides, recovery responses, hepatotoxicity, nephrotoxicity, hemotoxicity, fish.

### Introduction

Pesticides are natural compounds that are poisonous to pests and also life threatening to aquatic animals because they enter the water bodies through different processes such as drainage and droplets [1]. Emamectin benzoate is a member of the avermectins family and it is separated from the bacteria *Streptomyces avermitilis*. It is extensively used as a germicide and insecticide in the agricultural field to kill different pests, and is also used in the aquatic environment [2]. EMB is toxic to nerve cells and it remains deposited in the soil [3] and moves to marine and freshwater through different processes such as decaying feed and feces. It is less toxic to mammals, birds and some useful arthropods [4]. EMB is lethal to humans as it depressed the activity of different body organs and induces toxic effects on the kidney [5], liver [6], nervous system, heart [7].

EMB toxicity has side effects on different animals such as in rats it can cause problems in the eyes and nervous system, slow down the phagocytic process, and functioning of macrophages [8], cause

teratogenic effects [9]. EMB is also lethal to mice as it changes the histopathology of the liver, kidney, and brain [10] and it also causes reproductive toxicity [11].

EMB induces toxic effects on fish in many ways such as it affects the embryo, causing malformation, and slowing down the hatching process [7]. It is lethal to tissues, alters the heart working, decay epithelial tubes in the kidney and diminishes its working, blocks the glomerulus, and proximal and distal tubules become swollen [4, 12, 13]. It is also toxic to the liver [14], induces hyperglycemia, obesity, diabetes, and enhance the level of glucose [15].

Fish is a very sensitive and dominant organism in aquatic environments used for the detection of toxicity and also a very good bio-indicator in the research field to study the harmful and beneficial effects of chemicals in water bodies [16]. *Labeo (L.) rohita* (Rohu) is a freshwater fish and it is the most common and favorable fish in South Asian countries including Pakistan, India, Bangladesh and Nepal. It is adjusted to laboratory conditions easily. Many studies have been done to investigate the changes

in the hematology of *Labeo rohita* treated with emamectin benzoate [17].

To the best of our knowledge, it is first investigation on the effects of *Moringa oleifera* against the toxic effects in freshwater teleost. Therefore, present study aimed to check the ameliorative effects of *Moringa oleifera* against the toxic effects of emamectin benzoate in freshwater fish *L. rohita* using different biomarkers including, hematology, lipid profile, thyroid functioning, liver and kidney functioning and histological changes.

## Materials and methods

**Experimental animal.** The experimental fish used in the present study is *Labeo rohita* purchased from the Head Balloki fish hatchery, Kasur, Pakistan, and transported to the aquaculture lab of the University of Okara. No mortality was observed during transportation. Fish were acclimatized in a large glass tank for seven days. During the whole experiment, after every 48 hours, the excreta of fish and the remaining food were removed from the aquarium, by using a recirculation aerated system along with a water renewal system. Fish were kept at a set temperature of  $29.5 \pm 27^\circ\text{C}$ , pH of  $7.46 \pm 0.26$  of water, and oxygen concentration of  $7.25 \pm 0.23$  mg/L.

**Experimental chemical.** Emamectin benzoate was purchased from Punjab agrochemical trader, Okara, Pakistan. *Moringa oleifera* powder was purchased from an herbal store. Appropriate concentration of EMB was dissolved in distilled water for stock solution.

**Experimental design.** The present experiment was designed for 30 days. During the experiment fish were held in glass aquariums that contains 40 liters of water. Domestic feed was used after 48 hours during the duration of the experiment. Depending upon the concentration of emamectin benzoate four types of treatment groups were designed. Each group contained twenty fish. The first group without chemicals is the control group. 2<sup>nd</sup>, 3<sup>rd</sup> and 4<sup>th</sup> groups were exposed to emamectin benzoate concentrations of 3.64  $\mu\text{g/L}$ , 7.28  $\mu\text{g/L}$  and 14.56  $\mu\text{g/L}$ , respectively. The approval No. UO/ERC/2023/46A from September 14, 2023 was achieved from the ethical research committee of the University of Okara, Pakistan.

**Hematological analysis.** At day 30, fish (n=12) from each glass aquarium were removed for blood collection. Blood was extracted through BD syringe from caudal vein and stored in EDTA tubes for hematology and without EDTA for serum

biochemical analysis. Hematological parameters, such as RBC, HGB, HCT, MCV, MCH, MCHC, WBC, PDW, RDW-SD, Neutrophils, lymphocytes, monocytes, eosinophils, RDW-CD, PLT, MPV, and PCT were analyzed by automatic hematological analyzer SMT-50 (Chengdu Seamaty Technology Co., Ltd, China).

**Biochemical analysis.** Blood sample were left for coagulatory process for two hours at room temperature. Biochemical analysis was performed in Lifeline laboratory and diagnostic center in Lahore, Pakistan. Biochemical analysis of different parameters, such as cholesterol, triglycerides, HDL, LDL, VLDL, AST, ALT, total protein, albumin, globulin, blood glucose, BUN, urea, creatinine, T3, T4 and TSH hormones was performed in the laboratory conditions.

**Histological studies.** After blood collection, fish were dissected. All organs (gills, liver and kidney) were removed and fixed in a solution containing ethanol, formalin, and acetic acid (ALFAC), then stored in 70% ethanol. Tissues were embedded in paraffin, sectioned (5  $\mu\text{m}$ ), and the slides stained with hematoxylin and eosin. The sections were examined under light microscope using a digital camera.

**Recovery responses.** At day 30, five fish from group 4<sup>th</sup> (14.56  $\mu\text{g/L}$ ) removed and transferred to a chemical free freshwater aquarium. For recovery responses, fish were given moringa leaf powder mixed with feed according to body weight for seven days. After seven days, fish removed for above mentioned assays.

**Statistical analysis.** The completely randomized experimental design results are presented as mean  $\pm$  standard deviation and one-way analysis of variance ANOVA. Version of ANOVA that was used in analysis is ordinary one-way ANOVA from GraphPad prism (version 9.3.1).

## Results and discussion

The results of many studies show that teratological disorders, genotoxic effects, embryonic toxicity and histological damages can be caused by carbamate, organophosphate, and organochlorine pesticides [18, 19]. In our experiment, emamectin benzoate was used to test the toxicity based on changes in blood parameters, biochemical parameters, and histology of fish *Labeo rohita*.

**Hematological analysis.** Results of the hematological parameters of *L. rohita* are shown in Table 1.

**Table 1** – Showing alterations in hematological parameters of *L. rohita* in control group, emamectin benzoate exposed groups and *Moringa oleifera* exposed group. Data are represented as mean  $\pm$  SD. \*= $p < 0.05$  level of significance, NS=non-significant, Mo=*Moringa oleifera*

Parameters	Control	Low	Med	High	Mo
HGB (g/dl)	5.63 $\pm$ 0.25	4.53 $\pm$ 0.45 <sup>NS</sup>	3.70 $\pm$ 0.55*	2.83 $\pm$ 0.75*	4.66 $\pm$ 0.72*
WBC ( $\times 10^3/\mu\text{L}$ )	15.80 $\pm$ 0.55	14.20 $\pm$ 0.72*	12.13 $\pm$ 0.56*	10.23 $\pm$ 0.60*	13.20 $\pm$ 0.52*
RBC ( $\times 10^6/\mu\text{L}$ )	1.17 $\pm$ 0.02	1.05 $\pm$ 0.04 <sup>NS</sup>	1.00 $\pm$ 0.04*	0.91 $\pm$ 0.07*	1.04 $\pm$ 0.04*
HCT (%)	15.00 $\pm$ 0.55	12.70 $\pm$ 0.72*	11.90 $\pm$ 0.62*	10.80 $\pm$ 0.81*	11.27 $\pm$ 0.76 <sup>NS</sup>
MCV (fL)	141.9 $\pm$ 1.17	138.7 $\pm$ 1.10*	134.8 $\pm$ 1.22*	131.0 $\pm$ 1.48*	136.4 $\pm$ 1.22*
MCH (pg)	47.57 $\pm$ 0.60	46.07 $\pm$ 0.76*	42.97 $\pm$ 0.66*	41.20 $\pm$ 0.60*	43.70 $\pm$ 0.62*
MCHC (g/dl)	113.0 $\pm$ 2.00	98.33 $\pm$ 5.03*	76.67 $\pm$ 3.05*	65.67 $\pm$ 3.05*	50.67 $\pm$ 4.50*
RDW-CD (%)	23.80 $\pm$ 1.05	28.53 $\pm$ 0.60*	36.50 $\pm$ 1.70*	43.70 $\pm$ 0.98*	42.27 $\pm$ 0.86 <sup>NS</sup>
RDW-SD (%)	32.47 $\pm$ 3.90	24.40 $\pm$ 3.90*	17.67 $\pm$ 2.07*	9.50 $\pm$ 0.60*	10.50 $\pm$ 0.85 <sup>NS</sup>
PLT( $\times 10^3/\mu\text{L}$ )	219.0 $\pm$ 52.85	381.7 $\pm$ 45.08*	535.3 $\pm$ 38.19*	679.0 $\pm$ 38.74*	647.7 $\pm$ 37.63 <sup>NS</sup>
MPV (fL)	5.36 $\pm$ 0.55	7.30 $\pm$ 0.55*	8.56 $\pm$ 0.6506*	9.40 $\pm$ 0.65*	8.93 $\pm$ 0.70 <sup>NS</sup>
PDW (%)	15.50 $\pm$ 1.86	9.40 $\pm$ 1.45*	5.66 $\pm$ 0.85*	2.80 $\pm$ 1.15*	3.46 $\pm$ 0.49 <sup>NS</sup>
PCT (%)	0.10 $\pm$ 0.02	0.24 $\pm$ 0.03*	0.46 $\pm$ 0.06*	0.62 $\pm$ 0.05*	0.54 $\pm$ 0.06 <sup>NS</sup>
Neutrophils %	69.67 $\pm$ 5.50	81.67 $\pm$ 4.50*	89.33 $\pm$ 4.50*	97.33 $\pm$ 5.50*	87.33 $\pm$ 3.05 <sup>NS</sup>
Lymphocytes (%)	25.33 $\pm$ 7.02	54.33 $\pm$ 7.50*	74.33 $\pm$ 8.02*	87.67 $\pm$ 8.50*	84.63 $\pm$ 3.51 <sup>NS</sup>
Monocytes (%)	2.033 $\pm$ 0.55	4.10 $\pm$ 0.55*	5.96 $\pm$ 0.45*	8.96 $\pm$ 0.65*	7.86 $\pm$ 0.77 <sup>NS</sup>
Eosinophils (%)	2.26 $\pm$ 0.25	2.70 $\pm$ 0.20 <sup>NS</sup>	3.26 $\pm$ 0.25*	4.16 $\pm$ 0.15*	3.80 $\pm$ 0.26 <sup>NS</sup>

RBCs, HGB, HCT, MCV, MCH, MCHC, WBCs, PDW and RDW-SD were decreased significantly in the treated group as compared to the control group. Some other parameters, like neutrophils, lymphocytes, monocytes, eosinophils, RDW-CD, PLT, MPV and PCT increased significantly in experimental groups compared to the control group. Use of moringa leaf powder shows that some parameters including RBC, HGB, and WBC, MCV, MCH, and MCHC were significantly increased.

**Biochemical analysis.** Results of the effects of emamectin benzoate and recovery responses after moringa leaf powder on the biochemical parameters and thyroid hormone of *L. rohita* are presented on Figures 1, 2, and 3. Assessment of biochemical parameters reveals information on the functioning of important organ systems such as the immune system, hematopoietic system, kidneys, and liver. These are commonly employed in toxicological investigations to identify and assess cell damage [28]. According

to current study a significant increase was observed in lipid profile such as triglycerides, cholesterol, low density lipoproteins and very low-density lipoproteins except high density lipoproteins after exposure to EMB (Figure 1).

Results indicate that all the biochemical parameters (except high density lipoproteins, serum total proteins, T3 and T4) showed a significant increase in experimental groups than in control group. Blood sugar level undergoes a significant increase in EMB exposed group. The level of thyroid hormones T3 and T4 significant decrease but the level of TSH increased in the treated group as compared to the control group. After the recovery by using moringa leaf powder, the levels of cholesterol, triglyceride, LDL, urea, creatinine, blood glucose, ALT, AST, serum total proteins and albumin showed significant recovery responses. Remaining parameters were also restored to some extent.

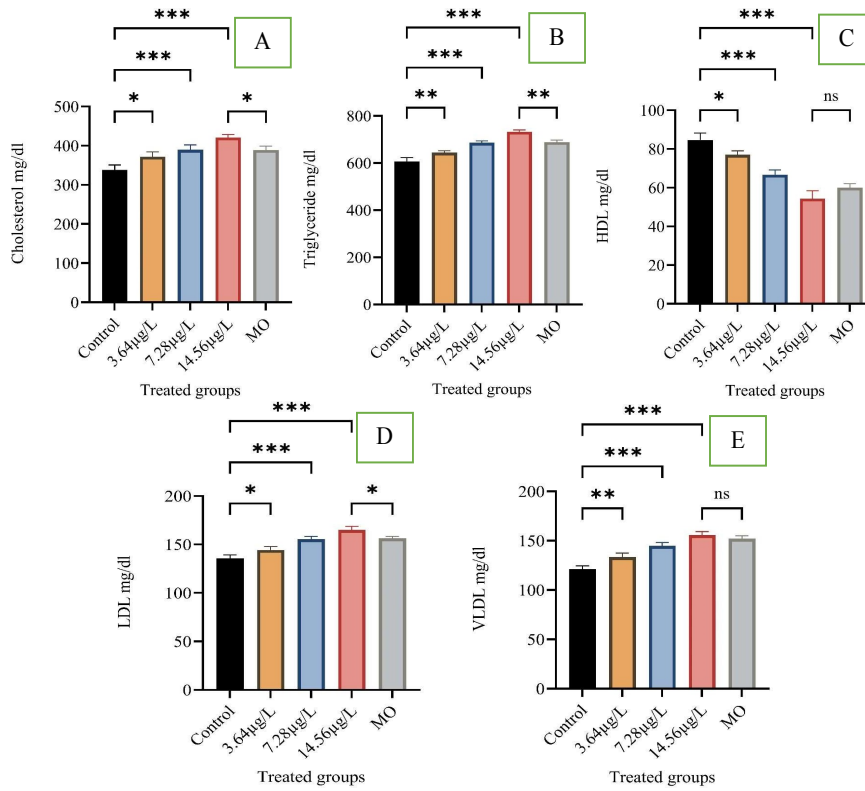


**Figure 1** – Graphical representation shows the variation in (A) cholesterol, (B) triglycerides, (C) HDL, (D) LDL and (E) VLDL of *L. rohita* after exposure of emamectin benzoate and *Moringa oleifera*.

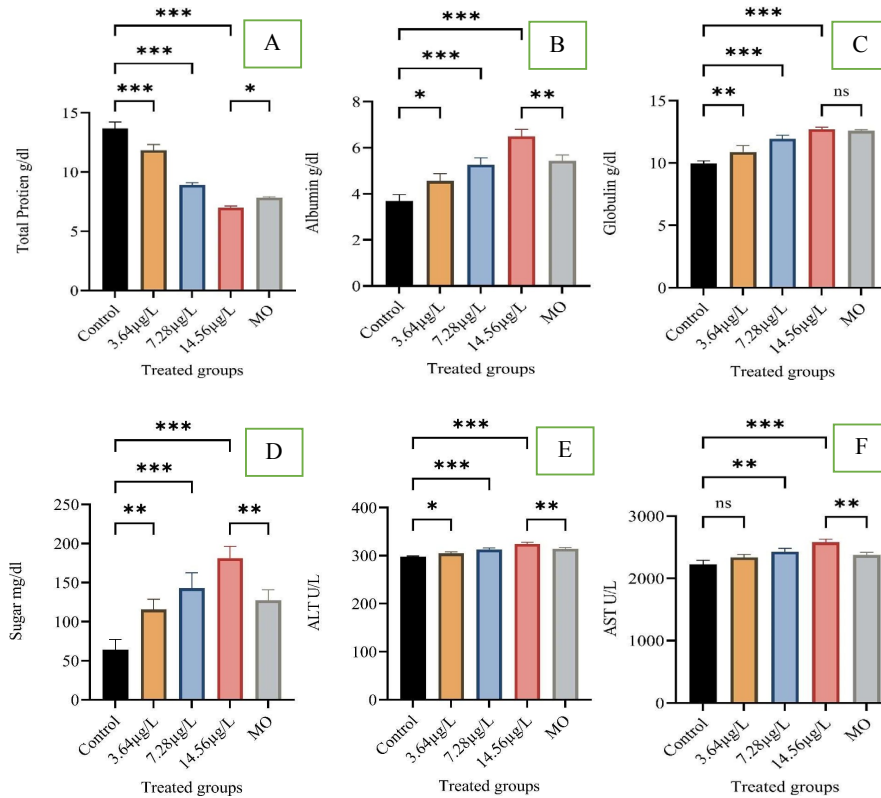


**Figure 2** – Graphical representation shows the variation in (A) total protein, (B) albumin, (C) globulin, (D) blood glucose, (E) ALT and (F) AST of *L. rohita* after exposure of emamectin benzoate and *Moringa oleifera*

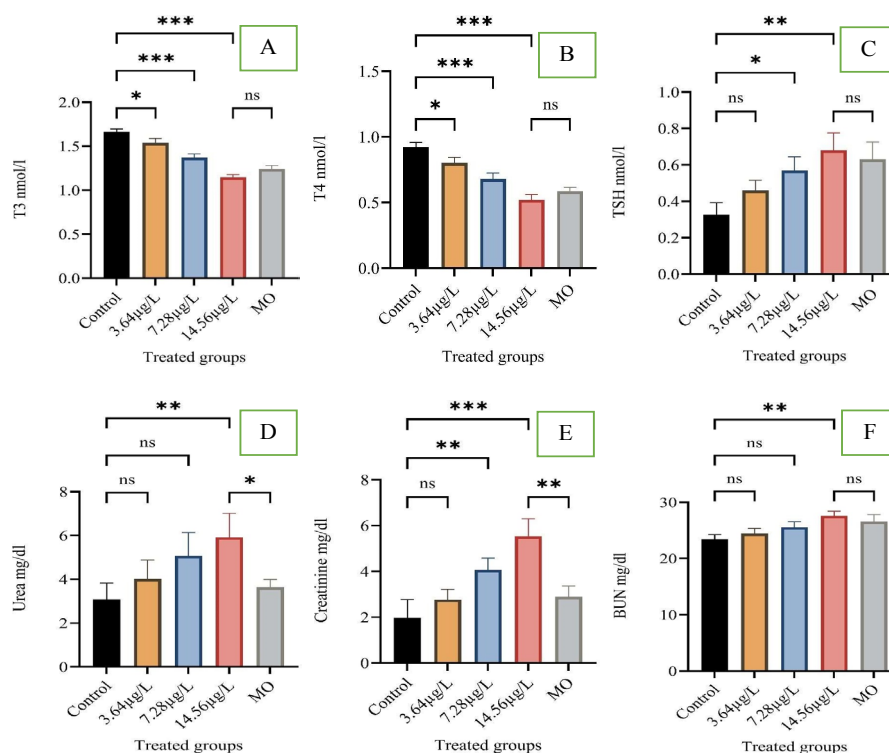


**Figure 3** – Graphical representation shows the variation in (A) T3, (B) T4, (C) TSH, (D) urea, (E) creatinine and (F) BUN (blood urea nitrogen) of *L. rohita* after exposure of emamectin benzoate and *Moringa oleifera*.

Hematological changes caused by exposure to xenobiotics serve as a good indication of the physiological condition in fish [20], birds [21] and other vertebrates [22].

The current study revealed that RBC, HGB, MCH, MCV, and MCHC were significant decreases in experimental groups in comparison to the control group. Toxicity of EMB causes direct injurious effects on the RBC cells, destruction of red blood cells, shrinkage of RBC, erythrocytic lysis, and inhibition of hematopoiesis, which causes the reduction of red blood cells. Similar findings were observed by Kumar et al. [17] and Alghamdi [23].

Results showed that WBCs significantly decreases in blood due to inhibition of the maturation process and immunity suppressions caused by toxicity after being exposed to EMB but significant increase in the lymphocytes, neutrophils, monocytes and eosinophils was indications of chronic infestations. Significant increase in platelets count observed due to infections caused by EMB

exposure. These observations are supported by Kumar et al. [17]. After the recovery by using moringa leaf powder showed that RBCs and HGB were significant increases in treated group. Similar findings were observed by Suzana et al. [24]. Other parameters such as WBC, MCV, MCH and MCHC were significant increased which are supported by previously published literature [25-27].

**Histology.** Histological studies of *Labeo rohita* after exposure to EMB showed that liver tissues undergo different changes such as pyknotic nuclei, cluster nuclei formation, and necrosis in exposed fish (Figure 4).

Gills tissues showed different changes like curved gill lamellae, damaged epithelial cell, bone cell deformities, edema and fused gill lamellae in exposed fish (Figure 5).

Kidney tissues demonstrated some alterations such as sinusoidal spaces, cluster nuclei formation, melanomacrophage, damaged epithelial cells, and elongated tubules in exposed fish (Figure 6).



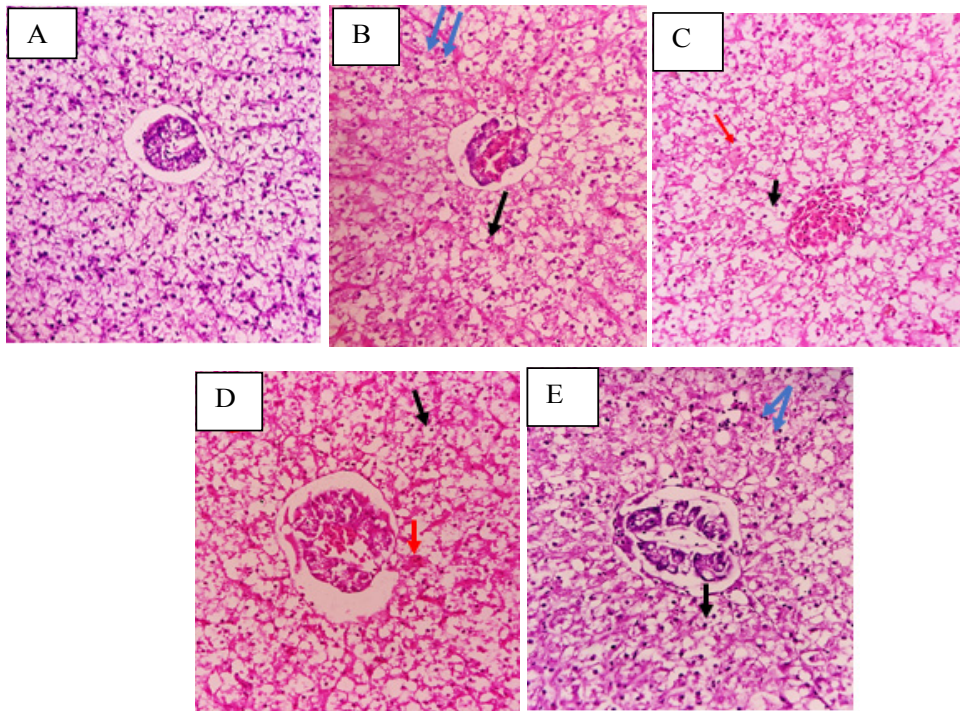


**Figure 4** – Histology of liver tissues of *Labeo rohita* at 40X. (A) control group, (B) low dose group, (C) medium dose group, (D) high dose group and (E) recovery group. Black arrows show pyknotic nuclei, blue arrows show cluster nuclei formation, red arrows show necrosis.

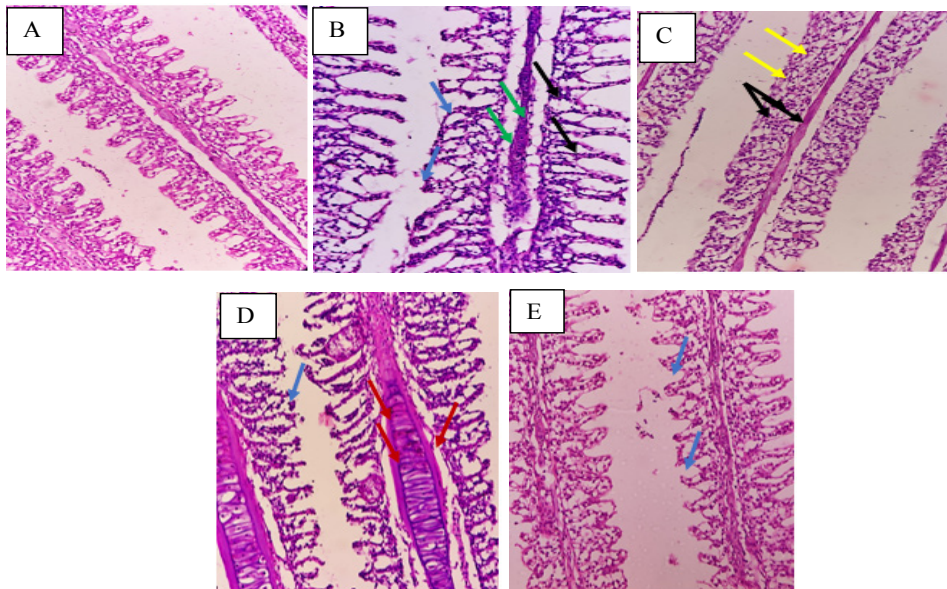


**Figure 5** – Histology of Gill tissues of *Labeo rohita* at 40X. (A) control group, (B) low dose group, (C) medium dose group, (D) high dose group and (E) recovery group. Blue arrows show curved gill lamellae, black arrows show damaged epithelial cell, green arrows show bone cell deformities, red arrows show oedema, yellow arrows show fused gill lamellae.

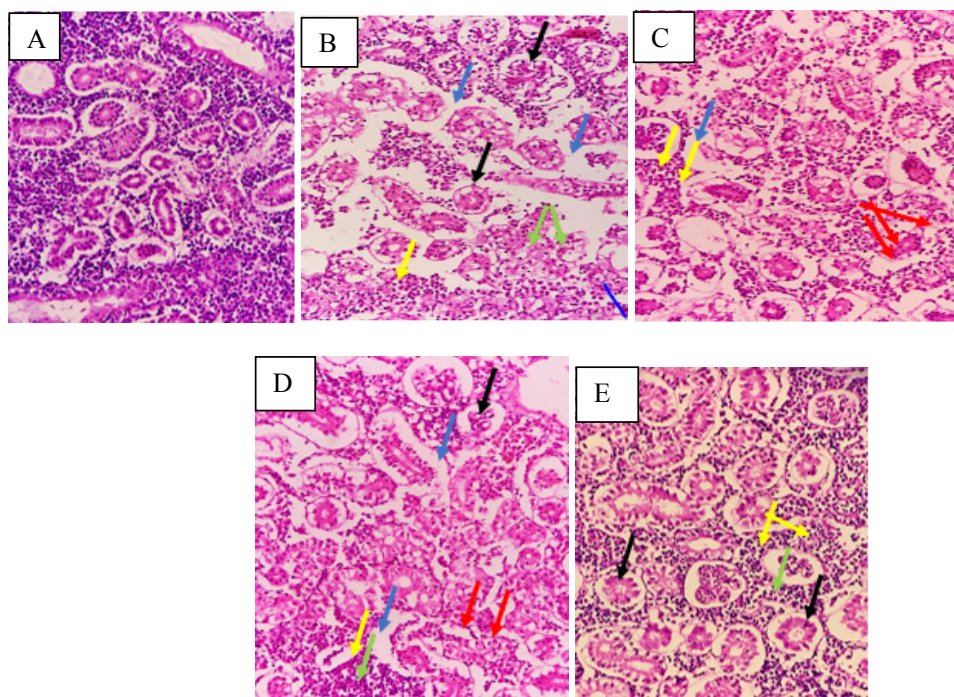


**Figure 6** – Histology of kidney tissues of *Labeo rohita* at 40X. (A) control group, (B) low dose group, (C) medium dose group, (D) high dose group and (E) recovery group. Blue arrows show sinusoidal spaces, yellow arrows show cluster nuclei formation, black arrows show melanomacrophage, green arrows show damaged epithelial cell, red arrows show elongated tubules

After recovery period, using moringa leaf powder, liver, kidney and gill tissues showed recovery to some extent from these damages.

It is because of liver damages (Figure 4) and malfunctioning of liver increase the level in blood. Cholesterol plays role in cell membrane and steroid hormone which act as major indicator to check the stress caused by any chemical. Increased cholesterol level showed the toxicity caused by EMB. Same observations noted by Lee, et al. [29]. ALT and AST showed significance increase in exposed groups in comparison to control. These enzymes present in liver cells help in conversion of amino acid into alpha-keto acids, any abnormality in hepatocytes lead to an increase the level of these enzymes in blood which show toxicity and necrosis in liver. Similar results observed by Ogueji, et al. [2], [17] and Cheng, et al. [3]. Higher levels of albumin and globulin may be due to increase excretory and synthetic functions of liver while decrease the level of serum total proteins in experimental animals due to decrease protein synthesis. Protein play the role in removal, transport and distribution of toxic substances [30]. Blood glucose level increased in the experimental animals exposed to EMB in comparison to control group.

Due to stress caused by toxic chemical, increased gluconeogenesis in liver and disturbance in the metabolism of protein and lipid in order to compensate the increased energy demand. Similar results were observed by Alghamdi [23] and Kumar, et al. [17]. A significant increase was observed in TSH level while decreased T3 and T4 levels in treated groups as compared with control group. Thyroid hormone plays important role in growth, differentiation and maintenance of metabolic process. Any abnormality in the thyroid hormones show that damages in the structure and functions of gland take place which leads to decrease the level of these two hormones in blood. Pituitary gland send signal for more TSH to fulfill the energy demands that is why TSH level increase in the blood. Our findings correspond with those of Azoz, et al. [31]. Increased levels of urea, blood urea nitrogen and creatinine in blood indicated that changes and malfunctioning of kidney due to toxic effects of EMB. Due to kidney damage (figure 6), it is unable to filter the urea, creatinine and BUN in blood and its level increase in blood [32, 33]. By using the moringa leaf powder, recovery responses showed that cholesterol, triglyceride, LDL, urea, creatinine, ALT, AST, serum proteins and blood

glucose levels were significantly restored to some extent. Our observations are similar to El-Kassas, et al. [34] and El-bakry, et al. [35].

Toxin-induced organ damage and injury level may be assessed by histological alterations, which have shown to be highly valuable assessments [36]. As the primary organ for detoxification, the liver serves as a useful biomarker of chemical toxicity. Histological studies of *Labeo rohita* after exposure to EMB showed that liver tissues undergo various changes such as pyknotic nuclei, cluster nuclei formation, and necrosis. Khaldoun-Oularbi, et al. [5] reported similar changes in rats. The gills are vital organs that play an important part in metabolic processes, act as a barrier, and regulate osmoregulation and excretion in addition to being the principal targeted tissues for respiration. Pesticides primarily enter the body through the gills [20, 37]. Fish exposed to EMB showed different changes in gill tissues such as curved gill lamellae, damaged epithelial cell, bone cell deformities, edema and fused gill lamellae. The kidneys play a crucial role in the body's waste removal process. Toxin concentrations affect the structural alterations that the kidneys go through in response to toxin elimination [16]. Fish exposed to EMB showed different changes in kidney tissues such as sinusoidal spaces, cluster

nuclei formation, melanomacrophage, damaged epithelial cells, and elongated tubules. Kumar, et al. [17] reported similar damage effects in *Labeo rohita*. After exposure to moringa leaf powder, liver, kidney and gill tissues showed good recovery responses from these damages. Moringa leaf powder is very effective for restoration of organ toxicity [38].

## Conclusion

Current results indicated that emamectin benzoate (EMB) have toxic effects on freshwater fish *Labeo rohita* at low concentrations. EMB undergoes alterations in hematological and biochemical parameters in experimental groups in comparison to control group. Changes in Lipid profile, serum proteins, thyroid hormones and urea levels are the evidence of emamectin benzoate toxicity. It also causes degenerative and damaging effects in gills, liver and kidney of exposed fish. Results indicated that *Moringa oleifera* is an excellent object for restoration of toxicity caused by EMB. The authors would like to acknowledge chairperson Department of Zoology, University of Okara, Pakistan. This research did not receive any kind of financial support and part of postgraduate research work.

## References

1. Ullah S. et al. (2018) Cypermethrin induced toxicities in fish and adverse health outcomes: its prevention and control measure adaptation, *J Environ Manage.*, 206, 863-871.
2. Ogueji E. et al. (2023) Histological and hematological changes to *Clarias gariepinus* juveniles exposed to acute doses of Emamectin benzoate in a static bioassay, *Ecotoxicol.*, pp. 1-14.
3. Cheng B. et al. (2020) The chronic toxicity of emamectin benzoate to three marine benthic species using microcosms, *Ecotoxicol Environ Saf.*, 194, 110452.
4. Raja R.A., Patil P.K., Avunje S., Aravind R.P., Alavandi S.V., Vijayan K.K. (2020) Biosafety, withdrawal and efficacy of anti-parasitic drug emamectin benzoate in Asian Seabass (*Lates calcarifer*) *Aquaculture*, 525, 735335.
5. Khaldoun-Oularbi H., Allorge D., Richeval C., Lhermitte M., Djenas N. (2015) Emamectin benzoate (Proclaim®) mediates biochemical changes and histopathological damage in the kidney of male Wistar rats (*Rattus norvegicus*), *Toxicol. Anal. Clin.*, 27(2), 72-80.
6. Temiz Ö. (2020) Biopesticide emamectin benzoate in the liver of male mice: evaluation of oxidative toxicity with stress protein, DNA oxidation, and apoptosis biomarkers, *ESPR*, 27(18), 23199-23205.
7. Lu J. et al. (2022) Induction of developmental toxicity and cardiotoxicity in zebrafish embryos by Emamectin benzoate through oxidative stress, *Sci. Total Environ.*, 825, 154040.
8. Wei Z. et al. (2023) The potential immunotoxicity of emamectin benzoate on the human THP-1 macrophages, *Environ. Toxicol.*, 38(3), 500-510.
9. Gabr G., Abdulaziz S.S., Al-Kahtani A.A., Ali B.E. (2015) Teratogenic effects in rat fetuses subjected to the concurrent in utero exposure to emamectin benzoate insecticide, *PJBS*, 18(7), 333-340.
10. Abou-Zeid S.M., AbuBakr H.O., Mohamed M.A., El-Bahrawy A. (2018) Ameliorative effect of pumpkin seed oil against emamectin induced toxicity in mice, *Biomed. Pharmacother.*, 98, 242-251.
11. Zhang Y. et al. (2020) Effect of a beta-cypermethrin and emamectin benzoate pesticide mixture on reproductive toxicity in male mice in a greenhouse environment, *Toxicol. Mech. Methods*, 30(2), 100-106.
12. Bowker J.D., Carty D., Bowman M.P. (2013) The safety of SLICE (0.2% emamectin benzoate) administered in feed to fingerling rainbow trout, *N. Am. J. Aquac.*, 75(4), 455-462.
13. Julinta R. et al. (2020) Effects of oral-dosing of an antiparasitic drug emamectin benzoate on the growth and serum biomarkers of *Oreochromis niloticus* (L.) juveniles, *J. Environ. Biol.*, 41(5), 973-979.

14. Choudhary P. et al. (2022) Effect of graded levels of dietary emamectin benzoate on immunity, enzyme activity, and withdrawal period in *Labeo rohita* Juveniles (Hamilton, 1822), *Aquac. Nutr.*, 2022.
15. Mobeen A., Ishrat I., Awan F.R., Mansoor S., Khan Q.M. (2022) *In vivo* toxicity assessment of biopesticide emamectin benzoate and its commercially used formulations in Pakistan, *J Pharm. Pharmacol.*, 10, 1-14.
16. Hong X., Zhao X., Tian X., Li J., Zha J. (2018) Changes of hematological and biochemical parameters revealed genotoxicity and immunotoxicity of neonicotinoids on Chinese rare minnows (*Gobiocypris rarus*), *Environ Pollut.*, 233, 862-871.
17. Kumar V. et al. (2022) Assessment of the effect of sub-lethal acute toxicity of Emamectin benzoate in *Labeo rohita* using multiple biomarker approach, *Toxicol. Rep.*, 9, 102-110.
18. Fetoui H., Makni M., Garoui E.M., Zeghal N. (2010) Toxic effects of lambda-cyhalothrin, a synthetic pyrethroid pesticide, on the rat kidney: Involvement of oxidative stress and protective role of ascorbic acid, *Exp. Toxicol. Pathol.*, 62(6), 593-599.
19. Akmal H., Ahmad S., Akram I. (2023) Assessment of water quality and targeted accumulation of some heavy metals in different organs of fresh water fish ompok bimaculatus in riverine system of Punjab, Pakistan: assessment of water quality, *PBMJ*, 24-29.
20. Mahmood A., Ahmad S., Akmal H., Shahzad K. (2023) Evaluation of hemotoxic, hepatotoxic and nephrotoxic potential of profenofos-based insecticide in freshwater *Labeo rohita* fish at low concentrations: evaluation of profenofos-based insecticide's potential, *PBMJ*, 32-40.
21. Akmal H. et al. (2023) Morphometry and food preference in relation to sex and hematological values of Eurasian collared dove (*Streptotella decaocto*), *JAVAR*, 10(2), 244.
22. Ahmad S., Akmal H., Jafar K. (2023) A comparative study of morphometric profiles and hematological analysis and food preference between male and female spotted redshank (*Tringa erythropus*) sampled from different wetlands of Punjab, Pakistan, *RADS J. Biol. Res. Appl. Sci*, 14(1).
23. Alghamdi S.A. (2020) Effect of *Nigella sativa* and *Foeniculum vulgare* seeds extracts on male mice exposed to carbendazim, *Saudi J. Biol. Sci.*, 27(10), 2521-2530.
24. Suzana D., Suyatna F.D., Andrajati R., Sari S.P., Mun'im A. (2017) Effect of *Moringa oleifera* leaves extract against hematology and blood biochemical value of patients with iron deficiency anemia, *JYP*, 9(1), S79.
25. Ncha O.S., Michael P.B., Nnabuchi U.O., Alex E. (2015) Effect of diets with moringa leaf meal on growth, carcass composition and haematology of *Clarias gariepinus*, *Int. J. Fish. Aquat.*, 3(2), 397-401.
26. Bbole I., Mumba C., Mupenda N., Kefi A.S. (2016) Analysis of growth performance and haematological parameters of *Oreochromis niloticus* fed on a varying diet of *Moringa oleifera* Lam. leaf meal as an additive protein source, *Int. J. Fish. Aquac.*, 8(11), 105-111.
27. Kavitha C., Ramesh M., Kumaran S.S., Lakshmi S.A. (2012) Toxicity of *Moringa oleifera* seed extract on some hematological and biochemical profiles in a freshwater fish, *Cyprinus carpio*, 64(7-8), 681-687.
28. Dzoyem J.P., Kuete V., Eloff J.N. (2014) Biochemical parameters in toxicological studies in Africa: significance, principle of methods, data interpretation, and use in plant screenings. In: *Toxicological survey of African medicinal plants*: Elsevier, pp. 659-715.
29. Lee D.-C., Choi Y.J., Kim J.-H. (2022) Toxic effects of waterborne cadmium exposure on hematological parameters, oxidative stress, neurotoxicity, and heat shock protein 70 in juvenile olive flounder, *Paralichthys olivaceus*, *Fish Shellfish Immunol.*, 122, 476-483.
30. Tang Y. et al. (2022) Sensitive determination of metalloprotein in salt-rich matrices by size exclusion chromatography coupled with inductively coupled plasma-mass spectrometry, *J. Chromatogr. A*, 1677, 463303.
31. Azoz A., Ibrahim K.A., Abdel Kader I., Tawfik A. (2020) Tracking of apoptosis induced by emamectin benzoate in fetuses of hypothyroid rats, *Int J Pharm Sci Rev Res.*, 13, 81-89.
32. Naik R.A., Rawat D., Ahi J.D., Koiri R.K. (2021) Ameliorative effect of piracetam on emamectin benzoate induced perturbations in the activity of lactate dehydrogenase in murine system, *Advances in Redox Research*, 3, 100019.
33. Afsar T., Razak S. (2017) Modulatory influence of *Acacia hydasypica* R. Parker ethyl acetate extract against cisplatin induced hepatic injury and dyslipidemia in rats, *BMC Complement Altern Med.*, 17(1), 1-13.
34. El-Kassas S. et al. (2020) Growth performance, serum lipid profile, intestinal morphometry, and growth and lipid indicator gene expression analysis of mono-sex Nile tilapia fed *Moringa oleifera* leaf powder, *Fish Shellfish Immunol.*, 18, 100422.
35. El-bakry K., Toson E.-s., Serag M., Aboser M. (2016) Hepatoprotective effect of *Moringa oleifera* leaves extract against carbon tetrachloride-induced liver damage in rats, *World J Pharm Sci.*, 5(5), 76-89.
36. Raibeemol K., Chitra K. Induction of immunological, hormonal and histological alterations after sublethal exposure of chlorpyrifos in the freshwater fish, *Pseudotroplus maculatus* (Bloch, 1795),” *Fish & shellfish immunology*, vol. 102, pp. 1-12, 2020.
37. Akmal H., Ahmad S., Abbasi M.H., Jabeen F., Shahzad K. (2024) A study on assessing the toxic effects of ethyl paraben on rohu (*Labeo rohita*) using different biomarkers; hemato-biochemical assays, histology, oxidant and antioxidant activity and genotoxicity, *PLoS one*, 19(5), e0302691.
38. Ashour E.A. et al. (2020) Effect of dietary supplementation with *Moringa oleifera* leaves and/or seeds powder on production, egg characteristics, hatchability and blood chemistry of laying Japanese quails, *Sustainability*, 12(6), 2463.

**Information about authors:**

*Iqra Jamil – Mphil, Department of Zoology, University of Okara (Okara, Pakistan, e-mail: hafzaiqrajamil@gmail.com)*

*Shabbir Ahmad – Mphil, Department of Zoology, University of Okara (Okara, Pakistan, e-mail: shabbir35303@gmail.com)*

*Hasnain Akmal – Mphil, Department of Zoology, University of Okara (Okara, Pakistan, e-mail: hasnain20156@gmail.com)*

*Iqra Akram– Mphil, Department of Zoology, University of Okara (Okara, Pakistan, e-mail: iqraakramhayat@gmail.com)*

*Muqadas Shahzadi – Mphil, Department of Zoology, University of Okara (Okara, Pakistan, e-mail: muqadas54111@gmail.com)*

*Sajid Ali – Mphil, Department of Zoology, University of Okara (Okara, Pakistan, e-mail: abidalisahibzada@gmail.com)*

*Sheraz Khan – Mphil, Department of Zoology, University of Okara (Okara, Pakistan, e-mail: sherazk0073@gmail.com)*

*Khurram Shahzad (corresponding author) – PhD, Assistant Professor, Department of Zoology, University of Okara (Okara, Pakistan, e-mail: dr.khurram@uo.edu.pk)*

S.N. Abdreshov<sup>1,2\*</sup>, M.A. Yessenova<sup>2</sup>, A.N. Yeshmukhanbet<sup>2</sup>,  
G.A. Demchenko<sup>1</sup>, V.N. Gorchakov<sup>3</sup>, G.K. Atanbaeva<sup>2</sup>,  
S.A. Mankibaeva<sup>2</sup>

<sup>1</sup>Institute of Genetics and Physiology CS MSHE RK, Almaty, Kazakhstan

<sup>2</sup>Al-Farabi Kazakh National University, Almaty, Kazakhstan

<sup>3</sup>Institute of Cytology and Genetics SB RAS, Novosibirsk, Russia

\*e-mail: snabdrshov@mail.ru

(Received 12 January 2024; received in revised form 20 March 2024; Accepted 26 April 2024)

## Morphofunctional and morphometric features of the small intestine in experimental rats with inflammation of the abdominal cavity

**Abstract.** The article presents studies of the effect of fecal suspension by introducing into the abdominal cavity at the rate of 0.5 ml of a 10% solution per 100 g of animal body weight. The morpho-functional state and morphometric analyzes of the small intestine were studied in normal conditions and with inflammation of the abdominal organs by introducing fecal suspension. The results showed that inflammation of the abdominal organs led to significant changes in the wall of the small intestine, multiple hemorrhages and fibrin clots were found. In the intestine, there is a change and violation of the structures of the small intestine, the total thickness of the mucous membrane increases. Violation of goblet cells, villus height and crypt depth occur. Analysis of the study showed that the walls of the small intestine, revealed structural changes, mainly in the mucosa, submucosa and muscle membranes. The mean value of the mucosal thickness in the control group was  $526.17 \pm 17.11$  micrometer; submucous layer –  $47.21 \pm 1.63$  micrometer. Phenomena of edema, inflammatory infiltration, and separation of muscle fibers were noted in both layers of the muscular membrane. The average layer of thickness of the muscular membrane was  $145.67 \pm 6.92$   $\mu\text{m}$ . Changes in the mucous membrane of the small intestine, at one time reflected in the structural changes in the villi-crypt of the small intestine. A violation of microcirculation in the tissues of the small intestine after the inflammatory process was revealed, which leads to aggravation of dystrophic and necrobiotic lesions of the overall state of the small intestine and is combined with the severity of the clinical picture in experimental animals.

**Key words:** goblet cells, abdominal cavity, villi, crypts, small intestine.

### Introduction

Inflammation of the parietal and visceral layers of the peritoneum, which is accompanied by a severe general state of the body. The most common cause of inflammation of the abdominal organs is hollow viscus perforation of the gastrointestinal tract, which includes a number of critically important stages that determine the further nature of the course of the disease [1, 2]. One of the leading factors in the progression of inflammatory processes with the development of multiple organ dysfunction and adverse outcomes is enteral insufficiency syndrome [3, 4]. Violation of the barrier function of the intestinal wall and the loss of colonization resistance lead to the development of uncontrolled processes of systemic inflammatory response and endogenous intoxication

[5, 6]. Currently, various changes are taking place in the understanding of inflammation of the abdominal organs, such as a systemic inflammatory response, oxidative stress and endothelial dysfunction, intestinal failure and intra-abdominal hypertension [7].

Morphological studies of the organs of the immune system of animals, which is the main defense system of the body, showed that the linear parameters of the thymus and lymph nodes depend on a high reactivity to exogenous and endogenous influences [8, 9]. Based on the data of modern literature, aggregated lymphoid nodules of the small intestine are secondary organs of the immune system [10, 11], which represent one of the first lines of defense against the penetration of pathogenic microorganisms, so their normal morpho-functional state is one of the conditions on which the

constancy of the internal environment, both the small intestine and the whole organism as a whole, depends [12, 13].

One of the models of inflammation is the peritoneal administration of a suspension of contents into the abdominal cavity, which leads to the development of progressive multiple organ failure, microcirculation dysfunction, including the colon [14].

Inflammation of the peritoneal cavity is the lining inner wall of the abdominal cavity and covers most of the abdominal organs. In most literary sources, the peritoneum is described only as a

“serous cover” lining the abdominal cavity. In the scientific literature, in most cases, references to the peritoneum are limited only to its representation as a mutually permeable membrane that provides fluid flow from the abdominal cavity to the circulatory and lymphatic systems and vice versa, using its capabilities as a dialysis surface or as a site for the manifestation of peritonitis [15]. Mortality in severe forms of inflammation of the abdominal cavity and an increase in the number of organs involved is very high. One of the most important organs, which is primarily exposed to pathological changes is the intestine. In the pathogenesis of its damage during inflammation, ischemia is of great importance. According to the nature of morphological changes in the intestinal wall, mild and severe degrees of ischemia are distinguished, in particular, it is characterized by necrosis of individual enterocytes in the region of the tip of the villi of the small intestine [16, 17].

The mucous membrane of the digestive tube is one of the most significant surfaces of the body in terms of area in constant interaction with the external environment [18]. Over the past decades, significant progress has been made in the study of inflammation in diseases of the internal organs. However, many issues of pathogenesis and various approaches to the study of inflammatory processes in the abdominal cavity remain unresolved. The purpose of the current study was to evaluate the morpho-functional state of the small intestine and to identify morphometric changes in the wall of the small intestine in rats with inflammation of the abdominal organs.

## Material and methods

*Animals.* The experiments were carried out on white male Wistar rats  $250 \pm 5$  g, obtained from the commercial supplier (Netherlands). All animals were kept under the same conditions at a constant ambient temperature of  $23-26^{\circ}\text{C}$ , fed the same

amount of food, and manipulated at the same time frame. All experiments with animals were carried out in accordance with the Directive of the European Parliament and the EU Council 2010/63/EU from September 22, 2010 on the protection of animals used in experimental studies for scientific purposes, and approved by the local ethical commission of the Institute of Genetics and Physiology, protocol No.4 from December 18, 2021. The experiments were carried out on 40 laboratory male rats weighing  $250 \pm 5$  g. Three groups of rats were created: one group contained control rats (15 rats), and the other two groups contained rats subjected to experimentally induced acute abdominal organ inflammation: I-experimental group (12 rats) experienced inflammation on the 2nd day, while the II-experimental group (13 rats) experienced inflammation on the 5th day. We have chosen a method for modeling inflammation of the abdominal organs, which is close to an acute inflammatory process, characterizing the completion of the acute phase of peritonitis in terms of etiopathogenesis, clinical evidence and flow phasal nature close to that in humans. Acute inflammation of the abdominal organs in rats was caused by introducing fecal suspension into the abdominal cavity at the rate of 0.5 ml of a 10% solution per 100 g of animal body weight. Animals for research were taken on the 2nd and 5th day after fecal injection. Anesthetization of animals was carried out by inhalation with ether through a mask into which a cotton wool with ether was placed [19].

*Morphometric analysis.* In all study groups, the state of the structural components of the small intestine was analyzed. Organs were fixed in 10% neutral formalin solution. According to the generally accepted histological method [19], the organs were passed through a series of alcohol of increasing concentration, xylene, and embedded in paraffin. Sections 5-7  $\mu\text{m}$  thick were made on a rotary microtome (Thermo Scientific HM 325, Roche) and stained with hematoxylin and eosin, light green, according to Masson [20]. The assessment of morphological changes was carried out at the light optical level with magnification  $\times 10$ ,  $\times 40$  and  $\times 100$ . Structural morphometric parameters of the intestine were performed using the Image ProPlus 4.1 program (Media cybernetics, Inc.) with the measurement of the diameters of the crypt, villus, mucous membrane, the thickness of the entire intestinal wall, which was superimposed on a section of the small intestine. We counted the intersections of the grid pertaining to the entire section of the small intestine, as a whole

and separately, for each of its structures, recalculated as a percentage, the thickness of the muscular and mucous membranes, mucous, muscular and serous membranes, the height and width of the villi, the depth and width of the crypts (in  $\mu\text{m}$ ) and the area of goblet cells, including the area of the nucleus (in  $\mu\text{m}^2$ ) [20, 21].

*Statistical analysis.* Statistical processing of the obtained results was carried out in the StatPlusPro 2009 program (AnalystSoft, Inc.) using Student's *t* test. Data are presented as arithmetic mean ( $M$ ) $\pm$ error of the mean ( $\pm m$ ). Differences were considered significant at  $p < 0.05$ .

## Results and discussion

To study the histological changes in the intestinal wall caused by inflammation of the abdominal cavity, we conducted a series of experiments to study the morphology of tissue samples of the intestine wall in the control and experimental groups of animals.

In the control group of animals, at autopsy, as has been shown by the macroscopy, the internal organs had the usual location, without abnormalities, the mucous membrane was at usual location, without abnormalities. Figure 1 shows control section of intestinal tissue sample from section of the villi.

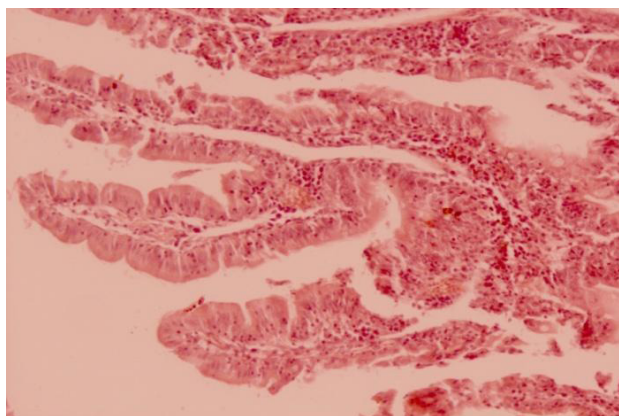


**Figure 1** – Section of the villi of the small intestine in control animals. Note: Abt. 40x0,65; ABT. 10x20

In the I-experimental group strong adhesion loops of the small intestine within itself and with abdominal peritoneum along with a decrease in the motion activity of rats, decreased food intake, and slight edema were observed. Visual examination of the mucosa revealed smoothness, atrophy and pallor of the latter, there were single structural defects in the form of petechial hemorrhages.

On the 5th day from the start of the experiment, the most pronounced changes in the behavior of animals were noted. In rats, the surface epithelium of the villi of the small intestine was flattened and necrotic. The villi and crypts of the small intestine were dystrophic, devoid of a brush border, and there was an increase in the number of goblet cells with a pyknotic nucleus. Vessels and capillaries of the villi are full-blooded and hemorrhages are noted, areas of erosion of the mucous membrane of the small intestine are characteristic. In these groups, the animals moved little, huddled in groups, ate scarcely; loose of stool and significant deterioration of wool were observed as well. In animals, 1.5-3.0 ml of a nebulous liquid with a milky tint was found in the abdominal cavity; in some animals a purulent effusion with an unpleasant odor was observed. At the end of the experiment, after the 5th day, the surviving animals did not move around the cage, sat motionless in a dark place, did not eat, and also loose stool and profuse hair loss were recorded in all animals.

When studying morphological changes, it was revealed that in the animals of the II-experimental group, the inflammation of the abdominal cavity was observed, especially in the walls of the abdominal, and intestines were less pronounced, cell tissue infiltration decreased. There was an increase in the number of collagen and elastic fibers in the adhesions, cells with large drops of fat, as well as fibroblasts, were located between them. The entire connective tissue of adhesions is permeated with blood vessels of various calibers (Figure 2).

Figure 2 shows a histological section of the wall of the small intestine on the second day after the inflammatory process of the abdominal cavity. The study of the morphofunctional features of the intestine in case of massive inflammation of the abdominal cavity confirmed with other authors that the mucous membrane suffers first of all in the form of desquamation, discomplexation of epithelial cells in the lining of the villi and crypts. It was noted that against the background of destruction, regeneration processes begin to occur, which are most pronounced in the small intestine [22, 23]. The results showed that microscopic examination of the small intestine revealed structural changes in the villi and deterioration of the mucous tissue of the intestinal wall. Structural changes in the villi were found, mainly related to the surface epithelium – the boundaries between individual epithelial cells are smoothed, decomplexation and desquamation of enterocytes are observed. The deterioration of the structural elements of enterocyte cells and the



beginning of perforation up to the detachment of the intestinal wall are visible. In the experiment, there is exfoliation of the intestinal wall and a complete violation and deterioration of the structural elements of the cells of the intestinal villi, perforation. At the end of the experiment on the 5th day, the complete deterioration of the villi of the small intestine with

inflammation caused by fecal suspension was noted. Violation of cell entanglement is a nonspecific reaction to various altering influences.

In the morphological study of the small intestine of intact rats, the morphometric parameters of the small intestine in terms of length and area were obtained (Figure 3).

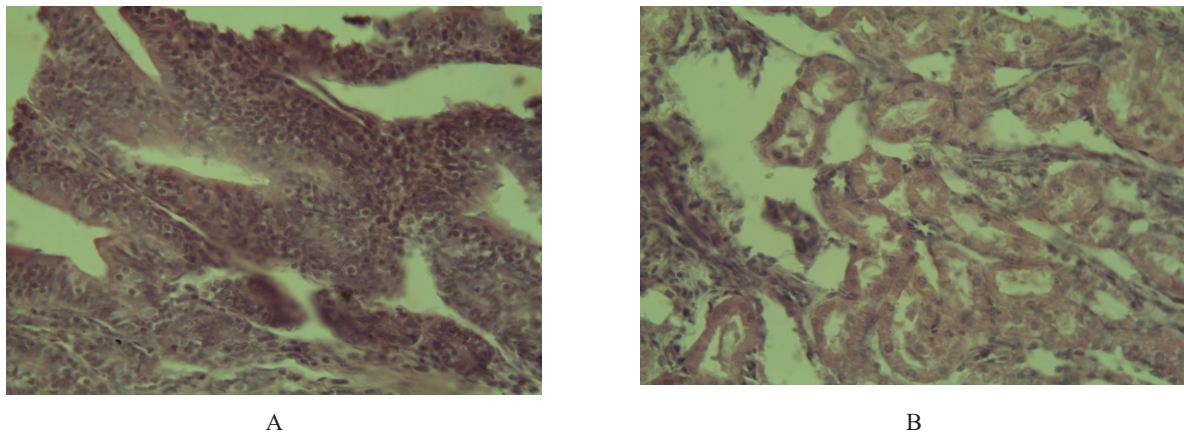


**Figure 2** – Deterioration of the villi of the intestinal wall in experimentally induced inflammation of the abdominal cavity.  
Designation: A – pronounced purulent inflammation of the mucous membrane with the destruction of the villi,  
B – inflammatory infiltration of the submucosa and muscle membranes. Dystrophic, necrobiotic and necrotic changes were most pronounced in the muscular layer of the small intestine. Note: Abt. 40x0,65; ABT. 10x20.

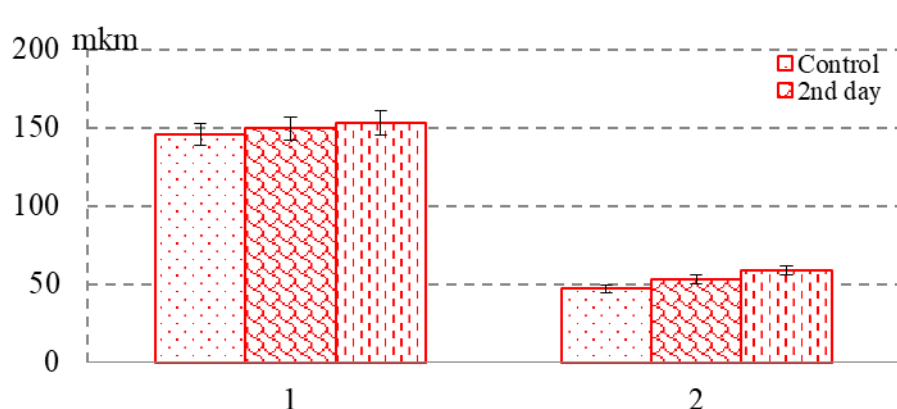


**Figure 3** – Morphometric indicators of the thickness of the muscular membrane and submucosa.  
Designation: On the ordinate axis: the measurement of the object in  $\mu\text{m}$ ,  
On the abscissa axis: 1 – the thickness of the muscle membrane, 2 – the thickness of the submucosa

The assessment of morphological changes was more often used in the diagnosis and assessment of the development of inflammatory processes in the abdominal cavity, including the small intestine. Normally, the small intestine is a long muscular tube of the gastrointestinal tract, which is the main site of absorption and digestion of nutrients and other

substances. Various substances and also various physiological or pathological conditions can change the rate of proliferation of enterocytes in the crypt and affect the rate of their migration to the top of the villi. The intercourse between the small intestine and nutritional factors is very complex. The mean value of the mucosal thickness in the control group was

526.17±17.11 µm; submucosal layer – 47.21±1.63 µm. Phenomena of edema, inflammatory infiltration, and separation of muscle fibers were noted in both

layers of the muscular membrane. The average layer thickness of the muscular membrane was 145.67±6.92 µm (Table 1).

**Table 1** – Morphometric characteristics of the small intestine in rats with experimental inflammation of the abdominal cavity

Indicators	Control	I – experimental group (2nd day)	II – experimental group (5th day)
Villus height, µm	267.21±9.91	260.4±11.3	253.86±10.4
Villus thickness, µm	71.46±3.08	75.9±2.17	79.86±3.8
Crypt depth, µm	203.19±6.11	198.2±2.34	195.6±4.13
Crypt thickness, µm	35.12±1.2	37.7±1.9	39.9±1.5
The thickness of the muscle membrane, µm	145.67±6.92	149.5±5.27	153.2±4.3
Submucosal thickness, µm	47.21±1.63	53.3±1.81	59.1±1.85*
Mucosal thickness, µm	526.17±17.11	554.24±12.6	631.65±14.9*
Goblet epithelial cells			
Quantity in the villus	8.7±0.52	15.1±0.69	17.1±0.73
Area, µm <sup>2</sup>	178.32±15.36	192.12±16.25	199.5±17.36
Core area, µm <sup>2</sup>	25.1±1.14	32.6±1.56*	34.3±2.39*

Note: \* – significance of differences compared to control, P<0.05

Morphological changes in the wall of the small intestine were more pronounced in animals 5 days after their removal from the experiment, and corresponded to the toxic stage of its development – the inflammatory process of the abdominal organs. The visceral and parietal layers of the peritoneum almost completely lost their mesothelial cover and were edematous. Multiple hemorrhages and fibrin clots were found in the wall of the small intestine. Analysis of the study showed that the walls of the small intestine revealed structural changes, mainly in the mucosa, submucosa and muscle membranes. The average value of the thickness of the mucous membrane in these periods exceeded the indicators of its thickness at the stage of inflammation of the internal organs, ranging from 554.24±12.6 to 631.65±14.9 µm, while the values of the submucosa ranged from 53.3±1.81 to 59.1±1.85\* µm. The average thickness of the muscular membrane increased from 152.5±5.27 to 163.8±4.3 µm (control values were 145.67±6.92 µm). Leukocyte infiltration of the lamina propria of mucous membrane and submucosa was noted.

An increase in the average value of the thickness of the mucous membrane (526.17±17.11 µm) and submucosa (47.21±1.63 µm) by 0.7-0.8 times was comparable to the characteristics in animals with the stage of inflammation, characterized by the

acute phase of peritonitis (Table 1). In experiments, desquamation of the surface epithelium and small necrosis were observed against the background of edema and infiltration of the mucosa and submucosa. The structural and functional unit of the mucous membrane of the small intestine is the crypt-villus system. Under normal conditions, the crypts are located in the lamina propria of the mucous membrane of the small intestine. The intestinal villus of the first part of the small intestine of the rat are flattened structures protruding into the intestinal lumen, the shape of which can be characterized as leaf-shaped, i.e. they are lined with low-prismatic epithelium, their height increases from the base to the mouth and amounts to 35.12±1.2 µm on average.

On the 5th day of the experiment, there was a significant increase in the thickness of the mucous membrane both due to the height of the villi and the depth of the crypts, despite the fact that the height of enterocytes at this time is greater than in the control. The trend towards an increase in the number of goblet cells in the area of the villi, as well as an increase in the depth of the crypt and villi, continued (Table 1). Thus, it can be observed that after the 5th day of inflammatory processes in the small intestine, there is a change in morpho-functional indicators compared to the control group. Atrophic processes were observed in the crypts, which indicates the failure of

regenerative processes in the mucous membrane of the small intestine [24].

In the experiments, it was observed that the wall of the small intestine underwent significant inflammatory changes, manifested primarily by an increase in the thickness of its layers, compared with the intact wall of the intestine; vascular reaction of the submucosa, changes in both layers of the muscular membrane in the form of the formation of spaces between muscle fibers. Morphological and morphometric indicators of the thickness of the layers of the wall of the small intestine in conditions of 2- and 5-days of inflammation of the abdominal organs were found. Inflammation of the abdominal cavity causes a decrease in the depth of intestinal crypts by 10%. According to the authors, the intestinal crypts are responsible for the renewal of the epithelial lining of the intestine for body balance control [25], it can be concluded that a decrease in the depth of the crypts is a morphological sign of a decrease in the regenerative activity of the epithelium of the small intestine [26]. The authors have shown that the absence of peristalsis leads to the loss of intestinal colonization resistance, translocation of pathogenic and opportunistic microflora to unusual habitats, bacteremia, the development of abdominal sepsis, and multiple organ failure [27, 28]. The mucous membrane of the small intestine has many finger-shaped villi, the surface consists of erythrocytes and individual goblet cells [29-31].

Studies have shown that after the 2nd and 5th days after the development of the inflammatory process in the abdominal cavity, inflammatory changes developed in the wall of the small intestine without a necrotic component. An increase in the thickness of the wall of the small intestine was noted in comparison with the intact group of animals. Quantitative morphometry showed that under the influence of fecal suspension there is an increase in the thickness of the entire wall of the small intestine due to the thinning of its membranes. The thickness of the muscular membrane was increased – by 5-12%, the mucous membrane – by 5-20% and the submucosa – by 13-25% compared to the control group. Changes in the mucous membrane of the small intestine, reflected at the time the structural changes in the villi-crypt of the small intestine. Studies have shown that there was a significant increase in the thickness of the villi by 6-12% due to a significant increase in the area of the villus by 5-11% and the area of the nucleus of the villus by 23-31%. In

rats after inflammation, there is an increase in the thickness of the intestinal wall and its layers, caused by dystrophic and necrotic processes, inflammatory infiltration and degeneration of the fibrous skeleton to the submucosa, dystrophic changes in the cells of the muscle layer and necrotic processes of the serous membrane. In the serous membrane, hyperemia, edema, punctate hemorrhages, and fibrin plaque were noted.

### Conclusion

The results of the study show that after the introduction of fecal suspension in the body of rats, an inflammatory process of the abdominal organs occurred, morphofunctional changes in the small intestine area and morphometric features of all layers of the wall of the small intestine were revealed. After the 5th day of the experiment, destructive and necrotic changes develop in the wall of the small intestine. During inflammatory processes, a morphological change begins from the mucous membrane of the small intestine, the surface epithelium flattens, the number of goblet cells decreases sharply, the crypts acquire an irregular shape, and microabscess develop in them. Thus, the introduction of fecal suspension in animals in the abdominal cavity caused a complete subsidence of the acute inflammatory process, which characterized the completion of acute widespread purulent peritonitis, in the form of the development of pronounced changes in the wall of the small intestine. Secretory and dystrophic disorders of the surface epithelium of the small intestine were observed along with vascular congestion, hemorrhages, edema and loosening in the mesentery. Quantitative morphometry indicated the pronounced edema of the peritoneum, small hemorrhages, and fibrin plaque on the peritoneum and on the abdominal organs. An analysis of morphological changes in the wall of the small intestine, carried out in dynamics, showed significant, gradually increasing, structural changes, showed significant, gradually increasing, structural changes during inflammation of the internal organs in rats.

### Acknowledgment

This study was supported within the framework of the research project AP23488476, funded by the Ministry of Science and Higher Education of the Republic of Kazakhstan.

## References

1. J.O.A.M van Baal, K.K.Va+n de Vijver, R. Nieuwland, C.J.F. van Noorden, W.J. van Driel, A. Sturk G.G.Kenter, L.G. Rikkers, C.A.R. Lok, The histophysiology and pathophysiology of the peritoneum, *Tissue and Cell*. (2017). <https://doi.org/10.1016/j.tice.2016.11.004>.
2. D. Holt, K.A. Agnello, *Peritoneum*, Elsevier Public Health Emergency Collection. (2014). doi: 10.1016/B978-0-7020-4336-9.00026-3
3. B.D. Levy, C.N. Serhan, *Resolution and Regulation of Inflammation, Pathobiology of Human Disease*. (2014).
4. Carolina Maciel Nogueira, Walter Mendes de Azevedo, Maria Lucia Zaidan Dagli, Sérgio Hiroshi Toma, André Zonetti de Arruda Leite, Maria Laura Lordello, Iêda Nishitokukado, Carmen Lúcia Ortiz-Agostinho, Maria Irma Seixas Duarte, Marcelo Alves Ferreira, Aytan Miranda Sipahi, Titanium dioxide induced inflammation in the small intestine, *World J Gastroenterol*. (2012). doi: 10.3748/wjg.v18.i34.4729.
5. K.M.Bajchorov, V.S. Botasheva, A.G.Bondarenko, V.N. Demyanova, Morphological reasons for miniinvasive video laparoscopic sanitation of abdominal cavity, *Medical News of the North Caucasus*. (2013).
6. D. Srinivas, Intraoperative Lavage in Peritonitis – Comparison between Saline and Metronidazole, *International Journal of Scientific Study*. (2020).
7. C.M. Ruthrauff, J. Smith, L.Glerum, Primary bacterial septic peritonitis in cats: 13 cases, *J Am Anim Hosp Assoc*. (2009). doi:10.5326/0450268.
8. E.A. Deitch, D. Xu, V.L. Kaise, Role of the gut in the development of injury- and shock induced SIRS and MODS: the gut-lymph hypothesis, *Front Biosci*. (2006). DOI 10.2741/1816
9. O. Gorchakova, V. Gorchakov, Yu. Kolmogorov, B. Nurmakhanova, G. Demchenko, S. Abdreshov, Microelement profile and structure of regional lymph nodes during senile involution of lymphoid tissue, *Archiv Euromedica*. (2021). <https://doi.org/10.35630/2199-885X/2021/11/1.9>.
10. Jung Camille, Hugot Jean-Pierre, Barreau Frédérick, Peyer's Patches: The Immune Sensors of the Intestine, *International Journal of Inflammation*. (2010). doi:10.4061/2010/823710.
11. G. Bouma, W. Strober, The immunological and genetic basis of inflammatory bowel disease, *Nature Reviews Immunology*. (2003). Doi:10.1038/nri1132.
12. Llamas M.A., Aller M.A., Marquina D. et al. Bacterial translocation to mesenteric lymph nodes increases in chronic portal hypertensive rats // *Dig. Dis. Sci.* – 2010. – Vol. 55, №8. – P. 2244-2254.
13. Steven M. Opal, Gary E. Garber, Steven P. LaRosa, Dennis G. Maki, Ross C. Freebairn, Gary T. Kinasewitz, Jean-Francois Dhainaut, S. Betty Yan, Mark D. Williams, Delores E. Graham, David R. Nelson, Howard Levy, Gordon R. Bernard, Systemic host responses in severe sepsis analyzed by causative microorganism and treatment effects of drotrecogin alfa (activated), *Clin Infect Dis*. (2003). Doi: 10.1086/375593.
14. Ordoñez Karlos, Carlos Puyana Juan, Management of Peritonitis in the Critically Ill Patient, *Surg Clin North Am*. (2006). doi:10.1016/j.suc.2006.09.006.
15. S.N. Abdreshov, G.A. Demchenko, V.N. Gorchakov, A.N. Yeshmukhanbet, M.A. Yessenova, Lymph flow and cellular composition, rheological properties of lymph and blood in animals with experimental peritonitis, *News NAS RK. Ser. biol. and med*. (2021). <https://doi.org/10.32014/2021.2519-1629.84>
16. D.V. Volkov, B.A. Stadnikov, V.S. Tarasenko, F.V. Basov, Influence anti-ischemic and antioxidant therapy on a morphofunctional state of the small intestine with the syndrome enteral insufficiency in experimental peritonitis, *Orenburg Medical Herald*. (2015).
17. L.M. Gonzalez, A.J. Moeser, A.T. Blikslager, Animal models of ischemia-reperfusion-induced intestinal injury: progress and promise for translational research, *Am. J. Physiol. Gastrointest. Liver Physiol*. (2015). <https://doi.org/10.1152/ajpgi.00112.2013>.
18. E.V. Johansson Malin, Sjövall Henrik, C. Hansson Gunnar, The gastrointestinal mucus system in health and disease, *Nat. Rev. Gastroenterol. Hepatol*. (2013). doi:10.1038/nrgastro.2013.35.
19. V.A. Lazarenko, V.A. Lipatov, Ju.Ju. Blinkov, D.V. Skorikov, Jeksperimental'naja model' rasprostranennogo kalovogo peritonita [Experimental model of diffuse fecal peritonitis], *Kursk scientific and practical bulletin «Man and his health»*. (2008).
20. Avtandilov, G.G. *Medical Morphometry; Medicine: Moscow, Russia*, 384p. (1990)
21. L.F. Rogers, Magnetic resonance images of reactive lymphadenitis, *Lymphology*, (2006).
22. Ohman Kwon, Tae-Su Han, Mi-Young Son, Intestinal Morphogenesis in Development, Regeneration, and Disease: The Potential Utility of Intestinal Organoids for Studying Compartmentalization of the Crypt-Villus Structure, *Front Cell Dev Biol*. (2020). Doi: 10.3389/fcell.2020.593969.
23. M. Iizuka, S. Konno, Wound healing of intestinal epithelial cells, *World J. Gastroenterol*. (2011). doi: 10.3748/wjg.v17.i17.2161.
24. R. De Mey Jan and Freund Jean-Noël, Understanding epithelial homeostasis in the intestine, *Tissue Barriers*. (2013). doi:10.4161/tisb.24965.
25. Stewart A. Stieler, J.M. Freund, A.T. Blikslager, L.M. Gonzalez, Intestinal stem cell isolation and culture in a porcine model of segmental small intestinal ischemia, *J. Vis. Exp.* (2018). doi: 10.3791/57647
26. Elyasin, S.B. Zalavina, A.N. Mashak, A.P. Nadeev, S.V. Aydagulova, Small intestine morphology of rats-Adolescents with chronic cadmium sulfate intoxication, *Ulyanovsk Medico-biological Journal*. (2018). Doi 10.23648/UMBJ.2018.31.17226.
27. V.K. Esipov, I. I. Kagan, S.V. Yashnikov, Features of Microsurgical Anatomy of the Small Intestine in Experimental Widespread Purulent Peritonitis, *Journal of anatomy and histopathology*. (2019). <https://doi.org/10.18499/2225-7357-2019-8-2-43-46>.

28. Joseph M. Pickard, Melody Y. Zeng, Roberta Caruso, Gabriel Núñez, Gut Microbiota: Role in Pathogen Colonization, Immune Responses and Inflammatory Disease, *Immunol Rev.* (2017). doi:10.1111/imr.12567.
29. Gunnar C. Hansson, Role of mucus layers in gut infection and inflammation, *Curr Opin Microbiol.* (2012). doi:10.1016/j.mib.2011.11.002.
30. Jonathan U. Peled, Alan M. Hanash, Robert R. Jenq, Role of the intestinal mucosa in acute gastrointestinal GVHD, *Boold.* (2016). doi:10.1182/asheducation-2016.1.119.
31. Silvia Clotilde Modena, Lucia Aidos, Raffaella Rossi, Paola Pocar, Carlo Corino, and Alessia Di Giancamillo, Stages of Gut Development as a Useful Tool to Prevent Gut Alterations in Piglets, *Animals.* (2021). <https://doi.org/10.3390/ani11051412>

**Information about authors:**

*Abdreshov Serik Nauryzbaevich (corresponding author) – candidate of biological sciences, associate professor, Leading Researcher of the Laboratory of Physiology of the Lymphatic System at the Institute of Genetics and Physiology CS MSHE RK (Almaty, Kazakhstan, email: snabdreshov@mail.ru)*

*Yessenova Makpal Abunasyrkyzy – PhD student, Junior Researcher of the Laboratory of Physiology of the Lymphatic System at the Institute of Genetics and Physiology CS MSHE RK (Almaty, Kazakhstan, email: esenova\_makpal@mail.ru)*

*Yeshmukhanbet Anar Nurzhankyzy – PhD student, Junior Researcher of the Laboratory of Physiology of the Lymphatic System at the Institute of Genetics and Physiology CS MSHE RK (Almaty, Kazakhstan, email: eshmukhanbet96@mail.ru)*

*Demchenko Georgiy Anatolevich – Doctor of Medical Sciences, Head of the Laboratory of Physiology of the Lymphatic System at the Institute of Genetics and Physiology CS MSHE RK (Almaty, Kazakhstan, email: georgiidemchenko@mail.ru)*

*Gorchakov Vladimir Nikolaevich – Doctor of Medical Sciences, professor, Head of the Laboratory, Research Institute of clinical and experimental Lymphology – branch of Institute of Cytology and Genetics of SB RAS (Novosibirsk, Russia, v.gorchakov@g.nsu.ru)*

*Atanbaeva Gulshat Kapalbaevna – candidate of biological sciences, associate professor at the Department of Department of Biophysics, Biomedicine and Neuroscience, al-Farabi Kazakh National University (Almaty, Kazakhstan, email: gulshat.atanbaeva.76@mail.ru)*

*Mankibaeva Sandugash Amanzholovna – Senior Lecturer, Department of Biodiversity and Bioresources, al-Farabi Kazakh National University (Almaty, Kazakhstan, email: mankibaevasandugash@gmail.com)*

*Kulbayeva Marzhan Susarovna – candidate of biological sciences at the Department of Department of Biophysics, Biomedicine and Neuroscience, al-Farabi Kazakh National University (Almaty, Kazakhstan, email: marzhan.kulbaeva@kaznu.edu.kz)*

I.Yu. Silachyov<sup>1\*</sup>, V.A. Glagolev<sup>2</sup>, M.N. Kokkuzova<sup>2</sup><sup>1</sup>Institute of Nuclear Physics, Almaty, Kazakhstan<sup>2</sup>Institute of Geological Sciences named after K.I. Satpayev, Almaty, Kazakhstan

\*e-mail: silachyov@inp.kz

(Received 17 May 2023; received in revised form 15 September 2023; accepted 3 November 2023)

## Gold content determination in small core-samples by instrumental neutron activation analysis

**Abstract.** Application of instrumental neutron activation analysis (INAA) based on the relative method of concentration standardization was considered to determine Au content in small solid core-samples of the gold-bearing ores and rocks up to 10 g of the mass. The small core-samples about 10 mm in diameter and 22-23 mm in length were cut from the previously collected ore lumps or in-situ using a handheld drilling rig. The studied small core-samples and the polyethylene capsules of the same dimensions filled up with the corresponding certified reference material (CRM) were irradiated for 2 min by a lower density neutron flux with the help of the automated pneumatic transport system (PTS). Maximum mass and dimensions of the core-samples corresponded to the PTS design and to the conditions of its safe operation. A special device was made to fix the transport capsules in the stable counting geometry making possible to eliminate the influence of the neutron flux gradient during irradiation. Due to the substantial differences in CRM and solid sample densities, corrections for neutron self-shielding and for gamma-ray self-absorption by the core-samples were applied. The method was tried to analyze Au content in 170 small core-samples presenting different gold-bearing ores and country rocks from the Kazakhstan's gold-barite-polymetallic deposit Maikain. This approach, rather simple methodically and requiring no unique equipment, can be used to assess gold resources together with the methods of geostatistics.

**Key words:** Neutron activation analysis, gold, small core-samples.

### Introduction

A main problem of gold dependable determination in ores and gold-bearing rocks comes from its extremely heterogeneous distribution. Together with finely dispersed "invisible" forms such as colloidal, cluster, and chemically bound, gold occurs as dissemination in a range of minerals (pyrite, chalcopyrite, arsenopyrite, quartz, etc.) forming native grains or discrete particles highly variable in size [1-3]. Anomalously high gold contents may be also caused by the secondary enrichment processes. To improve reliability of gold analysis representative samples should be used including "multiple smaller aliquots of the same sample" or larger sample aliquots [4]. The size of the latter depends on the variety of factors and, hence, is discussible, but its mass is unanimously considered beginning from 10 g, leastwise [5]. This is a rather large amount which can be scarcely introduced if the most commonly spread destructive pretreatment is applied followed by a high-sensitive instrumental analytical

technique. Moreover, the other challenges can arouse substantially diminishing reliability of gold content determination.

Firstly, grinding of geological samples presents a problem itself. Soft gold grains are resistant to milling and may be lost in one sample and contaminate the others via the milling vessels [6]. To avoid contamination, rock samples should be passed through the mill in the order of increasing of their gold content that is hardly possible before analysis.

On the other hand, Au mass fractions are frequently underestimated in silicates and in the resistant sulphide matrix due to incomplete dissolution when the classical acid digestion is applied, e.g. by aqua regia [7]. The popular up-to-date technique such as microwave-assisted pressure digestion at elevated temperatures is more effective and efficient, but all the same doesn't always solve the problem of complete sample decomposition. Its other disadvantages include a limited aliquot mass, complicated vessel constructions, and expensive equipment [8].

All these difficulties are avoided if the nondestructive pretreatment oriented to instrumental analytical techniques dealing with the intact larger samples can be applied. Advantages and limitations of such methods as laser ablation inductively coupled plasma mass spectrometry and high-energy instrumental photon activation analysis (IPAA) using both the reactions of isomeric state photoexcitation  $^{197}\text{Au}(\gamma, \gamma)^{197\text{m}}\text{Au}$  and photoneutron production  $^{197}\text{Au}(\gamma, n)^{196}\text{Au}$ , are discussed in [6] in the context of geochemical explorations. The last variant of IPAA is likely quite appropriate to analyze routinely large, up to 0.5 kg, rock samples for industrially significant gold mass fractions, except for the facilities to produce high-energy (20–30 MeV) gamma radiation – linear electron accelerators [9] or cyclotrons [10] – are mainly unique research installations.

Compact neutron generators to conduct the fast neutron (14 MeV) instrumental neutron activation analysis (INAA) are far more accessible [11, 12]. However, the sensitivity of gold determination is often insufficient due to a significantly (several orders of magnitude) lower flux density of 14 MeV neutrons comparing with the thermal neutron flux density  $\sigma_0$  produced by nuclear reactors, as well as due to the low cross-sections of activation by the fast neutrons ( $\approx 2.1$  barn,  $^{197}\text{Au}(n, 2n)^{196}\text{Au}$  and  $\approx 1.6$  barn,  $^{197}\text{Au}(n, 2n)^{196\text{m}}\text{Au}$ ).

Comparing with the methods above, high-sensitive thermal neutron INAA ( $\sigma_0 = 98.7$  barn,  $^{197}\text{Au}(n, \gamma)^{198}\text{Au}$ ), taking account of its advantages [5, 13, 14], seems being the most suitable method to analyze solid volumetric samples for Au content provided neutron self-shielding and gamma-ray self-absorption by the samples are considered, and the corrections for sample size deviation from the “point source” during irradiation and counting are made [15]. Different approaches both semi-empirical and theoretical are developed to evaluate and account these corrections mainly for the regular-shaped (cylindrical) samples [16, 17]. If the internal standard method (ISM) is used in comparator INAA, the corrections are basically reduced to zero or minimized. Moreover, irregular-shaped samples can be analyzed in this case too [18].

The ISM based comparator INAA was tried in the previous investigation [6] to determine Au content in the puck-like common rock samples 15–20 g of the mass which were cut off from the corresponding drill-cores. Fe mass fraction in the same volumetric samples by X-ray fluorescence (XRF) method was used as the internal standard. Only homogenous rocks with respect to the internal comparator content can

be reliably analyzed using this approach. Therefore, it is restricted by geochemical explorations of some types of more or less homogenous magmatic and metamorphic rocks characterized by Au contents close to that of the upper continental crust (UCC).

Subsequent investigations showed a great scope of heterogeneity for the similar puck-like samples cut off from the gold-bearing rocks and ores such as quartzites, black shales, and polymetallic ores. None of the potential comparator elements (Fe, As, Rb, Ba) can be used as the internal standard due to substantial unreliability of their determination by XRF resulted from high heterogeneity of these elements' distribution both in the volume and on the surface of the samples. After irradiation and counting, the samples could be powdered to analyze them reliably for, e.g., Fe content, but this idea was abandoned for the reasons of radiation safety.

That is why another approach was tried in the present work consisting in implementing INAA of the small core-samples using the simple way of relative standardization. This became possible due to the advantages of irradiation in a distant channel out of the reactor active zone, as well as due to small sizes and regular cylinder shape of the core-samples, resulted in minimum of the corrections which should be accounted. The method was applied to determine Au content both in the ores and some country rocks of the mined Maikain deposit in Kazakhstan.

## Materials and methods

Gold-barite-polymetallic deposit Maikain is located in Bayanaul district of the Pavlodar region, North-Eastern Kazakhstan. The gold-bearing ores form several associations differing in Au content. Gold occurs as inclusions in all main ore minerals, quartz and barite displaying irregular mottling. Native gold is found as intergrowth with bornite forming thin veins. The sizes of gold particles are 20 to 50  $\mu\text{m}$ , sometimes up to 200  $\mu\text{m}$  [19, 20].

A part of the studied geological material – lumps of ores and country rocks – was collected by M.Kokkuzova and delivered to a Satpayev Institute's laboratory. Several small core-samples were drilled out from every lump using a piped core bit with diamond chisels (inner diameter is 10 mm) installed into a portable drill. Then the billets were cut with a diamond saw to get the right cylinders 22–23 mm in length. The lump remainders were crashed and ground to the particle size about 0.07 mm to investigate them as the combined powder samples corresponding to several core-samples of the same origin.

Sizes of the small core-sample were selected to fit the dimensions of the standard HDPE capsules (inserted in the transport ones) to implement relative method of standardization. The masses of core-samples were evaluated preliminarily; none of them should exceed  $\approx 10$  g to provide safe operation of the automated pneumatic transport system (PTS) [21, 22], i.e. to avoid capsule jamming during irradiation.

The other samples under investigation were taken by V. Glagolev *in situ*, using the same equipment, from the different areas of Maikain deposit including the opencast workings and one or two new sites cleared from the surface to revise ore resources. The small core-samples of different geological objects were drilled out as close as possible one to another. Lumps of the same rocks were collected too to prepare powdered samples.

All cylinder samples turned out practically identical, even enough and without visible faults. Exterior view of several small core-samples drilled out of the same geological object is shown on Figure 1. As much as 170 volumetric samples were prepared on the whole.



**Figure 1** – Three small core-samples drilled out from the lump sample M2322 (banded quartz ore)

Masses of the core-samples were determined up to the third decimal with a Mettler Toledo analytical balance. Diameter of the cylinder samples depending on the piped core bit was ascribed to  $9.5 \pm 0.2$  mm; the height was measured with a caliper within the accuracy  $\pm 0.5$  mm. Based on these data, the combined relative standard uncertainty ( $\delta_\rho$ ) of the sample density evaluation was assessed [23] ( $\delta_\rho$  is used below to evaluate expanded uncertainty of Au determination) – about 3.5%.

Unlike the objects which were being studied earlier during geochemical explorations [6] the mined

Maikain deposit is characterized by much more Au contents. Hence short irradiation time and/or lower density of the thermal neutron flux  $\Phi_{th}$  are enough to implement INAA. Therefore, the horizontal channel of the WWR-K research reactor (INP, Almaty) equipped with PTS was selected.  $\Phi_{th}$  value in this channel is approximately one twentieths comparing with that ( $\approx 9 \times 10^{13} \text{ cm}^{-2} \text{ s}^{-1}$ ) in the vertical channel used to irradiate the samples [24, 25]. Since the PTS terminal is isolated from the reactor active zone cooled by water, there wasn't need to seal the samples in polyethylene before irradiation. The other advantages of the horizontal channel include invariability of the irradiation geometry and hence the same neutron flux gradient for the equal length cylinder samples, simple operation, promptness, and independence of the reactor personal. The limited mass of the studied samples comparing with irradiation in the vertical channels is a certain disadvantage, but the used PTS wasn't initially designed to transport heavy objects.

To conduct INAA, the small core-samples were fixed in the center of the HDPE transport capsules and irradiated one by one for 2 minutes. This irradiation time was selected before to avoid overheating of the capsules inside the non-cooled PTS terminal.

The corresponding powder samples intended for the detailed geochemical investigations were prepared for irradiation in the vertical channel No.10-6 of WWR-K in the usual manner [25]. Approximately 100 mg of the assays were sealed in plane double polyethylene bags and packed batchwise in aluminium foil. Every batch included a dozen samples and a neutron flux monitor ( $\approx 10$  mg of  $\text{ZrO}_2$ , the Institute of Reference Materials, Ekaterinburg, Russian Federation). No samples of certified reference material (CRM) were involved since the comparator model of concentration standardization based on the internal standard method was conceived [6, 21, 24]. All the packages were independently irradiated for 2.5 h.

Gamma-spectrometric measurements of the small core-samples were carried out for 20 minutes 7 days later when radionuclide  $^{76}\text{As}$  substantially decayed. The following equipment was used: a coaxial HPGe detector GC2018 with a horizontal dipstick cryostat (Canberra, 20% of a relative efficiency, and 1.80 keV at the 1332 keV peak of  $^{60}\text{Co}$  of an energy resolution) and a Canberra multi-channel analyzer DSA-1000, both incorporated into PTS.

Counting geometry was organized in a manner making possible to eliminate the influence of the neutron flux gradient in the irradiation terminal directed along the transport capsule axis. The special



Plexiglas attachment was made and mounted on the detector cap to fix the transport capsules parallel to the cap's plane surface as Figure 2 demonstrates. The small core-samples are located in the same position 25 mm distant from the detector cup, right opposite to its centre. That is the way the central symmetry of the counting geometry was achieved.



**Figure 2** – HPGe detector GC2018 with the Plexiglas attachment on its cap and a HDPE transport capsule held by a tweezers

The powder samples were counted for Au (and some other element) content for 40 minutes after 12–14 days of decay using an extended-range HPGe detector GX5019 (Canberra, 50% of a relative efficiency, and 1.86 keV of an energy resolution) and the similar multi-channel analyzer. All the samples were placed at the distance of 24 mm from the detector cap.

Both detectors were calibrated for relative detection efficiency with the help of a multi-gamma ray standard MGS-1 ( $^{152}\text{Eu}$ ,  $^{154}\text{Eu}$ ,  $^{155}\text{Eu}$ ) also by Canberra.

GENIE 2000 software was used for spectra collection in the first case, and the “AnalGamma” software developed in the INP – to analyze the powder samples. The last one was applied for spectra treatment as well, in the same way as before, e.g. [25].

Practically, there are no unresolved spectral interferences to the intensive analytical gamma-line of the radionuclide  $^{198}\text{Au}$  (411.80 keV of the energy  $E$ ) which should be accounted, especially when gold ore samples are analyzed. Only in the case of country

rock investigation count rate of  $^{198}\text{Au}$  was corrected by that of the low-intensive gamma-line of  $^{152}\text{Eu}$  ( $E = 411.12$  keV).

Fe content of the powder samples used as the internal standard to determine their Au mass fraction by comparator INAA was determined by XRF technique with a portable energy dispersive X-ray spectrometer RLP-21T by JSC “AspapGeo” (Almaty, Kazakhstan). This spectrometer is applied constantly to support comparator INAA and was mentioned in the previous investigations more than once. RLP-21T is enrolled in the State Register of Measuring Devices (Certificate № 670, valid to 27.07.2025), and the corresponding analytical technique is registered by the National Body for Certification of Kazakhstan (Certificate No. 69-2022, valid till 15.02.2027).

### Results and discussion

Gold content  $C_a$  (ppm) of the analyzed small core-samples was calculated as follows according to a variant of the relative method of concentration standardization:

$$C_a = \frac{J_a D_a}{G_a F_a m_a t_{irr}^a K_r}, \quad (1)$$

where  $J_a$  is net peak count rate of  $^{198}\text{Au}$  analytical gamma-line (cps);  $D_a = \exp(-\lambda_{\text{Au}}(7 - t_d))$  is decay factor depending on  $^{198}\text{Au}$  decay constant  $\lambda_{\text{Au}}$  and decay time  $t_d$  after the end of irradiation ( $D_a$  is normalized to  $t_d = 7$  d for convenience);  $G_a$  is the correction factor for neutron self-shielding by the samples;  $F_a$  is the correction factor for the analytical gamma-ray self-absorption by the sample;  $m_a$  is the sample mass (g);  $t_{irr}^a$  is irradiation time (min).

Coefficient  $K_r$  (cps ppm $^{-1}$  g $^{-1}$  min $^{-1}$ ) can be determined by the similar way with the help of a number of CRMs certified for Au content:

$$K_r = \frac{J_r D_r}{G_r F_r C_r m_r t_{irr}^r}. \quad (2)$$

$K_r$  corresponds to  $^{198}\text{Au}$  analytical gamma-line count rate  $J_r$  after 7 d of decay (corrected by the factors  $G_r$  and  $F_r$ ) per  $m_r = 1$  g of a CRM with gold content  $C_r = 1$  ppm irradiated for  $t_{irr}^r = 1$  min. Under the conditions of a stable neutron flux density in the irradiation channel equipped with PTS, for the same sample dimensions, irradiation and counting geometries,  $K_r$  is practically invariable.

To evaluate  $K_r$ , the next four CRMs were selected: OSO 163 and OSO 165 by the All-Russian Scientific-Research Institution of Mineral Resources (Moscow), GSO 1789 by the Vinogradov Institute of Geochemistry (Irkutsk, Russian Federation), and OREAS 684 by Ore Research & Exploration (Australia). Four standard HDPE capsules close by their inner dimensions to the analyzed core-samples

(22 mm of the height and 10 mm across the diameter) were filled up tightly with these CRMs and then welded all around. Since more than 2 g of the matter were tampered into the capsules (Table 1), the assays can be considered representative enough, despite the CRMs were produced from natural gold-bearing ores. Moreover, homogeneity of the CRMs was confirmed by their previous utilization in INAA.

**Table 1** – Au content of four small volumetric CRM samples ( $P = 0.95$ ), their masses, densities and correction factors for self-absorption of the 411.8 keV gamma-ray

CRM name	CRM type	$m_r$ , g	$\rho_r$ , g cm <sup>-3</sup>	$F_r$	Au, $\mu\text{g g}^{-1}$ (ppm)	
					Certified value	Measured value
OSO 163	Gold-bearing ore	2.286	1.386	0.945	$0.91 \pm 0.02$	$0.889 \pm 0.075$
OSO 165	Gold-bearing ore	2.223	1.348	0.947	$6.0 \pm 0.1$	$6.08 \pm 0.48$
GSO 1789	Gold-bearing ore	2.180	1.322	0.948	$4.5 \pm 0.1$	$4.61 \pm 0.39$
OREAS 684	Platinum group element ore	2.239	1.358	0.946	$0.248 \pm 0.007$	$0.244 \pm 0.022$

The capsules were irradiated for 1-3 min depending on Au content and counted in the same way as the investigated core-samples.

Correction factor for the neutron self-shielding  $G_r$  for Au was assessed with the help of the spreadsheet by C. Chilian et al. [26] supposing that major element contents in the samples correspond to that of UCC [27], and Sm, Eu and Gd mass fractions characterized by the maximum values of the thermal neutron cross-section are equal to their UCC values [28]. With the CRM masses presented in Table 1 the factor  $G_r$  is close to unity (0.991) and doesn't depend on Au content up to 100–200  $\mu\text{g g}^{-1}$ .

Correction factor for the  $^{198}\text{Au}$  analytical gamma-ray self-absorption  $F_r$  was evaluated following the next expression:

$$F_r = \frac{1 - \exp(-\rho_r \mu_\Sigma(E_{\text{Au}}) h_r)}{\rho_r \mu_\Sigma(E_{\text{Au}}) h_r}, \quad (3)$$

where  $\rho_r$  is core-sample density ( $\text{g cm}^{-3}$ );  $\mu_\Sigma(E_{\text{Au}})$  – total photon mass coefficient of  $^{198}\text{Au}$  analytical gamma-line attenuation ( $\text{cm}^2 \text{g}^{-1}$ ); and  $h_r$  – effective sample thickness (cm). Equating the area of the cylinder sample base to the equal-area square,  $h_r$  was taken equal to 0.886 cm. Individual  $\mu(E_{\text{Au}})$  values for the main rock-forming oxides were picked up from a NIST database [29]. These values are very close one to another since interaction of the high-energy gamma-rays with the matter is mainly brought to the

scattering processes. The issue is discussed in [6] in more details.  $\mu_\Sigma(E_{\text{Au}}) = 0.0927 \text{ cm}^2 \text{g}^{-1}$  corresponding to the composition of UCC is accepted to assess  $F_r$ . The values of  $F_r$  factor for four CRMs are presented in Table 1.  $F_r$  values depend linearly on the sample density up to  $5 \text{ g cm}^{-3}$ , i.e. including heavy rocks, therefore relative uncertainty of  $F_r$  factor evaluation can be accepted equal to  $\delta_\rho$  (see above).

Thus, taking account of the considerations above, four assessments of  $K_r$  coefficient were made according to Eq. 2. The mean value  $K_r = 0.9686$  was used to calculate Au content in the small core-samples (Eq. 1), and its relative standard deviation  $\delta_{K_r} = 2.2 \%$  – to evaluate uncertainty of the results.

Expanded uncertainty of Au determination  $U(C_a)$  was estimated as follows ( $P = 0.95$ ):

$$U(C_a) \approx 2C_a \sqrt{\frac{u(J_a)^2}{J_a^2} + (\delta_\rho)^2 + (\delta_{K_r})^2}, \quad (4)$$

where  $u(J_a)$  is the standard uncertainty of  $J_a$ ,  $\delta_\rho$  and  $\delta_{K_r}$  are evaluated above (all the summands are in %). Relative uncertainties of  $m$  and  $t_{\text{irr}}^a$  measuring (Eq. 1) are far lower than the terms accounted by Eq. 4 and are hence ignored.  $G_a$  is considered a constant.

The results of four small volumetric CRM analysis for Au content using Eq. 1 ( $P = 0.95$ ) are presented in Table 1. The measured values differ from the certified ones by no more than 2.5%. Expanded uncertainty

doesn't exceed the allowable standard deviation of the results of Au determination according to the III category of precision (of analysis) (12-30% for the intervals including these contents) according to OST 41-08-221-04 [30], for samples with fine-dispersed gold particles <0.1 mm of the size].

Unlike few CRMs above which were irradiated practically simultaneously, 16 days were spent to irradiate all the studied small core-samples divided

into a range of parties. To take account of possible  $K_r$  diminishing for such a long time due to nuclear fuel burn-out in the WWR-K active zone (the reactor is halted every three weeks to replace a part of uranium fuel elements), one more set of the same CRMs was prepared and irradiated in the end of the investigation. The assessed  $K_r$  value decreased by 5% only, so linear interpolation with time of the coefficient was used to calculate Au contents (Eq. 1).

**Table 2** – Gold content in the small core-samples and corresponding powder samples collected from the gold-polymetallic deposit Maikain, ore material ( $P = 0.95$ )

Sample number	Description	Core-sample			Powder sample
		Mass, g	Density, g cm <sup>-3</sup>	Au, µg g <sup>-1</sup> (ppm)	
M1859	Pyrite-barite-polymetallic ore	6.854	4.21	1.27 ± 0.11	1.30 ± 0.13
		6.826	4.19	1.26 ± 0.11	
		6.944	4.36	1.67 ± 0.14	
		7.385	4.34	1.56 ± 0.13	
		6.545	4.02	1.23 ± 0.11	
M2124	Pyrite-barite-polymetallic ore	7.354	4.51	2.09 ± 0.18	1.64 ± 0.16
		7.509	4.51	2.47 ± 0.21	
		7.275	4.47	1.23 ± 0.11	
		7.678	4.52	1.30 ± 0.11	
		7.299	4.48	1.54 ± 0.13	
M1998	Copper-pyrite ore	7.571	4.45	8.31 ± 0.71	6.41 ± 0.61
		7.558	4.54	10.0 ± 0.8	
		7.893	4.55	5.54 ± 0.47	
		7.519	4.52	9.18 ± 0.78	
		7.346	4.51	7.47 ± 0.63	
M2052	Copper-pyrite ore	7.290	4.47	2.79 ± 0.24	2.80 ± 0.26
		7.381	4.53	5.09 ± 0.43	
		7.309	4.49	9.19 ± 0.77	
		7.098	4.36	5.45 ± 0.46	
		7.462	4.39	1.90 ± 0.16	
M2514	Sulphide ore	7.678	4.61	0.292 ± 0.026	0.342 ± 0.034
		7.539	4.73	0.251 ± 0.023	
		7.043	4.52	0.311 ± 0.028	
		7.570	4.65	0.251 ± 0.023	
		7.685	4.72	0.277 ± 0.025	
M2684	Sulphide-polymetallic ore	6.911	4.15	2.63 ± 0.22	2.49 ± 0.24
		6.601	4.14	2.75 ± 0.23	
		6.757	4.06	2.44 ± 0.21	
		6.505	3.99	2.62 ± 0.22	
		6.836	4.11	2.71 ± 0.23	
M2691	Quartz sulphide ore	4.983	2.99	1.61 ± 0.14	1.51 ± 0.14
		4.790	2.88	3.20 ± 0.27	
		4.621	2.78	2.66 ± 0.23	
		5.118	2.95	0.906 ± 0.077	
		4.879	2.81	1.67 ± 0.14	

Table continuation

Sample number	Description	Core-sample			Powder sample
		Mass, g	Density, g cm <sup>-3</sup>	Au, µg g <sup>-1</sup> (ppm)	
M2821	Quartz sulphide ore	6.921	4.16	0.525 ± 0.047	
		6.767	4.15	1.21 ± 0.10	
		7.032	4.22	0.333 ± 0.030	
		7.180	4.31	0.376 ± 0.034	
		7.144	4.29	0.461 ± 0.040	
M2322	Banded quartz ore	5.336	3.28	0.684 ± 0.059	
		4.500	2.70	0.365 ± 0.033	
		4.539	2.79	0.560 ± 0.049	
		4.917	3.09	0.575 ± 0.050	
		5.264	3.16	0.312 ± 0.028	

The other distinction between powder CRM and core-sample investigation consists in the substantially higher density of the latter reaching approximately 2.5–4.5 g cm<sup>-3</sup> depending on the rock type. It results in small diminishing of  $G_a$  factor value to no less than 0.970 for the densest samples using the spreadsheet above.  $F_a$  factor varies in the broader range about 0.91–0.84 for the same interval of core-sample density.

At last, taking account of the high ratio of the resonance integral to the thermal neutron cross-section the isotope <sup>197</sup>Au is characterized (15.7 [31]), invariability of thermal to epithermal neutron flux ratio  $f$  in the beginning and in the end of core-sample irradiation was verified. The mentioned ZrO<sub>2</sub> flux monitors were used with this end in view, enlarged to ≈100 mg to compensate the lower neutron flux ratio in the horizontal channel. Two  $f$  values estimated using the “bare bi-isotopic method”, e.g. [25], actually did not differ from one another being close to the mean value 85.0 ± 3.5 assessed for the long observation period.

As an example, the results of Au content determination in several samples (as they were documented) presenting different types of the Maikain's gold-bearing ores are demonstrated in

Table 2. Five small core-samples were cut off from each sample, and the corresponding values of their mass and density are added to the table too. The last column shows the results of Au determination in the powder samples prepared as mentioned above.

Almost all ores displayed low density variations, no more than 8%, due to their composition variability, except for the banded quartz ore (up to 18%). Unlike this, gold revealed high degree of heterogeneity within the samples, especially for quartz and some polymetallic ores: Au contents in the small core-samples cut off from one lump differ three-five times. Sulphide ores turned out far more homogeneous in this respect.

The average gold mass fractions in the core-samples differ from that of the powdered samples to various extents, up to more than twice, and there may be a range of reasons for it. In any case, these powder samples, as they were prepared, seem far from being representative. To avoid this much more of rock material should be ground with all the problems mentioned in introduction.

Figure 3 presents in a log-linear scale a part of the gamma-ray spectrum of the small core-sample M2322 (Figure 1), number 2 (Table 2), counted after 7 days of decay.

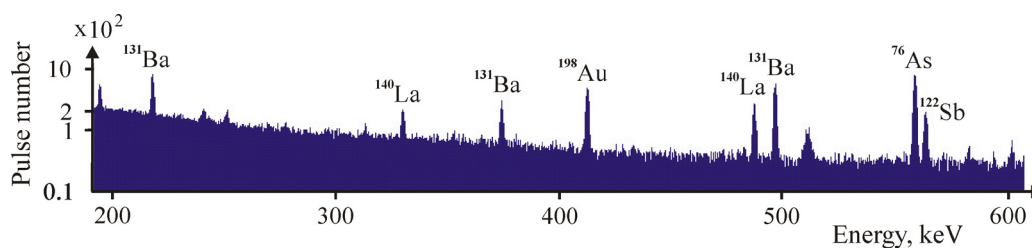
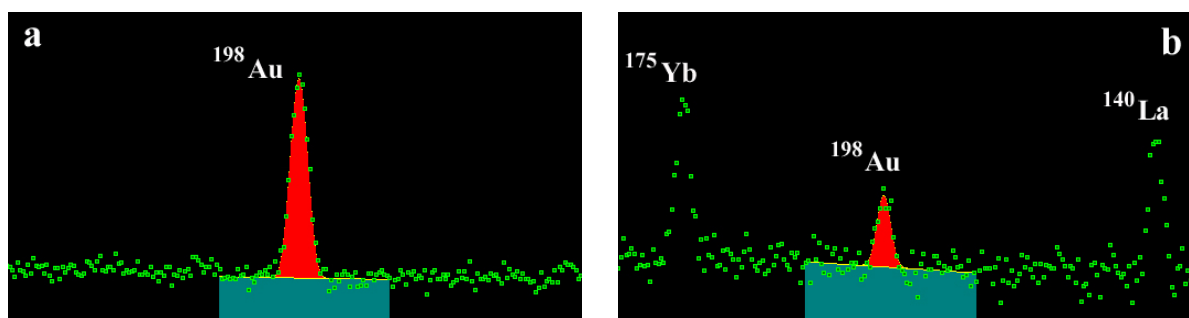


Figure 3 – A part of the gamma-ray spectrum of the small core-sample M2322(2) counted by GC2018 after 7 days of decay (in a log-linear scale)

Gamma-ray peaks of arsenic and antimony usually accompanying Au in gold deposits are noticeable, as well as some peaks of lanthanum and barium (the latter are due to the rather high Ba content about 1.5% measured in the corresponding powder sample). The volumetric sample spectrum is actually just the same as usual powder samples yield. The gist is to assess by sight sensitivity of the approach, i.e.  $^{198}\text{Au}$  background/

peak ratio, taking account of the short irradiation time (2 minutes) and a lower neutron flux in the horizontal channel. With the rather moderate Au mass fraction  $0.365 \mu\text{g g}^{-1}$ , substantial potential can be noted to determine far lower Au contents in the similar way.

Figure 4(a) displaying treatment of 411.80 keV gamma-line of  $^{198}\text{Au}$  by the “AnalGamma” software demonstrates it more visibly.



**Figure 4** – Net peak area of the  $^{198}\text{Au}$  analytical gamma-line in the “AnalGamma” treatment window: (a) – M2322(2), (b) – M2749(1)

The results of gold mass fraction determination in a range of the country rocks collected from Maikain deposit are presented in Table 3 following the same format as above. Three to five small core-samples were cut off from each lump, but only one of them is

put into the table if Au content turned out lower than the limit of detection (LOD). The latter was assessed separately for every small core-sample in the same way as in [21] according to the common expression applied in the spectroscopic methods.

**Table 3** – Gold content in the small core-samples and corresponding powder samples collected from the gold-polymetallic deposit Maikain, country rocks ( $P = 0.95$ )

Sample number	Description	Core-sample			Powder sample
		Mass, g	Density, g cm <sup>-3</sup>	Au, $\mu\text{g g}^{-1}$ (ppm)	
M1964	Gabbro dike	4.258	2.61	< 0.011	$0.019 \pm 0.004$
M2027	Andesite-basalt rock tuff	4.161	2.61	< 0.012	$0.067 \pm 0.008$
M2083	Sericite-quartz metasomatic rock	4.239	2.55	< 0.010	$0.038 \pm 0.005$
M2131	Sericite-quartz metasomatic andesite	4.115	2.58	$0.132 \pm 0.012$	$0.218 \pm 0.022$
		4.142	2.60	$0.149 \pm 0.013$	
		3.944	2.59	$0.158 \pm 0.014$	
		4.104	2.63	$0.166 \pm 0.015$	
M2135	Sericite-quartz metasomatic andesite	4.252	2.55	< 0.010	$0.064 \pm 0.008$
		4.218	2.53	$0.025 \pm 0.005$	
		4.173	2.56	$0.018 \pm 0.004$	
		4.212	2.59	$0.017 \pm 0.004$	
M2139	Sericite-quartz shale	3.730	2.34	< 0.013	$0.011 \pm 0.003$

Table continuation

Sample number	Description	Core-sample			Powder sample
		Mass, g	Density, g cm <sup>-3</sup>	Au, µg g <sup>-1</sup> (ppm)	
M2394	Quartzite	4.667	2.75	0.027 ± 0.005	
		4.261	2.80	0.043 ± 0.007	
		4.501	2.82	0.017 ± 0.004	
		4.504	2.83	0.018 ± 0.004	
		4.591	2.76	0.023 ± 0.005	
M2401	Schistose sericite-quartz rock	3.867	2.71	0.101 ± 0.010	
		4.589	2.70	0.108 ± 0.011	
		4.500	2.70	0.108 ± 0.011	
M2749	Schistose sericite-quartz rock	4.059	2.66	0.035 ± 0.005	
		4.261	2.62	0.040 ± 0.005	
		4.518	2.66	0.089 ± 0.011	
		4.247	2.61	0.051 ± 0.006	
M2824	Tuff	4.374	2.63	< 0.011	0.100 ± 0.10

As Table 3 shows, gold is distributed distinctly more homogeneous in the country rocks. This probably can be explained by vast prevalence of the finely dispersed forms over the native gold, if the last is present in these rocks at all. In this connection it should be noted that Au content in the majority of the powder samples exceeds notably that of the corresponding small core-samples. The situation is like the mentioned in introduction, i.e. the part of the powder samples were seemingly contaminated with gold during grinding.

Treatment of the low-intensity gamma-line of <sup>198</sup>Au when gold mass fraction in a core-sample is close to LOD is presented in Fig. 4(b) using specimen M2749, number 1, as the example. A rather low gold content about 0.035 µg g<sup>-1</sup> is surely distinguished above the background. On the whole, the LOD values of Au determination in the small core-samples after short irradiation in the horizontal channel are higher by one order of magnitude than the values usually achieved in geochemical investigations [6]. However, this scarcely can be regarded as a serious disadvantage of the approach since it is intended to analyze industrially significant gold contents which are at least two orders higher.

## Conclusion

A simple variant of INAA based on the relative method of concentration standardization was used to determine Au content in the small core-samples collected from a Kazakhstan's gold-bearing deposit. The core-sample mass was restricted to approximately 10 g to provide safe operation of the automated PTS. The height and diameter of the volumetric samples

(22–23 mm and ≈10 mm, respectively) are identical to the dimensions of the standard HDPE capsules filled up with the CRMs certified for Au content. So no corrections for the difference in sample geometry were necessary. Invariability of irradiation and counting geometries was ensured by the construction of the irradiation terminal and by the special Plexiglas attachment mounted on the detector cap. Due to the substantial difference in the densities of the CRMs and the small core-samples, corrections for neutron self-shielding and self-absorption of <sup>198</sup>Au analytical gamma-line were applied. The first one never exceeded 2% in the solid samples regardless of Au content, the latter reached 11% (both relatively to that for the CRMs). Influence of the neutron flux gradient during irradiation was eliminated owing to the centrally symmetric counting geometry.

INAA of small core-samples doesn't need any unique equipment, only the automated PTS, research reactors are usually equipped with. The tried approach can't solve all the problems connected with gold determination in highly heterogeneous ores. However, it can promote substantially to assess gold resources provided the small core-samples are collected in-situ and the methods of geostatistics are used to interpret the results.

## Acknowledgments

The work was supported by the grants BR23891691 from the Ministry of Energy of the Republic of Kazakhstan and BR10264324 from the Committee of Geology under the Ministry of Ecology, Geology and Mineral Resources of the Republic of Kazakhstan.

## References

1. Gas'kov I.V. (2017) Major impurity elements in native gold and their association with gold mineralization settings in deposits of Asian folded areas. *Russ Geol Geophys*, vol. 58(9), pp. 1080-1092. <http://doi.org/10.1016/j.rgg.2017.08.004>.
2. Matvienko V.N., Kalashnikov Y.D., Goncharov A.A. (2014) Natural clusters as the source of ore material formation in noble metals deposits: case study of gold fields in the Republic of Kazakhstan, Russia, Uzbekistan, and Kyrgyzstan. *Life Sci J*, vol. 11(1), pp. 269-281.
3. Dominy S.C., Platten I.M. (2007) Gold particle clustering: a new consideration in sampling applications. *Appl Earth Sci*, vol. 116(3), pp. 130-142. <https://doi.org/10.1179/174327507X207474>.
4. Pitcairn I.K. (2011) Background concentrations of gold in different rock types. *Appl Earth Sci*, vol. 120(1), pp. 31-38. <https://doi.org/10.1179/1743275811Y.0000000021>.
5. Balaram V. (2008) Analytical methods for gold and other precious metals in exploration studies. *J Appl Geochem*, vol. 10(2A), pp. 545-562.
6. Silachyov I.Yu., Glagolev V.A. (2022) Comparator neutron activation analysis of the solid volumetric rock samples for gold content. *IJBCh*, vol. 15(1), pp. 90-101. <https://doi.org/10.26577/ijbch.2022.v15.i1.010>.
7. Balaram V. (2008) Recent advances in the determination of PGE in exploration studies – A review. *J Geol Soc India*, vol. 72, pp. 661-677.
8. Balaram V., Subramanyam K.S.V. (2022) Sample preparation for geochemical analysis: Strategies and significance. *Adv Sample Prep*. <https://doi.org/10.1016/j.sampre.2022.100010>.
9. Alsufyani S.J., Liegey L.R., Starovoitova V.N. (2014) Gold bearing ore assays using  $^{197}\text{Au}(\gamma, n)^{196}\text{Au}$  photonuclear reaction. *J Radioanal Nucl Chem*, vol. 302(1), pp. 623-629. <https://doi.org/10.1007/s10967-014-3239-2>.
10. Lee M., Norman E.B., Akindele O.A., et al. (2022) Fast neutron activation of ubiquitous materials. *Appl Radiat Isot*, vol. 181, p. 110098. <https://doi.org/10.1016/j.apradiso.2022.110098>.
11. Marchese N., Cannuli A., Caccamo M.T., et al. (2017) New generation non-stationary portable neutron generators for biophysical applications of neutron activation analysis. *Biochim Biophys Acta*, vol. 1861(1), pp. 3661-3670. <http://dx.doi.org/10.1016/j.bbagen.2016.05.023>.
12. Nat A., Ene A., Lupu R. (2004) Rapid determination of gold in Romanian auriferous alluvial sands, concentrates and rocks by 14 MeV NAA. *J Radioanal Nucl Chem*, vol. 261(1), pp. 179-188. <https://doi.org/10.1023/B:JRNC.0000030954.29323.39>.
13. Rodríguez N., Yoho M., Landsberger S. (2016) Determination of Ag, Au, Cu and Zn in ore samples from two Mexican mines by various thermal and epithermal NAA techniques. *J Radioanal Nucl Chem*, vol. 307(2), pp. 955-961. <https://doi.org/10.1007/s10967-015-4277-0>.
14. Nyarku M., Nyarko B.J.B., Serfor-Armah Y., et al. (2010) Investigating concentration distributions of arsenic, gold and antimony in grain-size fractions of gold ore using instrumental neutron activation analysis. *Appl Radiat Isot*, vol. 68(2), pp. 378-383. <https://doi.org/10.1016/j.apradiso.2009.10.010>.
15. Bode P., Romanò S., Romolo, F.S. (2018) Large sample neutron activation analysis avoids representative sub-sampling and sample preparation difficulties: an added value for forensic analysis. *Forensic Chem*, vol. 7, pp. 81-87. <https://doi.org/10.1016/j.forc.2017.10.002>.
16. Menezes M.Â., Jaćimović R. (2014) Implementation of a methodology to analyse cylindrical 5-g sample by neutron activation technique,  $k_0$  method, at CDTN/CNEN, Belo Horizonte, Brazil. *J Radioanal Nucl Chem*, vol. 300(2), pp. 523-531. <https://doi.org/10.1007/s10967-014-3074-5>.
17. Farina Arbocò F., Vermaercke P., Sneyers L., et al. (2012) Experimental validation of some thermal neutron self-shielding calculation methods for cylindrical samples in INAA. *J Radioanal Nucl Chem*, vol. 291(2), pp. 529-534. <https://doi.org/10.1007/s10967-011-1211-y>.
18. Sudarshan K., Nair A., Goswami A. (2003) A proposed  $k_0$  based methodology for neutron activation analysis of samples of non-standard geometry. *J Radioanal Nucl Chem*, vol. 256(1), pp. 93-98. <https://doi.org/10.1023/A:1023356227170>.
19. Kokkuzova M., Bekenova G., Dyussebayeva K., et al. (2017) Gold-barite-polymetallic VMS deposit of Maikain, NE Kazakhstan. *Appl Earth Sci*, vol. 126(2), pp. 71-72. <https://doi.org/10.1080/03717453.2017.1306266>.
20. Kokkuzova M., Bekenova G., Dyussebayeva K. (2016) Gold-telluride association in the ores of gold-polymetallic deposits of Rudny Altai and Central Kazakhstan. *16<sup>th</sup> International Multidisciplinary Scientific GeoConference SGEM 2016*, Sofia, Bulgaria, vol. 2, pp. 1081-1088.
21. Silachyov I.Yu. (2021) Determination of indium in its ore resources by comparator neutron activation analysis. *IJBCh*, 14(2), 106-116. <https://doi.org/10.26577/ijbch.2021.v14.i2.015>.
22. Ismail S.S. (2010) A new automated sample transfer system for instrumental neutron activation analysis. *J Autom Methods Manage Chem*, vol. 2010(1), 8 pp. <https://doi.org/10.1155/2010/389374>.
23. Evaluation of measurement data – Guide to the expression of uncertainty in measurement. JCGM, 2008, 120 p.
24. Silachyov I. (2023) Zircon concentrate analysis for sixteen rare earth elements by the complex of nuclear analytical methods. *J Radioanal Nucl Chem*. Published online. <https://doi.org/10.1007/s10967-023-08844-1>.
25. Silachyov I.Yu. (2020) Instrumental neutron activation analysis of rhenium in uranium raw material. *IJBCh*, vol. 13(1), pp. 161-169. <https://doi.org/10.26577/ijbch.2020.v13.i1.17>.
26. Chilian C., St-Pierre J., Kennedy G. (2008) Complete thermal and epithermal neutron self-shielding corrections for NAA using a spreadsheet. *J Radioanal Nucl Chem*, vol. 278(3), pp. 745-749. <https://doi.org/10.1007/s10967-008-1604-8>.

27. Rudnick R.L., Gao S. (2014) Composition of the continental crust. In: Holland H.D., Turekian K.K. (Ed.) Treatise on Geochemistry, 2nd edition, vol. 4. Elsevier, pp. 1-51. <https://doi.org/10.1016/B978-0-08-095975-7.00301-6>.
28. Haynes W.M. (Ed.) (2016) Abundance of elements in the earth's crust and in the sea. CRC handbook of chemistry and physics, 97th edition. Boca Raton, Florida: CRC press, pp. 14-17. ISBN: 9781498754286.
29. Hubbell J.H., Seltzer S.M. (accessed May 15, 2023) X-ray mass attenuation coefficients. NIST standard reference database 126. <https://www.nist.gov/pml/x-ray-mass-attenuation-coefficients>.
30. OST 41-08-212-04 (2004) Standart otrasli. Upravlenie kachestvom analiticheskikh rabot. Normy pogreshnosti pri opredelenii himicheskogo sostava mineralnogo syr'ya i klassifikatsiya metodik laboratornogo analiza po tochnosti rezultatov (Industrial standard. Quality management of analytical work. Error guidelines for chemical analysis of mineral resources and precision classification of laboratory analytical techniques). Moscow, VIMS, 23 p. (in Russian).
31. Nuclear data sub-committee. K0-neutron activation analysis link page (accessed May 15, 2023). <http://www.kayzero.com/k0naa/k0naaorg/Links.html>.

**Information about authors:**

*Igor Yurievich Silachyov – candidate of engineering sciences, Institute of Nuclear Physics (Almaty, Kazakhstan, e-mail: silachyov@inp.kz*

*Glagolev Vladimir Andreyevich – senior research fellow, The Institute of Geological Sciences n.-a. K. I. Satpayev (Almaty, Kazakhstan; vaglag@mail.ru)*

*Kokkuzova Manshuk – Master of Technical Sciences, The Institute of Geological Sciences n.-a. K. I. Satpayev (Almaty, Kazakhstan; m.kokkuzova@satbayev.university)*



S.M. Adekenov



JSC “International Research and Production Holding “Phytochemistry”, Karaganda, Kazakhstan

e-mail: arglabin@phyto.kz

(Received 29 December 2023; received in revised form 8 February 2024; accepted 15 February 2024)

## Isoprenoids from *Rhaponticum carthamoides* (Willd.) Iljin and *Rhaponticum serratuloides* (Georgi.) Bobr

**Abstract.** The article presents the results of a chemical study of *Rhaponticum carthamoides* (Willd.) Iljin. and *Rhaponticum serratuloides* (Georgi.) Bobr., which are of interest as sources of new adaptogenic, anabolic, and antiparasitic drugs; a method for complex chemical processing of the raw materials of the above-mentioned plants has been proposed. The structure of new sesquiterpene lactones raposerine, raserolide, 15-deacetylraposerine, and raserine has been isolated and established. The content of pharmacologically active ecdysterone in various organs of the studied *Rhaponticum* species is discussed according to the phenological phases of plant development. The antiparasitic, antiviral activity and cytotoxicity of the isolated compounds were determined.

**Key words:** *Rhaponticum carthamoides* (Willd.) Iljin., *Rhaponticum serratuloides* (Georgi.) Bobr., isoprenoids, sesquiterpene lactones, ecdysterone.

### Introduction

Plants of the genus *Rhaponticum* Adans. (*rhaponticum*, *leuzea*) are promising sources of ecdysterone (20-hydroxyecdysone, 1) – a polyhydroxylated steroid that exhibits anabolic, adaptogenic, antiulcerogenic and other types of pharmacological activity and is the basis of the drug “Ecdisten”, recommended as an anabolic agent. Ecdysterone does not exhibit the androgenic effect characteristic of anabolic steroids of the testosterone series, which makes it promising for use in medical practice [1]. For the industrial production of ecdysterone, the roots of the *Rhaponticum carthamoides* (Willd.) Iljin. plant and inflorescences of *Rhaponticum integrifolium* Winkl. are recommended as raw materials [2,3].

Previously, research on the chemistry and technology of ecdysteroids had not been carried out in Kazakhstan; considering the need to develop original domestic adaptogenic and anabolic drugs, research on plants from Central Kazakhstan that are promising as raw materials for the production of ecdysterone has been started.

As objects of study, *Rhaponticum serratuloides* (Georgi.) Bobr, common in the steppe zone of Kazakhstan, *Rhaponticum carthamoides* (Willd.) Iljin, introduced into cultivation at the collection site

of the botanical garden of JSC International Research and Production Holding “Phytochemistry” were selected.

### Materials and methods

*Research methods* were performed as follows:

Melting points were determined using a Boetius apparatus.

IR spectra were recorded on Thermo Nicolet Avatar-360ESP instrument in KBr tablets and chloroform, UV spectra were recorded on an Agilent instrument Cary 60, in ethanol and the stop-flow method on an Agilent 1260 microcolumn liquid chromatograph.

NMR spectra were recorded on a Jeol JNM-ECA500 spectrometer (operating frequency – 500.13 MHz for  $^1\text{H}$ , 125.76 MHz for  $^{13}\text{C}$ ).  $\text{Py}-d_5$  and a mixture of  $\text{Py}-d_5 - \text{CDCl}_3$ , **1um serratulo**: 1 were used as solvents, tetramethylsilane ( $\delta$  scale) as an internal standard. For recording two-dimensional spectra  $^1\text{H}-^1\text{H}$  and  $^1\text{H}-^{13}\text{C}$  COZY and  $^1\text{H}-^{13}\text{C}$  COLOC (9Hz) standard programs from the Jeol company were used.

High-resolution mass spectra were recorded on a Finnigan MAT 8200 instrument using electron impact ionization with an energy of 70 eV.

Optical rotation was measured using a Polax 2L polarimeter at a wavelength of 580 nm.

Column chromatography was carried out on large silica gel, large porous and neutral aluminum oxide (IV degree of activity according to Brockman). For flash chromatography, silica gel "Armsorbsil" 100/160 and "Silpearl" (Czech Republic) 40/100 were used. For TLC, "Silufol -254" plates (Czech Republic) were used. Detection was carried out in UV light or using developers *A* and *B*.

Developers for TLC: *A* – solution of vanillin in sulfuric acid followed by heating at 100-110°C for 2-3 minutes, *B* – 1% solution of potassium permanganate; to detect substances, the plate was placed in the solution for 0.5-1 min, then washed with water.

HPLC of sesquiterpene lactones. Chromatography was carried out on an Agilent 1260 microcolumn liquid chromatograph. The column was 150 mm long, internal diameter 4.6 mm. Sorbent ZORBAX Eclipse XDB-C8, particle size 5 microns. Column temperature was 30 °C. The eluent was prepared by mixing MeOH and 0.05 M aqueous H<sub>3</sub>PO<sub>4</sub>. Eluent systems containing 40 and 50% methanol volumes were used. Detection of substances was carried out with a UV detector, operating wavelength 200 nm. The eluent flow rate was 0.5 ml/min. To record UV spectra, the eluent flow was stopped at the top of the chromatographic peak. The sample concentrations were about 1.2 mg/ml in MeOH; 1.4 µl of solution was applied to the column.

### *Sesquiterpene lactones of Rhaponticum serratuloides*

Leaves of the plant *Rhaponticum serratuloides* (Georgi.) Beaver. were collected during the flowering phase in the vicinity of the village of Aynabulak, Zhanaarkinskyi district, Ulytau region, air-dried and crushed.

The raw material weighing 5.5 kg was extracted four times with a mixture of ethanol and chloroform with a ratio of 1:4 (in volume ratios) 17 l each at the boiling point of the solvent for 1 hour. The extracts were combined, filtered and evaporated on a rotary evaporator under vacuum at a temperature not exceeding 45 °C. 1 liter of thick dark green mass has been obtained.

The resulting residue was dissolved in 1.5 L of hot (60 °C) ethanol and diluted with 3 L of hot water (60 °C). The precipitate of nonpolar components (chlorophylls, lipids) that formed after cooling the

solution was filtered off, the precipitate was similarly treated twice, and 1 and 0.5 L of ethanol were used. No sesquiterpene lactones were detected in the sediment by TLC method.

The combined filtrates were extracted with benzene six times, 2 L each. The combined benzene extracts were evaporated to dryness on a rotary evaporator under vacuum. The residue, 95 g, after distilling off the solvent was chromatographed on a silica gel column (2 kg).

Benzene – ethyl acetate systems were used as eluents, component ratio: 1) 40:1, 2) 25:1, 3) 20:1, 4) 10:1, 5) 7:1, 6) 5:1, 7) 4:1, 8) 3:1, 9) 2:1, 10) 1:1 and then benzene – acetone 11) 3:1, 12) 2:1, 13) 1:1, 14) ethyl acetate, ethyl acetate – ethanol: 15) 20:1, 16) 15:1. A number of fractions containing sesquiterpene lactones and related components were obtained.

Next, fractions of identical composition were combined and chromatographed on a flash column at a mass ratio of the chromatographed fraction and adsorbent of 1:50. The first 9 fractions contain lipids, colored non-crystalline components that were not further identified, and β-sitosterol (identified by TLC with a known sample). Fractions 9-11 contain loliolide as the main component. The last fractions (42 and further, see table 33) contain green and brown oils, in which no terpenoid and steroid substances were detected (TLC, developer *A*).

Systems for flash chromatography: benzene – ethyl acetate: 1) 5:1, 2) 4:1, and petroleum ether – ethyl acetate: 3) 10:7, 4) 5:4, 5) 1:1, 6) 5: 6) 5:7, 8) ethyl acetate.

The process was monitored by TLC, developer *B*.

For TLC the following solvent systems were used: petroleum ether – acetone: 1) 7:4, double elution 2) 5:3, double elution; 3) 2:1 three times elution.

The list of fractions and solvent systems for column and flash column chromatography is given in Table 1.

The lactones acroptilin (8) and raserolide (10) could not be separated chromatographically: a crystalline mixture was obtained, which gave one spot on TLC. Separation was carried out by fractional crystallization from system 1. Acroptilin is less soluble in this system and precipitates in the form of large cubic crystals; raserolide precipitates on the walls of the vessel in the form of small needle-shaped crystals.

**Table 1** – Chromatographic separation of *Rhaponticum serratuloides* sesquiterpene lactones

No. of factions	Solvent system for column chromatography	Faction composition	Solvent system for flash chromatography	Individual components
1	2	3	4	5
12, 13 14-17	6 7	Centaurepsin, acroptilin (8), minor cynaropicrin (2) and raserolide (10)	1 2	centaurepsin crystalline mixture of acroptilin and raserolide
18-23	8	Acroptilin (8), Raserolide (10), Raposerine (9)	3.4 4.5	crystalline mixture of acroptilin and raserolide raposerine
24-28	8-10	Cynaropicrin (2), raposerine (9), minor acroptilin (8) and raserolide (10)	4.5	cynaropicrin, raposerine
29-32	10.11	15-Deacetylraposerine (11), minor raposerine (9)	5	raposerine, 15-Deacetylraposerine
33.34	12, 13	15-Deacetylraposerine (11)	6	15-Deacetylraposerine
35-39	14-16	15-Deacetylraposerine (11), 15-deacetyl-2 $\alpha$ -hydroxyraserolide	6, 7.8	15-deacetylraposerine, 15-deacetyl-2 $\alpha$ -hydroxyraserolide
40-41	16	15-deacetyl- 2 $\alpha$ -hydroxyraserolide	7 8	15-deacetyl-2 $\alpha$ -hydroxyraserolide

(2'S)-3 $\beta$ ,4 $\alpha$ -dihydroxy-8 $\alpha$ -O-[2'-hydroxy-2'-methyl-3'-chloropropionyl]-15-chloro-1 $\alpha$ ,5 $\alpha$ ,6 $\beta$ ,7 $\alpha$ (H)-guai-10(14),11(13)-diene-6(12)-olide (centaurepsin) (7)

Compound (7): m.p. 221-223 °C (petroleum ether-acetone = 2:1)

$[\alpha]_{580}^{23} + 135.1^\circ$  (*c* 0.73; tetrahydrofuran).

UV:  $\lambda_{\max}^{23}$ : 196, 216 nm (shoulder)

TLC: system 1  $R_f$  0.39, system 2  $R_f$  0.46.

<sup>1</sup>H NMR spectra (Py-*d*<sub>5</sub>, 500 MHz,  $\delta$ , ppm, *J*, Hz) (7): 3.97 (1H, d.d.d., *J*<sub>1</sub>=11, *J*<sub>2</sub>=8, *J*<sub>3</sub>=8, H-1), 1.80 (1H, d.d., *J*<sub>1</sub>=14.5, *J*<sub>2</sub>=8, H-2a), 2.79 (1H, d.d.d., *J*<sub>1</sub>=14.5, *J*<sub>2</sub>=11, *J*<sub>3</sub>=6, H-2b), 4.65 (1H, br.d., *J* = 6, <1.5, H-3), 2.63 (1H, d.d., *J*<sub>1</sub>=8, *J*<sub>2</sub>=11, H-5), 5.32 (1H, d.d., *J*<sub>1</sub>=11, *J*<sub>2</sub>=9, H-6), 3.19 (1H, d.d.d.d., *J*<sub>1</sub>=9, *J*<sub>2</sub>=6.5, *J*<sub>3</sub>=3.5, *J*<sub>4</sub>=3.0, H-7), 5.39 (1H, d.d.d., *J*<sub>1</sub>=6.5, *J*<sub>2</sub>=5, *J*<sub>3</sub>=1, H-8), 2.59 (1H, d., *J*=14.5, H-9a), 2.94 (1H, d.d., *J*<sub>1</sub>=14.5, *J*<sub>2</sub>=5, H-9b), 5.75 (1H, d., *J*=3.0, H-13a), 6.18 (1H, d., *J*=3.5, H-13b), 5.07 (1H, br.d., *J*=1.5, H-14a), 5.12 (1H, d., *J*~1.5, H-14b), 4.34 (1H, d., *J*=11.5, H-15a), 4.78 (1H, d., *J*=11.5, H-15b), 4.00 (1H, d., *J*=11.5, H-18a), 4.10 (1H, d., *J*=11.5, H-18b), 1.70 (1H, s., H-19).

<sup>13</sup>C NMR spectra (Py-*d*<sub>5</sub>, 125 MHz,  $\delta$ , ppm) (7): 48.55 d. (C-1), 40.29 t. (C-2), 76.32 d. (C-3), 85.32 s. (C-4), 59.39 d. (C-5), 77.46 d. (C-6), 46.50 d. (C-7), 75.42 d. (C-8), 35.06 t. (C-9), 144.57 s. (C-10),

138.87 s. (C-11), 169.03 s. (C-12), 121.05 t. (C-13), 117.06 t. (C-14), 51.23 t. (C-15), 173.45 s. (C-16), 75.38 s. (C-17), 52.19 t. (C-18), 24.29 q. (C-19).

The following cross-peaks are observed in the two-dimensional COLOC spectrum, the presence of which was used to assign the indicated signals of carbon atoms: C(10)/H(8), H(9a), H(9b); C(11)/H(6), H(7), H(8), H(13a); C(12)/H(13a), H(13 b).

Crystal cell parameters (E): a = 10.47(1), b = 9.25(1), c = 11.49(2); p = 113.1(1).

The yield (7) was 0.008% (hereinafter the yields are given based on air-dry raw materials).

(2'S)-3 $\beta$ -dihydroxy-8 $\alpha$ -O-[2'-hydroxy-2'-methyl-3'-chloropropionyl]-15-chloro-1 $\alpha$ ,5 $\alpha$ ,6 $\beta$ ,7 $\alpha$ (H)-guai-10(14),11(13)-diene-6(12)-olide (acroptilin) (8)

Compound (8): m.p. 195-198 °C (petroleum ether-acetone = 2:1)

$[\alpha]_{580}^{23} + 110.7^\circ$  (*c* 0.62; methanol).

UV:  $\lambda_{\max}^{23}$ : 196, 216 nm (shoulder).

TLC: system 1  $R_f$  0.26, system 2  $R_f$  0.34.

IR spectrum (KBr),  $\nu$ , cm<sup>-1</sup>: 3450 (OH), 2950, 1640 (C=CH<sub>2</sub>), 1750 (C=O  $\gamma$ -lactone), 1275 (C-O, ester), 1180 (C-O).

<sup>1</sup>H NMR spectrum (Py-*d*<sub>5</sub>, 500 MHz,  $\delta$ , ppm, *J*, Hz): 3.28 (d.d.d., H-1, 1H, *J* 11, 8, 8, H-1), 2.10 (d.d.d.d, 1H, *J* 14.5, 8, 1.5, H-2a), 2.36 (d.d.d., 1H, *J*

14.5, 11, 6, H-2b), 4.23 (br.d.d., 1H,  $J$  6,  $\sim$ 1.5, H-3), 2.19 (d.d., 1H,  $J$  8, 11, H-5), 4.94 (d.d.,  $J$  11, 11.9, H-6), 3.10 (d.d.d., 1H,  $J$  9, 6.5, 3.5, 3, 11-7), 5.32 (d.d.d., 1H,  $J$  6.5, 5,  $\sim$  1.5, H-8), 2.47 (d.d., 1H,  $J$  14.5, 1.5, H-9a), 2.85 (d.d., 1H,  $J$  14.5, 5, H-9b), 5.75 (d., 1H,  $J$  3, H-13a), 6.15 (d. 1H,  $J$  3.5, H-13b), 5.08 (br.d., 1H,  $J$  1.5, H-14a), 5.10 (br.d., 1H,  $J$  1, H-14b), 3.20 (d., 1H,  $J$  5, H-15a), 3.40 (d., 1H,  $J$  5, H-15b), 3.95 (d., 1H,  $J$  11.5, H-18a), 4.06 (d., 1H,  $J$  11.5, H-18b), 1.65 (s., 3H, H-19).

$^{13}\text{C}$  NMR spectra (Py- $d_5$ , 125 MHz,  $\delta$ , ppm) (**8**): 46.05 d. (C-1), 38.90 t. (C-2), 75.26 d. (C-3), 69.05 s. (C-4), 53.22 d. (C-5), 77.25 d. (C-6), 47.58 d. (C-7), 75.16 d. (C-8), 36.08 t. (C-9), 142.80 s. (C-10), 138.53 s. (C-11), 168.98 s. (C-12), 121.26 t. (C-13), 117.98 t. (C-14), 48.89 t. (C-15), 173.33 s. (C-16), 75.27 s. (C-17), 52.02 t. (C-18), 24.19 q. (C-19).

Yield (**8**) was 0.004%

(2'**S**)-15-O-acetyl-3 $\beta$ ,4 $\alpha$ -dihydroxy-8 $\alpha$ -O-[2'-hydroxy-2'-methyl-3'-chloropropionyl]-1 $\alpha$ ,5 $\alpha$ ,6 $\beta$ ,7 $\alpha$ (H)-guai-10(14),11(13)-diene-6(12)-olide (raposerine) (**9**)

Compound (**9**): m.p. 191-193 °C (petroleum ether-acetone = 2:1)

$[\alpha]_{580}^{23} + 214^\circ$  ( $c$  0.35; methanol).

Found (%): C, 55.03; H, 6.21; Cl, 7.65.  $\text{C}_{21}\text{H}_{27}\text{O}_9\text{Cl}$ .

Calculated (%): C, 54.96; H, 5.91; Cl, 7.72.

UV:  $\lambda_{\text{max}}$ : 196, 216 nm (shoulder).

TLC: system 1  $R_f$  0.07, system 2  $R_f$  0.24.

IR spectrum (chloroform),  $\nu$ ,  $\text{cm}^{-1}$ : 3540 (OH), 3095, 1640 (C=CH<sub>2</sub>), 1765 (C=O  $\gamma$ -lactone), 1715 (C=O, ester), 1215, 1140, 1060 (C-O);

IR spectrum (KBr),  $\nu$ ,  $\text{cm}^{-1}$ : 1775 (C=O  $\gamma$ -lactone), 1737 (C=O, ester), 1715 (C=O, ester)

Mass spectrum,  $m/z$  ( $I_{\text{rel}}$  (%)): 429 (6), 427 (19), 260 (30), 247 (19), 243 (24), 242 (23), 229 (30), 203 (23), 175 (26), 43 (100).

Found:  $m/z$ : 427.11711  $[\text{M}-\text{CH}_3]^+$ .  $\text{C}_{20}\text{H}_{24}\text{O}_8\text{Cl}$ .

Calculated: 427.11596.

$^1\text{H}$  NMR spectra (Py- $d_5$ , 500 MHz,  $\delta$ , ppm,  $J$ , Hz) (**9**): 3.86 (1H, d.d.d.,  $J_1=11$ ,  $J_2=8$ ,  $J_3=8$ , H-1), 1.81 (1H, d.d.,  $J_1=14.5$ ,  $J_2=8$ , H-2a), 2.76 (1H, d.d.d.,  $J_1=14.5$ ,  $J_2=11$ ,  $J_3=6$ , H-2b), 4.57 (1H, br.d.,  $J=6$ ,  $<1.5$ , H-3), 2.66 (1H, d.d.,  $J_1=8$ ,  $J_2=11$ , H-5), 5.24 (1H, d.d.,  $J_1=11$ ,  $J_2=9$ , H-6), 3.17 (1H, d.d.d.,  $J_1=9$ ,  $J_2=6.5$ ,  $J_3=3.5$ ,  $J_4=3.0$ , H-7), 5.35 (1H, d.d.d.,  $J_1=6.5$ ,  $J_2=5$ ,  $J_3=1.5$ , H-8), 2.54 (1H, d.,  $J=14.5$ , H-9a), 2.92 (1H, d.d.,  $J_1=14.5$ ,  $J_2=5$ , H-9b), 5.74 (1H, d.,  $J=3.0$ , H-13a), 6.14 (1H, d.,  $J=3.5$ , H-13b), 5.04 (1H, s., H-14a), 5.11 (1H, br.d.,  $J\sim 1.5$ , H-14b),

5.04 (1H, s., H-15a), 5.04 (1H, s., H-15b), 3.97 (1H, d.,  $J=11.5$ , H-18a), 4.07 (1H, d.,  $J=11.5$ , H-18b), 1.67 (1H, s., H-19), 1.81 (1H, s., H-21).

$^{13}\text{C}$  NMR spectra (Py- $d_5$ , 125 MHz,  $\delta$ , ppm) (**9**): 47.60 d. (C-1), 40.10 t. (C-2), 77.01 d. (C-3), 84.26 s. (C-4), 58.32 d. (C-5), 77.46 d. (C-6), 46.76 d. (C-7), 75.47 d. (C-8), 35.50 t. (C-9), 144.48 s. (C-10), 139.06 s. (C-11), 169.20 s. (C-12), 121.00 t. (C-13), 117.02 t. (C-14), 67.50 t. (C-15), 173.44 s. (C-16), 75.37 s. (C-17), 52.17 t. (C-18), 24.28 q. (C-19), 171.13 s. (C-20), 20.85 q. (C-21).

The yield (**9**) was 0.03%.

15-O-acetyl-3 $\beta$ ,4 $\alpha$ -dihydroxy-8 $\alpha$ -O-[methacryloyl]-1 $\alpha$ ,5 $\alpha$ ,6 $\beta$ ,7 $\alpha$ (H)-guai-10(14),11(13)-diene-6(12)-olide (raserolide) (**10**)

Compound (**10**): m.p. 153-155 °C (petroleum ether-acetone = 2:1)

$[\alpha]_{580}^{23} + 126^\circ$  ( $c$  0.44; chloroform).

UV:  $\lambda_{\text{max}}$ : 198-208 nm (plateau)

TLC: system 1  $R_f$  0.24, system 2  $R_f$  0.30.

IR spectrum (CHCl<sub>3</sub>):  $\nu$ ,  $\text{cm}^{-1}$ : 3500 (broad) (OH), 3095, 1640, 1060 (C=CH<sub>2</sub>), 1765 (C=O  $\gamma$ -lactone), 1715 (C=O, ester), 1215, 1140 (C-O).

Mass spectrum,  $m/z$  ( $I_{\text{rel}}$  (%)): 375 (19), 333 (2), 259 (15), 69 (100).

Found:  $m/z$ : 375.14589,  $[\text{M}-\text{CH}_3\text{O}]^+$ .  $\text{C}_{20}\text{H}_{23}\text{O}_7$ .  
Calculated: 375.1443. Found:  $m/z$ : 333.13655,  $[\text{M}-\text{CH}_2\text{OAc}]^+$ .  $\text{C}_{18}\text{H}_{21}\text{O}_6$ . Calculated: 333.13380.

$^1\text{H}$  NMR spectra (Py- $d_5$ , 500 MHz,  $\delta$ , ppm,  $J$ , Hz) (**10**): 3.81 (1H, d.d.d.,  $J_1=11$ ,  $J_2=8$ ,  $J_3=8$ , H-1), 1.78 (1H, d.d.,  $J_1=14.5$ ,  $J_2=8$ , H-2a), 2.71 (1H, d.d.d.,  $J_1=14.5$ ,  $J_2=11$ ,  $J_3=6$ , H-2b), 4.53 (1H, br.d.,  $J=6$ ,  $<1.5$ , H-3), 2.64 (1H, d.d.,  $J_1=8$ ,  $J_2=11$ , H-5), 5.20 (1H, d.d.,  $J_1=11$ ,  $J_2=9$ , H-6), 3.16 (1H, d.d.d.,  $J_1=9$ ,  $J_2=6.5$ ,  $J_3=3.5$ ,  $J_4=3.0$ , H-7), 5.23 (1H, d.d.d.,  $J_1=6.5$ ,  $J_2=5$ ,  $J_3=1.5$ , H-8), 2.46 (1H, d.,  $J=14.5$ , H-9a), 2.87 (1H, d.d.,  $J_1=14.5$ ,  $J_2=5$ , H-9b), 5.46 (1H, d.,  $J=3.0$ , H-13a), 6.09 (1H, d.,  $J=3.5$ , H-13b), 5.01 (1H, s., H-14a), 5.05 (1H, br.d.,  $J\sim 1.0$ , H-14b), 5.01 (1H, s., H-15a), 5.01 (1H, s., H-15b), 5.52 (1H, br.d.,  $J=1.5$ , H-18a), 6.16 (1H, br.d.,  $J\sim 1.0$ , H-18b), 1.88 (1H, s., H-19), 1.78 (1H, s., H-21).

$^{13}\text{C}$  NMR spectra (Py- $d_5$ , 125 MHz,  $\delta$ , ppm) (**10**): 47.47 d. (C-1), 39.96 t. (C-2), 77.06 d. (C-3), 84.16 s. (C-4), 58.27 d. (C-5), 77.57 d. (C-6), 46.74 d. (C-7), 74.57 d. (C-8), 35.75 t. (C-9), 144.62 s. (C-10), 139.06 s. (C-11), 169.20 s. (C-12), 120.68 t. (C-13), 116.55 t. (C-14), 67.46 t. (C-15), 166.52 s. (C-16), 136.80 s. (C-17), 126.30 t. (C-18), 18.26 q. (C-19), 171.14 s. (C-20), 20.86 q. (C-21).

The yield (**10**) was 0.010%.

(2'S)-3 $\beta$ ,4 $\alpha$ ,15-trihydroxy-8 $\alpha$ -O-[2'-hydroxy-2'-methyl-3'-chloropropionyl]-1 $\alpha$ ,5 $\alpha$ ,6 $\beta$ ,7 $\alpha$ (H)-guaia-10(14),11(13)-diene-6(12)-olide (15-deacetylraserine) (11)

Compound (11): m.p. 153-155 °C (chloroform-petroleum ether = 1:1)

$[\alpha]_{580}^{23} + 48.8^\circ$  (*c* 0.66; acetone).

UV:  $\lambda_{\max}$ : 196, 216 nm (shoulder).

IR spectrum (KBr),  $\nu$ ,  $\text{cm}^{-1}$ : 1766 (C=O  $\gamma$ -lactone), 1739 (C=O), 1668, 1643 (C=C) 1274, 1226, 1158, 1113, 1065, 754 (C-Cl).

Mass spectrum (*EI*, 70 eV), (*m/z*, *I<sub>rel</sub>* (%)): 387 [M-CH<sub>2</sub>OM]<sup>+</sup> (<sup>37</sup>Cl)(18), 385 [M-CH<sub>2</sub>OH]<sup>+</sup> (<sup>35</sup>Cl)(54), 265(59), 247(87), 229(71), 201(52), 175(91), 93(100). Found (*m/z*): 385.10581, calculated for C<sub>18</sub>H<sub>22</sub>O<sub>7</sub>Cl: 385.10539.

TLC: system 2 R<sub>f</sub> 0.14

<sup>1</sup>H NMR spectra (Py-*d*<sub>5</sub>, 500 MHz,  $\delta$ , ppm, *J*, Hz) (11): 3.74 (1H, d.d.d., *J*<sub>1</sub>=11, *J*<sub>2</sub>=8, *J*<sub>3</sub>=8, H-1), 1.82 (1H, d.d.d.d., *J*<sub>1</sub>=14.5, *J*<sub>2</sub>=9.5, *J*<sub>3</sub>=7.5, *J*<sub>4</sub>=2, H-2a), 2.66 (1H, d.d.d., *J*<sub>1</sub>=14.5, *J*<sub>2</sub>=11.5, *J*<sub>3</sub>=6, H-2b), 4.63 (1H, br.d., *J*=6, <1.5, H-3), 2.57 (1H, d.d., *J*<sub>1</sub>=9.5, *J*<sub>2</sub>=10.5, H-5), 5.23 (1H, d.d., *J*<sub>1</sub>=11, *J*<sub>2</sub>=9, H-6), 3.12 (1H, d.d.d.d., *J*<sub>1</sub>=9, *J*<sub>2</sub>=6.5, *J*<sub>3</sub>=3.5, *J*<sub>4</sub>=3.0, H-7), 5.29 (1H, d.d.d., *J*<sub>1</sub>=7.5, *J*<sub>2</sub>=5, *J*<sub>3</sub>=2.5, H-8), 2.47 (1H, d.d., *J*<sub>1</sub>=15.0, *J*<sub>2</sub>=1.5, H-9a), 2.93 (1H, d.d., *J*<sub>1</sub>=14.5, *J*<sub>2</sub>=5, H-9b), 5.73 (1H, d., *J*=3.0, H-13a), 6.11 (1H, d., *J*=3.5, H-13b), 4.99 (1H, br.d., *J*=1.5 H-14a), 5.0 (1H, br.d., *J*=1.5, H-14b), 4.39 (1H, d., *J*=11.5 H-15a), 4.69 (1H, d., *J*=11.5, H-15b), 3.93 (1H, br.d., *J*=11.5, H-18a), 4.04 (1H, d., *J*=11.5, H-18b), 1.63 (1H, s., H-19).

<sup>13</sup>C NMR spectra (Py-*d*<sub>5</sub>, 125 MHz,  $\delta$ , ppm) (11): 47.07 d. (C-1), 39.84 d. (C-2), 77.07 d. (C-3), 85.77 s. (C-4), 57.74 d. (C-5), 77.89 d. (C-6), 47.00 d. (C-7), 75.57 d. (C-8), 36.22 t. (C-9), 144.61 s. (C-10), 138.91 s. (C-11), 169.36 s. (C-12), 121.09 t. (C-13), 116.65 t. (C-14), 63.92 t. (C-15), 173.45 s. (C-16), 75.38 s. (C-17), 52.17 t. (C-18), 24.31 q. (C-19).

The yield (11) was 0.015%.

2 $\alpha$ ,3 $\beta$ ,4 $\alpha$ ,15-tetrahydroxy-8 $\alpha$ -O-[methacryloyl]-1 $\alpha$ ,5 $\alpha$ ,6 $\beta$ ,7 $\alpha$ (H)guaia-10(14), 11(13)-diene-6(12)-olide (15-deacetyl-2 $\alpha$ -hydroxyraserolide; raserine) (12)

Compound (12): m.p. 168-171 °C (chloroform-methanol = 3:1)

$[\alpha]_{\text{D}}^{20} + 110.9^\circ$  (*c* 0.99; acetone).

UV:  $\lambda_{\max}$ : 198-208 nm (plateau)

IR spectrum (chloroform),  $\nu$ ,  $\text{cm}^{-1}$ : 1766 ( $\gamma$ -lactone), 1715 (C=O), 1632, (C=C), 1145, 1051, 910, 855.

Mass spectrum (*EI*, 70 eV), (*m/z*, *I<sub>rel</sub>* (%)): 362[M-H<sub>2</sub>O]<sup>+</sup>(3), 349 [M-CH<sub>2</sub>OH]<sup>+</sup>(5), 235 (10),

217(10), 175 (7), 69 (100). Found (*m/z*): 349.12884, calculated for C<sub>19</sub>H<sub>21</sub>O<sub>7</sub>: 349.12872.

TLC: system 3 R<sub>f</sub> 0.2

<sup>1</sup>H NMR spectra (Py-*d*<sub>5</sub>, 500 MHz,  $\delta$ , ppm, *J*, Hz) (12): 3.43 (1H, d.d., *J*<sub>1</sub>=11.5, *J*<sub>2</sub>=8, H-1), 4.74 (1H, d.d., *J*<sub>1</sub>=6.5, *J*<sub>2</sub>=8, H-2), 4.69 (1H, d., *J*=6.5, H-3), 2.95 (1H, d.d., *J*<sub>1</sub>=11.5, *J*<sub>2</sub>=11.5, H-5), 5.05 (1H, d.d., *J*<sub>1</sub>=11, *J*<sub>2</sub>=9, H-6), 3.18 (1H, d.d.d.d., *J*<sub>1</sub>=9, *J*<sub>2</sub>=6.5, *J*<sub>3</sub>=3.5, *J*<sub>4</sub>=3.0, H-7), 5.17 (1H, d.d.d., *J*<sub>1</sub>=10, *J*<sub>2</sub>=5, *J*<sub>3</sub>=5, H-8), 2.33 (1H, d.d., *J*<sub>1</sub>=14.0, *J*<sub>2</sub>=5, H-9a), 2.93 (1H, d.d., *J*<sub>1</sub>=14.0, *J*<sub>2</sub>=5, H-9b), 5.33 (1H, d., *J*=3.0, H-13a), 6.12 (1H, d., *J*=3.5, H-13b), 5.00 (1H, br.d., *J*=2, H-14a), 5.30 (1H, br.d., *J*=1.2, H-14b), 4.49 (1H, d., *J*=11.0, H-15a), 4.54 (1H, d., *J*=11.0, H-15b), 5.51 (1H, d.d., *J*<sub>1</sub>=1.5, *J*<sub>2</sub>=1.5, H-18a), 6.14 (1H, d., *J*<sub>1</sub>=1.5, *J*<sub>2</sub>=1.0, H-18b), 1.86 (1H, s., H-19).

<sup>13</sup>C NMR spectra (Py-*d*<sub>5</sub>, 125 MHz,  $\delta$ , ppm) (12): 52.46 d. (C-1), 78.36 d. (C-2), 84.46 d. (C-3), 80.97 s. (C-4), 54.79 d. (C-5), 77.70 d. (C-6), 47.84 d. (C-7), 74.45 d. (C-8), 39.59 t. (C-9), 141.41 s. (C-10), 138.22 s. (C-11), 169.27 s. (C-12), 121.01 t. (C-13), 116.81 t. (C-14), 63.63 t. (C-15), 166.01 s. (C-16), 136.32 s. (C-17), 126.04 t. (C-18), 17.90 q. (C-19).

The yield (12) was 0.002%.

#### Sesquiterpene lactones of *Rhaponticum carthamoides*

Leaves of *Rhaponticum carthamoides* (Willd.) Iljin plants were collected during the flowering phase in the botanical garden of JSC "IRPH "Phytochemistry" (Karaganda), air-dried and crushed.

A diagram of the process for isolating sesquiterpene lactones is shown in Figure 1. The raw material weighing 0.8 kg was extracted four times with a mixture of ethanol and chloroform with a ratio of 1:4 (in volume ratios), 7 l each at the boiling point of the solvent for 1 hour. The extracts were combined, filtered and evaporated on a rotary evaporator under vacuum at a temperature not exceeding 45 °C. 0.3 liters of thick dark green mass was isolated.

The resulting residue was dissolved in 0.5 L of hot (60 °C) ethanol and diluted with 1 L of hot water (60 °C). The precipitate of nonpolar components (chlorophylls, lipids) that formed after cooling the solution was filtered off, the precipitate was similarly treated twice, and 0.5 and 0.25 L of ethanol were used. No sesquiterpene lactones were detected in the sediment by TLC.

The combined filtrates were extracted with benzene six times, 0.5 L each. The combined benzene extracts were evaporated to dryness on a rotary evaporator under vacuum. The residue after distilling

off the solvent, 18 g, was chromatographed on a silica gel column (500 g).

Benzene – ethyl acetate systems were used as eluents with the component ratio: 1) 5:1, 2) 4:1, 3) 3:1, 4) 2:1, 5) 1:1, 6) ethyl acetate, 7) ethyl acetate – ethanol 10:1. A number of fractions containing sesquiterpene lactones and related components were obtained.

Next, fractions identical in composition were combined and chromatographed on a flash column at a mass ratio of the chromatographed fraction and adsorbent of 1 : 50. The first 11 fractions contain lipids, colored non-crystalline components that were not further identified, and  $\beta$ -sitosterol (identified

by TLC with a known sample). The last fractions contain green and brown oils, in which substances of a terpenoid and steroid nature (TLC, developer *A*) were not detected.

Systems for flash chromatography: petroleum ether – ethyl acetate: 1) 10:7, 2) 5:4, 3) 1:1

The process was monitored by TLC, developer *B*. Recrystallization of the isolated components was carried out from the following solvent systems: 1) petroleum ether – acetone 2 : 1; 2) petroleum ether – chloroform 1 : 1;

The list of fractions and solvent systems for column and flash column chromatography is presented in Table 2.

**Table 2** – Chromatographic separation of *Rhaponticum carthamoides* sesquiterpene lactones

No. fractions	Solvent system for column chromatographies	Fraction composition	Solvent system for flash chromatography	Individual components
12, 13 14-17	6 7	Chlorojanerin (3)	1	chlorojanerin
18-23	8	Chlorojanerin (3), Cynaropicrin (2)	1 2	chlorojanerin cynaropicrin
24-28	8-10	Cynaropicrin (2)	2	cynaropicrin

3  $\beta$ , 4  $\alpha$ -dihydroxy-8 $\alpha$ -O-[4'-hydroxymethacryloyl]-15-chloro-1 $\alpha$ ,5 $\alpha$ ,6 $\beta$ ,7 $\alpha$ (H)-guai-10(14),11(13)-diene-6(12)-olide (chlorojanerin) (3)

Compound (3): m.p. 160-162 °C (chloroform – petroleum ether)

$[\alpha]_{580}^{23} + 116.3^\circ$  (*c* 0.946; acetone).

<sup>1</sup>H NMR spectra (CDCl<sub>3</sub>, 500 MHz,  $\delta$ , ppm, *J*, Hz) (3): 3.59 (1H, d.d.d., *J*<sub>1</sub>=9, *J*<sub>2</sub>=9, *J*<sub>3</sub>=10.5, H-1), 1.58 (1H, d.d., *J*<sub>1</sub>=14.0, *J*<sub>2</sub>=8, H-2a), 2.52 (1H, d.d.d., *J*<sub>1</sub>=15.0, *J*<sub>2</sub>=11.5, *J*<sub>3</sub>=6.5, H-2b), 4.16 (1H, br.d., *J*=6.5, H-3), 2.31 (1H, d.d., *J*<sub>1</sub>=9, *J*<sub>2</sub>=11, H-5), 4.72 (1H, d.d., *J*<sub>1</sub>=11.5, *J*<sub>2</sub>=9.5, H-6), 3.15 (1H, d.d.d.d., *J*<sub>1</sub>=9, *J*<sub>2</sub>=6.5, *J*<sub>3</sub>=3.5, *J*<sub>4</sub>=3.0, H-7), 5.35 (1H, d.d.d., *J*<sub>1</sub>=7.5, *J*<sub>2</sub>=5.5, *J*<sub>3</sub>=2.0, H-8), 2.65 (1H, d.d., *J*<sub>1</sub>=15.5, *J*<sub>2</sub>=5, H-9a), 2.43 (1H, d., *J*<sub>1</sub>=15.5, H-9b), 5.59 (1H, d., *J*=3.5, H-13a), 6.19 (1H, d., *J*=3.5, H-13b), 4.81 (1H, br.d., *J*=1.5, H-14a), 5.12 (1H, br.d., *J*=1.5, H-14b), 3.94 (1H, d., *J*=12, H-15a), 4.32 (1H, d., *J*=12, H-15b), 5.94 (1H, br.d.d., *J*<sub>1</sub>=1, *J*<sub>2</sub>=1.5, H-18a), 6.32 (1H, br.d., *J*=1, H-18b), 4.37 (1H, br.s., H-19).

<sup>13</sup>C NMR spectra (CDCl<sub>3</sub>, 125 MHz,  $\delta$ , ppm) (3): 47.01 d. (C-1), 37.69 t. (C-2), 77.15 d. (C-3), 84.42 s. (C-4), 57.45 d. (C-5), 76.01 d. (C-6), 46.38 d. (C-7),

74.02 d. (C-8), 35.02 t. (C-9), 142.1 s. (C-10), 139.16 s. (C-11), 168.51 s. (C-12), 122.69 t. (C-13), 117.90 t. (C-14), 49.79 t. (C-15), 165.25 s. (C-16), 136.70 s. (C-17), 126.68 t. (C-18), 62.23 t. (C-19).

The yield was 0.01%.

3 $\beta$ ,-dihydroxy-8 $\alpha$ -O-[4'-hydroxymethacryloyl]-1 $\alpha$ ,5 $\alpha$ ,6 $\beta$ ,7 $\alpha$ (H)-guai-4(15),10(14),11(13)-triene-6(12)-olide (2) (cynaropicrin) (2)

Compound (2): a transparent yellowish oil, decomposes in air to form a cheesy precipitate insoluble in chloroform and ethyl acetate. Identified by TLC by comparison with a known sample isolated from *Chartolepis intermedia* Boiss. Yield (2) was 0.04%.

<sup>1</sup>H NMR spectra (125 MHz, CDCl<sub>3</sub>,  $\delta$ , ppm, *J*/Hz) (2): 2.96 (1H, d.d., *J*= 8.1, 7.5 Hz, H-1), 2.22 (1H, m, H-2a), 1.74 (1H, m, H-2b), 4.55 (1H, t.t.t., *J*= 7.2, 1.9, 1.9 Hz, H-3), 2.84 (1H, d.d., *J*= 10.4, 9.0 Hz, H-5), 4.24 (1H, d.d., *J*= 11.0 9.1 Hz, H-6), 3.20-3.16 (1H, m, H-7), 5.14-5.13 (1H, m, H-8), 2.40 (1H, d.d., *J*= 14.5, 3.8 Hz, H-9a), 2.72 (1H, d.d., *J*= 14.5, 5.1 Hz, H-9b), 6.22 (1H, d, *J*= 3.4 Hz, H-13a), 5.61 (1H, d, *J*= 3.0 Hz, H-9b), 5.14 (1H, d, *J*= 0.9 Hz,



*carthamoides*, depending on the phenophase, the content of ecdysterone (1) is relatively stable (0.18-0.30 %), and reaches a maximum in the dying phase (October). In the roots of *Rhaponticum serratuloides* ecdysterone (1) accumulates in amounts from 0.12 (phase of death of the aerial part) to 0.10% (phase

of spring growth). In the above-ground part of the specified plant, the maximum amount of ecdysterone (1) was noted in the regrowth phase (0.12 %) – during the development of shoots it decreases (0.11 in the budding and flowering phase and 0.02 % in the fruiting phase).

**Table 3** – Ecdysterone content (1) in various organs of *Rhaponticum carthamoides*, *Rhaponticum serratuloides* depending on the phenological phase (% of the weight of absolutely dry raw materials)

Phenophase	Roots	Leaves	Stems	Inflorescences/ Buds
<i>Rhaponticum carthamoides</i>				
Regrowth	0.20	0.60	0.12	-
<b>Budding</b>	0.18	0.58	0.06	0.49
Bloom	0.21	0.49	0.04	0.44
Fruiting	0.24	0.34	0.01	-
Dieback of the aboveground part	0.30	0.05	0.01	-
<i>Rhaponticum serratuloides</i>				
Regrowth	0.10	0.12	0.06	-
Budding	0.09	0.11	0.04	0.12
Bloom	0.10	0.11	0.02	0.07
Fruiting	0.11	0.05	-	-
Dieback of the aboveground part	0.12	0.02	-	-

Thus, the aerial parts of *Rhaponticum carthamoides*, cultivated under conditions of Central Kazakhstan, are distinguished by a high content of ecdysterone (1) and can be used as a raw material for its production, as well as for the production of ecdysteroid containing drugs.

In view of the complexity of the technology for isolating ecdysteroids from plant extracts, it is of interest to develop herbal preparations based on the studied plants, which, along with ecdysteroids, contain biologically active compounds of other classes. Studying the composition and biological activity of the latter was one of the objectives of this study.

Of the studied plants *Rhaponticum serratuloides* is the most adapted to the arid conditions of Central Kazakhstan and therefore, despite the fact that this plant contains a relatively small amount of ecdysterone, it was also of interest to study it for the content of biologically active components of other classes in order to predict the biological activity of herbal preparations based on these raw materials.

Subsequent studies consisted of searching for the most optimal methods for separating various

groups of biologically active compounds of the studied plants, and developing methods for complex chemical processing of raw materials.

It is known that the aerial parts of plants of the genus *Rhaponticum* contain sesquiterpene lactones of the guaian type. In particular, the composition of sesquiterpene lactones from *Rhaponticum carthamoides*, *Rhaponticum scariosum* subsp. *lyratum* (Bellardi/Hayek) and *Rhaponticum serratuloides*, introduced into Poland, was studied, and it was found that these species contain cynaropicrin (2). *Rhaponticum scariosum* subsp. *lyratum* and *Rhaponticum carthamoides* also contain chlorojanerin (3) and janerin (4); moreover, in *Rhaponticum carthamoides*, more polar lactones repdiolide (5) and cebellin E (6) were found [6-9].

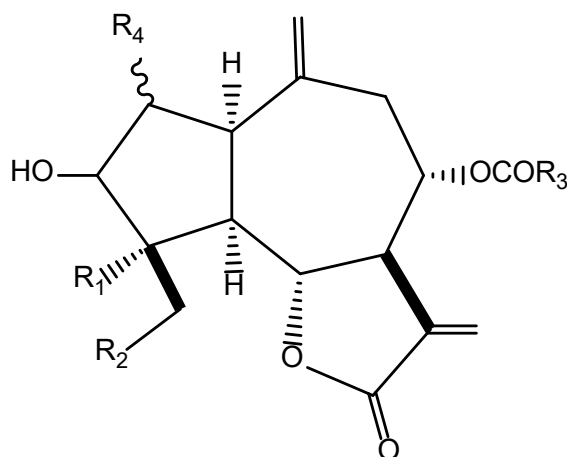
Cynaropicrin has been shown to have pronounced cytostatic and antiprotozoal activity. The presence of (2) and structurally similar lactones is associated with the presence of pronounced antiparasitic (antigiardiasis and antiopisthorchiasis) activity of extracts of various species of the genus *Saussurea* DC. [10].



Thus, it was of interest to study the composition of the sesquiterpene lactones of *Rhaponticum serratuloides* and *Rhaponticum carthamoides* with the aim of creating total herbal preparations with antiparasitic action based on the aerial parts of these plants.

Study of the composition of sesquiterpene lactones from *Rhaponticum serratuloides* showed

the presence of 2 in the plant, as well as known guaianolides centaurepensisin (7), acroptilin (8), which were not previously found in this plant [4], and four crystalline lactones, which turned out to be new. These compounds were named raposerine (9), raserolide (10), 15-deacetylraposerine (11) and raserine (12) [11,12].



Cynaropicrin (2)	$R_1+R_2 = \Delta^{4,15}$ ; $R_3 = C(CH_2OH)=CH_2$ ; $R_4 = H$
Chlorojanerin (3)	$R_1 = OH$ ; $R_2 = Cl$ ; $R_3 = C(CH_2OH)=CH_2$ ; $R_4 = H$
Janerin (4)	$R_1=R_2 = OH$ ; $R_3 = C(CH_2OH)=CH_2$ ; $R_4 = H$
Repdiolide (5)	$R_1+R_2 = \Delta^{4,15}$ ; $R_3 = C(CH_3)=CH_2$ ; $R_4 = \alpha-OH$
Cebellin E (6)	$R_1 = OH$ ; $R_2 = Cl$ ; $R_3 = C(CH_3)=CH_2$ ; $R_4 = \beta-OH$
Centaurepensisin (7)	$R_1 = OH$ ; $R_2 = Cl$ ; $R_3 = (17 S)C(OH)(CH_2Cl)CH_3$ ; $R_4 = H$
Acroptilin (8)	$R_1+R_2 = -O-CH_2-$ ; $R_3 = (17 S)C(OH)(CH_2Cl)CH_3$ ; $R_4 = H$
Raposerine (9)	$R_1 = OH$ ; $R_2 = OAc$ ; $R_3 = (17 S)C(OH)(CH_2Cl)CH_3$ ; $R_4 = H$
Raserolide (10)	$R_1 = OH$ ; $R_2 = OAc$ ; $R_3 = C(CH_3)=CH_2$ ; $R_4 = H$
15-Deacetylraposerine (11)	$R_1 = OH$ ; $R_2 = OH$ ; $R_3 = (17 S)C(OH)(CH_2Cl)CH_3$ ; $R_4 = H$
Raserine (12)	$R_1 = OH$ ; $R_2 = OH$ ; $R_3 = C(CH_3)=CH_2$ ; $R_4 = \alpha-OH$

Previously, the lactone, to which structure (11) is proposed, was isolated as an oil from the plant *Centaurea bella* by a group of Czech and Polish researchers and was named cebellin J. However, the configuration of the asymmetric C-17 center in this compound was not determined [13].

When acetylation of the mother liquor from the crystallization of raposerine (9) followed by chromatographic separation of the acetylation products oily lactone diacetate (5) was isolated [14].

Thus, discovered a significant difference has been discovered in the composition of lactones in the aerial parts of *Rhaponticum serratuloides*, cultivated in Poland and collected from nature in

Central Kazakhstan: in the first case (2) is the main component (no other lactones were detected by TLC and not isolated), in the second – the plant contains 7 lactones and at the same time content (2) does not prevail (Table 4).

Considering the discovered differences in the compositions of sesquiterpene lactones of *Rhaponticum serratuloides* collected in various habitats, a study of these components was conducted in the aerial part of *Rhaponticum carthamoides*, introduced into cultivation in Central Kazakhstan. In this case, lactones (2) and (3) were detected, the presence of which was also established in plants cultivated in Poland.

**Table 4** – Sesquiterpene lactones of *Rhaponticum serratuloides* and *Rhaponticum carthamoides*

Name	Yield, % by weight of air-dried raw materials
<i>Rhaponticum serratuloides</i>	
Raposerine (9)	0.030
15-Deacetylraposerine (11)	0.015
Cynaropicrin (2)	0.013
Raserolide (10)	0.010
Centaurepensin (7)	0.008
Acroptilin (8)	0.004
Raserine (12)	0.002
<i>Rhaponticum carthamoides</i>	
Cynaropicrin (2)	0.100
Chlorojanerin (3)	0.040

Based on our research, a technology for complex chemical processing of the aerial parts of *Rhaponticum serratuloides* and *Rhaponticum carthamoides* has been proposed, including the release of sesquiterpene lactones, ecdysteroids, and polyphenolic compounds (Figure 1).

Compared to the ecdysteroids and polyphenolic compounds present in the plant extract isolated with 70% ethanol, sesquiterpene lactones are less polar substances. In this regard, the separation of these compounds from the sum of extractive substances was carried out at the stage of liquid-liquid extraction.

To purify ecdysteroids from polyphenolic compounds close to them in polarity, as a rule, the method of column chromatography on a sorbent with basic properties (aluminum oxide, polyamide) is used. However, the technology for such purification, given the high cost of sorbents, eluents and the duration of the process, is quite expensive. In addition, the desorption of polyphenolic compounds from the main sorbents is an extremely labor-intensive process.

A method for separating ecdysteroids and polyphenolic compounds at the stage of liquid-liquid extraction has been proposed by converting the latter into water-soluble phenolates, based on the method described in [15].

Thus, the aerial parts of *Rhaponticum serratuloides* and *Rhaponticum carthamoides* are

of interest as sources of sesquiterpene lactones with antiparasitic and antitumor effects; aerial part of *Rhaponticum carthamoides* is a promising source of ecdysterone. The fraction of polyphenolic compounds is of particular interest, since the latter often exhibit antioxidant and hepatoprotective activity.

Anabolic activity of *Rhaponticum carthamoides* and *Rhaponticum serratuloides* root extracts were studied along with the amount of ecdysteroids from these plants. Tests were carried out on female outbred white rats, the magnitude of anabolic activity was assessed by the integral indicator of body weight gain in laboratory animals, as well as by the nature of the effect of drugs on motor activity and behavioral reactions. It was found that all studied samples exhibited anabolic activity at the level of the reference drug, methandrostenolone.

It is known that ecdysterone (1) exhibits antiulcerogenic activity. In this regard, the gastroprotective effect of *Rhaponticum serratuloides* root extract has been studied when modeling psycho-emotional stress in rats caused by their twelve-hour fixation. It was found that the extract exhibits a pronounced gastroprotective effect.

A study was carried out of the effect of sesquiterpene lactones centaurepensin (7) and raposerine (9) on the reproduction and infectivity of influenza virus (strain A/FPV/Rostock/34) and Newcastle disease virus (strain La Sota). It was determined that both (7) and (9) exhibit antiviral activity comparable to that of a widely used commercial drug "Remantadine", which is effective against the influenza A virus.

Antifungal activity of acroptilin (8), cynaropicrin (2), raposerine (9) and raserolide (10), as well as the sum of sesquiterpene lactones with accompanying components of *Rhaponticum carthamoides*, obtained according to the scheme shown in Fig. 1, was determined *in vitro* against *Aspergillus niger*, *Candida albicans*, *Trichophyton rubrum*, *Trichophyton mentagrophytes* and *Microsporum canis*. Nystatin and nitrofungin were used as comparison drugs. The lactone fraction from *Rhaponticum carthamoides* showed relatively pronounced antifungal activity, samples of these lactones showed somewhat low activity, (9) turned out to be inactive against all the studied strains. The activity of all studied samples is inferior to the activity of commercial drugs nystatin and nitrofungin.

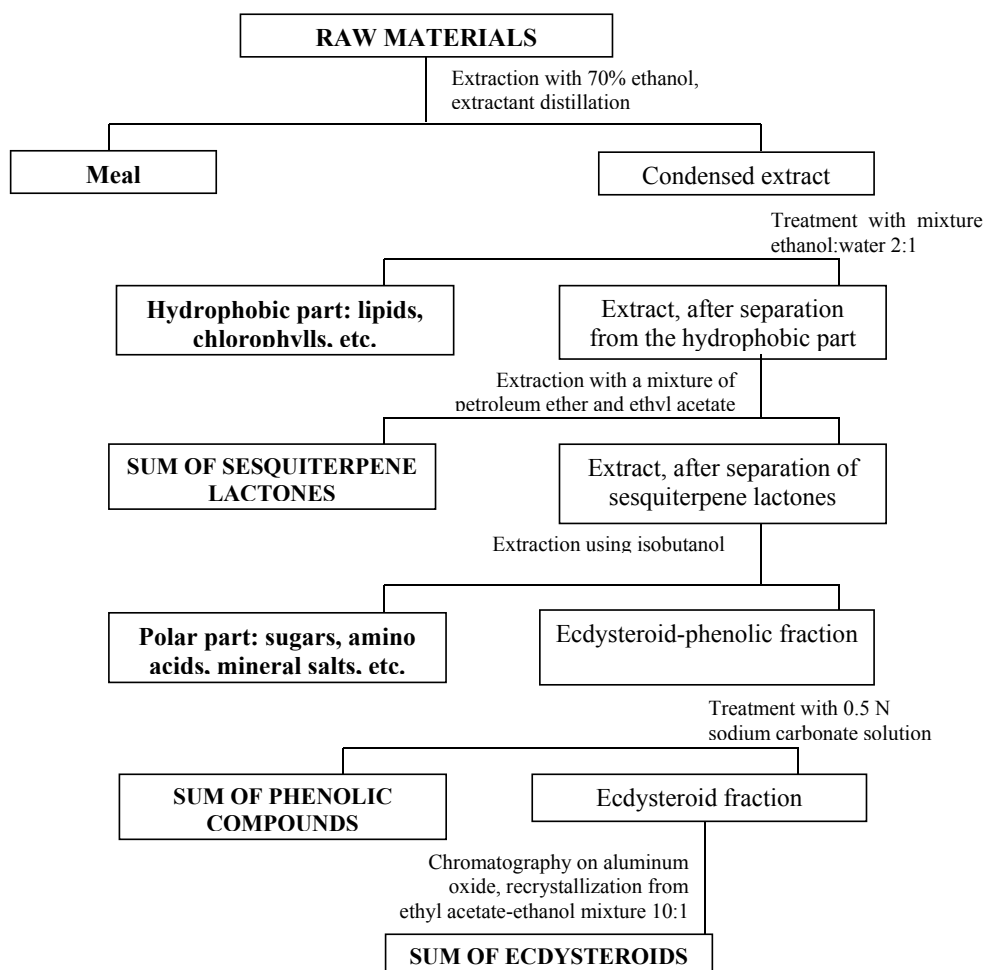


**Figure 1** – Scheme of complex chemical processing of raw materials from the aerial parts of *Rhaponticum carthamoides* and *Rhaponticum serratuloides*

Thus, it has been established that the roots and aerial parts of the plant *Rhaponticum serratuloides* contain ecdysterone, and, in addition, the aerial part of this plant is a promising source of sesquiterpene lactones with cytostatic, antiviral and antiparasitic activity. The aerial part of *Rhaponticum carthamoides*, which also contains sesquiterpene lactones that have antiparasitic and cytostatic activity, is of significant interest in terms of ecdysterone release.

### Conclusion

Plants of the genus *Rhaponticum* Adans. (*Rhaponticum*, *Leuzea*, tribe of the family *Asteraceae* L.) are sources of valuable biologically active substances, primarily ecdysones and sesquiterpene lactones, as well as polyacetylenes and flavonoids.

All studied plants of this genus contained ecdysterone, which is used as a substance in the tonic drug “Ecdisten”. The roots with rhizomes

of *Rhaponticum carthamoides*, as well as the inflorescences of *Rhaponticum integrifolium*, are industrially important raw materials for the production of ecdysterone. The presence of ecdysterone and accompanying ecdysteroids necessitated intensive study of the ecdysteroid composition of various representatives of this genus. However, the composition of ecdysteroids in some species of the genus remains unknown.

At the same time, the composition of other components of plants of the genus *Rhaponticum* Adans. remain little studied or not studied at all. Thus, in the literature there is only isolated information about the composition of such valuable components of plants of the genus *Rhaponticum* as sesquiterpene lactones. The composition of sesquiterpene lactones of this genus, growing in Central Asia, has not been studied.

Therefore, the search and study of biologically active isoprenoids among plants of the genus

*Rhaponticum* growing in the territory of Central Kazakhstan or introduced into culture in this territory, with the prospect of large-scale production of raw materials for the production of practically valuable drugs, is an urgent task. The second problem that arises when processing plant raw materials is the problem of its rational use, that is, complex processing with the fullest possible use of all valuable components.

A comprehensive study of the biologically active components of *Rhaponticum serratuloides* (Georgi.) Bobr. and *Rhaponticum carthamoides* (Willd.) Iljin allowed to establish that all organs of *Rhaponticum serratuloides* contain ecdysterone as the main ecdysteroid, the yield of which from the aerial part is 0.015%, and from the roots 0.014% based on air-dried raw materials.

The minor ecdysteroid amarasterone A and two new ecdysteroids, 25-epi-amarasterone and 25-deoxy-24-hydroxyethylideneecdysterone (rasersterone), were isolated from the roots of *Rhaponticum serratuloides*, the structure of which was determined by NMR spectroscopy methods, including two-dimensional COLOC and COSY.  $\beta$ -sitosterol, which has depyrogenized and anti-sclerotic effect, and its glycoside, a possible raw material for the production of polyoxysteroids, were obtained as accompanying components in the isolation of ecdysterone.

A number of sesquiterpene lactones have been isolated from the leaves of *Rhaponticum serratuloides*, including the well-known cynaropicrin, centaurepensin, acroptilin and new ones named raposerine, raserolide, raserine and 15-deacetylraposerine. Details of the structure of these sesquiterpene lactones were established on the basis of data from the  $^1\text{H}$  and  $^{13}\text{C}$  NMR spectra, including using the methods of two-dimensional NMR spectroscopy  $^1\text{H}$ - $^1\text{H}$  and  $^1\text{H}$ - $^{13}\text{C}$  COSY,  $^1\text{H}$ - $^{13}\text{C}$  COLOC and X-ray diffraction. To prove the structure of the isolated compounds, chemical modification of sesquiterpene lactones was carried out. Thus, the spatial structure of the new sesquiterpene lactones raposerine and 15-deacetylraposerine was established by obtaining acetates of these compounds, which turned out to be identical substances.

For the isolated lactones, the optimal parameters for analysis by HPLC on a reverse-phase sorbent were determined, which made it possible to select the conditions for separating a mixture of lactones.

Ecdysterone was isolated from the leaves and roots of the introduced *Rhaponticum carthamoides*. From the roots of *Rhaponticum carthamoides*, an industrial raw material for the production of

ecdysterone, the yield was 0.05%, which corresponds to industrial value and allows us to consider the raw materials produced in Central Kazakhstan as a promising source of ecdysterone. The yield from the leaves of *Rhaponticum carthamoides* was 0.07%, which allows us to recommend the leaves of this plant as a new potential source of ecdysterone.

In addition to ecdysterone, the well-known sesquiterpene lactones cynaropicrin and chlorojanerin have also been isolated from the leaves of *Rhaponticum carthamoides*.

A method has been developed and processes for complex chemical processing have been optimized for the most promising in terms of production of ecdysterone-containing drugs – leaves of *Rhaponticum carthamoides*, which consists in the joint release of ecdysteroids, sesquiterpene lactones and phenolic components.

A study of the antiviral activity of the sesquiterpene lactones centaurepensin and raposerine isolated from the leaves of *Rhaponticum serratuloides* showed that both compounds can effectively inhibit the process of reproduction of the influenza virus (strain A/FPV/Rostock/34) and the virus that causes Newcastle disease (strain La Sota), in addition, both centaurepensin and raposerine reduce the infectivity of the above viruses.

The results obtained during the research allows recommending:

- the aerial part of *Rhaponticum carthamoides*, introduced in Central Kazakhstan, as a raw material for the production of ecdysterone and the release of sesquiterpene lactones;
- roots of *Rhaponticum carthamoides*, introduced in Central Kazakhstan as a high-quality raw material for the production of ecdysterone;
- roots and aerial parts of *Rhaponticum serratuloides* as additional raw materials for the production of ecdysterone;
- aerial part of *Rhaponticum serratuloides* for the production of ecdysterone and sesquiterpene lactones with antiviral, cytotoxic, antiprotozoal activity.

### Acknowledgments

The work was carried out under the scientific and technical program BR21882180 “Development of a program for the conservation and development of the resource base of plants of Kazakhstan that are promising for medicine and veterinary medicine in a changing climate,” financed by the Science Committee of the Ministry of Science and Higher Education of the Republic of Kazakhstan.

### References

1. Todorova V., Ivanov K., Ivanova S. (2022) Comparison between the biological active compounds in plants with adaptogenic properties (*Rhaponticum carthamoides*, *Lepidium meyenii*, *Eleutherococcus senticosus* and *Panax ginseng*), *Plants*, 11(64), 1-32.
2. Baltayev U.A. (2000) Phytoecdysteroids – structure, sources and pathways of biosynthesis in plants, *Bioorg. Chem.*, 26(12), 892-925.
3. Mamathanov A.U., Shamsutdinov M.-R.I., Shakirov T.T. (1979) On the isolation of ecdysterone from the inflorescences of *Rhaponticum integrifolium* // *Chem. Nat. Compd.*, 5, 667-669.
4. Patent RU 2174397, publ. 10.10.2001 Method for obtaining a concentrate of ecdysteroids and ecdysterone from plant materials. Nedopekin D.V., Galyautdinov I.V., Odinkov V.N.
5. Patent RU 2582282, publ. 20.04.2016 A method for producing a product with stress-protective and antihypoxic activity. Nikolayev S.M., Nikolayeva I.G., Shantanova L.N., Nikolayeva G.G., Garmayeva L.L., Tatarinova N.K., Razuvayeva Ya.G., Mathanov I.E., Seng L., Song P.
6. Nowak G., Drozd B., Holub M., Budesinsky M., S'Man D. (1986) New guaianolides in *Centaurea bella* Trautv. and *Centaurea adjarica* Alb, *Acta Soc. Bot. Pol.*, 55(2), 227-231.
7. Nowak G., Holub M., Budesinsky M. (1988) Sesquiterpene lactones. XXXIV. Guaianolides in the genus *Leuzea* DC, *Acta Soc. Bot. Pol.*, 57(1), 157-163.
8. Gonzalez A.G., Darias V., Alonso G., Boada G.M., Ferrá M. (1978) Cytostatic activity of sesquiterpene lactones from Compositae of the Canary Islands, *Planta Medica*, 33(4), 356-359.
9. Sulsen V., Martino V. (2018) Sesquiterpene lactones. Advances in their chemistry and biological aspects. Springer International Publishing AG, Cham, Switzerland, 381 p.
10. Adekenov S.M. (2019) Study of antiopisthorchiasis activity of sesquiterpene lactones and their derivatives, *Fitoterapia*, 133, 200-211.
11. Berdin A.G., Adekenov S.M., Raldugin V.A., Shakirov M.M., Druganov A.G., Kulyyasov D.G., Tolstikov G.A. (1999) Raposerine and raserolide – new sesquiterpene lactones from *Rhaponticum serratuloides*, *News of the Russian Academy of Sciences (Chemical series)*, 10, 2010-2014.
12. Berdin A.G., Adekenov S.M., Raldugin V.D., Shakirov M.M., Druganov A.G., Gatilov Yu.V., Bagryanskaya I.Yu., Kulyyasov A.T., Tolstikov G.A. (2001) 15-O-Deacetylraposerine and raserine – new components of the sum of lactones from *Rhaponticum serratuloides*, *News of the Russian Academy of Sciences (Chemical series)*, 3, 515-520.
13. Nowak G., Drozd B., Holub M., Budesinsky M., S'Man D. (1986) New guaianolides in *Centaurea bella* Traut and *Centaurea adjarica* Alb, *Acta Soc. Bot. Pol.*, 55(2), 227-231.
14. Stevens K.L. (1982) Sesquiterpene lactones from *Centaurea repens*, *Phytochem.*, 21, 1093-1098.
15. Galbraith M.N., Horn D.H.S. (1969) Insect moulting hormones: crustecdysone (20-hydroxyecdysone) from *Podocarpus elatus*, *Aust. J. Chem.*, 22, 1045- 1057.

#### Information about author:

Adekenov Sergazy Mynzhasarovich – President of the joint-stock company “International Research and Production Holding” Phytochemistry”, Kazakhstan, e-mail: arglabin@phyto.kz

O.Yu. Maslov<sup>1\*</sup>, M.A. Komisarenko<sup>1</sup>, S.V. Ponomarenko<sup>2</sup>,  
 S.V. Kolisnyk<sup>1</sup>, T.P. Osolodchenko<sup>2</sup>, M.Yu. Golik<sup>1</sup>,  
 S.I. Polishchuk<sup>1</sup>

<sup>1</sup>National University of Pharmacy, Kharkiv, Ukraine

<sup>2</sup>I. Mechnikov Institute of Microbiology and Immunology, NAMSU, Kharkiv, Ukraine

\*e-mail: alexmaslov392@gmail.com

(Received 10 January 2024; received in revised form 13 February 2024; accepted 20 February 2024)

### Antimicrobial, antifungal, antioxidant activity a nd phytochemical investigation of fatty acids by GS/MS of raspberry (*Rubus idaeus* L.) shoot lipophilic extract

**Abstract.** The aim of the study was to determine the content of fatty acids using GC-MS in the obtained extract, conduct a study of the antimicrobial, antifungal and antioxidant activities of *Rubus idaeus* shoot lipophilic extract. The quantification of fatty acids was accomplished through GC-MS, antioxidant activity was assessed by potentiometric method, antimicrobial and antifungal activity was determined by well method. The 18 compounds were identified by the GS-MS. The levulenic acid (64.47±0.08 mg/100 g), linoleic acid (8.50±0.08 mg/100 g) and linolenic acid (6.80±0.04 mg/100 g) dominated in the obtained lipophilic *R. idaeus* shoot extract. *Bacillus subtilis* (17.00±0.50 mm) was the most sensitive to lipophilic extract whereas *P. vulgaris* was the most resistant to the lipophilic extract. Moreover, *Candida albicans* was medium sensitive to lipophilic extract (13.50±0.50 mm). The antioxidant activity was 1.00 mmol-equiv./m<sub>dry res</sub>, according to Maslov's antioxidant level classification it has low level. The extract exhibited antimicrobial activity against all tested strains, with the most significant impact observed against *B. subtilis*. However, the obtained lipophilic extract showed a relatively low level of antioxidant activity. Consequently, the derivatives of fatty acids play a substantial role in the antimicrobial and antifungal effects, whereas their contribution to antioxidant activity appears to be limited.

**Key words:** raspberry, fatty acids, lipophilic extract, antimicrobial activity, antioxidant activity.

#### Introduction

The bacterial infection diseases have caused about 14% of all deaths and 56% of sepsis cases throughout the world in 2019. The mortality level was 100 deaths per 100,000 of population. The 55% out of 7.7 million deaths have been caused with 3 Gram-negative (-) strains: *Escherichia coli*, *Klebsiella pneumonia*, *Pseudomonas aeruginosa*; and 2 Gram-positive (+): *Staphylococcus aureus* and *Streptococcus pneumonia*, with over 1.1 million deaths from *S. aureus* [1]. Over a 1.0 billion patients suffer from fungal infections of skin, nails, and hair, with over 150 million affected by serious fungal diseases that can be fatal [2]. Therefore, the search and elaboration of new antimicrobial medicines against G(+) and G(-), fungi strains is topical for medicine and pharmacy.

The temperate climate is the optimal conditions for genus *Rubus*, this genus is presented by 700 species [3]. Raspberries are cultivated throughout America, Eastern Europe, Russia, Asian as well as raspberry are closely related to blackberries and other brambles or cranberries. A red and black raspberry is the most widespread on the global range [4].

The raspberry leaves and fruits composition is represented by a variety of flavonoid derivatives, is represented by quercetin derivatives as well as phenolicarboxylic acids, organic acids, vitamin C [5]. Phenolicarboxylic acids are represented by ferulic acid, gentisic acid, syringic acid, vanillic acid and ellagic acid in *R. idaeus* leaf and shoot. The recent study showed that main compound in *R. idaeus* leaf and shoot are ellagotannins [6].

The recent literature search has showed that in many researches was estimated antimicrobial

and antifungal activities against G (+) and G (-) of ethanolic-aqueous and aqueous-ethanolic *R. idaeus* shoot and leaf extracts [7]. The results showed that all obtained extracts had high level of inhibition growth of bacteria and fungi strains. Moreover, the researches have been concluded that exactly derivatives of ellagotannins and flavan-3-ols responsible for antimicrobial and antifungal actions. There are no doubts that ellagotannins and flavan-3-ols are inhibited the growth of bacteria and fungi strains. However, in our view, the derivatives of fatty acids contribute to antimicrobial and antifungal effect of *R. idaeus* extracts. Therefore, the aim of study is to determine the content of fatty acids using GC-MS in the obtained extract, conduct a study of the antimicrobial, antifungal and antioxidant activities of *R. idaeus* shoot lipophilic extract.»

### Materials and methods

**Plant material.** The *Rubus idaeus* shoots were the objective of the study, which were gathered from places of its native cultivation. The leaves were collected in 2021 after the fruiting phase in the village of Ternova, Kharkiv region, Ukraine (50.193116162220264, 36.66935288403296).

**Reagents.** Hexane (purchased from Allchem), chloroform (purchased from Allchem), vanillic, benzoic, ferulic, *p*-oxybenzoic, syringic, gentisic, salicylic and phenylacetic acids from Sigma Aldrich Company.

**Extraction technique.** A 250.0 (exact mass) g of *Rubus idaeus* shoots were drudgery in the size 1-2 mm. The leaves were extracted by 60% EtOH at the proportion of leaf: solvent 1:20 (*m/v*) on water bath with a reflux condenser for 60 minutes at 80° C, the extraction was made two times. Following the cooling process, the solutions were filtered and concentrated to a final volume of 250 mL using a rotatory evaporator at 40°C under vacuity conditions than obtained extract was extracted by a chloroform with volume 125 mL for 15 min two times.

**GC-MS method of analysis.** The chromatographic separation of fatty acids was carried out on gas chromatography-mass spectrometer 5973N/6890N MSD/DS «Agilent Technologies» (USA). The mass spectrometer detector is a quadrupole, ionization method is chosen an electron impact, and ionization energy is 70 eV. For the analysis is applied a full ion current. A capillary column was made by HP-INNOWAX (30 m × 250 μm). «The stationary phase was INNOWAX as well as mobile phase was helium,

gas flow rate was 1 ml/min; the sample was introduced at 250 °C. The introduction of a sample of 2 μL into the chromatographic column was performed in the splitless mode (without flow distribution), which allows you to do this without loss of separation and significantly (up to 20 times) increase the sensitivity of the chromatography method. Sample injection speed – 1 mL/min, time – 0.2 min.

The research was done according following way: 0.50 mg of the dried extract in a 2 mL vial was added an internal standard (50 μg of tridecane in hexane) and 1.0 mL of a methylating agent – 14% BCl<sub>3</sub> in methanol, Supelco No. 3-3033. The mixture was kept in a hermetically sealed vial for 8 hours at a temperature of 65 °C. During this time, fatty acids are completely extracted from the extract and transesterification of acids occurs. The reaction mixture was drained from the sediment and diluted with 1 ml of distilled water. To obtain methyl esters of fatty acids, 0.2 mL of methylene chloride was added, shaken for 1 hour «and subjected to chromatography.

Identification of the methyl esters of the acids was based on the calculation of the equivalent aliphatic chain length using data from the NIST 05 and Willey 2007 mass spectra library. The retention time was also compared with the retention time of standard compounds (“Sigma”). The quantitative content was calculated by a formula:

$$C(\text{mg/kg}) = K_1 \times K_2 \times 100.$$

where,  $K_1 = S_1/S_2$  ( $S_1$  – square peak of analyzed substance,  $S_2$  – square peak of standard substance);  $K_2 = 50/M$  (50 – mass of internal standard, that injected with analyzed substance, μg); M – sample mass, mg.

**Antioxidant activity.** «Antioxidant activity of extract was evaluated by potentiometric method and calculated according to the following equation and expressed as mmol-equiv./m<sub>dry, res.</sub> [8-10].»

**Test organisms.** Test strains of *Staphylococcus aureus* ATCC 25923, *Proteus vulgaris* NTCS 4636, *Escherichia coli* ATCC 25922, *Bacillus subtilis* ATCC 6538, *Candida albicans* ATCC 885/653, *Pseudomonas aeruginosa* ATCC 27853 were applied in accordance with the approvals for the assessment of drugs antimicrobial activity.

**Antifungal and antibacterial activities assays.** The concentration of lipophilic extract was 1% as a solvent of which were 40% EtOH. The method of diffusion of the drug into agar carried out using the method of “wells” [11].

## Results and discussion

The GC-MS method was used to carry out a qualitative and quantitative analysis of fatty acids in the obtained lipophilic extract of *Rubus idaeus* shoot. According to the results of the study, 18 compounds were identified: levulinic, linoleic,

linolenic, palmitic, oleic, stearic, arachidic, heneicosanoic, behenic, tetracosanoic, heptadecanoic, 2-hydroxypalmitic, azelaic, palmitoleic acid, myristic, lauric, tricosanoic, pentadecanoic acids (Figure 1).

The sum of the fatty acids in the obtained extract was 92.11 mg/100 g (Table 1).

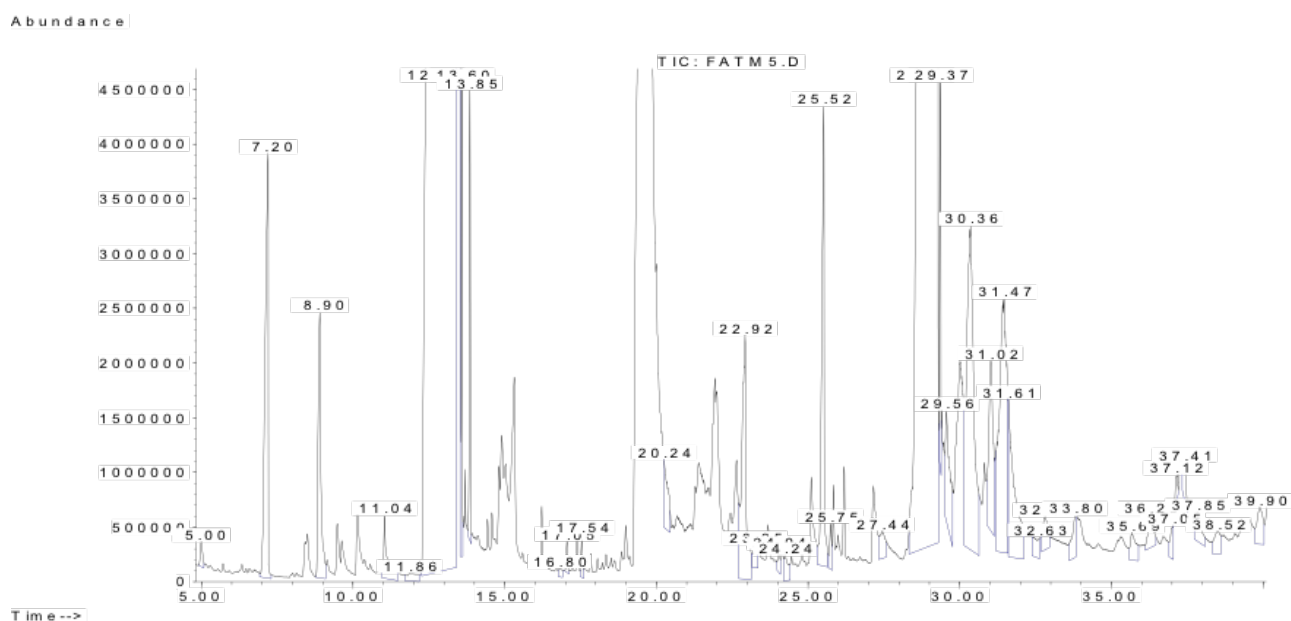


Figure 1 – GC-MS fingerprint of *Rubus idaeus* shoot lipophilic extract

Table 1 – Fatty acid composition in *R. idaeus* shoot lipophilic extract

No.	Compound	Rt, min	Quantitative content in extract, mg/100 g $\pm$ SD	% out of sum fatty acids
1	Levulinic acid	12.689	64.47 $\pm$ 1.00	69.99
2	Linoleic acid	30.294	8.50 $\pm$ 0.08	9.23
3	Linolenic acid	31.580	6.80 $\pm$ 0.08	7.38
4	Palmitic acid	25.433	4.06 $\pm$ 0.08	4.41
5	Oleic acid	30.183	1.91 $\pm$ 0.04	2.07
6	Stearic acid	30.061	1.68 $\pm$ 0.04	1.82
7	Arachidic acid	32.659	0.64 $\pm$ 0.04	0.69
8	Heneicosanoic acid	34.236	0.58 $\pm$ 0.04	0.63
9	Behenic acid	35.601	0.58 $\pm$ 0.04	0.63
10	Tetracosanoic acid	38.494	0.55 $\pm$ 0.04	0.60
11	Heptadecanoic acid	26.410	0.54 $\pm$ 0.04	0.59
12	2-hydroxypalmitic acid	32.043	0.43 $\pm$ 0.04	0.47
13	Azelaic acid	24.764	0.41 $\pm$ 0.04	0.45
14	Palmitoleic acid	25.776	0.34 $\pm$ 0.04	0.37
15	Myristic acid	21.738	0.33 $\pm$ 0.04	0.36



Table continuation

No.	Compound	Rt, min	Quantitative content in extract, mg/100 g $\pm$ SD	% out of sum fatty acids
16	Lauric acid	17.634	0.22 $\pm$ 0.01	0.24
17	Tricosanoic acid	37.173	0.21 $\pm$ 0.01	0.23
18	Pentadecanoic acid	24.099	0.19 $\pm$ 0.01	0.21
Total content of identified compounds			92.11	100

As shown in Table 1, levulinic acid dominates among all fatty acids (69.99% out of the total fatty acids), linoleic acid is in second place (7.38% out of the total fatty acids), and linolenic acid is in the third place, and the lowest content was pentadecanoic acid (4.41% out of the total fatty acids). As can be seen from the above results, the content of levulinic, linoleic and linolenic acids is 81.78% out of total fatty acids (Table 1).

Analyzed extract showed the antimicrobial and antifungal against *S. aureus*, *E. coli*, *P. vulgaris*, *P. aeruginosa*, *B. subtilis*, *C. albicans* strains.

According to the conducted research, it was found that extract strongly inhibited the growth of *B. subtilis* (17.00 $\pm$ 0.50 mm). In the case of G(-) bacteria, it was found that strongly inhibited the growth of *E. coli* (15.00 $\pm$ 0.50 mm) and *P. aeruginosa* (17.00 $\pm$ 0.50 mm). *P. vulgaris* strain was the most resistant among bacteria turned out to be. *C. albicans* was medium sensitive for lipophilic extract (13.50 $\pm$ 0.50 mm). In addition, it was found that *R. idaeous* shoot lipophilic extract had higher antimicrobial activity against G(+) than G(-) bacteria strains. (Table 2)

Table 2 – Antimicrobial and antifungal activities of *R. idaeous* shoot lipophilic extract

Sample	The diameter growth retardation zone, mm $\pm$ SD					
	<i>S. aureus</i> ATCC 25923	<i>E. coli</i> ATCC 25922	<i>P. vulgaris</i> ATCC 4636	<i>P. aeruginosa</i> ATCC 27853	<i>B. subtilis</i> ATCC 6633	<i>C. albicans</i> ATCC 653/885
Lipophilic extract	16.50 $\pm$ 0.50	15.00 $\pm$ 0.50	14.00 $\pm$ 0.50	15.00 $\pm$ 0.50	17.00 $\pm$ 0.50	13.50 $\pm$ 0.50
40%EtOH	Growth	Growth	Growth	Growth	Growth	Growth

SD –standard deviation, n=3

The antioxidant effect was determined with the potentiometric method. Table 3 shows that the antioxidant activity of lipophilic extract was 1.00 $\pm$ 0.01 mmol-equiv./m<sub>dry res.</sub> Comparing with standard «Ascorutin» the antioxidant effect level of analyzed

extract lower in 98%. According to developed a novel conditional classification of antioxidant action by Maslov [12] the lipophilic extract had a low level of scavenging activity of free radicals, whereas the standard «Ascorutin» – medium level (Table 3).

Table 3 – Result of antioxidant activity of *R. idaeous* shoot lipophilic extract

Sample	AOA, mmol-equiv./m <sub>dry res.</sub> $\pm$ SD	The conditional level of antioxidant activity
Lipophilic extract	1.00 $\pm$ 0.01	Low level
«Ascorutin»	51.10 $\pm$ 1.05	Medium level

SD –standard deviation, n=3

Fatty acids, whether free or part of complex lipids, play crucial roles in metabolism. They serve as a major source of metabolic fuel by storing and transporting energy, are essential components of all cell membranes, and act as gene regulators. Fatty acids are carbon chains that have a methyl group at one end (designated as omega,  $\omega$ ) and a carboxyl group at the other end. They are divided in two sub-groups: saturated and unsaturated acids, it dependence on the presence of double bonds in the structure [13]. In a recent research of Celik *et al.* [14], it has been evaluated the extract obtained with chloroform from *R. idaeus* fruit from cultivated fruit. It was found that total fatty acids content was 290.0 mg/100 g in extract, the 10 fatty acids were identified: linoleic, linolenic, palmitic, oleic, stearic, arachidic, lauric, azelaic, behenic, and myristic acids. The main fatty acids were represented by unsaturated acids: linoleic (35%) and linolenic (20%) acids. Compared with our results, the total content of fatty acids was 68% lower, the content of linolenic acid was lower in 50%, and the content of linoleic acid in 45%. In our view, levulinic acid is a specific marker of *R. idaeus* shoot, whereas in fruit are linolenic and linoleic acid. According to compared results, the sum content of fatty acids in *R. idaeus* fruit extract is higher than in the obtained lipophilic extract from shoot. In our view, it relates with the biometabolism of flavonols in plant. According to the theory of growing plant, derivatives of fatty acid involved in responses to stress, growth, and development that is quite important for fruit, whereas for shoot fatty acids play only role of transporters.

In our recent studies, it has been demonstrated that the primary groups of biologically active compounds in *R. idaeus* shoots are derivatives of catechins and ellagitannins. Due to the presence of these compound groups, the extracted *R. idaeus* shoot extract exhibits powerful antioxidant, antimicrobial, and antifungal effects. However, other phenolic compounds, such as fatty acids (levulinic acid, linoleic acid, linolenic acid, etc.), are also present in *R. idaeus* shoots but in minor quantities. We were interested in understanding whether these fatty acids possess antioxidant, antimicrobial, and antifungal

properties, or if they are merely inert compounds with no pharmacological value.

To investigate this hypothesis, we conducted the following extraction method: initially, a dual extraction of the raw material was performed using 60% ethanol, followed by ethanol evaporation and liquid-liquid extraction with chloroform. This is because fatty acids acid derivatives have high solubility in nonpolar solvents. The obtained extract was evaporated to a 1:2 mass ratio relatively to the raw material, and subsequent analysis was conducted to evaluate antimicrobial, antifungal, and antioxidant activities.

Our study revealed that the obtained lipophilic extract demonstrates antimicrobial activity against both G(+) and G(-) bacterial strains and exhibits antifungal activity against *Candida albicans*. However, it shows low level of antioxidant activity. Consequently, derivatives of fatty acids contribute significantly to the antimicrobial and antifungal actions, while catechin and ellagitannins derivatives are responsible for the antioxidant activity. Based on these findings, it can be concluded that in the development of a pharmaceutical product with antioxidant properties, fatty acid derivatives should be eliminated.

## Conclusion

The lipophilic extract from *R. idaeus* shoots contains various fatty acids, including levulinic, linoleic, linolenic, palmitic, oleic, stearic, arachidic, heneicosanoic, behenic, tetracosanoic, heptadecanoic, 2-hydroxypalmitic, azelaic, palmitoleic, myristic, lauric, tricosanoic, pentadecanoic acids with the highest concentrations observed for levulinic, linoleic, and linolenic acids. This study highlights the antimicrobial and antifungal properties of the *R. idaeus* shoot lipophilic extract. The extract exhibited antimicrobial activity against all tested strains, with the most significant impact observed against *Bacillus subtilis*. However, the obtained lipophilic extract showed a relatively low level of antioxidant activity. Consequently, the derivatives of fatty acids play a substantial role in the antimicrobial and antifungal effects, whereas their contribution to antioxidant activity appears to be limited.

## References

1. Ikuta, K.S., Swetschinski, L.R., Robles Aguilar, G., et al. (2022). Global mortality associated with 33 bacterial pathogens in 2019: a systematic analysis for the Global Burden of Disease Study 2019. *The Lancet*, vol. 400, pp. 2221-2248. [https://doi.org/10.1016/s0140-6736\(22\)02185-7](https://doi.org/10.1016/s0140-6736(22)02185-7)
2. Bongomin, F., Gago, S., Oladele, R., Denning, D. (2017). Global and Multi-National Prevalence of Fungal Diseases – Estimate Precision. *Journal of Fungi*, vol. 3, no. 4, p. 57. <https://doi.org/10.3390/jof3040057>

3. Maslov, O., Komisarenko, M., Kolisnyk, S., Kostina, T., Golik, M., Moroz, V., Tarasenko, D., & Akhmedov, E. (2023). Investigation of the extraction dynamic of the biologically active substances of the raspberry (*Rubus idaeus* L.) shoots. *Current Issues in Pharmacy and Medical Sciences*, 36(4), 194–198. <https://doi.org/10.2478/cipms-2023-0034>
4. Maslov, O.Y., Komisarenko, M.A., Golik, M.Y., et al. (2023). Study of total antioxidant capacity of red raspberry (*Rubus idaeus* L.) shoots. *Vitae*, vol. 30, no 1, pp. 1-8 <https://doi.org/10.17533/udea.vitae.v30n1a351486>
5. Komisarenko, M.A., Polischuk, I.M., Upyr, T.V., Saidov, N.B. (2021). Study of Amino acid composition and immunomodulatory activity of *Rubus idaeus* alcoholic extract. *Research journal of pharmacy and technology*, vol. 14, no 3, pp. 1329–1332. <https://doi.org/10.5958/0974-360x.2021.00236.5>
6. Derymedvid L.V., Komisarenko M.A. et al. (2021) Anti-inflammatory properties of raspberry shoot extract. *Pharmacologyonline*, no 2, pp. 657-662. <https://doi.org/10.5281/zenodo.10464322>
7. Maslov, O., Komisarenko, M., Ponomarenko, S., et al. (2022). Investigation the influence of biologically active compounds on the antioxidant, antibacterial and anti-inflammatory activities of red raspberry (*Rubus idaeus* L.) leaf extract. *Current Issues in Pharmacy and Medical Sciences*, vol. 35, no. 4, pp. 229-235 <https://doi.org/10.2478/cipms-2022-0040>
8. Maslov O, Kolisnyk S, Komisarenko M, Golik M. (2022) Study of total antioxidant activity of green tea leaves (*Camellia sinensis* L.). *Herba Pol*, vol. 68, no 1, pp. 1-9. <https://doi.org/10.2478/hepo-2022-0003>
9. Maslov O.Y., Kolisnyk S.V., Komisarenko N.A., Kostina T.A. (2021) Development and validation potentiometric method for determination of antioxidant activity of epigallocatechin-3-o-gallate. *Pharmacologyonline*, no 2, pp. 35-42. <https://doi.org/10.5281/zenodo.7813097>
10. Maslov O.Y., Kolisnyk S.V., Komisarenko M.A., Kolisnyk O.V., et al. (2021) Antioxidant activity of green tea leaves (*Camellia sinensis* L.) liquid extracts. *Pharmacologyonline*, no 3, pp. 291-298. <https://doi.org/10.5281/zenodo.7813114>.
11. Maslov O., Kolisnyk S., Komisarenko M., et al. (2022) In vitro antioxidant and antibacterial activities of green tea leaves (*Camellia sinensis* L.) liquid extracts. *An Mechnikov's Inst*, 2, pp. 64–67. doi: <https://doi.org/10.5281/zenodo.6634846>
12. Maslov O.Y., Kolisnyk S.V., Komisarenko M.A., et al. Study and evaluation antioxidant activity of dietary supplements with green tea extract. *Curr Issues Pharm Med*, vol. 14, no 2, pp. 215-219. <https://doi.org/10.14739/2409-2932.2021.2.233306>
13. Lund J., Rustan, A.C. (2024). Fatty Acids: Structures and Properties. NY: John Wiley & Sons, Ltd. (Ed.), 283-292 ISBN 9780470015902 <https://doi.org/10.1002/9780470015902.a0029198>
14. Celik F., Ercisli S. (2009) Lipid and fatty acid composition of wild and cultivated red raspberry fruits (*Rubus idaeus* L.). *Journal of Medicinal Plants Research*, vol. 3, no 8, pp. 583-585. <https://doi.org/10.5281/zenodo.10464340>

**Information about authors:**

Olexander Maslov (corresponding author) – PhD, National University of Pharmacy, Kharkiv 61001, Ukraine, e-mail: [alexmaslov392@gmail.com](mailto:alexmaslov392@gmail.com)

Mykola Komisarenko – PhD, National University of Pharmacy, Kharkiv 61001, Ukraine, e-mail: [a0503012358@gmail.com](mailto:a0503012358@gmail.com)

Svitlana Ponomarenko – PhD, Mechnikov Institute of Microbiology and Immunology of the NAMS of Ukraine, Kharkiv 61001, Ukraine, Puskinskay 53, e-mail: [syonomarenko@i.ua](mailto:syonomarenko@i.ua)

Sergii Kolisnyk – DSc, professor, National University of Pharmacy, Kharkiv 61001, Ukraine, e-mail: [s\\_kolesnik@nuph.edu.ua](mailto:s_kolesnik@nuph.edu.ua)

Tetiana Osolodchenko – PhD, associate professor, Mechnikov Institute of Microbiology and Immunology, NAMS, Kharkiv 61001, Ukraine, e-mail: [imi\\_lbb@ukr.net](mailto:imi_lbb@ukr.net)

Mykola Golik – DSc, professor, National University of Pharmacy, Kharkiv 61001, Ukraine, e-mail: [aptekar4009@gmail.com](mailto:aptekar4009@gmail.com)

Sofia Polishchuk – student, National University of Pharmacy, Kharkiv 61001, Ukraine, e-mail: [chemistry29@meta.ua](mailto:chemistry29@meta.ua)

M. Siddiqui<sup>1</sup>, Atia-tul-Wahab<sup>2</sup>, B.M. Kudaibergenova<sup>3\*</sup>,  
Zh.A. Abilov<sup>3</sup>, M.I. Choudhary<sup>1,2,3</sup>

<sup>1</sup>H.E.J. Research Institute of Chemistry, University of Karachi, Karachi, Pakistan

<sup>2</sup>Dr. Panjwani Center for Molecular Medicine and Drug Research, University of Karachi, Karachi, Pakistan

<sup>3</sup>Al-Farabi Kazakh National University, Almaty, Kazakhstan

\*e-mail: bateskudaibergenova@yahoo.com

(Received 2 May 2024; received in revised form 13 May 2024; accepted 24 May 2024)

## Biotransformation of anabolic drug Dianabol with *Rizhopus oryzae*

**Abstract.** Microbial biotransformation technique is an excellent approach for the synthesis of stereo-, enantio-, chemo-, and regio-selective/specific analogues of existing steroidal and non-steroidal drugs by using bacteria, fungi, algae, actinomycetes, yeast, and plants and animals cell cultures. This technique is effectively used to synthesize compounds whose structures resemble to the substrates (parent drugs) without using protecting/deprotecting steps. In the current study, an anabolic-androgenic steroid (AAS) based drug, methandienone (dianabol) (1) was incubated with the filamentous fungi *Rizhopus oryzae* ATCC 11145 for twelve days under ambient reaction conditions (at room temperature and neutral pH) by using aqueous media. Therefore, the present study has successfully helped to produce the structural analogues of inert steroidal anabolic drug dianabol (1) without using expensive and toxic chemicals. This yielded five known structural analogues of dianabol (1), *i.e.*, 17 $\beta$ ,11 $\beta$ -dihydroxy,17 $\alpha$ -methyl-androsta-1,4-diene-3-one (2), 17 $\beta$ -hydroxy,17 $\alpha$ -methyl-androsta-1,4-diene-3,11-dione (3), 17 $\beta$ ,6 $\beta$ -dihydroxy,17 $\alpha$ -methyl-androsta-1,4-diene-3-one (4), 17 $\beta$ ,6 $\beta$ -dihydroxy,17 $\alpha$ -methyl-androsta-4-ene-3-one (5), and 17 $\beta$ -hydroxy,17 $\alpha$ -methyl-androsta-4,6-diene-3-one (6). Structures of transformed products 2-6 were determined through <sup>1</sup>H-NMR, and FAB-MS spectroscopic techniques.

**Key words:** microbial biotransformation, fungi, *Rizhopus oryzae*, anabolic-androgenic drug, Dianabol.

### Introduction

Derivatization of organic compounds through conventional synthetic methodologies is a difficult task, as they typically involve the use of expensive and toxic chemicals, and extreme pressure, temperature and pH during the transformations, along with the protection/deprotection steps. In contrast, microbial biotransformation is a robust approach that can effectively modify the structures of almost all classes of organic compounds. This technique is generally performed at ambient temperature and pressure, and neutral pH by using aqueous media. Microbial biotransformation technique is therefore, an efficient way to synthesize regio-, chemo-, and stereo-specific/selective derivatives of existing drugs. The chemical conversion of substrates is catalyzed by various enzymes (biological catalysts) without using protection, deprotection, and functional group activation steps. At present microbial biotransformation is recognized as a green

chemistry approach, because it generates less toxic wastes as compared to chemical syntheses. Currently the use of microbial biotransformation is increasing significantly in the production of pharmaceutical products, *i.e.*, vitamins, hormones, enzymes, enzyme inhibitors, vaccines, *etc.* as it preserves the original skeleton of starting material during the formation of products, making it important for industries [1-7].

Methandrostenolone/methandienone (1) is an anabolic-androgenic steroidal drug, used to improve physical performances, and increase muscles without gaining fat. Previously, it was sold under the brand name of dianabol (1) in USA and Germany. Like other steroids, methandienone also has some side effects, including acne, increased hair growth on body, change in voice, estrogenic effects, and liver damage [8, 9]. It is therefore, important to synthesize its analogues by environmentally friendly methods.

In continuance of our biocatalytic studies of steroidal-based compounds/drugs [5-7, 10-13], we

report here biotransformation of dianabol (1) with *Rhizopus oryzae* under mild reaction conditions. This yielded five known transformed products (Figure-1), 17 $\beta$ , 11 $\beta$ -dihydroxy, 17 $\alpha$ -methyl-androsta-1,4-diene-3-one (2), 17 $\beta$ -hydroxy,17 $\alpha$ -methyl-androsta-1,4-diene-3,11-dione (3), 17 $\beta$ ,6 $\beta$ -dihydroxy,17 $\alpha$ -methyl-androsta-1,4-diene-3-one (4), 17 $\beta$ ,6 $\beta$ -dihydroxy,17 $\alpha$ -methyl-androsta-4-ene-3-one (5), and 17 $\beta$ -hydroxy,17 $\alpha$ -methyl-androsta-4,6-diene-3-one (6). Structures of metabolites 2-6 were identified through <sup>1</sup>H-NMR, and FAB-MS spectroscopic techniques.

## Materials and methods

**Fungi.** Fungal cell culture *e.g.*, *Rhizopus oryzae* ATCC 11145 was purchased from ATCC (American Type Culture Collection, USA). Fungal cell culture was grown on SDA at 3-4 °C.

**Media.** Five liters of media for the growth of *R. oryzae* was prepared by using following ingredients: Glucose (50 g), NaCl (25 g), peptone (25 g), KH<sub>2</sub>PO<sub>4</sub> (25 g), and glycerol (50 mL) in five liters of distilled water.

Ingredients for the preparation of media were acquired from Scharlau Chemicals and Reagents (Spain), VWR Chemicals (USA), Dae-Jung Chemicals and Metals Company Limited (Korea), Sigma-Aldrich (Germany), and Oxoid Limited (England).

**General.** Dianabol (1), (*m/z* = 300.4, C<sub>20</sub>H<sub>28</sub>O<sub>2</sub>), was procured from the Shenzhen Simeiquan Biotechnology Company Limited, (China). Silica coated (PF<sub>254</sub>) TLC plates (Merck KGaA, Germany) were used to determine the transformations, and purity of compounds. Fractions were obtained by performing silica gel (70–230 mesh) (E. Merck, Germany) column chromatography. Final purifications of fractions were performed *via* recycling reverse phase HPLC (LC-908, YMC L-80) using methanol/water. The <sup>1</sup>H-NMR spectra of compounds 1-6 were run in CDCl<sub>3</sub> on the Bruker Avance-NMR (Bruker, Switzerland). FAB-MS of compounds 1-6 were performed on the Joel JMS H×110 mass spectrometer (Joel, Japan).

**Fermentation of Dianabol (1).** Media (5 L) was prepared by aforementioned recipe. Media (400 mL) was transferred to each 20 flasks of 1 L. Each flask was cotton plugged, and autoclaved. All the flasks were then cooled at room temperature. Media was inoculated with the culture of *R. oryzae* under sterilized conditions, and placed for four days on rotary shaker at 25 °C. After maximum growth of *R.*

*oryzae*, 2 g of dianabol (1) was dissolved in 20 mL of methanol, and fed 1 mL in each *R. oryzae*-containing flask. These flasks were again placed on rotary shaker at 25 °C for twelve days.

**Extraction of Transformed Products.** After incubation, EtOAc (ethyl acetate) was added in each flask. Flasks were filtered, and rinsed with EtOAc. The filtrate was extracted three times with EtOAc, and biomasses were discarded. Sodium sulfate was added in each extracted flask to absorb water, and filtered. The extracted was then evaporated by using rotary evaporator. As a result, a brown color gummy crude extract was obtained.

**Purification of Transformed Products.** Crude extract was fractionated by silica-gel column chromatography using hexanes-acetone mixture (5-100%), passing 400 mL at each mixture concentration. TLCs were taken for each fractions. TLCs were stained by ceric sulfate spraying reagent. Fractions were purified through recycling RP-HPLC using methanol (70%) and water (30%) solvent system.

## Results and discussion

*R. oryzae*-mediated structural modification of dianabol (1) afforded five derivatives, presented on Figure 1.

Their structures were determined by comparing their <sup>1</sup>H-NMR and FAB-MS data with the spectral data reported in the literature.

Metabolite 2 showed its [M-H]<sup>+</sup> at *m/z* 315.3 in the FAB-MS (-ve mode). Newly appeared H-11 of compound 2 was observed at  $\delta$  4.40, d ( $J_{11,12/11,9} = 2.88$  Hz). Compound 2 was previously reported by our research group [14].

Transformed product 3 showed its [M+H]<sup>+</sup> at *m/z* 315.1 in the FAB-MS (+ve). <sup>1</sup>H-NMR spectrum of compound 3 was distinctly similar to compound 2. Signals for methylene protons (H<sub>2</sub>-12) were found missing in the <sup>1</sup>H-NMR spectrum of 3. Compound 3 was also previously reported by our research group [14].

[M-H]<sup>+</sup> of compound 4 was observed at *m/z* 315.2 in the FAB-MS (-ve mode). Newly appeared H-6 of compound 4 was observed at  $\delta$  4.53, d ( $J_{6,7} = 2.18$  Hz) in the <sup>1</sup>H-NMR spectrum. Compound 4 was previously reported by our research group [14].

Derivative 5 displayed its [M-H]<sup>+</sup> at *m/z* 317.2 in the FAB-MS (-ve mode). Newly appeared H-6 of compound 5 was observed at  $\delta$  4.53, d ( $J_{6,7} = 2.22$  Hz) in the <sup>1</sup>H-NMR spectrum. Signals for olefinic protons H-1 and H-2 were found missing in the <sup>1</sup>H-NMR spectrum of 5 [15].

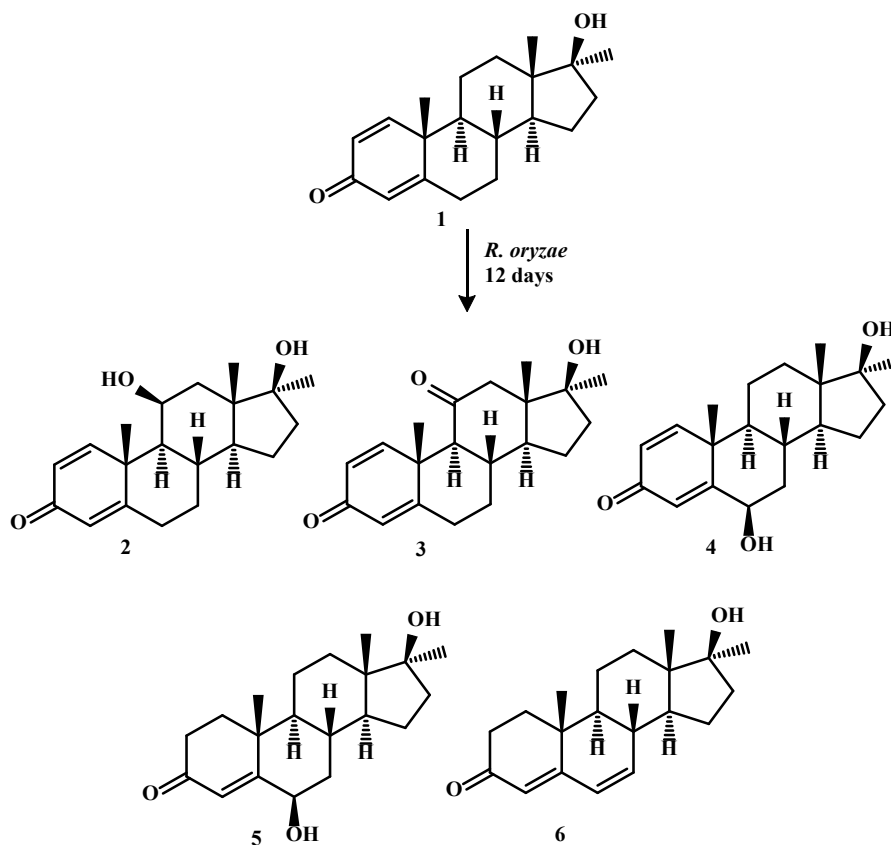


Figure 1 – Biotransformation of dianabol (1) with *R. oryzae*

Compound 6 showed its  $[M+H]^+$  at 301.0 in the FAB-MS (+ve). Olefinic protons H-1 and H-2 were found missing while new downfield signals for olefinic protons H-6, and H-7 were observed at  $\delta$  6.09 s in the  $^1\text{H-NMR}$  spectrum of 6 [16].

### Conclusion

In the present study biotransformation of dianabol (1) was performed at ambient reaction conditions

with *R. oryzae*. This afforded five known structural analogues of anabolic drug 1. The study indicates that *R. oryzae* was able to catalyze  $\beta$  hydroxylation at C-6, and C-11 of drug 1. Dehydrogenation, reduction, and ketone formation was also observed during the transformation of dianabol (1). In future, transformed products 2-6 will be evaluated against various biological activities. These derivatives will also be studied at enzymatic levels for their mechanism of production.

### References

- Adams, J. P., Brown, M. J., Diaz-Rodriguez, A., Lloyd, R. C., et al. (2019). Biocatalysis: A pharma perspective. *Adv Synth and Catal.*, 361 (11), 2421-2432. <https://doi.org/10.1002/adsc.201900424>
- Alcántara, A. R. (2018). Biotransformations in drug synthesis: a green and powerful tool for medicinal chemistry. *J Med Chem and Drug Design*, 1 (1), 1-7. DOI: 10.16966/2578-9589.102
- Atia-tul-Wahab, Siddiqui, M., Ibrahim, I., Hussain, A., et al. (2018). *Cunninghamella blakesleeana*-mediated biotransformation of a contraceptive drug, desogestrel, and anti-MDR-*Staphylococcus aureus* activity of its metabolites. *Bioorg Chem.* 77, 152-158. <https://doi.org/10.1016/j.bioorg.2017.12.027>
- Bianchini, L. F., Arruda, M. F., Vieira, S. R., Campelo, P., et al. (2015). Microbial biotransformation to obtain new antifungals. *Front Microbiol*, 6, 1433. <https://doi.org/10.3389/fmicb.2015.01433>
- Chegaing, S. P. F., Kengni, A. D. M., Siddiqui, M., Fowa, A. B., et al. (2020). Fungal transformation of norandrostenedione with *Cunninghamella blakesleeana* and anti-bacterial activity of the transformed products. *Steroids*, 162, 108679. <https://doi.org/10.1016/j.steroids.2020.108679>

6. Siddiqui, M., Atia-tul-Wahab, Jabeen, A., Wang, Y., et al. (2020). Whole-cell fungal-mediated structural transformation of anabolic drug metenolone acetate into potent anti-inflammatory metabolites. *J Adv Res.*, 24, 69-78. <https://doi.org/10.1016/j.jare.2020.02.009>
7. Siddiqui, M., Ahmad, M. S., Atia-tul-Wahab, Yousuf, S., et al. (2017). Biotransformation of a potent anabolic steroid, mibolerone, with *Cunninghamella blakesleeana*, *C. echinulata*, and *Macrophomina phaseolina*, and biological activity evaluation of its metabolites. *PLoS one*, 12 (2), e0171476. <https://doi.org/10.1371/journal.pone.0171476>
8. Dürbeck, H. W., and Büker, I. (1980). Studies on anabolic steroids. The mass spectra of 17 $\alpha$ -methyl-17 $\beta$ -hydroxy-1,4-androstadien-3-one (dianabol) and its metabolites. *Biomed Mass Spectrom.*, 7 (10), 437-445. <https://doi.org/10.1002/bms.1200071007>
9. Van der Kuy, P. H., Hooymans, P. M., Stegeman, A., and Looij jr, B. J. (1997). Falsification of Thai dianabol. *Pharm World Sci.*, 19 (4), 208-209. <https://doi.org/10.1023/A:1008669917252>
10. Ahmad, M. S., Yousuf, S., Atia-tul-Wahab, Jabeen, A., et al. (2017). Biotransformation of anabolic compound methasterone with *Macrophomina phaseolina*, *Cunninghamella blakesleeana*, and *Fusarium lini*, and TNF- $\alpha$  inhibitory effect of transformed products. *Steroids*, 128, 75-84. <https://doi.org/10.1016/j.steroids.2017.04.001>
11. Bano, S., Atia-tul-Wahab, Yousuf, S., Jabeen, A., et al. (2016). New anti-inflammatory metabolites by microbial transformation of medrysone. *PLoS One*, 11 (4), e0153951. <https://doi.org/10.1371/journal.pone.0153951>
12. Choudhary, M. I., Siddiqui, M., Atia-tul-Wahab, Yousuf, S., et al. (2017). Bio-catalytic structural transformation of anti-cancer steroid, drostanolone enanthate with *Cephalosporium aphidicola* and *Fusarium lini*, and cytotoxic potential evaluation of its metabolites against certain cancer cell lines. *Front Pharmacol.*, 8, 900. <https://doi.org/10.3389/fphar.2017.00900>
13. Farooq, R., Hussain, N., Yousuf, S., Atia-tul-Wahab, A., et al. (2018). Microbial transformation of mestanolone by *Macrophomina phaseolina* and *Cunninghamella blakesleeana* and anticancer activities of the transformed products. *RSC Adv.*, 8 (39), 21985-21992. DOI: 10.1039/C8RA01309H
14. Khan, N. T., Zafar, S., Noreen, S., Al Majid, A. M., et al. (2014). Biotransformation of dianabol with the filamentous fungi and  $\beta$ -glucuronidase inhibitory activity of resulting metabolites. *Steroids*, 85, 65-72. <https://doi.org/10.1016/j.steroids.2014.04.004>
15. Kolet, S. P., Nilofarjahan, S., Haldar, S., Gonnade, R., et al. (2013). Biocatalyst mediated production of 6 $\beta$ ,11 $\alpha$ -dihydroxy derivatives of 4-ene-3-one steroids. *Steroids*, 78 (11), 1152-1158. <https://doi.org/10.1016/j.steroids.2013.08.004>
16. Cooper, E. R., McGrath, K. C., Li, X., Akram, O., et al. (2017). The use of tandem yeast and mammalian cell *in vitro* androgen bioassays to detect androgens in internet-sourced sport supplements. *Drug Test Anal.*, 9 (4), 545-552. <https://doi.org/10.1002/dta.2000>

**Information about authors:**

Mahwish Siddiqui – PhD at H.E.J. Research Institute of Chemistry (Karachi, Pakistan, e-mail: mahwish.siddiqui88@gmail.com)

Atia-Tul-Wahab – Professor at ICCBS, University of Karachi (Karachi, Pakistan, e-mail: tulwahab@yahoo.com)

Kudaibergenova Bates – PhD, Acc.professor at Al-Farabi Kazakh National University (Almaty, Kazakhstan, e-mail: bateskudaibergenova@yahoo.com)

Zharylkasyn Abilov – Professor at Al-Farabi Kazakh National University (Almaty, Kazakhstan, e-mail: abilov229@mail.ru)

Choudhary, Mohammed Iqbal – Director and Professor of Bioorganic and Natural Product Chemistry at the International Center for Chemical and Biological Sciences (H. E. J. Research Institute of Chemistry and Dr. Panjwani Center for Molecular Medicine and Drug Research), University of Karachi (Karachi, Pakistan, e-mail: iqbal.choudhary@iccs.edu)

O. Sarikaya<sup>1\*</sup> , S. Parlak<sup>1</sup> , Y. Yildiz<sup>2</sup> , T. Gencal<sup>1</sup> ,  
I.M. Ozcankaya<sup>3</sup> , F. Selek<sup>3</sup> , O. Acici<sup>4</sup> , H. Can<sup>4</sup> 

<sup>1</sup>Bursa Technical University, Bursa, Turkey

<sup>2</sup>Bartın University, Faculty of Forestry, Bartın, Turkey

<sup>3</sup>Aegean Forestry Research Institute, Urla, Izmir, Turkey

<sup>4</sup>Bursa Regional Forestry Directorate, Osmangazi, Bursa, Turkey

\*e-mail: oguzhan.sarikaya@btu.edu.tr

(Received 13 February 2024; received in revised form 12 March 2024; accepted 19 March 2024)

## Insecticide applications with trunk injection method for reducing the damage level of *Leptoglossus occidentalis* (Heidemann, 1910) in stone pine stands

**Abstract.** *Leptoglossus occidentalis* was first detected in Turkey in 2009. The pest's damage to stone pine trees and its effects on seeds cause economic losses. In recent years, observations and predictions show that there is a significant threat not only to stone pine but also to other coniferous forests throughout country. In this study, pesticides were applied by trunk injection method in the experiment areas taken in stone pine stands of Bergama – Kozak region. In the systemic application carried out in 2020 and 2021, the Arborjet system was used and the insecticide with the active ingredient Azadirachtin (0.3 g/Lt) was used as an organic insecticide, as well as pesticide with the active ingredient Imidacloprid (200 g/Lt). In 2020, the highest seed filling rate was achieved after systemic Imidacloprid insecticide application with the Arborjet system. As a result of this application, the full seed rate reached 70.7% in Asagicuma, while this rate was 63.6% in the Karaveliler. The seed occupancy rate obtained from control trees in the Asagicuma was 37.96% and this rate reached 70.7% after systemic Imidacloprid application in the same field. Similarly, in the studies carried out in Asagicuma and Yukaribey experiment sites in 2021, only 35% of the seeds were filled in the cones taken from control trees, while the occupancy rate in the cones without insecticide application in the Yukaribey was determined to be 32.76%. In both trial sites, the highest seed fill rate was achieved after systemic Imidacloprid insecticide application with the Arborjet system. As a result of this application, the filled seed rate reached 67.89% in the Asagicuma and 69.86% in Yukaribey experiment sites.

**Key words:** *Leptoglossus occidentalis*, pine seeds, trunk injection, pesticides, Turkey.

### Introduction

Climate change is one of the most effective factors on forests. In recent years, with the impact of climate change, invasive species have been causing significant destruction in forests of Turkey and are turning into natural species day by day. *Leptoglossus occidentalis* Heidemann (1910) (Hemiptera: Coreidae), which was first detected in Turkey in 2009, stands out with its damage to stone pine trees and economic losses due to its effects on seeds. It is noteworthy that it also poses a significant threat to the forests of other coniferous species throughout Turkey.

Since stone pine seed is an edible species with high economic returns, its damage is considered mostly from its economic perspective. But there is

also a great danger for other forest tree seeds. Studies have shown that it also causes significant damage to the seeds of other species. In this respect, it is a pest that has a great potential to affect our forestry activities. As a result of the damage, problems such as rising stone pine nut prices and foreign market contractions in exports began to be encountered. If an effective and fast method of combating the pest cannot be introduced, significant negative consequences will occur, both in terms of economic losses and the natural forests in Turkey being affected by these damages.

The pest was first described by Heidemann in North America in 1910, and began to spread rapidly in central and eastern America after the 1950s. The insect, which was first seen in Italy in 1999, quickly spread to every part of the country and was also



found in Switzerland in 2005 [1,2]. Its spread after 2000 was very rapid, and in just ten years it colonized most of the continent, from Norway to Sicily, from Portugal to Turkey [3]. It was seen in Russia and Ukraine in 2012 [4]. The pest, which was first seen in our country in 2009, has attracted attention with its damage in a large part of our country in recent years, especially in coniferous forests. *Leptoglossus occidentalis* was found on *Pinus brutia*, *P. nigra*, *P. pinea*, *P. radiata*, *P. sylvestris*, *Abies nordmanniana* subsp. *bornmulleriana* and *A. concolor* in Turkey [5-11].

In the controlling of harmful insects, chemical control methods have not been a preferred method in recent years due to the damage they cause to the environment and their side effects. Instead, it is recommended to use biological and biotechnical control methods, which stand out as alternative methods. Chemical controlling is a method that requires the most care in its application in terms of the environment and human health. It appears as a method of control that can still be preferred today due to reasons such as seeing the results in a short time and preventing the high investment made in intensive cultures from being endangered, but it needs to be carried out with great care and should be carried out with selective pesticides that will not harm the nature.

Trunk injection is an alternative technique in chemical controlling of pest insects. The main advantages of trunk injection is providing a higher efficiency of product delivery, reduced risk for worker exposure, reduced risk to the environment, reduced harm to non-target organisms, and the possibility for use in populated areas where other methods are not an option [12-14].

In this study, systemic pesticides were applied by injection into the trunk in the trial areas taken in the stone pine fields of Bergama-Kozak region of Turkey. In this context, trials were carried out with products containing Azadirachtin and Imidacloprid actives.

### Materials and methods

Experimental areas were selected in the areas of stone pine with different elevation levels in the Bergama-Kozak region. The project studies were carried out in the trial areas (Figure 1) in the Karaveliler, Yukaribey and Asagicuma provinces, which are located at different altitudes where stone pine (*Pinus pinea*) is distributed in the Bergama region. In the experiment, 10 trees (Figure 2) were taken as a parcel, with the number of replications being 3.

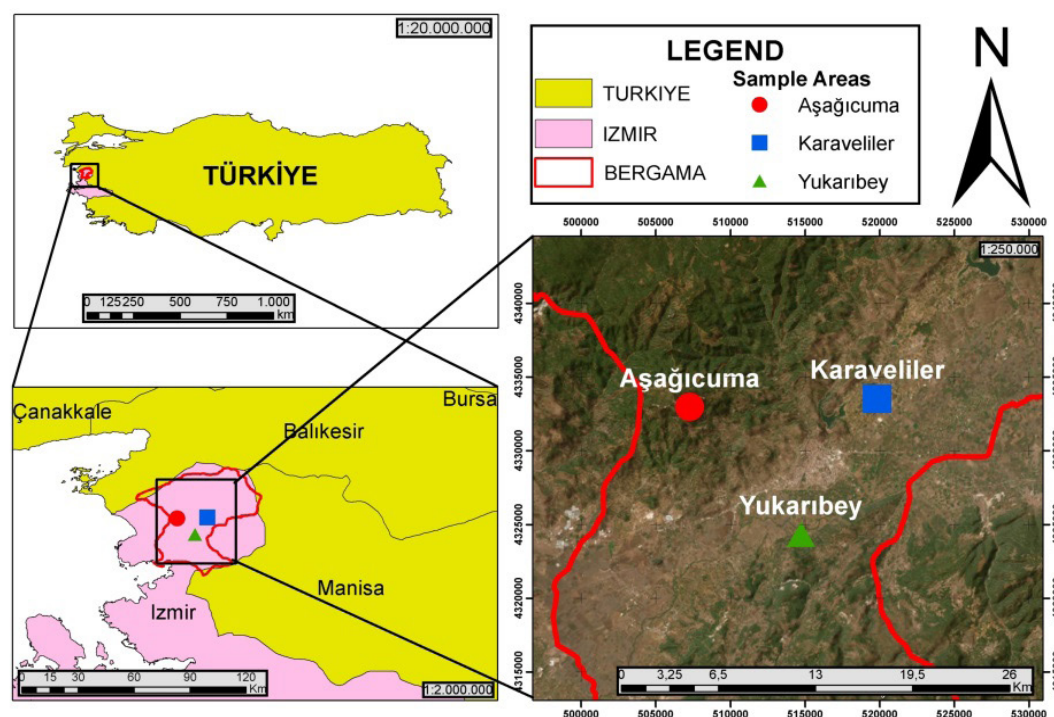


Figure 1 – Research area and experiment sites



**Figure 2** – Stone pine trees in research area

Chemical applications were carried out twice on the same trees in 2020 and 2021, in the first week of April and the second week of July when the first and second generation of *L. occidentalis* adults were occurred. Arborjet system was used in systemic spraying and application was carried out with the insecticide containing the active ingredient

Azadirachtin (0.3 g/Lt) as an organic pesticide, as well as the pesticides containing the active ingredient Imidacloprid (200 g/Lt). In systemic application, the injection method applied directly to the tree trunk was used. The main reason for this is that this method is seen as a more effective, environmentally friendly and safe systemic application than the systemic application method from the soil. Unlike spraying and applying pesticides through soil, Arborjet does not harm the person applying, other people in the environment, or non-target creatures, as the product is applied directly to the trunk of the tree.

In the systemic application with the Arborjet system, the pesticides were injected into the tree at the rate of 50 ml per tree. For this purpose, 6-10 arbor plugs per tree (Figure 3) were placed on the trees where the application would be made, after drilling the bark with a cordless drill, depending on the diameter and thickness of the tree. These plugs are used in different sizes, with a length of at least 15 mm and a width of at least 6 mm, and can be applied to all trees. Its special structure ensures fast and consistent release by holding the plug tightly to the tree, ensuring that the pressure is not lost during the injection process, and the special gasket inside prevents product leakage and “rebound” of the applied insecticide. In practice, a 1/1 solvent-insecticide mixture was injected into each plug as 5 ml (Figure 4). Solvent formulation is a mixture as Surfactant System – 31.20%, Organic Solvent 1- 24.40%, Organic Solvent 2- 24.40% and water 20.00%.



**Figure 3** – Plug settled in stem for injection



Figure 4 – Pesticide injection



Figure 5 – Separation of full and empty seeds

The cones were collected and the necessary counts were carried out in January of the year following the years of applications. Seeds obtained from trees that received systemic injection by injection in 2020 and 2021 were also subjected to residue analysis for both years.

### Results and discussion

In the studies carried out in Asagicuma and Karaveliler experiment sites in 2020; in the cones

taken from the control trees where no application was made, only 37.96% of the seeds were filled in Asagicuma experiment site, while the occupancy rate was determined as 48.44% in the cones without any insecticide application in the Karaveliler experiment site. In both sites, the highest seed filling rate was achieved after systemic Imidacloprid insecticide application with the Arborjet system. As a result of this application, the full seed rate reached 70.7% in Asagicuma, while this rate was 63.6% in the Karaveliler. The seed occupancy rate obtained from

control trees in the Asagicuma was 37.96% and this rate reached 70.7% after systemic Imidacloprid application in the same field (Table 1).

**Table 1** – Comparison of seed filled percentages in Asagicuma and Karaveliler experiment sites at the end of 2020

2020	Experiment Sites	
	Asagicuma	Karaveliler
Application / Active Ingredient	Seed occupancy (%)	
Azadirachtin	46.06%	43.8%
Imidacloprid	70.7%	63.6%
Control trees	37.96%	48.44%

In the studies carried out in Asagicuma and Yukaribey experiment sites in 2021, only 35% of the seeds were filled in the cones taken from control trees, while the occupancy rate in the cones without insecticide application in the Yukaribey was determined to be 32.76%. In both trial sites, the highest seed fill rate was achieved after systemic Imidacloprid insecticide application with the Arborjet system. As a result of this application, the filled seed rate reached 67.89% in the Asagicuma and 69.86% in Yukaribey (Table 2).

**Table 2** – Comparison of seed filled percentages in Asagicuma and Yukaribey experiment sites at the end of 2021

2021	Experiment Sites	
	Asagicuma	Yukaribey
Application / Active Ingredient	Seed occupancy (%)	
Azadirachtin	37.23%	42.29%
Imidacloprid	67.89%	69.86%
Control trees	35%	32.76%

“Residue Analysis” was also performed on the seeds collected in December 2021 from the trees to which imidacloprid was applied. According to the Residue Analysis Report, no Imidacloprid residue was found in the seeds. According to the control results of both years, the use of the insecticide containing the active ingredient Imidacloprid in systemic application by trunk injection gave the most successful results.

In previous studies regarding the chemical control of *Leptoglossus occidentalis*, it has been reported that there is no chemical preparation registered for the pine cone sucking insect so far. Mostly, there are recommendations for combating the insect in closed areas where it enters for wintering and is used by humans or pets.

Jacobs [15] states that the most effective insecticides against *Leptoglossus occidentalis* are broad-spectrum ones such as permethrin and pyrethroid-based ones such as deltamethrin, cyfluthrin, lambda-cyhalothrin, cypermethrin. Summers and Ruth [16] report that dimethoate and permethrin are successful against *L. occidentalis*, and diatom soil is successful under laboratory conditions, but they are ineffective under field conditions. Grossman et al. [17] state that a single systemic pesticide mixture of thiamethoxam with benzoate administered by injection in the USA reduced seed loss by 72%.

In a limited number of studies on the use of chemical insecticide against *Leptoglossus occidentalis*, results show that systemic application by injection is successful. In our study, we observed that the insecticide, especially with the active ingredient Imidacloprid, reached a significant success rate on trees where it was applied systemically.

## Conclusion

It is important and a priority to choose methods such as mechanical or biotechnical controlling methods, especially biological control, which does not harm to nature, instead of chemical applications against *Leptoglossus occidentalis*. In addition, systemic application by injection into trees, which has a higher success rate compared to others in our studies, is not considered easy to prefer in forest areas, both in terms of economy and labor force. However, our results reveal that it is possible to use systems such as arborjet instead of contact chemical spraying, and that systemic application through injection into the tree can be used as an alternative method in regions or seed stands that make their living entirely from stone pine nut production, as in the Bergama-Kozak region. Applying the insecticide directly to the tree by injection can eliminate the negative effects on the environment and other living things that the contact effect may cause. The most important concern is the possible negative effects on human health if the pesticide penetrated into the seed

leaves residue. Starting from this point, after the systemic applications of Imidacloprid, the most successful insecticide in our study, in the obtained seeds in April and August, residue analyzes were made in the following January, which is also the month of harvest, and no residue was found.

## Acknowledgments

This study was a part of Turkish Forestry General Directorate project. We express our sincere appreciation to Turkish Forestry General Directorate for their support of the project.

## References

1. Lesieur, V., Yart, A., Guilbon, S., Lorme, P., Auger-Rozenberg, M.A., Roques, A. (2014) The invasive *Leptoglossus* seed bug, a threat for commercial seed crops, but for conifer diversity? *Biological Invasions*, 16, 1833-1849.
2. Tescari, G. (2001) *Leptoglossus occidentalis*, coreidae neartino rinvenuto in Italia (Heteroptera, Coreidae). *Torymidae* native and introduced to the West Palearctic region: taxonomy, host specificity and distribution. *J Naturali, Lavori.*, 26, 3-5.
3. Fent M., Kment P. (2011) First record of the invasive western conifer seed bug *Leptoglossus occidentalis* Heteroptera: Coreidae) in Turkey. *North-West. J. Zool.*, 7, 72-80.
4. Gapon, D.A. (2012) First records of the western conifer seed bug *Leptoglossus occidentalis* Heid. (Heteroptera, Coreidae) from Russia and Ukraine, regularities in its distribution and possibilities of its range expansion in the Palearctic region. *Ent. Obzrenie.*, 91, 559-568.
5. Arslangundogdu, Z., Hizal, E. (2010) The western conifer seed bug, *Leptoglossus occidentalis* (Heidemann, 1910), recorded in Turkey (Heteroptera: Coreidae). *Zool. Middle East.*, 50, 138-139.
6. Dursun G. (2016) Investigation on determination of Heteroptera (Hemiptera) fauna of Balıkesir Urban Forest and Baun Çağış Campus area by hibernation traps. Master Thesis, Balıkesir University, Balıkesir.
7. Hizal E., Inan M. (2012) *Leptoglossus occidentalis* (Heidemann, 1910) is an invasive insect species. *BAROFD*, 14, 56-61.
8. Oguzoglu S., Avci M. (2018) Isparta ve Burdur İllerinde *Leptoglossus occidentalis* Heidemann, 1910 (Hemiptera: Coreidae)'e Ait Gözlemler ve Türkiye'deki Durumu. III. Türkiye Orman Entomolojisi ve Patolojisi Sempozyumu 10-12 May 2018, Artvin, pp. 13-14
9. Ozek T., Avci M. (2017) Cone pests of fir, pine and cedar forests in Isparta Forest Regional Directorate. *Turk J For.*, 18, 178-186.
10. Ozgen I., Dioli P., Celik V. (2017) New and interesting record of western conifer seed bug: *Leptoglossus occidentalis* (Heidemann, 1910) (Heteroptera: Coreidae) in Eastern Turkey. *J. Entomol. Zool. Stud.*, 5, 830-833.
11. Parlak S. (2017) An invasive species: *Leptoglossus occidentalis* (Heidemann) how does it affect forestry activities? *Kastamonu univ. orman fak. derg.*, 17, 531-542
12. Sánchez Zamora M.A., Fernández Escobar R. (2000) Injector-size and the time of application affects uptake of tree trunk-injected solutions. *Sci. Hortic.*, 84, 163-177.
13. Wise J.C., VanWoerkom A.H., Acimovic S.G., Sundin G.W., Cregg B.M., Vandervoort, C.V. (2014). Trunk injection: a discriminating delivering system for horticulture crop IPM. *Entomol. Ornithol. Herpetol. Cur. Res.*, 3, 1.
14. Archer L., Crane J.H., Albrecht U. (2022) Trunk injection as a tool to deliver plant protection materials – an overview of basic principles and practical considerations. *Hortic.*, 8, 552.
15. Jacobs S.B. (2013) Western conifer seed bug, *Leptoglossus occidentalis*. Penstate College of Agricultural Sciences, Department of Entomology, Entomological Notes.
16. Summers D., Ruth D.S. (1987) Effect of diatomaceous earth, malathion, dimethoate and permethrin on *Leptoglossus occidentalis* (Hemiptera: Coreidae): a pest of conifer seed. *JESBC*, 84, 33-38.
17. Grosman D.M., Upton W.W., McCook F.A., Billings R.F. (2001) Control of cone and seed insects with systemic injections in a southern pine seed orchard. In: Volney WJA, Spence JR, Lefebvre EM (eds.) *Proceedings of the North American Forest Insect Work Conference*. May 14-18, 2001, Edmonton, Alberta, Canada. Canadian Forest Service, p. 260.

### Information about authors:

Oguzhan Sarikaya (corresponding author) – Professor, Faculty of Forestry, Bursa Technical University, Yildirim, 16350, Bursa, Turkey, e-mail: oguzhan.sarikaya@btu.edu.tr

Salih Parlak – Associate Professor, Faculty of Forestry, Bursa Technical University, Yildirim, 16350, Bursa, Turkey, e-mail: salih.parlak@btu.edu.tr

Yafes Yildiz – Associate Professor, Faculty of Forestry, Bartın University, 74110, Bartın, Turkey, e-mail: yyildiz@bartin.edu.tr





Tutku Gencal – MsC, Faculty of Forestry, Bursa Technical University, Yildirim, 16350, Bursa, Turkey, e-mail: tutku.gencal@btu.edu.tr

I.Meltem Ozcankaya – PhD., Aegean Forestry Research Institute, Urla, 35430, Izmir, Turkey, e-mail: meltemozcankaya@ogm.gov.tr

Fazil Selek – PhD, Aegean Forestry Research Institute, Urla, 35430, Izmir, Turkey, e-mail: fazilselek@ogm.gov.tr

Ozden Acici – MsC., Bursa Regional Forestry Directorate, Osmangazi, 16250, Bursa, Turkey, e-mail: ozdenacici@ogm.gov.tr

Hacer Can – Bursa Regional Forestry Directorate, Osmangazi, 16250, Bursa, Turkey, e-mail: hacercan@ogm.gov.tr

N.A. Nursapina<sup>1,2</sup> , I.V. Matveyeva<sup>1,2\*</sup> ,  
Sh.N. Nazarkulova<sup>1,2</sup> , R. Jačimović<sup>3</sup> 

<sup>1</sup>al-Farabi Kazakh National University, Almaty, Kazakhstan

<sup>2</sup>Center of Physical-Chemical Methods of Research and Analysis, Almaty, Kazakhstan

<sup>3</sup>Department of Environmental Sciences, Jožef Stefan Institute, Ljubljana, Slovenia

\*e-mail: Iona.matveyeva@kaznu.kz

(Received 17 May 2024; received in revised form 22 May 2024; accepted 23 May 2024)

## Determination of impurities in fertilizers purchased in Almaty (Kazakhstan)

**Abstract.** Two solid (Double superphosphate and Phosphoric) and two liquid (Peat and Microfertilizer) fertilizers from Russia and Kazakhstan were evaluated with regard to macronutrients content (K, Ca), transition elements (Cr, Fe, Co, Zn, Hg), alkaline earth (Sr), semi-metals (As), rare earth elements (Ce, Eu, La, Nd, Sc, Sm, Tb, Yb) and Th and U. For analysis, the  $k_0$ -INAA was used. For QA/QC purposes for  $k_0$ -INAA the certified reference material BCR-320R channel sediment was used and irradiated together with the samples. The highest content of REEs was obtained in Double superphosphate, while in liquid fertilizers REEs were mostly below the limit of detection of the method used. Most elements in liquid organic fertilizers (Peat and Microfertilizer) were determined in insignificant level, except iron, which belongs to the essential micronutrients. The content of iron was at least 57 times higher in case of Peat fertilizer in comparison to Microfertilizer. Content of iron was higher in case of Phosphoric fertilizer than in Double superphosphate (about five times).

**Key words:** fertilizers, Kazakhstan, impurities, nutrients,  $k_0$ -INAA.

### Introduction

For modern society, sustainable agriculture plays essential role. Although techniques applied during the production of the target crop can have delayed consequences. One of the common techniques is the application of the different types of fertilizers. Due to the intensive cultivation, the fertility of soil decreased in many parts of the world. In order to sustain crop yields more fertilizers might be required, leading to the environmental concern [1].

Most of the fertilizers have complicated composition, which can content not only target elements-nutrients, but also contaminants, which is tending to accumulate in agricultural soils over the years, and have negative influence on the nature [2]. Radionuclides and rare earth elements (REEs) are common contaminants in fertilizers, especially in the case of P-containing mineral fertilizers [3-7]. Phosphorus-containing mineral fertilizers have high concentration of toxic elements, due to the rock phosphates, which are used as a raw material during their production [8]. The negative effect of continuous

application of mineral fertilizers was demonstrated in several studies [9-11]. For instance, the combined application of mineral and organic fertilizers leads to enhance of content of trace elements in maize [10], which is evident of accumulation of trace elements in soil and following transfer to crop. Have to be mentioned that one of the main sources of REEs pollution of the soil is P-containing mineral fertilizers. Soils, which were longingly fertilized by phosphate fertilizers, received high doses of REEs [12].

In addition, REEs contamination leads to reduction in soil macro and micro fauna diversity [13]. There is scarce information about different contaminants in mineral fertilizers, which may be purchased on the local markets of Kazakhstan, or produced in the country. In Kazakhstan, there is no regulation related to permissible concentration of toxic elements, such as As, Pb or Hg in mineral fertilizers. For instance, Technical regulations "Requirements for the safety of fertilizers" [14] provides only general information about regulation of mass fraction of biuret, the specific activity of phosphorus containing fertilizers and biological safety of organic and organo-mineral

fertilizers, without any specification of permissible concentration of contaminants. In addition, have to be mentioned, that there is no limitation in content of REEs in mineral fertilizers. Fertilizers, which are exported from Eurasian Economic Union countries regulates by technical regulations of the Eurasian Economic Union “Requirements for mineral fertilizers” [15], where provided general terms about radiation and chemical safety of fertilizers, without specification of limit of each toxic element, except copper in ammonium nitrate fertilizer.

It is evident that the applied fertilizers should be controlled systematically for content of toxic elements. At the same time, most of the commonly used fertilizers have complicated composition and it takes long time for the analysis of their composition. We focused on two solid and two liquid mineral fertilizers, which are available on the local market in Almaty (Kazakhstan). For determination of mass fractions of major, minor and trace elements, the  $k_0$ -instrumental neutron activation analysis ( $k_0$ -INAA) was used. The method is validated and widely used for simultaneous determination of major, minor and trace elements in various materials [16-18].

### Materials and methods

*Sample description.* In the presented work four different fertilizers were analyzed. Double superphosphate (20% of  $P_2O_5$ , 5% of N in Garden Retail Service, Russia) and Pphosphoric (20% of  $P_2O_5$ , 8% of N in Garden Retail Service, Russia) are solids; Peat (3% of  $P_2O_5$ , 3% of  $K_2O$ , 1% of N in AgroSnabRetail, Russia) and Microfertilizer (1% of N in Scientific production and technical center

“Zhalyn”, Kazakhstan) are liquid organic fertilizers. All samples are commonly used in agriculture and can be purchased in specialized shops of Kazakhstan. The samples of solid fertilizers were crushed in mortar and homogenized before the analysis.

*$k_0$ -INAA analysis.* For  $k_0$ -INAA an aliquot of fertilizer sample (varied from 190 mg to 240 mg) and a liquid sample (varied from 2.6 g to 2.9 g) was sealed into polyethylene ampoule. For determination of intermediate/median and long-lived radionuclides an aliquot and standard Al-0.1%Au (ERM-EB530A alloy) were stacked together, fixed in polyethylene vial and irradiated for 12 hours in the carousel facility of the TRIGA Mark II reactor (Ljubljana, Slovenia) with a thermal neutron flux of  $1.1 \times 10^{12} \text{ cm}^{-2} \text{ s}^{-1}$  [17].

After irradiation, the aliquot was measured after 4, 8 and 23 days cooling time on absolutely calibrated HPGe detectors (40 % and 45 % relative efficiency). For peak area evaluation, the HyperLab program was used [19]. The values  $f = 22.54$  (thermal to epithermal flux ratio) and  $\alpha = -0.0075$  (epithermal flux deviation from the ideal 1/E distribution) in the chosen irradiation channel of the carousel facility were used to calculate mass fractions. For mass fractions and effective solid angle calculations the software package Kayzero for Windows V3 [20] was applied, where the  $k_0$ -database from the year 2020 was used [21].

For QA/QC purposes for  $k_0$ -INAA the certified reference material BCR-320R channel sediment was used and irradiated together with the samples. The data obtained by  $k_0$ -INAA are evaluated using  $E_n$ -score as defined in ISO 13528 [22] and graphically presented on Figure 1 only for certified elements.

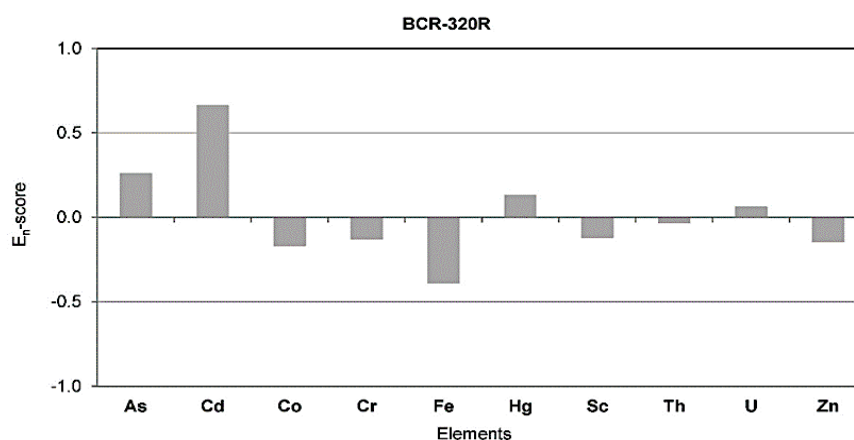


Figure 1 – Evaluation of  $k_0$ -INAA data by  $E_n$ -score for BCR-320R channel sediment

As can be seen from the Figure 1, calculated  $E_n$ -scores are within the following inequality  $E_n \leq 1.0$ , which indicate successful performance of the  $k_0$ -INAA method.

### Results and discussion

The mass fractions of elements obtained by  $k_0$ -INAA with combined standard are in Table 1, uncertainty for studied fertilizers is given in mg/kg.

The highest content of K and Ca, which belongs to the macronutrients, were obtained in Phosphoric mineral fertilizer. Comparing our data presented in the Table 1 with producers' data, it can be seen that, the content of K in Peat fertilizer is low than content provided by the producer. This finding can cause concern about the reliability of the information provided by the producer, which can lead to inappropriate fertilizer use by a farmer.

**Table 1** – The content of element obtained by  $k_0$ -INAA

El.	Double superphosphate/solid form <sup>a</sup>	Phosphoric/solid form <sup>a</sup>	Peat/liquid	Microfertilizer/liquid
K	1400 ± 80	82700 ± 2900	< 12 <sup>b</sup>	6.21 ± 0.33
Ca	184600 ± 6500	194500 ± 7000	85.8 ± 4.1	< 3.2 <sup>b</sup>
Ba	51.2 ± 3.9	91.9 ± 5.6	0.800 ± 0.044	< 0.078 <sup>b</sup>
Cs	0.356 ± 0.015	0.597 ± 0.022	0.00130 ± 0.00011	< 0.0005 <sup>b</sup>
Na	1524 ± 53	4273 ± 150	430 ± 15	2.73 ± 0.10
Rb	8.86 ± 0.37	23.0 ± 0.8	0.0301 ± 0.0056	< 0.017 <sup>b</sup>
Sr	1205 ± 43	866 ± 32	2.40 ± 0.12	< 0.20 <sup>b</sup>
Cr	12.9 ± 0.5	19.9 ± 0.7	0.0734 ± 0.0030	< 0.0046 <sup>b</sup>
Fe	2630 ± 100	12470 ± 440	22.6 ± 0.8	< 0.39 <sup>b</sup>
Co	1.00 ± 0.04	17.0 ± 0.6	0.00993 ± 0.00043	< 0.0007 <sup>b</sup>
Zn	24.4 ± 0.9	46.2 ± 1.7	0.428 ± 0.018	0.131 ± 0.007
Hg	< 0.23 <sup>b</sup>	< 0.07 <sup>b</sup>	< 0.0021 <sup>b</sup>	< 0.0013 <sup>b</sup>
As	1.57 ± 0.07	10.8 ± 0.4	0.0139 ± 0.0009	< 0.0008 <sup>b</sup>
Sb	0.172 ± 0.008	0.325 ± 0.013	0.00401 ± 0.00016	< 0.00011 <sup>b</sup>
Se	< 0.55 <sup>b</sup>	< 0.39 <sup>b</sup>	0.00380 ± 0.00054	< 0.0023 <sup>b</sup>
Ce	194 ± 7	43.1 ± 1.5	0.0301 ± 0.0013	< 0.002 <sup>b</sup>
Eu	4.72 ± 0.17	0.849 ± 0.036	0.000421 ± 0.000088	< 0.00003 <sup>b</sup>
La	112 ± 4	20.1 ± 0.7	0.0128 ± 0.0005	< 0.0002 <sup>b</sup>
Nd	85.1 ± 3.0	18.7 ± 0.9	< 0.0001 <sup>b</sup>	< 0.002 <sup>b</sup>
Sc	0.647 ± 0.023	2.43 ± 0.09	0.00514 ± 0.00018	< 0.00004 <sup>b</sup>
Sm	14.8 ± 0.5	4.00 ± 0.14	0.00254 ± 0.00009	< 0.00006 <sup>b</sup>
Tb	1.84 ± 0.06	0.533 ± 0.019	0.00037 ± 0.00004	< 0.00016 <sup>b</sup>
Yb	3.94 ± 0.14	1.44 ± 0.05	< 0.00067 <sup>b</sup>	< 0.00001 <sup>b</sup>
Th	8.76 ± 0.29	1.76 ± 0.06	0.00489 ± 0.00021	< 0.0003 <sup>b</sup>
U	8.37 ± 0.29	12.8 ± 0.5	0.00139 ± 0.00011	0.000899 ± 0.000047

a – mass fractions are given on air dry mass basis;

b – limit of detection (LD) of the method used calculated using equation



The highest content of K and Ca, which belongs to the macronutrients, were obtained in Phosphoric mineral fertilizer. Comparing our data presented in the Table 1 with producers' data, it can be seen that, the content of K in Peat fertilizer is low than content provided by the producer. This finding can cause concern about the reliability of the information provided by the producer, which can lead to inappropriate fertilizer use by a farmer.

$LD = 2.706 + 4.653 \sqrt{B}$ , where B is the background calculated in the gamma energy region where the peak in question is supposed to be present. It should be mentioned that KayWin software then calculates the mass fraction of an element taking the LD (net peak counts) as the input parameter in its basic equation of the  $k_0$ -method.

The highest concentration of Co, Cr, Zn and As among the investigated samples were determined in Phosphoric mineral fertilizer, meanwhile the lowest values were determined in liquid organic Microfertilizer. Due to lack of information about permissible concentration of toxic elements in fertilizer according to local regulations, there was no option for comparison of obtained values to standard. For all investigated samples, mercury was below the limit of detection of the used method.

Most elements in liquid organic fertilizers (Peat and Microfertilizer) were determined in insignificant level, except iron, which belongs to the essential micronutrients (see Table 1). The content of iron was at least 57 times higher in case of Peat fertilizer in comparison to Microfertilizer. Content of iron was higher in case of Phosphoric fertilizer than in Double superphosphate (about five times). Despite that fact that iron is essential components for plants, its high concentration may lead to decrease in P availability for plants due to the formation of iron-phosphate salts and it is therefore harmful to plants indirectly [8].

It should be mentioned that significant content of strontium in both solid fertilizers was determined. The content of strontium was 1.4 times higher for Double superphosphate in comparison to the Phosphoric fertilizer. Strontium can substitute calcium in biological system due to their chemical properties similarity, which can cause different illness of plant. For instance, strontium affected to photosynthesis, decreasing the level of chlorophyll in algae and higher plant, which can cause chlorosis [23].

Among the rare earth elements significant differences were determined for solid fertilizers. The content of Ce, Eu, La, Nd, Sm, Tb, Yb in Double superphosphate was 4.5, 5.6, 5.6, 4.5, 3.7, 3.5,

2.7 times higher in comparison to the Phosphoric fertilizer. Only content of Sc was 3.8 times higher in case of Phosphoric fertilizer. It is interesting to note that, both of phosphate containing fertilizers are produced by same producer, however as it can be seen from the results, there is significant difference in REEs content, which can be explained with the usage of different raw materials and different processing methods. The differences of REEs content in solid fertilizers might indicate the different origin of raw material used for production of fertilizers. In series of studies [12, 24, 25] are shown that apatite carbonate minerals are more enriched in REEs. In case of investigated Double superphosphate, raw material used for production could be apatite carbonate minerals. Among the liquid fertilizer, REEs was detected using  $k_0$ -INAA mostly in Peat sample, while in Microfertilizer sample their contents were below the limit of detection due to low induced activity of radionuclides by neutrons in the sample. In order to increase the sensitivity of the  $k_0$ -method for such kind of samples, the pre-concentration procedures should be applied before the sample irradiation or appropriate radiochemical procedures.

In comparison of two solid fertilizers, content of thorium was lower in case of Phosphoric fertilizer, nevertheless the content of uranium was vice versa, slightly lower in case of Double superphosphate. Based on our results presented in Table 1 it is evident that the producer used different processing methods and raw materials for production of phosphate containing fertilizers.

## Conclusion

The highest content of K and Ca, which belongs to the macronutrients, were obtained in Phosphoric mineral fertilizer. The highest concentration of Co, Cr, Zn and As among the investigated samples were determined in Phosphoric mineral fertilizer, meanwhile the lowest values were determined in liquid organic Microfertilizer. For all investigated samples, mercury was below the limit of detection of the used method.

Most elements in liquid organic fertilizers (Peat and Microfertilizer) were determined in insignificant level, except iron, which belongs to the essential micronutrients. The content of iron was at least 57 times higher in case of Peat fertilizer in comparison to Microfertilizer. Content of iron was higher in case of Phosphoric fertilizer than in Double superphosphate (about five times).

The present study explores that high concentration of iron was determined in Phosphoric fertilizer, despite that iron mostly nontoxic for plants, it can have hidden negative side effect, which leads to reduce the availability of P in plant [8]. Our study revealed another problem, there is no regulation on the content of REEs and toxic elements in mineral fertilizers in Kazakhstan and more specific research about their effect on plants. The addition of REEs and other metals due to regularly usage of phosphate containing mineral fertilizers might lead to potential risk for agriculture and environment sustainability. Future investigation of other different mineral fertilizers which are available on local market is necessary. In addition, risk assessment study is

needed for evaluation of impact of REEs to soil and plant.

### Acknowledgments

This work was supported by the Ministry of Education and Science of the Republic of Kazakhstan, grant number AP08052224. The Slovenian co-author would like to thank Slovenian Research Agency (ARRS) for financial support of programme P1-0143 and Metrology Institute of the Republic of Slovenia (MIRS) under contract No. C3212-10-000071 (6401-5/2009/27) for activities and obligations performed as a Designate Institute.

### References

1. Abbady, A.G.E., Uosif, M.A.M., Ei-Taher, A. (2005) Natural radioactivity and dose assessment for phosphate rocks from Wadi El-Mashash and El-Mahamid Mines, Egypt. *J Environ Radioact.* 84:65-78. <https://doi.org/10.1016/j.jenvrad.2005.04.003>
2. Ayoub, A.T. (1999) Fertilizers and the environment. *Nutr Cycl Agroecosys.* 55:117-121.
3. Burger, A., Lichtscheidl, I. (2019) Strontium in the environment: Review about reactions of plants towards stable and radioactive strontium isotopes. *Sci Total Environ.* 653:1458-1512. <https://doi.org/10.1016/j.scitotenv.2018.10.312>
4. Chauhan, P., Chauhan, R.P., Gupta, M. (2013) Estimation of naturally occurring radionuclides in fertilizers using gamma spectrometry and elemental analysis by XRF and XRD techniques. *Microchem J.* 106:73-78. <https://doi.org/10.1016/j.microc.2012.05.007>
5. De Corte, F., van Sluijs, R., Simonits, A., Kučera, J., Smodiš, B., Byrne, A.R., De Wispelaere, A., Bossus, D., Frána, J., Horák, Z., Jaćimović, R. (2001) The validation of Kayzero-assisted NAA in Budapest, Rež, and Ljubljana via the analysis of three BCR certified reference materials, Fresenius. *J Anal Chem.* 370:38-41. <https://doi.org/10.1007/s002160100765>
6. Dissanayake, C.B., Chandrajith, R. (2009) Phosphate mineral fertilizers, trace metals and human health. *J Natn Sci Foundation Sri Lanka.* 37:153-165
7. HyperLab 2014, Quick Start Guide for Main Module, HyperLabs Software, Budapest, Hungary (2014). [http://www.hlabsoft.com/web/hl2014/docs/MainModule\\_QuickStartGuide.pdf](http://www.hlabsoft.com/web/hl2014/docs/MainModule_QuickStartGuide.pdf)
8. ISO 13528:2015, Statistical methods for use in proficiency testing by interlaboratory comparisons, 2nd ed. 2015-08-01, issued by ISO-Geneva (CH), International Organization for Standardization. <https://www.iso.org/standard/56125.html>
9. Jaćimović, R., De Corte, F., Kennedy, G., Vermaercke, P., Revay, Z. (2014) The 2012 recommended  $k_0$  database. *J Radioanal Nucl Chem.* 300:589-592. <https://doi.org/10.1007/s10967-014-3085-2>
10. Jaćimović, R., Matveyeva, I.V., Nursapina, N.A., Shynybek, B.A., Nazarkulova, Sh.N., Ponomarenko, O.I. (2020), Assessment of minor and trace elements in mineral fertilizers purchased in Almaty city, Kazakhstan, using  $k_0$ -INAA. *Int J Biol Chem.* 13:130-140. <https://doi.org/10.26577/ijbch.2020.v13.i2.15>
11. Jaćimović, R., Smodiš, B., Bučar, T., Stegnar, P. (2003)  $k_0$ -NAA quality assessment by analysis of different certified reference materials using the KAYZERO/SOLCOI software. *J Radioanal Nucl Chem.* 257:659-663. <https://doi.org/10.1023/a:1026116916580>
12. [http://www.kayzero.com/k0naa/k0naaorg/Nuclear\\_Data\\_SC/Nuclear\\_Data\\_SC.html](http://www.kayzero.com/k0naa/k0naaorg/Nuclear_Data_SC/Nuclear_Data_SC.html)
13. Kassir, L.N., Darwish, T., Shaban, A., Olivier, G., Ouaini, N. (2012) Mobility and bioavailability of selected trace elements in Mediterranean red soil amended with phosphate fertilizers: Experimental study. *Geoderma.* 189: 357-368.
14. Kayzero for Windows (KayWin<sup>®</sup>), User's Manual, for reactor neutron activation analysis (NAA) using the  $k_0$ -standardization method, Version 3.30 (2017).
15. Kratz, S., Schick, J., Schnug, E. (2016) Trace elements in rock phosphates and P containing mineral and organo-mineral fertilizers sold in Germany. *Sci Total Environ.* 542:1013-1019. <https://doi.org/10.1016/j.scitotenv.2015.08.046>
16. Mar, S.S., Okazaki, M. (2012) Investigation of Cd contents in several phosphate rocks used for the production of fertilizer. *Microchem J.* 104:17-21.
17. Morvedt, J.J. (2005) Heavy metals in fertilizers: their effects on soil and plant health. Proceedings No 575. The International Fertilizer Society, York, UK.
18. Nursapina, N.A., Shynybek, B.A., Matveyeva, I.V., Nazarkulova, Sh.N., Štrok, M., Benedik, L., Ponomarenko, O.I. (2022) Effect of mineral fertilisers application on the transfer of natural radionuclides from soil to radish (*Raphanus sativus* L.). *J Environ Radioact.* 247:106863. <https://doi.org/10.1016/j.jenvrad.2022.106863>
19. Otero, N., Vitória, L., Soler, A., Canals, A. (2005) Fertiliser characterisation: major, trace and rare earth elements. *Appl. Geochem.* 20:1473-1488. <https://doi.org/10.1016/j.apgeochem.2005.04.002>

20. Ramos, S.J., Dinali, G.S., Carvalho, T.S., Chaves, L.C., Siqueira, J.O., Guilherme, L.R.G. (2016) Rare earth elements in raw materials and products of the phosphate fertilizer industry in South America: content, signature and crystalline phases. *J Geochem Explor.* 168:177-186. <https://doi.org/10.1016/j.gexplo.2016.06.009>
21. Rim, K.T., Koo, K.H., Park, J.S. (2013) Toxicological evaluations of rare earths and their health impacts to workers: a literature review. *Saf. Health Work.* 4:12-26. <https://doi.org/10.5491/SHAW.2013.4.1.12>
22. Silva, F.B.V., Nascimento, C.W.A., Alvarez, A.M., Araújo, P.R.M. (2019) Inputs of rare earth elements in Brazilian agricultural soils via P-containing fertilizers and soil correctives. *J Environ Manag.* 232:90-96. <https://doi.org/10.1016/j.jenvman.2018.11.031>
23. Technical regulations «Requirements for the safety of fertilizers» Order of the Minister of Agriculture of the Republic of Kazakhstan No.143 dated April 29, 2020. <https://adilet.zan.kz/rus/docs/V2000020547>
24. Technical Regulations of the Eurasian Economic Union “On requirements for mineral fertilizers”. [https://docs.eaeunion.org/docs/ru-ru/01413088/encd\\_28022017\\_150](https://docs.eaeunion.org/docs/ru-ru/01413088/encd_28022017_150).
25. Wajid, K., Ahmad, K., Khan, Z.I., Nadeem, M., Bashir, H., Chen, F., Ugulu, I. (2020) Effect of Organic Manure and Mineral Fertilizers on Bioaccumulation and Translocation of Trace Metals in Maize. *Bull Environ Contam Toxicol.* 104:649-657. <https://doi.org/10.1007/s00128-020-02841-w>

**Information about authors:**

Nursapina Nurgul Armarkyzy – PhD student, al-Farabi Kazakh National University (Almaty, 050040, Kazakhstan, e-mail: [nurgulya13@mail.ru](mailto:nurgulya13@mail.ru))

Matveeva Ilona Valerievna (corresponding author) – PhD, Associate Professor, al-Farabi Kazakh National University, (Almaty, 050040, Kazakhstan, e-mail: [ilona.matveyeva@kaznu.kz](mailto:ilona.matveyeva@kaznu.kz))

Nazarkulova Sholpan Nurlanovna – PhD, Senior Lecturer, al-Farabi Kazakh National University (Almaty, 050040, Kazakhstan, e-mail: [sholpan.nazarkulova@kaznu.kz](mailto:sholpan.nazarkulova@kaznu.kz))

Radojko Jačimovič – Senior Researcher, Jožef Stefan Institute (Ljubljana, 1000, Slovenia, e-mail: [radojko.jacimovic@ijs.si](mailto:radojko.jacimovic@ijs.si))

S. Kashif<sup>1\*</sup> , S. Feroz<sup>2</sup> , A.A. Sethi<sup>1</sup> <sup>1</sup>NED University of Engineering & Technology, Karachi, Pakistan<sup>2</sup>Biological and Biomedical Sciences, Medical College, Aga Khan University, Karachi, Pakistan

\*e-mail: ssoomro@neduet.edu.pk

(Received 23 May 2024; received in revised form 30 May 2024; accepted 1 June 2024)

## Targeting beta-amyloid plaques and neurofibrillary tangles: a proteomic approach towards Alzheimer's disease therapy

**Abstract.** Alzheimer's disease (AD) stands as the most prevalent form of dementia affecting elderly individuals and ranks as the sixth leading cause of death globally. The pathological hallmarks of AD involve the formation of beta-amyloid plaques and neurofibrillary tangles in the brains of affected individuals, contributing to progressive brain degradation. This study aimed to utilize molecular modeling methods as a theoretical approach to explore the inhibition of beta-amyloid plaques and neurofibrillary tangles. Beta-amyloid and tau receptors were employed to carry out molecular docking with the ligands, including curcumin, memantine, nicotine, and caffeine. The selected compounds demonstrated minimum binding affinity and interactions with the active sites of the receptors while docking studies were performed. Notably, molecular interactions of the receptor complexes with curcumin compounds exhibited prominence in number. Curcumin, known for its antioxidant, anti-inflammatory, and lipophilic properties, has shown promise in enhancing cognitive function in AD patients. The findings of this study highlight the potential for further research aimed at developing improved drugs based on curcumin for the treatment of AD.

**Key words:** Alzheimer's, Dementia, Virulence Factor, Active Site, Docking, Binding affinity.

### Introduction

Neurological diseases, characterized by disruptions in regular electrical impulses within the brain or nervous system, pose significant challenges to global health. Among these, Alzheimer's disease (AD) represents a significant and growing public health concern worldwide, particularly among the aging population [1]. As the most common form of dementia, AD poses substantial challenges to both affected individuals and healthcare systems, significantly impacting quality of life and imposing a significant socioeconomic burden [2]. AD is a degenerative condition involving a myriad of symptoms, including motor dysfunction, sensory impairment, cognitive decline, and memory loss. Alongside memory deficits, individuals may struggle with language difficulties, including trouble finding words, following conversations, or understanding written text [3].

One of the defining pathological features of AD is the presence of aberrant protein aggregates in the brain, notably beta-amyloid plaques and neurofibrillary tangles [4]. Beta-amyloid plaques consist of extracellular deposits of amyloid-beta

peptides, while neurofibrillary tangles comprise intracellular accumulations of hyperphosphorylated tau protein. These proteinaceous aggregates disrupt neuronal function, leading to synaptic dysfunction, neuronal loss, and ultimately, cognitive decline characteristic of AD [5, 6]. These pathological hallmarks, along with genetic predispositions, underscore the intricate interplay between genetic and environmental factors in AD etiology [7].

Various hypotheses have been proposed to elucidate the etiology of AD, including the cholinergic, amyloid, and tau theories. The cholinergic theory implicates reduced acetylcholine synthesis in neuronal degeneration, while the amyloid theory posits extracellular beta-amyloid accumulation as a primary instigator of the disease process [8, 9]. Conversely, the tau hypothesis suggests that abnormalities in tau protein initiate neurofibrillary tangle formation, leading to neuronal collapse [10]. Despite extensive research, current treatments for AD are limited to symptomatic management with cholinesterase inhibitors, including tacrine, donepezil, rivastigmine, and galantamine. However, these treatments fail to address the underlying pathology, highlighting the urgent need for novel therapeutic interventions [11].

Given the central role of beta-amyloid plaques and neurofibrillary tangles in AD pathogenesis, targeting these pathological structures represents a promising therapeutic strategy [12, 13]. Molecular modeling methods offer a powerful tool for elucidating the molecular mechanisms underlying disease progression and identifying potential therapeutic interventions. They play a crucial role in drug discovery and development for Alzheimer's disease (AD) [14, 15]. By employing computational techniques, researchers can predict the interactions between target proteins, such as beta-amyloid peptides, tau protein, cholinesterases, and others, and small molecule ligands (potential drugs), facilitating the rational design of novel therapeutics.

The primary aim of this study is to investigate potential therapeutic strategies for Alzheimer's disease (AD) by utilizing molecular modeling methods to target and inhibit beta-amyloid plaques and neurofibrillary tangles, the two abnormal structures implicated in AD pathogenesis.

## Materials and methods

In this study, various tools and software were employed to analyze protein structures and assess binding energy properties with active compounds. The Tools and Software employed in this Molecular Docking Analysis are presented on Figure 1.

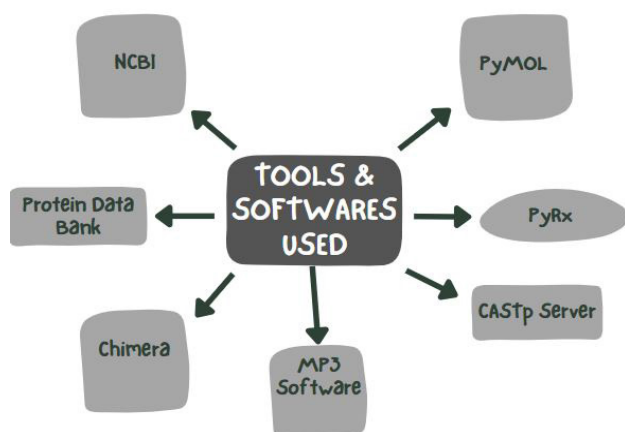


**Figure 1** – Schematic representation of tools and software utilized in molecular docking analysis

**1. Target identification and retrieval.** The study focused on molecular docking analyses of four active compounds against the tau protein (PDB: 2MZ7) and beta-amyloid protein (PDB: 1IYT), both implicated in Alzheimer's disease. Both protein sequences were retrieved from The National Center

for Biotechnology Information (NCBI) [16], and the corresponding 3D structures were obtained from the Protein Data Bank (PDB) [17].

**2. Choice of ligands.** caffeine [18], Curcumin [19], Nicotine [20], and Memantine [21] were selected as ligands based on previous research indicating their potential efficacy against Alzheimer's disease. These ligands were retrieved from NCBI and converted from SDF to PDB format using the Online Smiles Converter.

**3. Virulence prediction.** MP3 software [22] is used for the prediction of virulent and non-virulent protein properties. In this study, Virulence factor analysis was conducted using MP3 software that predicted the pathogenicity of proteins associated with Alzheimer's disease.

**4. Active site analysis.** The CASTp Server [23] was utilized for predicting the active sites of the tau protein and beta-amyloid. This online tool identifies and measures pockets and voids within 3D protein structures, providing annotated functional information on specific residues.

**5. Chimera visualization.** Visualization of the beta-amyloid and tau proteins was performed using UCSF Chimera software [24], enabling interactive visualization and analysis of molecular structures.

**6. Molecular docking analysis.** Molecular docking was performed using AutoDock Vina software [25] to predict binding modes of protein-ligand complexes. The ligand's rotational bonds were treated as flexible, while those of the protein were kept rigid. Grid boxes were positioned around the active site of the protein to guide the docking process. The resulting poses were ranked based on affinity scores in kcal/mol. PyRx software [26] was utilized for predicting the binding energy of ligands when interacting with receptors.

**7. Visualization of docking results.** PyMOL software [27] was utilized for visualizing the protein-ligand complexes, generating high-quality 3D images for further analysis. This aided in understanding the active site, binding modes, and interactions between the tau protein and beta-amyloid targets with the ligand molecules.

## Results and discussion

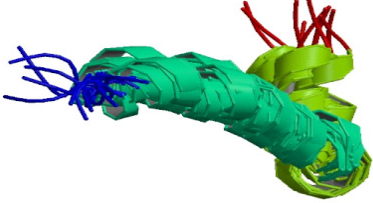
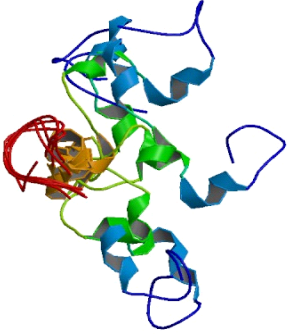
### 1. Virulence factor analysis of Alzheimer's protein

Predicting virulence factors is essential for the understanding of infectious diseases, identifying targets for therapeutic intervention, improving diagnostics, assessing disease risk, and elucidating

host-pathogen interactions. The virulence factor was analyzed using MP3 software. The virulence factor prediction indicated the number of pathogenic and non-pathogenic sequences identified for each protein

as shown in Table 1. The beta-amyloid protein (PDB code: 1YIT) exhibited 1 non-pathogenic sequence, while the tau protein (PDB code: 2MZ7) displayed 1 pathogenic sequence.

**Table 1** – Virulence factor analysis of Alzheimer's protein

Protein	Gene PDB Code	Structure Protein Model	MP3 RESULTS
Beta-Amyloid	1YIT		Total Sequences in File: 1 Total Pathogenic sequences: 0 Total Non-Pathogenic sequences: 1
Tau Protein	2MZ7		Total Sequences in File: 1 Total Pathogenic sequences: 1 Total Non-Pathogenic sequences: 0

## 2. Active Site Analysis

Predicting the active site of a protein is essential in drug discovery and design processes as it provides crucial insights into the molecular interactions between potential drug candidates and their target proteins. Next, active sites of beta-amyloid and tau protein were identified by using CASTp server. The results obtained from the CASTp server provided valuable structural insights. CASTp identified and characterized the locations and properties of binding sites or pockets on the surface of beta-amyloid and tau proteins. It also calculated the surface area and volume of the identified binding sites. It identified several active pockets within the beta-amyloid protein. Notable active pockets included residues DA, RH, I, D, V, K, II, and M as shown on Figure 2.

For the Tau protein, CASTp revealed active pockets including residues QP, NK, D, Q, K, VQSK, GSK, G, K, V, Q, and IP as shown in Figure 3. In

addition, the number, area, and circumference of the mouth openings for each pocket were also measured.

All measurements were given in two values, one for the solvent-accessible surface (SA) and one for the molecular surface (MS).

## 3. Visualization using Chimera

The interactive visualizations of the beta-amyloid and tau proteins generated through UCSF Chimera software are shown in Figures 4a & 4b. This visualization helped in analyzing the intricate three-dimensional structures of beta-amyloid and tau proteins, allowing for the identification of key features such as active sites, structural motifs, and binding pockets.

## 4. Selection of ligands for molecular docking

Following four FDA-approved ligands were selected to determine and compare their binding efficacy with beta-amyloid and tau protein. The selected ligands are shown in Table 2.

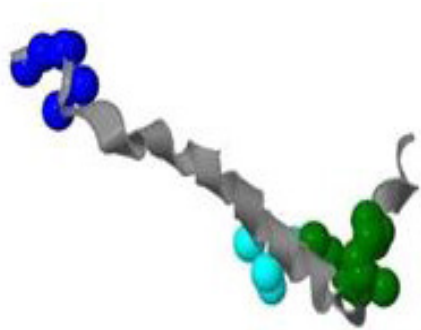


**Figure 2** – Visual Representation of Beta-amyloid generated through CASTp Server. Blue spheres show DA and RH active pockets of Amino Acid residue. Cyan spheres show I, and D active pockets of amino acid residue. Green spheres show V, K, II, and M active pockets of amino acid residue.

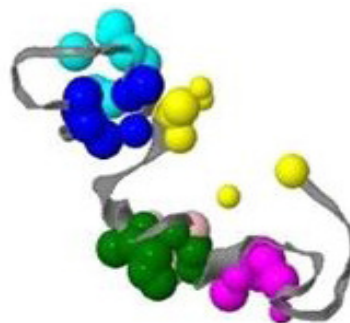
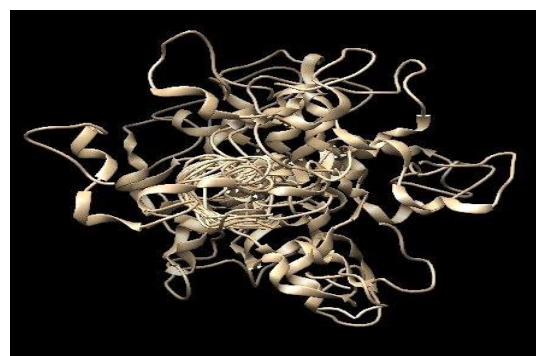


**Figure 3** – Visual Representation of Tau protein generated through CASTp Server. Blue spheres show QP, NK, and D active pockets of amino acid residue. Cyan spheres show Q and K active pockets of Amino Acid residue. Green spheres show VQSK and GSK active pockets of amino acid residue. Purple spheres show G, K, V, and Q active pockets of amino acid residue. Yellow spheres show I P active pockets of amino acid residue.



A



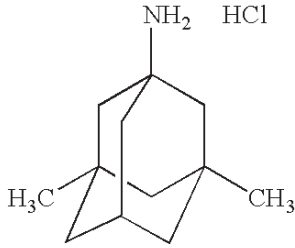
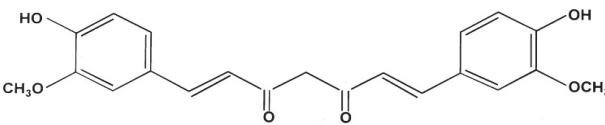
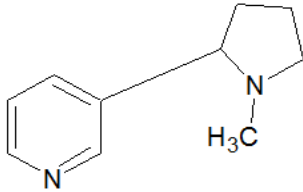
B

**Figure 4** – Visualization of Beta-amyloid chimera (A), Tau protein chimera (B)

**Table 2** – Name, Pubchem ID, and structure of selected Ligands

S.No	PubChem ID	Name of compound	Molecular weight (g/mol)	Structure
1	2519	Caffeine	194.1906	

Table continuation

S.No	PubChem ID	Name of compound	Molecular weight (g/mol)	Structure
2	181458	Memantine	215.765	
3	89594	Nicotine	162.23156	 <p style="text-align: center;"><b>CURCUMIN</b></p>
4	969516	Curcumin	368.3799	

### 5. Molecular Docking of Beta-amyloid and Tau protein

The molecular docking results of Beta Amyloid indicate that Caffeine exhibited a binding affinity of -4.3 kcal/mol, However, Memantine and nicotine

displayed -4.8 and -4.1 kcal/mol, and Curcumin demonstrated the highest binding affinity of -5.7 kcal/mol as shown in Table 3. This binding energy makes it the most suitable candidate. Results of Beta-Amyloid Ligand Docking Analysis are shown in Table 3.

**Table 3** – Results of Beta-Amyloid Ligand Docking Analysis

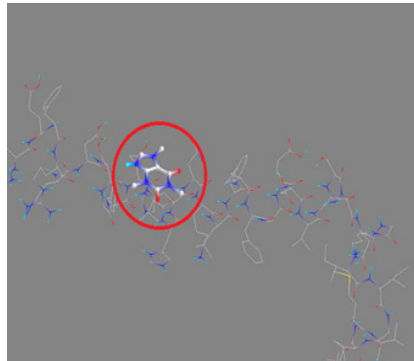
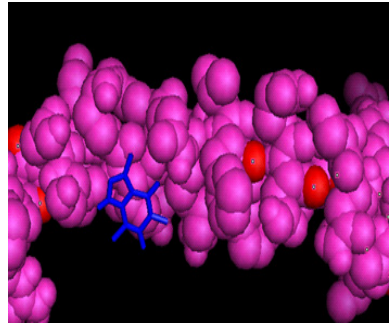
Ligand	PyRx Visualization	Binding Affinity	PyMol Visualization
Caffeine		-4.3 Kcal/Mol	



Table continuation

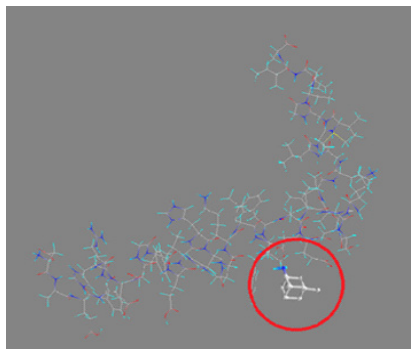
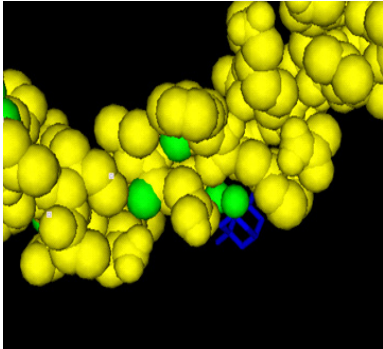
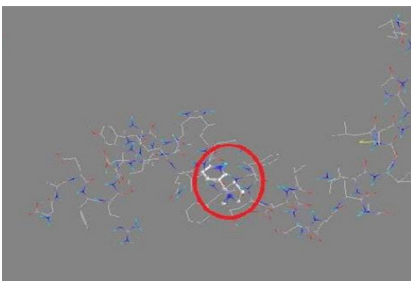
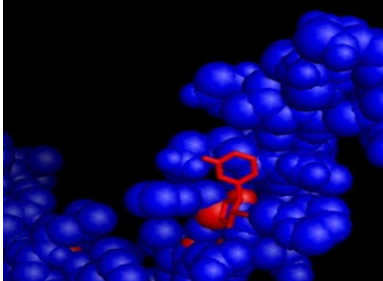
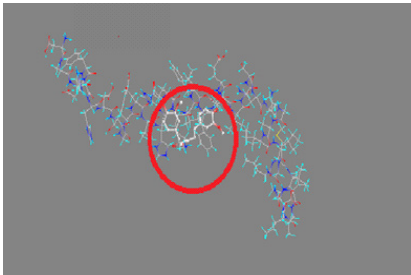
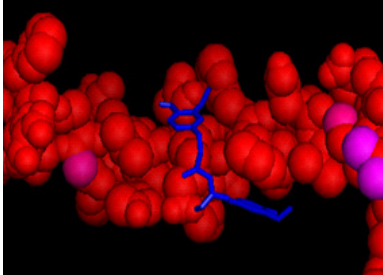
Ligand	PyRx Visualization	Binding Affinity	PyMol Visualization
Memantine		-4.8 Kcal/Mol	
Nicotine		-4.1 Kcal/Mol	
Curcumin		-5.7 Kcal/Mol	

Table 4 shows the Results of Tau Proteins Ligand Docking Analysis. It was analyzed that Caffeine exhibited a binding affinity of -5.1 kcal/

mol, Memantine showed -5.6 kcal/mol, Nicotine displayed -5.0 kcal/mol, and Curcumin demonstrated the highest binding affinity of -5.8 kcal/mol.

**Table 4** – Results of Tau Proteins Ligand Docking Analysis

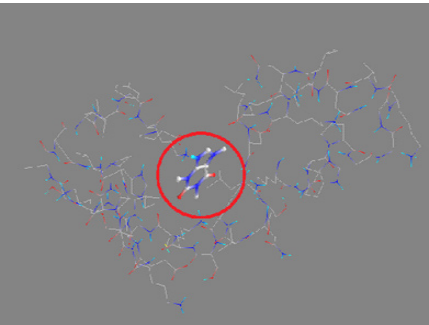
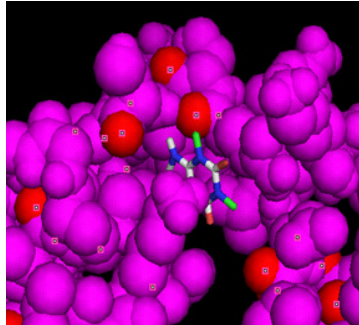
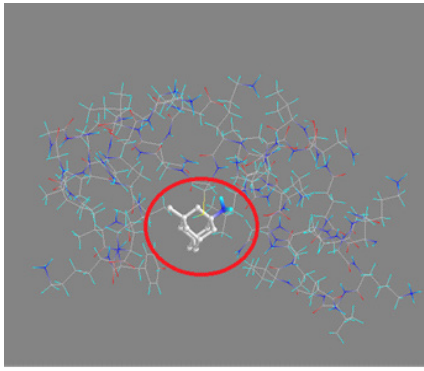
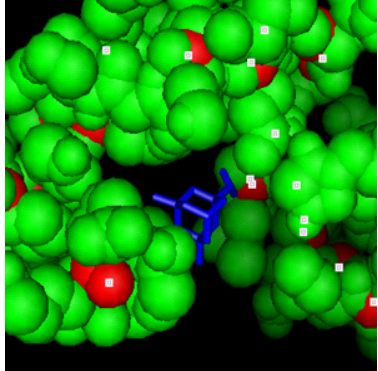
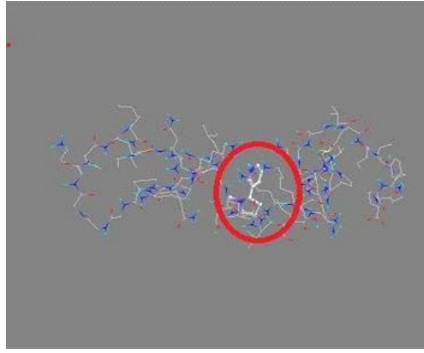
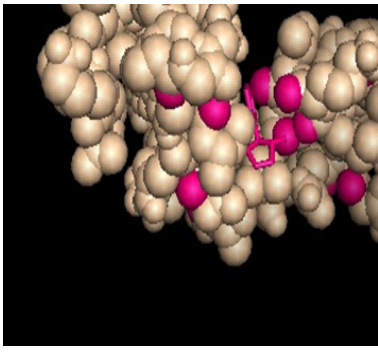
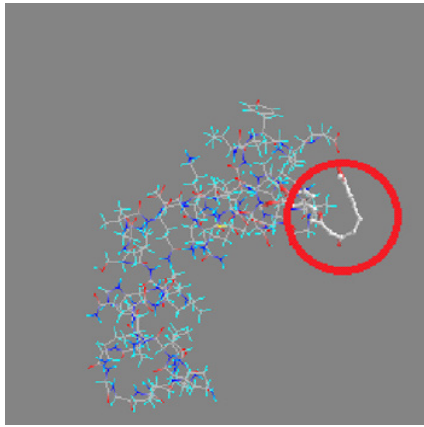
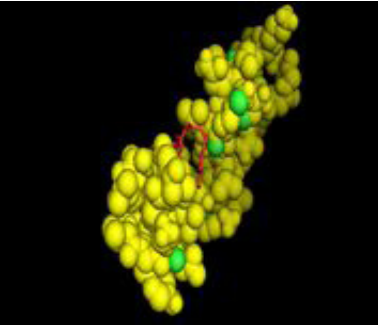
Ligand	PyRx Visualization	Binding Affinity	PyMol Visualization
Caffeine		-5.1 Kcal/Mol	

Table continuation

Ligand	PyRx Visualization	Binding Affinity	PyMol Visualization
Mamantine		-5.6 Kcal/Mol	
Nicotine		-5.0 Kcal/Mol	
Curcumin		-5.8 Kcal/Mol	

The findings of this study provide valuable insights into potential therapeutic strategies for Alzheimer's disease (AD) targeting beta-amyloid and tau proteins. Through molecular docking analysis, the binding affinities of four active compounds, including Caffeine, Curcumin, Memantine, and Nicotine, were evaluated against beta-amyloid and tau proteins.

The molecular docking results revealed varying degrees of binding affinities among the tested ligands. Curcumin exhibited the highest binding affinity to both beta-amyloid and tau

proteins, with binding energies of -5.7 kcal/mol and -5.8 kcal/mol, respectively. The ability of Curcumin to bind effectively to these proteins may impede their aggregation and potentially mitigate neurodegenerative processes associated with AD. Different molecular docking studies have also indicated the potential therapeutic benefits of curcumin and its derivatives for Alzheimer's disease (AD) (20 – 22). This suggests that Curcumin may possess strong inhibitory effects against the aggregation of beta-amyloid and tau proteins, which are characteristic features of AD pathogenesis.

Additionally, Memantine demonstrated notable binding affinity to beta-amyloid protein with a binding energy of -4.8 kcal/mol, suggesting its potential as a therapeutic agent for targeting beta-amyloid aggregation in AD. Some molecular docking studies also provided valuable insights into the therapeutic potential of memantine (23, 24).

Nicotine and Caffeine displayed moderate binding affinities to beta-amyloid protein, indicating their potential as adjunctive therapeutic agents in AD management. While their exact mechanisms of action in AD pathogenesis remain to be elucidated, their ability to interact with beta-amyloid protein suggests potential neuroprotective effects.

The visualization of protein-ligand complexes using PyRx and PyMOL software provided valuable insights into the binding modes and interactions between ligands and target proteins. These visualizations aided in understanding the structural basis of ligand-protein interactions and facilitated the identification of key binding sites and residues involved in ligand binding. Overall, our study underscores the importance of interdisciplinary approaches in drug discovery and highlights the potential of computational techniques in accelerating the development of effective treatments for Alzheimer's disease. These findings contribute to the growing body of research aimed at understanding the molecular mechanisms underlying AD pathogenesis and identifying novel therapeutic targets.

## Conclusion

In conclusion, this study highlights the potential of natural compounds such as Curcumin, Memantine, Nicotine, and Caffeine as therapeutic agents for AD by targeting beta-amyloid and tau proteins. The high binding affinity of Curcumin to both proteins suggests its promise as a multifaceted therapeutic agent capable of inhibiting beta-amyloid and tau aggregation, thereby potentially slowing the progression of AD. These findings suggest its potential therapeutic efficacy in preventing the formation of neurofibrillary tangles associated with Alzheimer's disease. The results of this study highlight the need for the exploration of natural compounds as novel treatments for AD and underscore the importance of further research to validate their efficacy and safety profiles in clinical settings. Further experimental validation of the computational predictions presented in this study is warranted to confirm the efficacy of the identified compounds in mitigating AD-associated pathology.

## Acknowledgments

The authors acknowledge support from the Department of Biomedical Engineering, NED University of Engineering and Technology for providing us with the platform to accomplish our work.

## References

1. Suresh, S., Singh S, A., Rushendran, R., Vellapandian, C., & Prajapati, B. (2023). Alzheimer's disease: the role of extrinsic factors in its development, an investigation of the environmental enigma. *Frontiers in neurology*, 14, 1303111. <https://doi.org/10.3389/fneur.2023.1303111>
2. Ding, C., Wu, Y., Chen, X., Chen, Y., Wu, Z., Lin, Z., Kang, D., Fang, W., & Chen, F. (2022). Global, regional, and national burden and attributable risk factors of neurological disorders: The Global Burden of Disease study 1990-2019. *Frontiers in public health*, 10, 952161. <https://doi.org/10.3389/fpubh.2022.952161>
3. Breijyeh, Z., & Karaman, R. (2020). Comprehensive Review on Alzheimer's Disease: Causes and Treatment. *Molecules* (Basel, Switzerland), 25(24), 5789. <https://doi.org/10.3390/molecules25245789>
4. Abubakar, M. B., Sanusi, K. O., Ugusman, A., Mohamed, W., Kamal, H., Ibrahim, N. H., Khoo, C. S., & Kumar, J. (2022). Alzheimer's Disease: An Update and Insights Into Pathophysiology. *Frontiers in aging neuroscience*, 14, 742408. <https://doi.org/10.3389/fnagi.2022.742408>
5. Serrano-Pozo, A., Frosch, M. P., Masliah, E., & Hyman, B. T. (2011). Neuropathological alterations in Alzheimer disease. *Cold Spring Harbor perspectives in medicine*, 1(1), a006189. <https://doi.org/10.1101/cshperspect.a006189>
6. Jankovska, N., Olejar, T., & Matej, R. (2020). Extracellular Amyloid Deposits in Alzheimer's and Creutzfeldt-Jakob Disease: Similar Behavior of Different Proteins?. *International journal of molecular sciences*, 22(1), 7. <https://doi.org/10.3390/ijms22010007>
7. Boyd, R. J., Avramopoulos, D., Jantzie, L. L., & McCallion, A. S. (2022). Neuroinflammation represents a common theme amongst genetic and environmental risk factors for Alzheimer and Parkinson diseases. *Journal of neuroinflammation*, 19(1), 223. <https://doi.org/10.1186/s12974-022-02584-x>
8. Chen, Z. R., Huang, J. B., Yang, S. L., & Hong, F. F. (2022). Role of Cholinergic Signaling in Alzheimer's Disease. *Molecules* (Basel, Switzerland), 27(6), 1816. <https://doi.org/10.3390/molecules27061816>
9. Ma, C., Hong, F., & Yang, S. (2022). Amyloidosis in Alzheimer's Disease: Pathogeny, Etiology, and Related Therapeutic Directions. *Molecules* (Basel, Switzerland), 27(4), 1210. <https://doi.org/10.3390/molecules27041210>

10. Arnsten, A. F. T., Datta, D., Del Tredici, K., & Braak, H. (2021). Hypothesis: Tau pathology is an initiating factor in sporadic Alzheimer's disease. *Alzheimer's & dementia : the journal of the Alzheimer's Association*, 17(1), 115–124. <https://doi.org/10.1002/alz.12192>
11. Alhazmi, H. A., & Albratty, M. (2022). An update on the novel and approved drugs for Alzheimer disease. *Saudi pharmaceutical journal : SPJ : the official publication of the Saudi Pharmaceutical Society*, 30(12), 1755–1764. <https://doi.org/10.1016/j.jsps.2022.10.004>
12. Sharma, K., Pradhan, S., Duffy, L. K., Yeasmin, S., Bhattarai, N., & Schulte, M. K. (2021). Role of Receptors in Relation to Plaques and Tangles in Alzheimer's Disease Pathology. *International journal of molecular sciences*, 22(23), 12987. <https://doi.org/10.3390/ijms222312987>
13. Yin, X., Qiu, Y., Zhao, C., Zhou, Z., Bao, J., & Qian, W. (2021). The Role of Amyloid-Beta and Tau in the Early Pathogenesis of Alzheimer's Disease. *Medical science monitor : international medical journal of experimental and clinical research*, 27, e933084. <https://doi.org/10.12659/MSM.933084>
14. Abraham, J. T., Maharifa, H. N. S., & Hemalatha, S. (2022). In Silico Molecular Docking Approach Against Enzymes Causing Alzheimer's Disease Using *Borassus flabellifer* Linn. *Applied biochemistry and biotechnology*, 194(4), 1804–1813. <https://doi.org/10.1007/s12010-021-03779-3>
15. Gnanaraj, C., Sekar, M., Fuloria, S., Swain, S. S., Gan, S. H., Chidambaram, K., Rani, N. N. I. M., Balan, T., Stephenie, S., Lum, P. T., Jeyabalan, S., Begum, M. Y., Chandramohan, V., Thangavelu, L., Subramaniyan, V., & Fuloria, N. K. (2022). In Silico Molecular Docking Analysis of Karanjin against Alzheimer's and Parkinson's Diseases as a Potential Natural Lead Molecule for New Drug Design, Development and Therapy. *Molecules (Basel, Switzerland)*, 27(9), 2834. <https://doi.org/10.3390/molecules27092834>
16. Sayers, E. W., Bolton, E. E., Brister, J. R., Canese, K., Chan, J., Comeau, D. C., Connor, R., Funk, K., Kelly, C., Kim, S., Madej, T., Marchler-Bauer, A., Lanczycki, C., Lathrop, S., Lu, Z., Thibaud-Nissen, F., Murphy, T., Phan, L., Skripchenko, Y., Tse, T., ... Sherry, S. T. (2022). Database resources of the national center for biotechnology information. *Nucleic acids research*, 50(D1), D20–D26. <https://doi.org/10.1093/nar/gkab1112>
17. Burley, S. K., Bhikadiya, C., Bi, C., Bittrich, S., Chao, H., Chen, L., Craig, P. A., Crichlow, G. V., Dalenberg, K., Duarte, J. M., Dutta, S., Fayazi, M., Feng, Z., Flatt, J. W., Ganesan, S., Ghosh, S., Goodsell, D. S., Green, R. K., Guranovic, V., Henry, J., ... Zardecki, C. (2023). RCSB Protein Data Bank (RCSB.org): delivery of experimentally-determined PDB structures alongside one million computed structure models of proteins from artificial intelligence/machine learning. *Nucleic acids research*, 51(D1), D488–D508. <https://doi.org/10.1093/nar/gkac1077>
18. Schreiner, T. G., & Popescu, B. O. (2022). Impact of Caffeine on Alzheimer's Disease Pathogenesis-Protective or Risk Factor?. *Life (Basel, Switzerland)*, 12(3), 330. <https://doi.org/10.3390/life12030330>
19. Shabbir, Umair, Momna Rubab, Akanksha Tyagi, and Deog-Hwan Oh. (2021). Curcumin and Its Derivatives as Theranostic Agents in Alzheimer's Disease: The Implication of Nanotechnology. *International Journal of Molecular Sciences* 22, no. 1: 196. <https://doi.org/10.3390/ijms22010196>
20. Newhouse, P.A., Raman, R., Saykin, A.J., Dumas, J., Levin, E., Kellar, K. and Aisen, P.S. (2023), Long-term nicotine treatment of mild cognitive impairment (The MIND Study): Baseline characteristics and study progress. *Alzheimer's Dement.*, 19: e064697. <https://doi.org/10.1002/alz.064697>
21. Tang B-C, Wang Y-T, Ren J. (2023). Basic information about memantine and its treatment of Alzheimer's disease and other clinical applications. *ibrain.*; 9: 340-348. doi:10.1002/ibra.12098
22. Gupta, A., Kapil, R., Dhakan, D. B., & Sharma, V. K. (2014). MP3: a software tool for the prediction of pathogenic proteins in genomic and metagenomic data. *PloS one*, 9(4), e93907. <https://doi.org/10.1371/journal.pone.0093907>
23. Binkowski, T. A., Naghibzadeh, S., & Liang, J. (2003). CASTp: Computed Atlas of Surface Topography of proteins. *Nucleic acids research*, 31(13), 3352–3355. <https://doi.org/10.1093/nar/gkg512>
24. Pettersen, E. F., Goddard, T. D., Huang, C. C., Couch, G. S., Greenblatt, D. M., Meng, E. C., & Ferrin, T. E. (2004). UCSF Chimera--a visualization system for exploratory research and analysis. *Journal of computational chemistry*, 25(13), 1605–1612. <https://doi.org/10.1002/jcc.20084>
25. Trott, O., & Olson, A. J. (2010). AutoDock Vina: improving the speed and accuracy of docking with a new scoring function, efficient optimization, and multithreading. *Journal of computational chemistry*, 31(2), 455–461. <https://doi.org/10.1002/jcc.21334>
26. Dallakyan, S., & Olson, A. J. (2015). Small-molecule library screening by docking with PyRx. *Methods in molecular biology (Clifton, N.J.)*, 1263, 243–250. [https://doi.org/10.1007/978-1-4939-2269-7\\_19](https://doi.org/10.1007/978-1-4939-2269-7_19)
27. Rigsby, R. E., & Parker, A. B. (2016). Using the PyMOL application to reinforce visual understanding of protein structure. *Biochemistry and molecular biology education: a bimonthly publication of the International Union of Biochemistry and Molecular Biology*, 44(5), 433–437. <https://doi.org/10.1002/bmb.20966>
28. Mokhamad Fahmi Rizki Syaban, Rislan Faiz Muhammad, Basyar Adnani, Gumilar Fardhani Ami Putra, Nabila Erina Erwan, Safira Dita Arviana, Agung Dwi Krisnayana, Dedy Budi Kurniawan.(2022). Molecular Docking Studies of Interaction Curcumin against Beta-secretase 1, Amyloid A4 Protein, Gamma-secretase and Glycogen Synthase Kinase-3β as Target Therapy for Alzheimer Disease. *Research Journal of Pharmacy and Technology*. 15(7):3069-4. <https://doi.org/10.52711/0974-360X.2022.00513>
29. Dai, R., Sun, Y., Su, R., & Gao, H. (2022). Anti-Alzheimer's disease potential of traditional chinese medicinal herbs as inhibitors of BACE1 and AChE enzymes. *Biomedicine & pharmacotherapy = Biomedecine & pharmacotherapie*, 154, 113576. <https://doi.org/10.1016/j.biopha.2022.113576>
30. Waseem, R., Shamsi, A., Khan, T., Hassan, M. I., Kazim, S. N., Shahid, M., & Islam, A. (2022). Unraveling the Binding Mechanism of Alzheimer's Drugs with Irisin: Spectroscopic, Calorimetric, and Computational Approaches. *International journal of molecular sciences*, 23(11), 5965. <https://doi.org/10.3390/ijms23115965>

31. Siddiqui AJ, Badraoui R, Jahan S, Alshahrani MM, Siddiqui MA, Khan A and Adnan M (2023) Targeting NMDA receptor in Alzheimer's disease: identifying novel inhibitors using computational approaches. *Front. Pharmacol.* 14:1208968. <https://doi.org/10.3389/fphar.2023.1208968>







32. Marotta, Giambattista, Filippo Basagni, Michela Rosini, and Anna Minarini. (2020). "Memantine Derivatives as Multitarget Agents in Alzheimer's Disease" *Molecules* 25, no. 17: 4005. <https://doi.org/10.3390/molecules25174005>

**About the authors:**

*Saima Kashif (corresponding author) – Assistant Professor, Department of Biomedical Engineering, NED University of Engineering & Technology Karachi 74800, Pakistan, e-mail: ssoomro@neduet.edu.pk*

*Samreen Feroz – MPhil Student, Aga Khan University Hospital, Karachi 3500, Pakistan, e-mail: samreen.feroz@gmail.com*

*Amna Amin – Lecturer, Department of Biomedical Engineering, NED University of Engineering & Technology, Karachi 74800, Pakistan, e-mail: amnasethi@neduet.edu.pk*

A.B. Niyazbekova<sup>1</sup> , T.A. Shakirov<sup>1</sup> , L.I. Baytlesova<sup>1</sup> ,  
N.M. Zhunusbekova<sup>2</sup> , A.I. Niyazbaeva<sup>3\*</sup> , G.M. Gubaidullina<sup>4</sup> 

<sup>1</sup>West Kazakhstan Innovation Technology University, Uralsk, Kazakhstan

<sup>2</sup>Satbayev University, Almaty, Kazakhstan

<sup>3</sup>Al-Farabi Kazakh National University, Almaty, Kazakhstan

<sup>4</sup>Zhangir Khan West Kazakhstan Agrarian Technical University, Uralsk, Kazakhstan

\*e-mail: [Almagul.Niyazbaeva@kaznu.edu.kz](mailto:Almagul.Niyazbaeva@kaznu.edu.kz)

(Received 16 May 2024; received in revised form 24 May 2024; accepted 27 May 2024)

## Effect of phosphate nature on the inhibitory capability of phosphate compositions

**Abstract.** Corrosion inhibitors find ubiquitous application across diverse sectors to formulate robust coatings and chemical compounds. Serving as pivotal additives in compositions, they play a vital role in crafting coatings for circulating water systems, water supply networks, oil refining, petrochemical industries, and power plants. Incorporation extends to fuels, oils, lubricants, and construction materials. In industries oxidation inhibitors is particularly high as chemical, electrochemical, petrochemical, and gas, as well as in water supply networks and circulating water systems. The utilization of inhibitors obviates the necessity for treating metal surfaces with protective enamels and mastics. Effectively preventing oxidation involves the introduction of chemical contributions into aggressive ecology, thereby neutralizing or retarding the oxidation processes. This article explores the anti-oxidation properties of inhibitors in compositions related to St-3 steel. The study includes factors such as the pH of the medium, the nature and concentration of phosphate in compositions simulating reservoir water under stationary and aerated conditions. Investigation methods as potentiometry and photolorimetry used in research. Experimental data, quantitative parameters of the oxidation process, oxidation rate, and degree of protection, depth index, and stability of the film formed were determined. These indicators were assessed on the oxidation resistance scale relative to steel. Analysis of the data shows that out of 63 compositions, seven systems demonstrate the most significant protective effects, with five containing sodium orthophosphate and two containing sodium hydroorthophosphate. The effective, surrounding friendly and cost-effective steel oxidation inhibitors using materials from Kazakhstan will main contribute to the development.

**Key words:** oxidation, inhibitor, orthophosphates, degree of protection, depth index.

### Introduction

In various sectors like power engineering, mechanical engineering, and mining are used corrosion inhibitors. Through the deposition of corrosion inhibitor thin films on their surfaces is achieved metals against atmospheric corrosion. This method stands out for its technological sophistication, preserving the original dimensions of the protected product while exerting minimal impact on subsequent manufacturing processes. The approach is economically viable, as protective coatings can be readily disposed of in industrial wastewater, offering a sustainable solution that minimizes the need for re-preservation.

In based aqueous surroundings and aggressive steamy airs, metallic oxidization classically effects in contained surface damage. Traditional inhibitors similar chromates and nitrites are used no longer generally due to ecological concerns. Carbon-based acid salts have the capacity to become constant metals and compounds when showing to ecological components like chlorides and sulfates. These composites, such as carboxylic acids and alkylphosphonic acids, not only encourage inactivity but also have minimal environmental impact. Water-soluble compounds are mostly preferred due to growing ecological criteria [1].

As such composites, it is particularly worth importance the salts of carboxylic acids R-COOH,

alkylphosphonic acids  $\text{Alk-P(0)(OH)}_2$  and phosphoric acid esters, since in addition to protecting things, they have a low polluting effect on the surroundings. Among them, you can find composites that have good solubility in water. At the same time, there is a vital for the development of environmentally benign and effective formulations of metal corrosion inhibitors, especially those characterized by low concentrations [2].

The consequence of oxidization studies is triple. Principally, from a financial standpoint, the objective is the modification of material losses incurred due to the oxidization of pipelines, boilers, machine components, vessels, bridges, marine structures, and the like. The second is to improve the reliability of apparatus that can oxidize with catastrophic significances, such as pressure containers, vapor boilers, metal containers for toxic materials, turbine blades and rotors, bridges, aircraft parts and autonomous automated machinery. Stability is the main state in the increase of nuclear power plant equipment and radioactive waste disposal systems. The third dimension revolves around the safeguarding of the metal reserve. Assumed the limited nature of global metal resources, corrosion-induced metal losses entail supplementary expenditures in terms of energy and water resources. So imperative is the redirection of social effort spent on the design and modernization of oxidized metal apparatus toward addressing other publically useful activities [3, 4].

### Materials and methods

Oxidization inhibitors have been essential to the oil and gas manufacturing since the 1940s, usually calculated in parts per million, ranging from 15 to 50 grams per ton of liquid. In the complicated network of field pipeline systems resembling the branches of a tree, emanating in divergent directions from a common origin point, the strategic addition of inhibitors at the pipeline inlet ensures comprehensive protection over vast distances, extending up to some hundred kilometers [5].

The NACE usual are distinguished by an appropriately significant acidity, with a hydrogen ion concentration yielding a pH of 3.6 in the absence of hydrogen sulfide and carbon dioxide additives. Summary of these acid agents does not precipitate a pH reduction. The totaling of acid substances does not lower the pH, since hydrogen sulfide and carbon dioxide in solution are current in molecular form at the specified pH values. When carbon steel corrodes in an environment saturated with carbon dioxide,

the surface of the electrodes becomes covered with a gray film with rust spots, consisting of  $\text{Fe}_3\text{O}_4$  with traces of  $\text{FeCO}_3$ . In the presence of hydrogen sulfide, a layer of iron sulfides forms on the metal surface, which is easily indifferent with an etching solution. The investigational results obtained confirm the essential remarkable effect of hydrogen sulfide and carbon dioxide on the oxidization rate of steel [6].

Improving device reliability, mainly for oxidation-prone modules in pressure vessels, condensation boilers, and nuclear power plants, is crucial. The presence of hydrogen sulfide and carbon dioxide can meaningfully accelerate the corrosion rate of steel, with hydrogen sulfide proving to be a stronger activating than  $\text{CO}_2$ . Inhibition of corrosion through the formation of a protective layer on the metal surface is observed over time.

Giving to the moments of daily investigations, in the occurrence of hydrogen sulfide  $K_0$  is 0.46  $\text{g/m}^2$  hour, and in carbon dioxide environments, it is meaningfully lower – 0.192  $\text{g/m}^2$  hour, which is 2 times upper than the oxidization rate in the background solution. In a combined environment containing both hydrogen sulfide and carbon dioxide,  $K_0$  values are slightly lower than in hydrogen sulfide. This element is probably connected with the reasonable adsorption of  $\text{CO}_2$  and hydrosulfide ions on the active centers of the metal surface. As the time of the research increases, the oxidization rate values decrease, which is due to the adding of a deposit of oxidization produces on the surface of the steel, which builds a certain barrier to the supply of an acid average [7].

The oxidization analysis approach engaged adhered to widely accepted practices [8]. Oxidization experiments were carried out on ST-3 steel samples with the components, wt. %: C – 0.2; Mn – 0.5; Si – 0.15; P – 0.04; S – 0.05; Cr – 0.30; Ni – 0.20; Cu – 0.20; Fe – 98.36.

To carry out oxidization analysis, rectangular plates made of St-3 steel were used. The samples were cleaned, degreased and weighed. A solution volume of at least 15  $\text{cm}^3$  per 1  $\text{cm}^2$  of sample surface was used and tests lasted from 24 to 480 hours [9].

The oxidization rate assessed by the weight loss of the samples at certain time intervals. Quantitative oxidation indicators calculated using the Student's t coefficient with a confidence level of 0.95.

During the work, potentiometric measurements of pH, electrical conductivity and total mineralization, conductometric measurements and determination of iron (III) content using potassium thiocyanate were carried out [10].

## Results and discussion

Experimental data elucidating the protective efficacy of formulations containing sodium dihydroorthophosphate are depicted on Figure 1.

Examination of pure phosphate inhibitors at concentrations of 0.01, 0.025, and 0.05 mol/dm<sup>3</sup>, both in a composition with a simulated reservoir water under stationary conditions and with intensive aeration, unveiled a notable elevation in the corrosion process rate in pure media, correspondingly resulting in a low inhibition coefficient. In media with IPV NACE and IPV NACE during aeration,

the inhibition coefficient is notably low, indicating an absence of protective effects in these systems. The highest value of the inhibition coefficient is observed at a concentration of sodium dihydrogen orthophosphate of 0.025 mol/dm<sup>3</sup> in the control sample – tap water.

Further investigations under stationary conditions revealed that, in the mediums of IP in NACE and with IPV NACE during aeration, compositions containing NaH<sub>2</sub>PO<sub>4</sub> do not manifest a significant protective effect. Experimental data on the protective effect of inhibitors in compositions containing sodium hydroorthophosphate are presented on Figure 2.

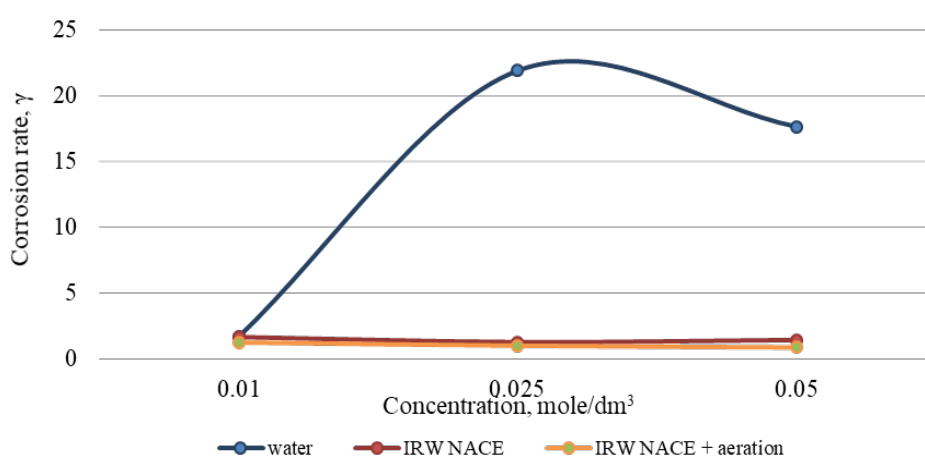


**Figure 1** – Inhibition of corrosion of steel St3 by compositions with sodium dihydroorthophosphate NaH<sub>2</sub>PO<sub>4</sub> in various media depending on concentration

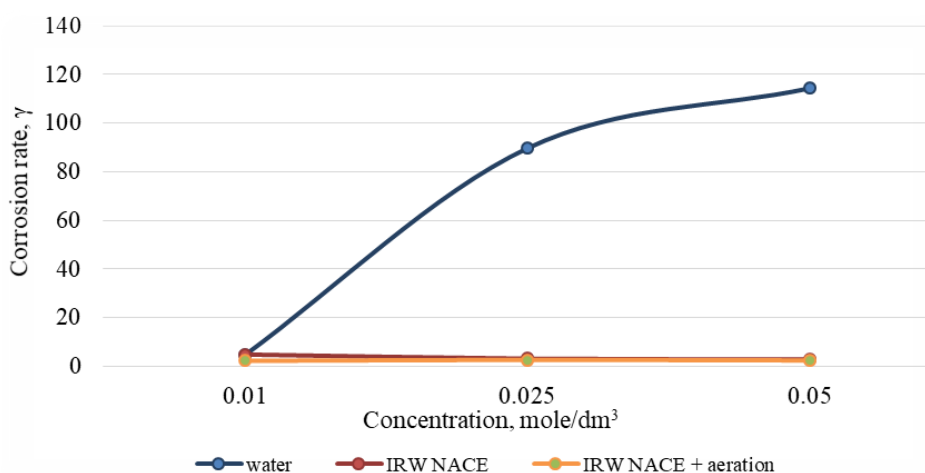


**Figure 2** – Inhibition of corrosion of steel St3 by compositions with sodium hydroorthophosphate Na<sub>2</sub>HPO<sub>4</sub> in various media depending on concentration



The study of the protective effect of pure  $\text{Na}_2\text{HPO}_4$  and its compositions with IPV NACE and with IPV NACE during aeration showed that in all media at  $0.01 \text{ mol/dm}^3$  the effect in all media of the inhibitor is insignificant. Upon escalating the concentration to  $0.025$  and  $0.05 \text{ mol/dm}^3$ , a

substantial augmentation in the inhibitory effect of  $\text{Na}_2\text{HPO}_4$  is observed in pure water. However, concomitantly, this enhanced effect is practically non-evident in the other two media, exhibiting a diminishing trend with the escalating concentration of the phosphate component.

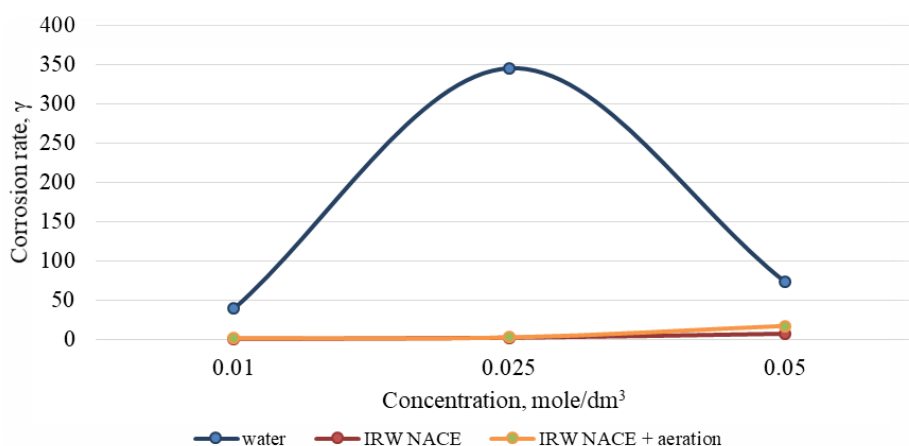


**Figure 3** – Inhibition of corrosion of steel St3 by compositions with sodium orthophosphate  $\text{Na}_3\text{PO}_4$  in various media depending on concentration

Figure 3 presents experimental data elucidating the protective efficacy of compositions incorporating sodium orthophosphate. For compositions of  $\text{Na}_3\text{PO}_4$  with IPV NACE and IPV NACE with intense aeration at concentrations of  $0.01$ ,  $0.025$ ,  $0.05 \text{ mol/dm}^3$ , it was found that the best inhibitory effect is demonstrated by  $\text{Na}_3\text{PO}_4$  in pure water at a

concentration of  $0.025 \text{ mol/dm}^3$  ( $\gamma = 345.22$ ), which is the best result. All data show that a concentration of  $0.025 \text{ mol/dm}^3$  for sodium orthophosphate is optimal.

Experimental data on the protective effect of compositions containing sodium dihydrodiphosphate is presented on Figure 4.

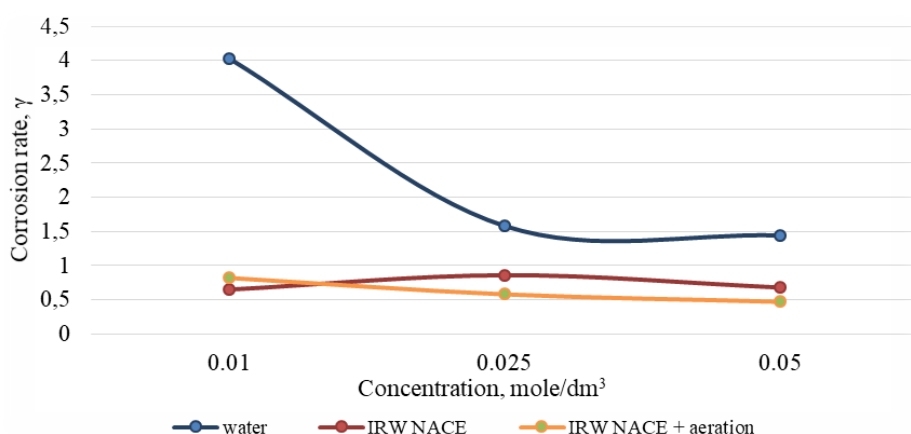


**Figure 4** – Inhibition of corrosion of steel St3 by compositions with sodium dihydrogen phosphate  $\text{Na}_2\text{H}_2\text{P}_2\text{O}_7$  in various media depending on concentration

The investigation into the inhibitory effect of compositions incorporating  $\text{Na}_2\text{H}_2\text{P}_2\text{O}_7$  reveals that the composition with water attains the highest inhibition coefficient at a concentration of  $0.01 \text{ mol/dm}^3$ . Notably, an augmentation in the concentration of sodium dihydrodiphosphate

systematically diminishes the protective effect. In compositions involving  $\text{Na}_2\text{H}_2\text{P}_2\text{O}_7$  with IPV NACE and compositions under IPV NACE with intensive aeration, the inhibition coefficient falls below unity. Consequently, under these conditions,  $\text{Na}_2\text{H}_2\text{P}_2\text{O}_7$  serves as a corrosion stimulator.

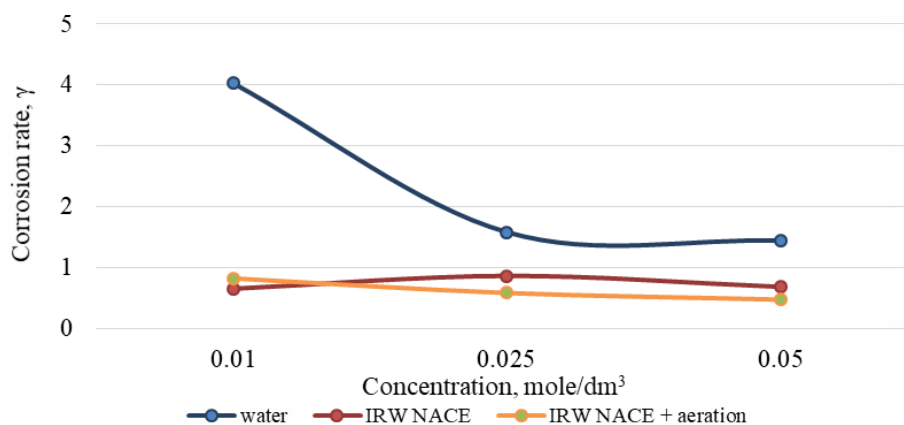


**Figure 5** – Inhibition of oxidation of steel St3 by compositions with sodium diphosphate  $\text{Na}_4\text{P}_2\text{O}_7$  in various media depending on concentration

Experimental data on the protective effect of compositions containing sodium diphosphate is presented in Figure 5.

Analysis of the obtained data on the main indicators characterizing the corrosion process of the composition of sodium diphosphate with  $0.01 \text{ mol/dm}^3$  shows the manifestation of similar values of the protective effect.

Upon escalating the inhibitor concentration in compositions with reservoir water during aeration, a

slight increase in protective efficacy was observed. Conversely, in other conditions, an elevation in concentration resulted in corrosion stimulation. Generally, these compositions lack discernible effectiveness in the studied media.

Information on the protective effect of compositions containing sodium cyclotriphosphate was obtained from experiments and is presented on Figure 6.

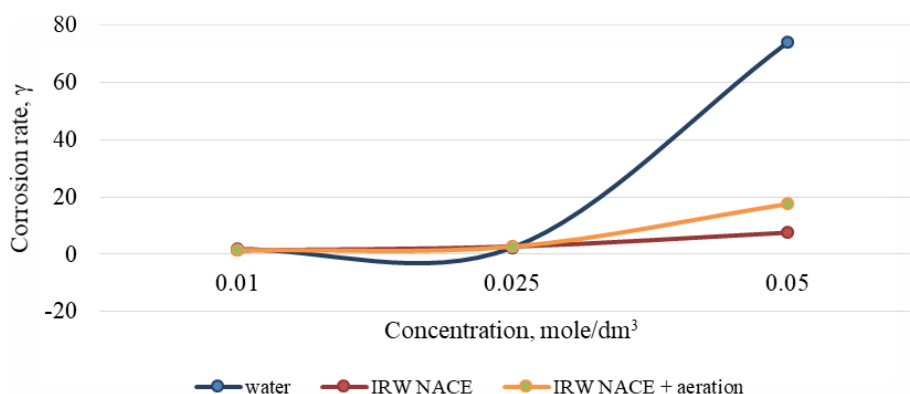


**Figure 6** – Inhibition of corrosion of steel St3 by compositions with sodium cyclotriphosphate  $\text{Na}_3\text{P}_3\text{O}_9$  in various media depending on concentration

The inhibitory capabilities of trimetaphosphate compositions were systematically explored, both in their pure form and as compositions with IPV NACE and compositions with IPV NACE under intensive aeration.

The findings indicate that the  $\text{Na}_3\text{P}_3\text{O}_9$  inhibitor, within the composition involving IPV NACE under intensive aeration, exhibits superior protective

efficacy compared to other systems, albeit not surpassing 3 in terms of the protective effect. Increasing in the content of inorganic components in the compositions leads to a slight increase in the protective effect. Experimental data shows that the best combination of anti-corrosion components for maximum protection in clean water is a composition with  $\text{Na}_3\text{PO}_4$  at  $0.025 \text{ mol/dm}^3$ .

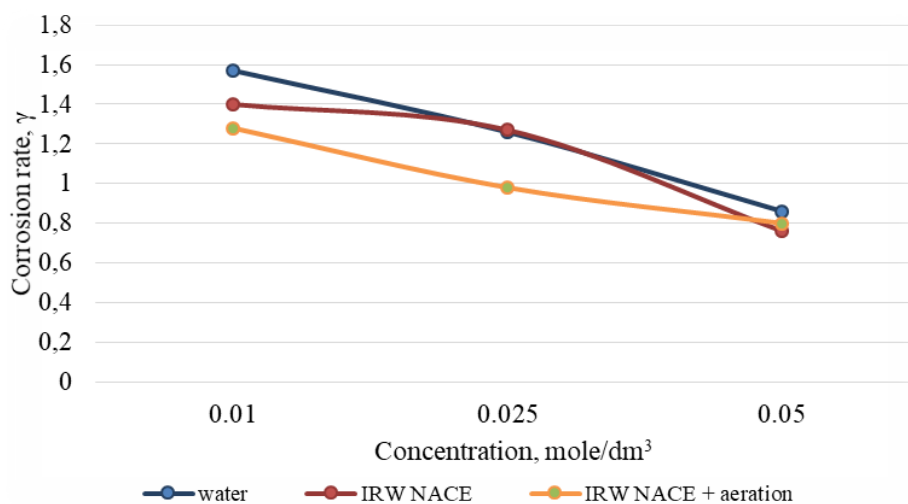


**Figure 7** – Inhibition of corrosion of steel St3 by compositions with sodium cyclohexaphosphate  $\text{Na}_6\text{P}_6\text{O}_{18}$  in various media depending on concentration

Experimental data on the protective effect of compositions containing sodium cyclohexaphosphate is presented on Figure 7.

The outcomes from the investigation into the protective efficacy of compositions containing sodium cyclohexaphosphate  $\text{Na}_6\text{P}_6\text{O}_{18}$  across diverse media lead to the conclusion that an elevation in concentration does not contribute to the enhancement of the inhibitor's protective properties. The inhibition coefficient values remain small across all systems. In the composition with IPV NACE, sodium cyclohexaphosphate acts as a corrosion stimulant, but under conditions of intensive aeration, the protective effect experiences a marginal increase, albeit insignificant.

1. The anticorrosive efficacy of phosphorus-containing inorganic compositions in diverse media has been systematically evaluated. Quantitative parameters delineating the corrosion process were ascertained employing both chemical and physicochemical methodologies.

2. Based on the results of experimental work, it established that the more effective combination of

anti-corrosion components to ensure the maximum possible protection for the environment is:

- tap water – composition with  $\text{Na}_3\text{PO}_4$  at  $0.025 \text{ mol/dm}^3$ ;

- for IPV NACE – composition with  $\text{Na}_3\text{PO}_4$  at  $0.025 \text{ mol/dm}^3$ ;

- for IPV NACE during aeration – composition  $\text{Na}_3\text{PO}_4$  at  $0.05 \text{ mol/dm}^3$ .

It was found that, compared to tap water, the protective effect of phosphate compositions in IPV is reduced, and becomes even less with intense aeration.

In pure water medium the anticorrosive activity increases in the following range:

$\text{Na}_4\text{P}_2\text{O}_7 < \text{Na}_6\text{P}_6\text{O}_{18} < \text{Na}_3\text{P}_3\text{O}_9 < \text{Na}_2\text{H}_2\text{P}_2\text{O}_7 < \text{NaH}_2\text{PO}_4 < \text{Na}_2\text{HPO}_4 < \text{Na}_3\text{PO}_4$ .

In the IPV NACE medium, the anticorrosive activity increases in a number of:

$\text{Na}_2\text{H}_2\text{P}_2\text{O}_7 < \text{Na}_6\text{P}_6\text{O}_{18} < \text{NaH}_2\text{PO}_4 < \text{Na}_4\text{P}_2\text{O}_7 < \text{Na}_3\text{P}_3\text{O}_9 < \text{Na}_2\text{HPO}_4 < \text{Na}_3\text{PO}_4$ .

In the IPV NACE media with intensive aeration, the anticorrosive activity increases in the row:

$\text{Na}_2\text{H}_2\text{P}_2\text{O}_7 < \text{Na}_6\text{P}_6\text{O}_{18} < \text{NaH}_2\text{PO}_4 < \text{Na}_4\text{P}_2\text{O}_7 < \text{Na}_3\text{P}_3\text{O}_9 < \text{Na}_2\text{HPO}_4 < \text{Na}_3\text{PO}_4$ .

## Conclusions

The undeniable importance and significance of metal corrosion inhibitors are highlighted, as evidenced by the extension of the service life of metal structures from the conventional 2 years to an impressive 5-6 years, exceeding the baseline by 2.5-3 times, contingent upon the steel grade.

In the largest countries globally, the production landscape of metal corrosion inhibitors is characterized by a diverse array of chemical products, yielding substantial financial returns for producers [11]. Annually, manufacturers from both non-CIS and CIS countries introduce new, ostensibly more effective metal corrosion inhibitors to the market. However, industrial viability depends on the economic costs of a particular product and its compliance with chemical reagent specifications.

The experimental exploration involved the study of 63 compositions, analyzing their anticorrosive effectiveness in relation to the concentration and nature of the phosphate component. Additionally, three systems without inhibitors were investigated.

The use of all systems depends on the pH of the solution and the overall mineralization. An increase in pH and mineralization corresponds to an increase in the protective effect.

The effectiveness of all systems depends on the pH of the solution and the total mineralization. An increase in pH and mineralization corresponds to an increase in the protective effect.

Based on the acquired investigational data, it was assumed that among the 63 compositions, 7 systems exhibit the most basically significant protective result. This subset comprises 5 systems with sodium orthophosphate and 2 with sodium hydroorthophosphate.

The patterns established during the study not only develop, but also addition current ideas about the protective effect of compounds based on inorganic phosphate compounds. The results obtained promise a significant support to the increasing of effective, ecologically responsive and cost-effective steel oxidation inhibitors based on Kazakhstani raw materials. The collected data represents a significant step in advancing the scientific frontiers of effective inhibitory protection of metals.

## References

1. McCafferty E. (2010) Introduction to Corrosion Science. Springer, New York, NY.
2. Tosun A., Ergun M. (2006) Protection of corrosion of carbon steel by inhibitors in chloride containing solutions. *Gazi Univ. J. Sci.*, 19(3), 149-154.
3. Fouda A.S., Elewady G.Y., El-Haddad M.N. (2011) Corrosion inhibition of carbon steel in acidic solution using some azodyes. *Can. J. Sci. Ind. Res.*, 2(1), 1-19.
4. Niyazbekova A.B., Akatyev N.V., Sulekeshova G.K., Shakirov T.A. (2013) Chromatographic study of systems cyclotri-, cyclotetra- and cyclohexaphosphate with two and trivalent cations of p- and d-elements. Materials of the VI international research and practice conference, Munich, Germany.
5. Kuanysheva G.S., Makasheva G.R., Kamalova G., Niyazbekova A.B. (1999) Complexa formation of salts of some d-elements with a diphosphate anion. *Bull. of KazGU*, 1(13), 71-73.
6. Brown B., Saleh A., Moloney J. (2016) A comparison of mono- to di- phosphate ester ratio in inhibitor formulations in the mitigation of under deposit corrosion. *CORROSION*, Vancouver, Canada.
7. Narayana N., María Rao, Gómez-García R., Kornberg A. (2009) Inorganic polyphosphate: essential for growth and survival. *Annu. Rev. Biochem.*, 78, 605-647.
8. Durif A. (2005) The development of cyclophosphate crystal chemistry. *Solid State Sci.*, 7(6), 760-766.
9. Bhajiwala H.M., Vashi R.T. (2001) Ethanolamine, diethanolamine and triethanolamine as corrosion inhibitors for zinc in binary acid mixture [ $\text{HNO}_3 + \text{H}_3\text{PO}_4$ ]. *Bull. Electrochem.*, 17(10), 441-448.
10. Kura G. (1987) Hydrolysis reaction of inorganic cyclophosphates at various acid strengths. *Polyhedron*, 6(3), 531-533.
11. Niazbekova A., Akatyev N., Mukasheva M., Rakhova A. (2012) Quantum- chemical calculations of electronic structure of polyphosphate complexes of manganese, cobalt, copper and zinc. Materials of the international research and practice conference "European Science and Technology", Wiesbaden: Germany, 82-85.

**Information about authors:**

*Niyazbekova Aktoty – candidate of chemical Science, Associate Professor, West-Kazakhstan Innovation Technology University (Uralsk, Kazakhstan, e-mail: abnyazbekova@mail.ru)*

*Shakirov Timur – magister of engineering and technology, West-Kazakhstan Innovation Technology University (Uralsk, Kazakhstan, e-mail: Shakirov.timur.0585@gmail.com)*

*Baytlesova Laura – candidate of chemical Science, Associate Professor, West-Kazakhstan Innovation Technology University (Uralsk, Kazakhstan, e-mail: beu@mail.ru)*

*Zhunusbekova Nazym – candidate of chemical Science, Associate Professor, Satbayev University (Almaty, Kazakhstan, e-mail: znazym@mail.ru)*

*Niyazbayeva Almagul (corresponding author) – candidate of chemical science, associate professor, Al-Farabi Kazakh National University (Almaty, Kazakhstan, e-mail: Almagul.Niyazbaeva@kaznu.edu.kz)*

*Gubaidullina Gulkhan – candidate of technical Sciences, Associate Professor, West-Kazakhstan agrarian-technical University named after Zhangir Khan (Uralsk, Kazakhstan, e-mail: ggulkhan@mail.ru)*

## Content

Editorial.....	3
E.S. Seitkozhanova, S.M. Shalgimbayeva, S.S. Barinova, Dh. Makhmetova, G.B. Jumakhanova, A.E. Nurgaliev, Z.S. Omarova, D.A. Yussayeva, G.T. Zhanysbay Study of Charyn river naked osman ( <i>Diptychus dybowskii</i> ) nutrition and ichthyopathological analysis .....	4
M. Ozdal, O. Gulmez, E. Gökçe, O.F. Algur Purification and characterization of glutaminase and urease-free L-asparaginase from <i>Bacillus atrophaeus</i> with acrylamide reduction potential .....	13
Y.M. Toishibekov, D.Y. Toishybek, T.T. Nurkenov, B.S. Katubayeva, M.Y. Salmenova, A.V. Perfilyeva Optimization of cryopreservation methods for somatic cells of the Tobet dog breed .....	23
A.K. Shokan, D.M. Yergozova, T.N. Kobylina, N.O. Kudrina, Yu.A. Litvinenko, G.A. Seitimova, T.E. Kulmanov, N.V. Terletsкая, I.M. Zharkova Effect of the complex extract from <i>Rumex</i> plants on quantitative parameters of blood cells and bone marrow in <i>vivo</i> .....	31
M. Kamalabadi, Gh. Chehardoli Aspects of DNA interaction with the natural heterocyclic compounds .....	40
Zh.K. Batykova, A.S. Kistaubayeva, I.S. Savitskaya, V. Pidlisnyuk Isolation and study of plant growth promoting rhizobacteria from Triticosecale Wittmack growing in Almaty region.....	53
J. Iqra, A. Shabbir, A. Hasnain, A. Iqra, S. Muqadas, A. Sajid, K. Sheraz, Sh. Khurram The potential ameliorative effects of <i>Moringa oleifera</i> in emamectin benzoate induced toxicity in freshwater <i>Labeo rohita</i> fish.....	60
S.N. Abdreshov, M.A. Yessenova, A.N. Yeshmukhanbet, G.A. Demchenko, V.N. Gorchakov, G.K. Atanbaeva, S.A. Mankibaeva Morphofunctional and morphometric features of the small intestine in experimental rats with inflammation of the abdominal cavity.....	70
I.Yu. Silachyov, V.A. Glagolev, M.N. Kokkuzova Gold content determination in small core-samples by instrumental neutron activation analysis.....	78
S.M. Adekenov Isoprenoids from <i>Rhaponticum carthamoides</i> (Willd.) Iljin and <i>Rhaponticum serratuloides</i> (Georgi.) Bobr .....	89
O.Yu. Maslov, M.A. Komisarenko, S.V. Ponomarenko, S.V. Kolisnyk, T.P. Osolodchenko, M.Yu. Golik, S.I. Polishchuk Antimicrobial, antifungal, antioxidant activity and phytochemical investigation of fatty acids by GS/MS of raspberry ( <i>Rubus idaeus</i> L.) shoot lipophilic extract.....	102
M. Siddiqui, Atia-tul-Wahab, B.M. Kudaibergenova, Zh.A. Abilov, M.I. Choudhary Biotransformation of anabolic drug Dianabol with <i>Rizhopus oryzae</i> .....	108
O. Sarikaya, S. Parlak, Y. Yildiz, T. Gencal, I.M. Ozcankaya, F. Selek, O. Acici, H. Can Insecticide applications with trunk injection method for reducing the damage level of <i>Leptoglossus occidentalis</i> (Heidemann, 1910) in stone pine stands.....	112
N.A. Nursapina, I.V. Matveyeva, Sh.N. Nazarkulova, R. Jaćimović Determination of impurities in fertilizers purchased in Almaty (Kazakhstan) .....	118
S. Kashif, S. Feroze, A.A. Sethi Targeting beta-amyloid plaques and neurofibrillary tangles: a proteomic approach towards Alzheimer's disease therapy .....	124
A.B. Niyazbekova, T.A. Shakirov, L.I. Baytlesova, N.M. Zhunusbekova, A.I. Niyazbaeva, G.M. Gubaidullina Effect of phosphate nature on the inhibitory capability of phosphate compositions .....	134